Thermal Treatment of Bitumen Froth at 400 °C: Impact of Water and Minerals on Bitumen Properties and Reaction Chemistry

by

Joao Felipe Pereira Bassane

A thesis submitted in partial fulfillment of the requirements for the degree of

Doctor of Philosophy

in

Chemical Engineering

Department of Chemical and Materials Engineering
University of Alberta

© Joao Felipe Pereira Bassane, 2024

Abstract

The production of oilsands bitumen from mining operations requires its recovery from the mineral matter through a hot water extraction process, which generates a bitumen froth comprising about 60 wt% bitumen, 30 wt% water, and 10 wt% mineral solids. The challenging separation of water and solids from bitumen is achieved in the froth treatment unit employing a light hydrocarbon solvent. The bitumen product, after solvent recovery, is very viscous and dense, requiring dilution and/or upgrading to be transported through pipelines.

The thermal treatment of bitumen froth has potential to integrate froth treatment and partial upgrading of bitumen. With this prospect in mind, the current thesis investigated the impact of water and oilsands minerals on the bitumen properties and the reaction chemistry during the thermal treatment of bitumen froth at 400 °C.

The visbreaking of bitumen in the presence of water and solids, with and without solvent addition, was investigated at 400 °C. While visbreaking of froth led to a bitumen product with lower density and viscosity, it was surprising that the treatment in the presence of water and/or solids resulted in a bitumen product with slightly higher viscosity and density as compared to visbreaking of bitumen alone. This finding was contrary to reports in literature that claimed improved quality of the bitumen product when bitumen was thermally treated in the presence of water and solids. Changes in the physicochemical properties of bitumen indicated a decreased aromatic H content when bitumen was treated in the presence of water and/or solids as compared to bitumen alone, a sign that hydrogen transfer reactions were influenced by these components. The study found that it was advantageous to perform bitumen visbreaking in the presence of a lighter hydrocarbon solvent (*n*-hexane) when compared to a heavier solvent (kerosene) or visbreaking without a solvent.

To gain a better fundamental understanding of the influence of water and minerals on bitumen conversion in froth, α-methylstyrene (AMS) was employed as a probe molecule. The presence of water during the treatment resulted in decreased AMS conversion, lowered the formation of addition products, and favored hydrogen transfer reactions. However, it was unclear if water had a direct effect on influencing these changes or if it altered the system properties, which subsequently resulted in the observed changes. There was evidence that the froth minerals favored hydrogen transfer during the treatment, which can potentially be advantageous to bitumen upgrading by suppressing coke formation. The Brønsted-Lowry acidity of clays found in oilsands, such as kaolinite, was expected to enable cationic conversion during the treatment. Nevertheless, due to the complexity of a reaction medium containing bitumen, it was not possible to distinguish between free radical and cationic conversion, which motivated the use of simpler model systems to facilitate interpretation of the results.

The specific contributions of water and kaolinite to the reaction rates and pathways during thermal treatment of a model system comprising AMS, tetralin, and *n*-pentadecane were studied through detailed characterization of the reaction products. The dilution of the reaction medium by water was presented as a potential effect that resulted in decreased conversion rates of AMS. This finding highlighted a possible deleterious effect of water during thermal treatment. Although water affected the conversion rates and promoted the hydration of unsaturated species, there was no evidence that water was a net hydrogen donor during the treatment. The choice of the model systems allowed for differentiating between free radical and cationic conversion. The Brønsted-Lowry acidity of kaolinite had an impact on the reaction pathways by enabling cationic dealkylation to form benzene and cationic dimerization to form the tricyclic AMS dimer 1,1,3-trimethyl-3-phenyl indane. The presence of kaolinite also resulted in increased reaction rates and favored hydrogen transfer reactions. Although kaolinite was catalytically active during the conversion, its catalytic sites were rapidly fouled due to its low surface area.

It can be concluded that visbreaking of bitumen froth at 400 °C, particularly in the presence of a light solvent such as *n*-hexane, has the potential to combine froth treatment and upgrading. Water and mineral matter caused a minor suppression of conversion, but at the same time improved hydrogen transfer, with kaolinite also being responsible for limited cationic conversion.

Preface

(Mandatory due to collaborative work)

Chapter 3 of this thesis was published as "Bassane, J. F. P.; de Klerk, A. Visbreaking of Bitumen Froth: Influence of Minerals, Water, and Solvent on the Physicochemical Changes in the Bitumen Phase. *Energy Fuels* **2023**, 37 (16), 11820–11837". I was responsible for concept formation, experimental design, data collection and analysis, as well as manuscript composition. I was also the corresponding author for this manuscript. I presented parts of this study at the American Chemical Society (ACS) Spring Meeting 2021 (oral presentation) and the Future Energy Systems Digital Research Showcase 2020 (poster presentation). Arno de Klerk acted as the supervisory author and was involved in the concept formation, data interpretation and manuscript composition.

Chapter 4 of this thesis was published as "Bassane, J. F. P.; de Klerk, A. Hydrothermal Treatment of Oilsands Bitumen Froth at 400 °C: Influence of Minerals and Water on Hydrogen Transfer, Cracking, and Addition Reactions. *Energy Fuels* **2024**, 38 (2), 1032–1046". I was responsible for concept formation, experimental design, data collection and analysis, as well as manuscript composition. I was also the corresponding author for this manuscript. I presented parts of this study at the American Chemical Society (ACS) Spring Meeting 2023 (oral presentation). Arno de Klerk acted as the supervisory author and was involved in the concept formation, data interpretation and manuscript composition.

To my beloved wife, Lays Gaudio, for all the love and support.

To my dear parents, Joao and Mari Bassane, for all the love and encouragement.

Acknowledgements

I would like to start by acknowledging the creator of the universe and all science, the One who is the source of all wisdom. Thank you, God, for giving me strength and supporting me through all the challenges. I dedicate every achievement in my life to glorify your name.

There are insufficient words to adequately express my gratitude to my supervisor, Prof. Arno de Klerk, for his patience, guidance, and support throughout this journey. I truly appreciate all the wise advice and feedback that have contributed significantly to my growth, both professionally and personally, during this period. Your wealth of knowledge and dedication have been truly inspiring. Thank you for being an outstanding supervisor and professor.

I am deeply grateful to my parents, Mari and Joao Bassane, for being the ones who taught me the essential principles that have defined who I am. Thanks so much for loving me and for your countless efforts in investing in my education and future. Without you, I would not have come close to where I am today. I love you both.

I am so thankful to my beloved wife, Lays Gaudio, for continually holding my hand and making me believe that I was able to advance and overcome the challenges even when I felt weak and hopeless. I am so blessed to have you by my side. Your love and radiance inspire me, making each day the brightest and happiest. I love you.

Next, I am thankful to my entire research group, composed of such talented people. Their friendship and support encouraged me during my studies. I am very thankful to Cibele for all her leadership, training, technical support, and for being a good friend, whose advice was greatly appreciated. I would like to thank Shruthi and Natalia for being such good friends and for their patience in listening and advising me in moments of joy and struggle. Also, thanks to Glaucia and Lina for their friendship, advice, and words of encouragement.

I am grateful to my family and friends, both in Brazil and Canada. I would like to thank Jorge Correa, who, despite the distance, always makes an effort to show his closeness. I am blessed to have you as a friend. I am thankful to Lucas Giovenardi for being such a supportive friend and consistently motivating me to pursue my goals. I am thankful to Nayara for the words of

encouragement and for the shared moments of coffee breaks and thesis writing. Additionally, I am thankful to Laine for her friendship and for supporting me with her technical expertise.

Lastly, I would like to acknowledge Future Energy Systems for all the financial support.

Table of Contents

List of Tables

List of Figures

Chapter 1

Introduction

1.1 Background

Road transportation, aviation and shipping, as well as industry and petrochemicals, are the primary drivers of the increase in global oil demand. Unconventional oil sources, such as extra-heavy oil and bitumen, play an important role in meeting current and future demand scenarios and are expected to increase production from 3.7 million barrels per day in 2021 to 6.2 million barrels per day in 2050 [1].

The Canadian oilsands are one of the largest proven oil reserves in the world [2]. Oilsands bitumen is classified as unconventional oil due to its low fluidity at reservoir conditions and its tendency to strongly interact with mineral matter. These characteristics pose significant challenges for both the recovery and transportation of bitumen, often making them impractical through conventional methods [3]. The method employed for oilsands recovery depends on the depth of the reservoir. Shallow deposits, typically at depths of 30 meters or less, are recovered through mining, whereas deeper deposits require subsurface recovery methods such as cyclic steam stimulation [4].

Roughly 50% of the bitumen produced in Alberta is derived from mining operations [5]. The Athabasca oilsands comprise a mixture of mineral solids, water, and bitumen. A typical ore comprises approximately 6–12 wt% bitumen, 5–6 wt% water, and the remaining portion as solids, categorized as fines and coarse solids. Fines (i.e., solids with a diameter less than 44 μm) include very fine quartz, clay minerals (predominantly kaolinite and illite), and small amounts of heavy minerals like rutile. Coarse solids are primarily composed of silica sand (quartz) with some feldspar [4, 6].

A simplified overview of the bitumen production process from mining is illustrated in **Figure 1.1**. When bitumen is produced through mining, it needs to be disengaged from the bulk of the mineral matter through a process known as hot water extraction. In this process, crushed oilsands ores are pumped with warm water (40–50 °C) through a conditioning pipeline, forming a slurry of oilsands and water. Subsequently, this slurry undergoes further separation steps to produce a froth composed of 45–65 wt% bitumen, 20–35 wt% water, and 5–15 wt% mineral solids [7].

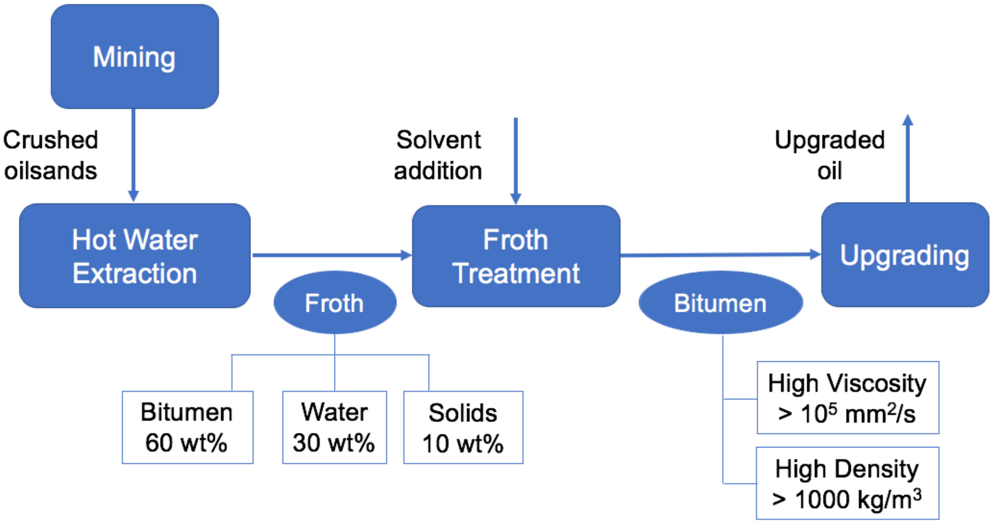

Figure 1.1: Simplified block flow diagram of bitumen production process from mining.

The separation of water and mineral solids from bitumen froth is challenging because bitumen and water have similar densities, which makes gravitational separation impractical. Also, the high viscosity of bitumen hinders the separation of fines, while water-in-oil emulsions are stabilized by natural surfactants in bitumen and by the fines, impeding the separation of water [8]. In order to achieve such separation, a light solvent is added to the froth in the froth treatment unit. Depending on the type of solvent used, the froth treatment can be classified as either paraffinic froth treatment (PFT) or naphthenic froth treatment (NFT). In the NFT, the addition of naphtha enables solids and water separation from bitumen, yielding a bitumen product that still contains some residual water and solids and therefore requires further separation steps. In the PFT, the addition of a paraffinic solvent (usually a mixture of pentane and hexane) results in the precipitation of some asphaltenes, yielding a clean bitumen product that does not need further separation steps [4, 8].

After the separation of water and solids in the froth treatment and solvent recovery, the resulting bitumen product exhibits high density and viscosity. Three primary methods can be utilized to transport the bitumen product to its primary market, namely, refineries: (1) dilution with a light hydrocarbon solvent; (2) full upgrading of bitumen, transforming it into a higher quality/value synthetic crude oil (SCO); and (3) partial upgrading of bitumen as an intermediate option between dilution and full upgrading [9, 10]. Although partial upgrading is not an industrially applied method at present, it is an approach that has attracted attention.

The primary goal in partial upgrading of bitumen is to decrease its density and viscosity to a level where the required amount of diluent for transportation is minimized, at a lower cost than that of the bitumen dilution alone (i.e., dilution without any upgrading benefit) and that of full upgrading [9]. One of the technologies that can be applied for partial upgrading of bitumen is visbreaking, which is a thermal cracking process.

The aforementioned stages of mining, hot water extraction, froth treatment, and upgrading, represent the typical steps in oilsands bitumen production. The majority of research associated with the froth treatment process has focused on enhancing the efficiency of separation in the process (i.e., the removal of water and solids from bitumen). There has been little emphasis on investigating potential physicochemical changes in the bitumen phase throughout the process [11, 12]. Froth treatment is usually operated in the temperature range of 70–90 °C, which is too low to achieve any upgrading benefit. However, intrigued by the possible integration of the froth treatment step and upgrading, a previous study investigated the impact of the hydrothermal treatment of froth at 250 °C on the physicochemical changes in the bitumen phase [13]. The study revealed that the treatment did not result in any partial upgrading benefits. Instead, an increase in bitumen's viscosity and density was observed in the presence of water and mineral solids, which pointed out that both water and minerals played a role during the treatment, influencing changes in the bitumen phase.

The thermal treatment of bitumen and heavy oils in the presence of water and mineral solids has been mainly explored in studies related to subsurface upgrading of these oils. Studies that subjected bitumen to thermal treatment in the presence of sub- and supercritical water have reported benefits such as coke suppression and increased yields of liquid products [14, 15]. Nevertheless, it remains unclear whether water actively participates as a reactant in the process of bitumen upgrading or if the observed effects are a result of water dilution in the reaction medium. Also, numerous studies in this regard involved extended reaction times and elevated pressures, which may not be practical for industrial applications in on-surface installations.

Studies that investigated the thermal conversion of bitumen in the presence of oilsands minerals suggested that some of these minerals act as catalysts during the oil conversion, affecting reaction rates and influencing the composition of the resulting products [16]. Some of the minerals found in oilsands possess surface acidity. Clays, such as kaolinite, possess Brønsted-Lowry and Lewis acidity, whereas non-clays, such as rutile, possess mainly Lewis acidity. The acidity of these minerals could potentially influence reaction pathways, enabling, for instance, cationic conversion during the treatment.

While the individual effects of water and minerals during the thermal treatment of bitumen have been explored, only a few studies have concentrated on the potential results of thermally treating froth. Additionally, there is a limited body of research addressing the influence of water and minerals on the properties, reaction chemistry, and composition of the bitumen product. The role of water is still unclear. The effect of oilsands minerals on specific reactions with relevance to bitumen upgrading, such as cracking, hydrogen transfer, and addition reactions, is also little explored.

In the present thesis, the thermal treatment of bitumen froth at 400 °C was investigated, with emphasis on the impact of water and minerals on the physicochemical properties and composition of the resulting bitumen product, as well as their influence on the reaction rates and pathways during the conversion. It has been reported that visbreaking of bitumen can be effectively conducted at 400 °C, a temperature milder than those commonly employed in oil refining [17]. The froth used in this study was obtained from the Canadian oilsands mining industry. The specific reaction pathways impacted by water and minerals were investigated by thermally treating both froth and organic model compounds.

1.2 Objectives

The main objective of this work was to investigate the impact of water and oilsands minerals on the physicochemical changes on the bitumen phase during thermal conversion of bitumen froth at 400 °C, as well as their influence on the reaction chemistry taking place during the conversion. To achieve the main objective, the following sub-objectives were proposed:

(a) To investigate the role of water, minerals, and solvent dilution on the physicochemical changes in the bitumen phase during visbreaking of froth at 400 °C, with focus on identifying if the presence water, minerals, and solvent dilution could improve the quality of bitumen (**Chapter 3**);

(b) To evaluate the impact of water and minerals on cracking, hydrogen transfer, and addition reactions during thermal treatment of froth at 400 °C (**Chapter 4)**;

(c) To assess the role of water and typical oilsands minerals on the reaction rates and pathways during the thermal conversion of model systems at 400 °C (**Chapter 5**). Model systems were employed instead of bitumen froth with the objective of limiting the number of species involved during the conversion while at the same time capturing relevant information about the reaction chemistry.

1.3 Scope of work

Chapter 2 contains a literature review on the key topics used for concept development, experimental design, and the interpretation and discussion of the works presented in this thesis. The covered topics include factors that influence the physicochemical properties of bitumen, particularly focusing on density and viscosity and examining the effects of dilution on these properties. Additionally, the literature review explores the composition of bitumen froth, addressing challenges encountered in the separation of water and minerals. It also explores the technologies utilized for froth treatment, bitumen upgrading, and the influence of minerals and water during the thermal conversion of both bitumen and model compounds.

Chapter 3 investigated the impact of water, mineral solids, and solvent on the physicochemical changes in the bitumen phase during the thermal conversion of froth at 400 °C. The primary focus was on evaluating whether the presence of water, solids, and/or minerals during the treatment could improve the quality of bitumen by lowering its density and viscosity. A froth sample obtained from the Canadian oilsands mining industry was used in this study. Mineral solids and water were removed from the froth, whenever necessary, in order to decouple the effects of each of these components during the treatment. The effect of bitumen dilution with both a paraffinic and a naphthenic solvent (*n*-hexane and kerosene, respectively) during the thermal conversion was also evaluated in this study.

Chapter 4 evaluated the impact of water and minerals on reactions with relevance to bitumen upgrading, including cracking, hydrogen transfer, and addition reactions, during the thermal conversion of froth at 400 °C. Although the outcomes from **Chapter 3** indicated that the presence of water and minerals did not enhance the density and viscosity reduction of bitumen, there were indications that these components did influence the physicochemical changes during the treatment. In order to understand the influence of water and minerals on the reaction chemistry taking place during the thermal treatment of froth, **Chapter 4** focused on evaluating the individual and collective contributions of water and minerals to reactions with relevance to bitumen upgrading. This was performed by monitoring selected chemical species identified in the feed and thermally converted products. The possible free radical and cationic pathways for the conversion of chemical species were assessed by analyzing the product composition of various reaction systems. The same froth sample used in **Chapter 3** was employed in this study. α-Methylstyrene was added to the feed as a probe molecule.

Chapter 5 explored the effect of water and typical minerals found in oilsands, including kaolinite, rutile, and quartz, on the reaction rates and pathways during the thermal conversion of model systems at 400 °C. The outcomes from **Chapter 4** indicated that water and minerals had an impact on the conversion of α-methylstyrene and the selectivities to specific products during the thermal treatment of froth. However, the complexity of a reaction medium containing bitumen made it challenging to attribute the impact of water and minerals to specific reaction pathways. Therefore, simpler model systems (one containing α-methylstyrene, tetralin, and *n*-pentadecane, and another comprising α-methylstyrene alone) were employed in **Chapter 5** instead of bitumen froth. Additionally, there was an interest in determining whether the minerals were catalytically active during the conversion process. Previous studies had suggested that both water and minerals influence reaction rates during the thermal conversion of oil and organic model compounds.

1.4 References

(1) IEA *World Energy Outlook*, 2022, https://www.iea.org/reports/world-energy-outlook-2022 (accessed 2023/2/10).

(2) Bennett, B.; Jiang, C. Oil-source and oil-oil correlations and the origin of the heavy oil and bitumen accumulations in Northern Alberta, Canada. *Org. Geochem.* **2021**, *153*, 104199.

(3) De Klerk, A. Chapter 3 - Unconventional oil: Oilsands, In *Future Energy - Improved, Sustainable and Clean Options for our Planet*, ed. by Letcher, T. M., 3rd edition, Elsevier: 2020, pp 49–65.

(4) Gray, M. R., *Upgrading oilsands bitumen and heavy oil*; Pica Pica Press - Edmonton: 2015.

(5) AER *Alberta Energy Outlook*, 2023, https://www.aer.ca/providing-information/data-and-reports/statistical-reports/st98 (accessed 2024/1/9).

(6) Strausz, O. P.; Lown, E. M., *The Chemistry of Alberta Oil Sands, Bitumens and Heavy Oils*; Alberta Energy Research Institute: Calgary, 2003, p 695.

(7) Czarnecki, J.; Masliyah, J.; Xu, Z.; Dobras, M., *Handbook on Theory and Practice of Bitumen Recovery from Athabasca Oil Sands - Volume 2: Industrial Practice*; Kingsley Knowledge Publishing: 2013, p 717.

(8) Rao, F.; Liu, Q. Froth treatment in Athabasca oil sands bitumen recovery process: A review. *Energy Fuels* **2013**, *27* (12), 7199–7207.

(9) De Klerk, A. Processing unconventional oil: partial upgrading of oilsands bitumen. *Energy Fuels* **2021**, *35* (18), 14343–14360.

(10) Gray, M. R. Fundamentals of partial upgrading of bitumen. *Energy Fuels* **2019**, *33* (8), 6843–6856.

(11) Gu, G.; Zhang, L.; Xu, Z.; Masliyah, J. Novel bitumen froth cleaning device and rag layer characterization. *Energy Fuels* **2007**, *21* (6), 3462–3468.

(12) Chen, Q.; Stricek, I.; Cao, M.; Gray, M. R.; Liu, Q. Influence of hydrothermal treatment on filterability of fine solids in bitumen froth. *Fuel* **2016**, *180*, 314–323.

(13) Turuga, A. S. S.; de Klerk, A. Hydrothermal Treatment of Bitumen Froth: Impact of Mineral Solids and Water on Bitumen Properties. *Energy Fuels* **2021**, *35* (21), 17536–17550.

(14) Canıaz, R. O.; Arca, S.; Yaşar, M.; Erkey, C. Refinery bitumen and domestic unconventional heavy oil upgrading in supercritical water. *J. Supercrit. Fluids* **2019**, *152*, 104569.

(15) Dutta, R. P.; McCaffrey, W. C.; Gray, M. R.; Muehlenbachs, K. Thermal cracking of Athabasca bitumen: influence of steam on reaction chemistry. *Energy Fuels* **2000**, *14* (3), 671–676.

(16) He, M.; Wang, Z.; Moldowan, M. J.; Peters, K. Insights into catalytic effects of clay minerals on hydrocarbon composition of generated liquid products during oil cracking from laboratory pyrolysis experiments. *Org. Geochem.* **2022**, *163*, 104331.

(17) Wang, L.; Zachariah, A.; Yang, S.; Prasad, V.; De Klerk, A. Visbreaking oilsands-derived bitumen in the temperature range of 340-400 °C. *Energy Fuels* **2014**, *28* (8), 5014–5022.

Chapter 2

Literature Review

2.1 Introduction

The Canadian oilsands are the world's third-largest proven oil reserve, accounting for 97% of Canada's oil reserves [1]. In 2021, Canada's oilsands were responsible for 3.8% of the total world oil supply, which was double compared to 2010 [2]. Despite its impressive abundance, bitumen exploration and production from oilsands is challenging and costly due to its physicochemical properties. The high viscosity and density of bitumen, along with its high heteroatom and metal content, associated with substantial amounts of heavy components, have driven the development of technologies to make bitumen processing economical in both upstream and downstream applications.

The bituminous material is found impregnated in shallow sand and sandstone strata [3]. The required method for oilsands recovery depends on the depth of the deposit [4]. Surface mining and subsurface (or *in situ*) production are the two primary methods for recovering oilsands. When the deposits are too deep to be mined, subsurface recovery methods, such as steam-assisted gravity drainage (SAGD), are used. When the deposits are close enough to the surface, oilsands bitumen are recovered through mining. For example, the mineable oilsands of northern Alberta are deposits with approximately 30 m of depth, which is considered feasible for mining operations [5]. About half of the bitumen production in Alberta comes from mining operations [6]. This chapter focused on bitumen recovery through mining.

An overview of bitumen production process from mining is shown in **Figure 2.1**. The bitumen contained in the mined oilsands ores needs to be extracted from the bulk of the mineral matter. The oilsands ores are crushed and sieved, resulting in oilsands lumps of about 5 cm in diameter. These lumps are pumped through a conditioning pipeline with warm water (40–50 °C), in a process known as hot water extraction. The temperature of the warm water serves to decrease the viscosity of bitumen, allowing it to separate from the sand grains and bond with air bubbles in the flow. If the quantity of entrained air in the ores is insufficient, external air can be introduced into the pipeline. The product from the hot water extraction process is a conditioned oilsands-and-water slurry. In the separation unit, this conditioned slurry undergoes mixing and aeration in flotation cells, generating a froth containing bitumen, water, and minerals. Then, bitumen needs to be extracted from the froth, which is accomplished in the froth treatment process. In the froth treatment unit, the froth is combined with either a naphthenic (naphthenic froth treatment) or paraffinic (paraffinic froth treatment) solvent and passed through separation units, removing water and solids and yielding a "clean bitumen" product [5]. The recovery of solvent added during the froth treatment can take place either in the upgrader or as part of the froth treatment unit. In naphtha-based operations, froth treatment plants are colocated with the upgrader, and naphtha is recovered within the upgrader. In paraffin-based operations, diluted bitumen is fed to the solvent recovery unit, and complete solvent recovery is achieved only when a distinct diluent is employed for pipeline transportation [7]. At the upgrader, bitumen is converted into a higher-quality and higher-value synthetic crude oil that is ready to be refined.

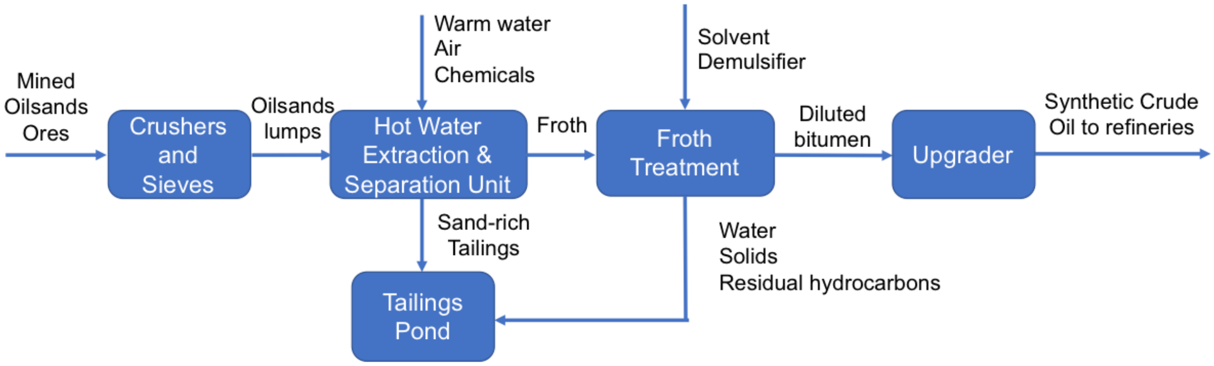

Figure 2.1: Overview of bitumen production process from mining operations.

The separation of bitumen from water and minerals in froth is challenging because: (i) bitumen and water have similar densities, making separation by gravity impractical [8]; (ii) the water-in-oil emulsions, formed during the hot water extraction, are stabilized by natural surfactants in bitumen and fine mineral particles [9]; (iii) the high density and viscosity of bitumen hinder the separation of fine mineral solids dispersed throughout the bitumen phase [9].

The aforementioned overview of bitumen production highlighted the key topics addressed in this chapter. Since bitumen dilution is critical during froth treatment and bitumen transportation, the effect of solvent addition to bitumen is emphasized in many topics of this chapter. First, the physicochemical properties of bitumen are presented, with a focus on the effect of dilution on these properties (**Section 2.2**). Then, the froth characteristics are introduced, along with the current applied technologies for the froth treatment and a review of recent studies aiming for process improvements (**Section 2.3**). Next, a review of bitumen upgrading is presented, with an emphasis on the chain reactions taking place during the treatment but also presenting the effects of performing bitumen upgrading in the presence of water and minerals (**Section 2.4**). All of these topics were relevant to laying the foundations for the experimental chapters presented in this thesis.

2.2 Physicochemical properties of bitumen and bitumen/solvent mixtures

2.2.1 Bitumen's composition

Before looking into the physicochemical characteristics of bitumen, it is crucial to understand the key components of bitumen's composition that contribute to its properties. Oilsands bitumen is classified as an unconventional oil source due to its low fluidity (density > 1000 kg/m^3 and viscosity $> 10^5$ mPa·s) at reservoir conditions, making conventional production and transportation unfeasible [4]. The challenges encountered as a result of bitumen's properties are a direct consequence of its composition.

Bitumen is a complex mixture of hydrocarbons and heteroatom-containing compounds with a similar chemical composition compared to typical crude oils but with different relative abundances of the chemical species. The main compound classes found in bitumen are paraffins (alkanes), naphthenes (cycloparaffins), aromatics, and heteroatom-containing compounds. A well-known characteristic of bitumen is its high amount of heavy material (little or no material boiling below 250 °C and around 50 vol% of vacuum residue) in its composition [5]. The substantial concentration of heavy substances in bitumen results in its categorization as an extra-heavy crude oil.

The hydrogen-to-carbon atomic ratio (H:C) is an important property of bitumen, as it serves as an indicator of both the degree of aromaticity and the propensity for coke formation during the upgrading process. A low H:C ratio is indicative of a high presence of aromatics in its composition and a great tendency for coke production. The H:C ratio of crude oils varies in the range of 1.4–1.9, with bitumen having a H:C ratio that tends to be situated at the lower end of this range. For instance, Athabasca bitumen has a H:C ratio of 1.53 [10]. The low H:C ratio of bitumen indicates that it has a higher aromatic content compared to many conventional oils and also suggests challenging bitumen processing during upgrading due to its expected higher tendency to form coke.

Bitumen is also recognized for its high heteroatom (S, O, and N) and metal content. The heteroatom content of bitumen varies in the range of 4.17–5.90 wt% of S, 0.88–1.61 wt% of O, and 0.34–0.51 wt% of N. The most abundant heteroatom in bitumen is sulfur, which is found mainly in the forms of thiols, thioethers, and thiophenes. When compared to conventional oils, bitumen has a higher metal content, including Ni, V, Fe, and Zn. Ni and V are mostly found in porphyrin complexes [10].

Table 2.1 contains some characterization properties of bitumen alongside a well-recognized benchmark crude oil, namely WTI (West Texas Intermediate). **Table 2.1** illustrates some of the significant differences between the properties of bitumen and those of conventional oils. The density of Athabasca bitumen is significantly higher in comparison to WTI and similar to the density of water. The viscosity of Athabasca bitumen is five orders of magnitude higher than that of WTI at 15.6 °C. In contrast to WTI, Athabasca bitumen has higher concentrations of sulfur, nitrogen, and metals.

The distillation characteristics of Athabasca bitumen and WTI are also presented in **Table 2.1**. Bitumen exhibits a high initial boiling point (260 °C) and a low amount of material collected at the atmospheric distillation unit (9 vol%). Conversely, WTI has a lower initial boiling point (60 °C) and around 70 vol% of material being collected at atmospheric pressure. Half of the volume of Athabasca bitumen is made of non-distillable material, whereas the non-distillable fraction of the WTI accounts for only 10 vol%.

A traditional characterization method used for the quantification of the relative amounts of chemical classes in bitumen is the SARA (saturates, aromatics, resins, and asphaltenes) solubility classification recommended by ASTM D-2007 [11]. When assessing the solubility classes of bitumen using the SARA classification, the results are typically in the range of 15–21 wt% of saturates, 18–19 wt% of aromatics, 44–46 wt% of resins, and 16–20 wt% of asphaltenes [10]. The high levels of resins and asphaltenes in bitumen are indicative of a substantial amount of complex, polar, large-sized molecules within its composition.

Table 2.1: Characterization properties of Athabasca bitumen and West Texas Intermediate (WTI) [4, 5, 12].

Property	Oil	
	Athabasca bitumen	WTI
Density at 15.6 °C (kg/m^3)	1007	820
Viscosity at 15.6 °C (Pa·s)	402	0.004
Sulfur Content (wt%)	4.8	0.34
Nitrogen Content (wt%)	0.4	0.08
Metals Content – V and Ni (wppm)	290–390	4
Distillation data		
Initial boiling point (°C)	260	60
Cumulative distilled at atmosphere (material collected up to 360 °C, vol%)	9	70
Non-distillable material (vol%)	50	10

The asphaltenes fraction is defined as a solubility class (i.e., components that are soluble in toluene and insoluble in *n*-alkanes) composed of aromatic polycyclic clusters variably substituted with alkyl groups and containing heteroatoms and metals in its structure [13]. The characteristics of the asphaltenes precipitated from the bitumen phase vary according to the nature and amount of the solvent used for their precipitation. The high asphaltenes content in bitumen is problematic not only from the perspective of bitumen's processing but also from the perspective of its transportation because the precipitation of asphaltenes can lead to the fouling of equipment and pipelines [14].

Another important and intriguing aspect of bitumen is that it naturally contains free radicals in its composition (commonly referred to as persistent free radicals), but these highly reactive species are surprisingly stabilized in the medium [15]. This is further discussed in **Section 2.4.2.1**.

2.2.2 Implications of bitumen's composition on transportation and processing

Transporting crude oils to the market is most efficiently and economically achieved through pipelines. The crude oil must meet some requirements in order to ensure proper flow rates, preserve product quality, and maintain the integrity of the pipeline [5, 16]. The Canadian pipeline specifications are shown in **Table 2.2**.

Table 2.2: Canadian pipeline specifications [17].

Property	Pipeline Specification
Viscosity	$<$ 350 cSt at the pipeline temperature[a]
Density	< 940 kg/m^3
Gravity	$>$ 19 °API
Bottom solids and water	$<$ 0.5 vol%
Olefin content	$<$ 1 wt%
Reid vapor pressure	$<$ 100 kPa

[a] Pipeline temperature varies in the range of 7.5–18.5 °C throughout the year.

Due to its poor fluidity at ambient conditions, straight-run bitumen is usually diluted with a light solvent (C_5–C_7) to meet pipeline specifications for density and viscosity. The addition of light paraffinic solvents to bitumen affects the stability of the oil phase, making it more susceptible to asphaltenes precipitation [18].

The quality of a solvent has an impact on asphaltenes aggregation. In this context, the terms good and poor solvents refer to the solvent's ability to dissolve or not dissolve asphaltenes. When a solvent is added to bitumen at a high dilution, the solubility parameter of the bulk liquid is changed to be near that of the solvent. In general, the increase in the difference between the solubility parameters of the asphaltenes and the bulk liquid promotes an increase in the attraction between the asphaltenes molecules. Poor solvents for heavy polar species, like the *n*-paraffins, change the solubility parameter of the bulk liquid in such a way that they facilitate the formation of asphaltenes aggregates [19]. The addition of a poor solvent increases the adhesion forces between the asphaltenes, increasing the aggregates' size. When a good solvent (e.g., toluene) is added to bitumen, the adhesion forces are weak and repulsion forces dominate, creating smaller asphaltenes aggregates [20, 21].

2.2.3 Bitumen's density: effect of composition, dilution, and temperature

2.2.3.1 Relation between bitumen's density and composition

The density of pure hydrocarbons typically increases as the hydrogen content decreases. Aromatic compounds, for example, are more hydrogen-depleted than paraffins with comparable carbon numbers and hence have a higher density [22]. Bitumen density is also strongly dependent on its hydrogen content; however, carbon and hydrogen content alone are insufficient to predict bitumen's density. Other elements, such as nitrogen, oxygen, and sulfur might also impact bitumen's density [5]. Metals, such as vanadium and nickel, are present at low concentrations, and their influence on bitumen's density is expected to be minor.

A correlation between the density of Alberta heavy oils and bitumen and its bulk elemental composition is shown in **Eq. 2.1**, where ρ is the density of the oil in kg/m^3, H is the hydrogen content in wt$\%$, S is the sulfur content in wt$\%$, and N is the nitrogen content in wt$\%$. This correlation was established by combining data from several sources of hydrocarbons, including residues from Alberta crudes (such as Athabasca, Cold Lake, and Peace River), hydroconversion products, deasphalted residual oils, and hydrotreated gas oils. Each component in **Eq. 2.1** (i.e., H, S, and N) was found to make a significant contribution to the density prediction [23].

$$\rho = 1033 - 13.69H + 13.85S + 115.7N \tag{2.1}$$

In order to meet the density requirement for pipeline transportation (see **Table 2.2**), bitumen needs to be diluted with a light solvent. A brief review of the mixing rules used to predict the density of diluted bitumen is presented next.

2.2.3.2 Density prediction of bitumen/solvent mixtures

The dilution of bitumen with a light hydrocarbon contributes to a decrease in the average molecular weight of the mixture containing bitumen, thereby causing a decrease in the density of the resulting mixture. Density prediction of bitumen/solvent mixtures is essential in applications where density measurements are not practical.

The volumes of hydrocarbons in a mixture are not necessarily additive, resulting in a non-zero excess volume of mixing. Nevertheless, the excess volumes observed in liquid hydrocarbon mixtures are relatively small [24]. Two primary methods are used to predict the density of hydrocarbon mixtures, namely equations of state (EoS) and mixing rules [25]. Detailed information on each of these methods is presented as follows.

(a) Equations of state (EoS)

The equations of state are widely employed to model the phase behavior and volumetric properties of petroleum fluids. These equations rely on the critical properties of each pure component in the mixture combined with mixing rules. A common example found in the literature is the Peng-Robinson cubic equation of state (PRCEOS). Nonetheless, it is necessary to estimate the critical properties of bitumen and heavy oils, as they cannot be measured directly due to thermal conversion occurring below their critical temperatures [26]. Therefore, the use of an EoS to predict the density of bitumen/solvent mixtures is dependent on another estimated value, namely the critical properties of bitumen.

The application of EoS to predict bitumen and bitumen/solvent mixtures shows high deviations in density prediction at high pressures and close to the critical point. In order to get more accurate predictions, the EoS model needs to be modified or tuned to fit experimental density data for the mixtures of interest [24]. EoS are a better method for predicting the density of mixtures of bitumen and dissolved gases (e.g., bitumen/CO_2 mixture), but the mixing rules method is a simpler method to be applied when bitumen is diluted with liquid solvents [25].

(b) Mixing rules

The use of mixing rules is a more practical approach for predicting the density of bitumen/solvent mixtures (ρ_m). It depends on knowledge of the densities of each component as well as data on the volumetric changes upon mixing. Regular (or ideal) solutions have additive volumes, and the mixing rule for this case is based only on the density (ρ) and the weight fraction (w) of bitumen (subscript B) and solvent (subscript S), as indicated in **Eq. 2.2**.

$$\rho_m = \frac{1}{\dfrac{w_s}{\rho_s} + \dfrac{1 - w_s}{\rho_B}} \tag{2.2}$$

Normally, the addition of light hydrocarbons to bitumen forms nearly regular solutions, and the regular mixture model can be applied to give estimated density values with an average absolute relative deviation (AARD) of about 2% [24]. However, any application that requires more accurate predictions could make use of the excess volume model. In this approach, the deviations from the ideal mixture assumption are measured in terms of excess volumes. A positive excess volume indicates volume increase upon mixing, whereas a negative excess volume indicates volume shrinkage upon mixing [25]. The value of the excess volume term depends on the size and interaction forces among each component in the mixture, and consequently, it varies with the bitumen composition and type of solvent used for bitumen dilution [25].

In the excess volume mixing rule, the regular solution equation (**Eq. 2.2**) is modified in order to account for volume changes upon mixing by the introduction of a binary interaction parameter (β_{ij}), as shown in **Eq. 2.3**. The value of β_{ij} is determined through regression analysis of experimental density data collected for various mixture compositions [25].

$$\frac{1}{\rho_m} = \frac{w_s}{\rho_s} + \frac{1 - w_s}{\rho_B} - w_s\,(1 - w_s)\left[\frac{1}{\rho_s} + \frac{1}{\rho_B}\right]\beta_{ij} \tag{2.3}$$

The density of mixtures of bitumen and aromatic solvents, such as toluene and xylene, can be accurately described by the use of the ideal mixture model (**Eq. 2.2**) in a wide range of solvent concentrations [27, 28]. On the other hand, the dilution of bitumen with paraffinic solvents results in a volume shrinkage upon mixing, and correlations that introduce correction factors for the mixture volume would better predict the mixture density. Practical examples of density prediction for bitumen/solvent mixtures are presented in the following subsection [29, 30].

2.2.3.3 Impact of dilution on the density of bitumen/solvent mixtures

Density is not as sensitive to dilution as viscosity (discussed in **Section 2.2.3**). In this section, practical examples from the literature on the density prediction of bitumen/solvent mixtures are presented, as well as the impact of solvent concentration on the ideality or non-ideality of the mixtures. The thermal dependence of the density of bitumen/solvent mixtures is addressed in **Section 2.2.3.4**.

Nourozieh et al.[29–31] studied the density behavior of bitumen/*n*-alkane mixtures in the range from C_5 to C_7. **Figure 2.2** shows the densities of non-diluted bitumen and mixtures of bitumen/*n*-pentane (C_5) and bitumen/*n*-heptane (C_7) at different concentrations and temperatures. The highest reductions in density, when comparing non-diluted bitumen and bitumen/solvent mixtures with the same solvent concentrations, were observed in the presence of *n*-pentane. This is attributed to the lower density of *n*-pentane in comparison to *n*-heptane (i.e., the densities of *n*-pentane and *n*-heptane at 25 °C and 1 atm are 621 and 679 kg/m^3, respectively).

Some models for predicting the density of bitumen mixtures with C_5 to C_7 were examined in the studies developed by Nourozieh et al.[29–31]. The mixtures deviated from the ideal mixture behavior at solvent concentrations greater than 20 wt%. In these cases, the mixture densities were better predicted using the excess volume mixing rule (average absolute relative deviation, AARD, of 1% compared to 1.7% using the ideal mixture assumption). The mixtures presented a shrinkage upon mixing, and the higher the solvent concentration, the higher the deviation from the ideal mixture assumption.

Excess volume tends to be negative when bitumen is diluted with light paraffins (e.g., C_5 and C_7) but positive when bitumen is diluted with toluene. Nevertheless, as mentioned earlier, the positive excess volume for aromatic compounds, such as toluene, is typically minimal (i.e., bitumen/toluene presented an excess volume of about +0.0009 cm^3/g compared to -0.0118 cm^3/g in bitumen/pentane), and the ideal mixture model (**Eq. 2.2**) accurately predicts the density of bitumen and aromatic compound mixtures [25].

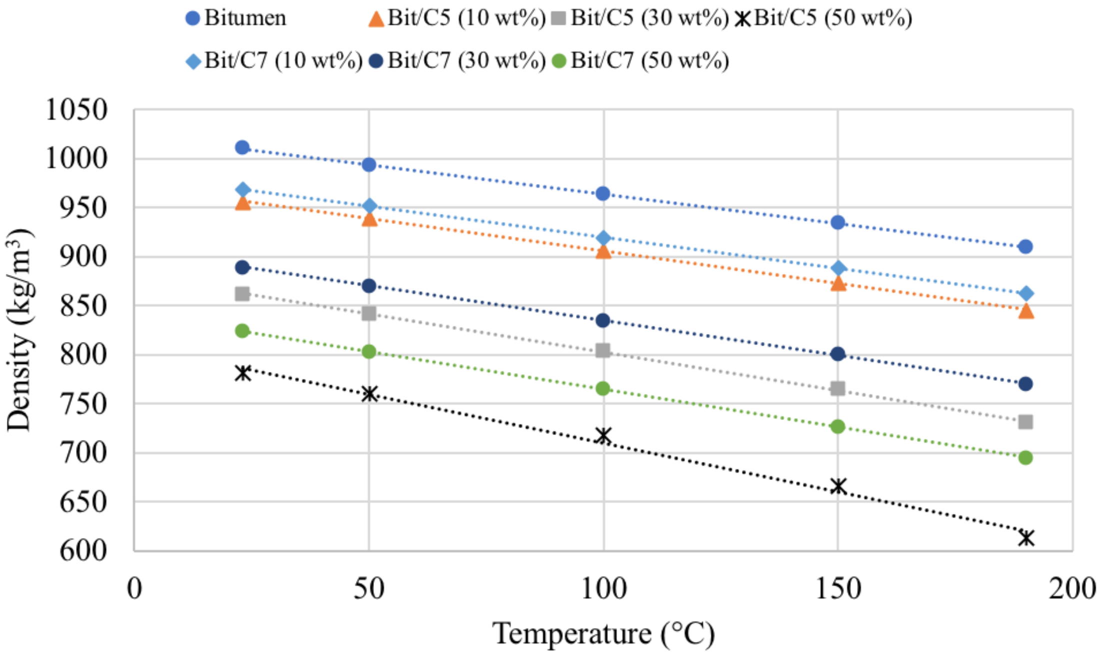

Figure 2.2: Density of bitumen/C_5 and bitumen/C_7 mixtures at various concentrations and temperatures. Density measurements were performed at 4 MPa, and the mixture concentrations are given in wt% of solvent [29, 31].

Sanchez-Lemus et al.[25] studied the density modeling of mixtures of deasphalted oil (DAO) with commercial naphtha and natural gas condensate. Both solvents presented a positive excess volume upon mixing, and the use of the excess volume model yielded better predictions than the regular mixing model (AARD of 0.4% compared to 0.6–1%).

2.2.3.4 Thermal dependence of density in bitumen/solvent mixtures

The linear relationship between the density of bitumen and bitumen/solvent mixtures and temperature is expressed in **Eq. 2.4**, where d_2 represents the density (in kg/m^3) at temperature T_2 (in °C), d_1 is the density at temperature T_1, and α denotes the slope. The temperature dependence of Athabasca bitumen was found to be well described by a slope (α) value of 0.62 [10].

$$d_2 = d_1 + \alpha (T_1 - T_2) \tag{2.4}$$

The impact of temperature on the density of bitumen and bitumen/solvent mixtures is also shown in **Figure 2.2**. The slopes and coefficients of determination of the trendlines shown in **Figure 2.2** are listed in **Table 2.3**. The densities of most of the mixtures of of bitumen/C_5 and bitumen/C_7 decreased linearly with temperature (i.e., most of the bitumen/solvent mixtures presented a R^2 higher than 0.999; refer to **Table 2.3**). However, a clear deviation from linearity was observed for the bitumen/C_5 mixture at a concentration of 50 wt%, which trendline presented a R^2 of 0.9912. The nature of that deviation was not discussed by the authors but could be related to any factor affecting the density measurements, such as phase separation due to solvent volatilization or precipitation of C_5-insolubles.

Table 2.3: Slopes and coefficients of determination of the linear regressions of density vs. temperature of bitumen, bitumen/pentane, and bitumen/heptane. The trendlines are shown in **Figure 2.2**.

Components[a]	Linear relation between density and temperature	
	Slope	R^2
Bitumen	-0.601	1
Bit/C_5 (10 wt%)	-0.660	0.9998
Bit/C_5 (30 wt%)	-0.783	0.9992
Bit/C_5 (50 wt%)	-0.996	0.9912
Bit/C_7 (10 wt%)	-0.634	1
Bit/C_7 (30 wt%)	-0.711	0.9998
Bit/C_7 (50 wt%)	-0.770	0.9997

[a] Solvent concentration in parenthesis

The slopes of the linear relationship between density and temperature can potentially indicate variations in the composition of the medium. In the studies by Nourozieh et al.[29, 31], the slopes of density vs. temperature (given in **Table 2.3**) exhibited an increase with higher solvent concentrations, likely reflecting alterations in the medium's composition following the addition of the solvent. The authors noticed that at a fixed solvent concentration, the higher the temperature, the higher the volume change upon mixing, and, consequently, a high deviation from the regular solution behavior was observed. In fact, when the temperature approaches the critical temperature of the solvent, large negative deviations from the ideal behavior are expected [32].

Nourozieh et al.[29–31] also tested the accuracy of a prediction method for the bitumen/solvent density, which relies on known density data of the raw bitumen at a given temperature and pressure, and calculated density of the pure *n*-alkane solvent using effective liquid density correlations. The authors used the ideal mixture model (**Eq. 2.2**) to combine the known density of bitumen at a given temperature and pressure with the density of the pure *n*-alkane calculated using the effective liquid density equations given in **Table 2.4**. The effective liquid density is a function of temperature and pressure. The authors claimed that this method gave the best prediction results as compared to the other prediction methods in their studies (AARD in the range of 0.31% to 0.63%). However, the authors did not address how the results obtained using the effective liquid density differed from the measured density values for the bitumen/C_5 mixture at 50 wt%, where a noticeable deviation from the linearity of density vs. temperature was observed (see **Figure 2.2**).

Table 2.4: Effective liquid density equations for *n*-alkanes from C_5 to C_7. ρ in kg/m^3, T in K, and P in MPa [29–31].

Solvent	Effective liquid density equation for pure *n*-alkanes
n-Pentane	$\rho = 878.006 - 0.82817T + (- 0.0923 + 2.6481 \times 10^{-3}) T) P$
n-Hexane	$\rho = 901.512 - 0.80985T + (- 0.142 + 2.6846 \times 10^{-3} T) P$
n-Heptane	$\rho = 918.603 - 0.79155T + (- 0.177 + 2.6919 \times 10^{-3} T) P$

2.2.4 Bitumen's viscosity: effect of composition, dilution, and temperature

Bitumen is a complex mixture, and, as expected, it presents a complex rheological behavior. Not all factors governing bitumen's viscosity are known. However, there is evidence in the literature that bitumen's viscosity is influenced by its chemical composition and asphaltenes content [33, 34].

2.2.4.1 Relation between bitumen's viscosity and composition

The molecular weight of the species within a fluid, along with the intermolecular interactions between these species, have a significant influence on the fluid's viscosity. The higher the density and molecular weight of a petroleum fraction, the higher its viscosity [5, 35]. Bitumen has larger molecular weight components than conventional oils, which contributes to its higher viscosity (ranging from 10^4 to 10^6 mPa·s at 25 °C) [5].

The high viscosity of bitumen is also attributed to its high asphaltenes content. As noted in **Section 2.2.1**, asphaltenes are characterized as a solubility class, encompassing species that are insoluble in n-alkanes but soluble in toluene. The molecular weight of asphaltenes is relatively high, and their structure consists of polycyclic species containing multiple branches. These characteristics, along with the presence of structural sites that allow for the formation of both weak and strong intermolecular forces such as London forces and hydrogen bonds, contribute to an increase in resistance to flow and, consequently, result in a high viscosity [13, 36, 37].

Previous research has shown that asphaltenes content and inter-particle interactions have a significant impact on bitumen viscosity [33, 34]. Asphaltenes molecules connect to one another via $\pi - \pi$ stacking due to the large number of polycondensed aromatic rings in their structures. Furthermore, the presence of polar groups and metal complexes increases the surface activity of asphaltenes, favoring their aggregation.

The effect of asphaltenes concentration on the viscosity of reconstituted heavy oils was studied by Luo and Gu [34], who discovered that as the volume fraction of n-pentane asphaltenes increased above 12.2%, the relative viscosity increased faster. The authors concluded that as asphaltenes molecules get closer to each other, they become entangled due to stronger inter-particle interactions, resulting in increased viscosity.

The asphaltenes are found in bitumen in the form of aggregates. When the aggregates are solvated, some molecules of the continuous-phase fluid might be trapped in the solvated aggregates. The aggregates concentration can be quantified by the calculation of an effective volume fraction (Φ_{eff}) which takes into account both the asphaltenes aggregates and the trapped molecules in the solvated aggregates [33, 38].

The viscosity of bitumen (μ_b) is a function of the effective volume fraction of the aggregates and can be related to the viscosity of the maltenes fraction (μ_m) by the use of the Roscoe-Brinkman model (**Eq. 2.5**) [33, 39, 40]. This model is based on Einstein's viscosity equation, which specifically applies to highly diluted suspensions of hard spheres and neglects particle-particle interactions. In contrast, the Roscoe-Brinkman model considers the hydrodynamic interactions between particles, providing accurate predictions for the relative viscosity of hard sphere suspensions at low to moderate concentrations of the dispersed phase [41]. According to **Eq. 2.5**, the viscosity of bitumen rises with an increase in the effective volume of asphaltenes, which accounts for both asphaltenes aggregates and the species trapped from the continuous phase within these aggregates. The Roscoe-Brinkman model tends to underestimate viscosity when the volume fraction of the dispersed phase is high [33, 42].

$$\frac{\mu_b}{\mu_m} = (1 - \Phi_{eff})^{-2.5} \tag{2.5}$$

2.2.4.2 Impact of dilution on the viscosity of bitumen/solvent mixtures

The addition of even a small amount of a solvent to bitumen has a significant impact on the mixture's viscosity. The dilution of bitumen with common *n*-paraffins is illustrated in **Figure 2.3**. For example, at a solvent/bitumen ratio of 10 wt$\%$, the viscosity drastically decreased by 1–2 orders of magnitude. The general observation is that the mixture's viscosity follows an exponential decrease with the increase in the solvent-to-bitumen ratio, suggesting that bitumen dilution could be modeled by a relation of the type $log\mu \times w_s$, where μ is the dynamic viscosity of the mixture and w_s is the bitumen-to-solvent mass ratio.

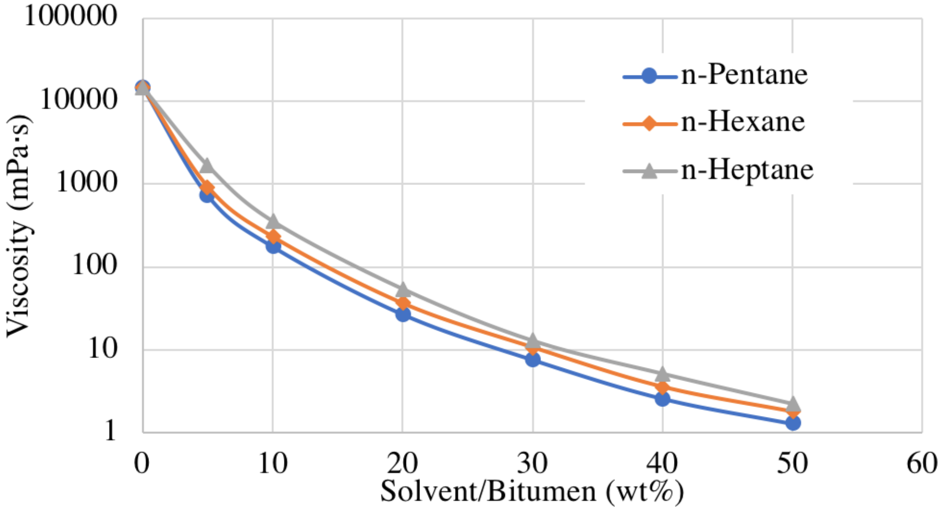

Figure 2.3: Viscosity of bitumen/*n*-alkanes (C_5-C_7) mixtures at 50 °C and 2 MPa [31, 43, 44].

As the *n*-alkanes used for bitumen dilution shown in **Figure 2.3** have similar chemical natures and similar viscosities, the decrease in bitumen viscosity when adding C_5 to C_7 followed a similar trend. The slight difference in the diluted bitumen viscosity values when the three solvents are compared is due to small differences in the dynamic viscosities of the pure compounds (i.e., $\mu_{C_5} < \mu_{C_6} < \mu_{C_7}$).

Employing mixing rules to predict the viscosity of bitumen/solvent mixtures is essential for improvements to processes that involve bitumen dilution [45]. **Table 2.5** provides examples of common mixing rules used for predicting the viscosity of bitumen/solvent blends. The simplest types of mixing rules are those that require only the dynamic viscosities of the individual components and the composition of the mixture, such as the Arrhenius (**Eq. 2.6**) and Centeno et al. (**Eq. 2.7**) models. The Chirinos et al. model (**Eq. 2.8**) requires not only the dynamic viscosities but also the densities of the individual components. The power law model (**Eq. 2.9**) requires the calculation of the parameter “z” (flow behavior index) by regression analysis. The value of “z” depends on the type of compositional parameter chosen for the correlation and how the fluid molecules reorganize their structure due to flow (i.e., Newtonian or non-Newtonian behavior) [46].

A comprehensive study on the viscosity behavior of bitumen/*n*-alkane mixtures (C_5 to C_8) in a wide range of concentrations was conducted by Nourozieh et al. [31, 43, 44] and Ghao et. al. [47]. Viscosity predictions for bitumen dilution using low-chain paraffins in the temperature range from 25 to 190 °C were best represented by the power law model (**Eq. 2.9**) once an appropriate value of ’z’ was found by regression. The best predictions were obtained for bitumen dilution with *n*-pentane, *n*-hexane, and *n*-heptane (with AARD in the range of 7–14%) while a higher deviation from measured to predicted values was obtained for *n*-octane (AARD of 34%).

Wallace et al.[48] studied the viscosity of different types of bitumen diluted with naphtha and concluded that the viscosity of the mixtures could be modeled by the Cragoe equation (**Eq. 2.13**). The predicted viscosities were, in general, within 20% of the measured values. A model with better predictions when using naphtha as a diluent was developed in the study done by Miadonye et al.[49]. In their study, the authors tested their model using mixtures of bitumen and some hydrocarbon solvents (condensate, naphtha, toluene, and diesel) in concentrations up to 80 wt% of solvent. Miadonye et al.’s model (**Eq. 2.10-2.12**) was able to predict the mixtures’ viscosities with a lower overall average absolute deviation (AAD of 13.5%) than Cragoe’s equation (22.6%) and Chirinos et al.’s model (16.9%).

Table 2.5: Examples of mixing rules used to predict the viscosity of bitumen/solvent mixtures.

Author	Mixing Rule^a	
Arrhenius	$log\mu_m \, x_s \, log\mu_s + x_B \, log\mu_B$	(2.6)
Centeno et al.[50]	$log\,(log\,(\mu_m + 1)) = \sum w_i \, log\,[log\,(\mu_i + 1)]$	(2.7)
Chirinos et al.[49]	$log\,(log\,(v_m + 0.7)) = \sum w_i \, log\,[log\,(v_i + 0.7)]$	(2.8)
Power Law[29]	$\mu_m = [x_s \, \mu_s^z + (1 - x_s \,) \, \mu_B^z]^{\frac{1}{z}}$	(2.9)
Miadonye et al.[49]	$v_m = exp\,(exp\,(a\,(1 - w_S^n)) + ln\,(v_S) - 1)$	(2.10)
	$a = ln\,(ln\,(v_B) - ln\,(v_S) + 1)$	(2.11)
	$n = \frac{v_S}{0.9029\, v_S + 0.1351}$	(2.12)
Cragoe [51]	$\frac{1}{ln\,(2000\mu_m)} = \frac{w_s}{ln\,(2000\mu_m)} + \frac{w_b}{ln\,(2000\mu_b)}$	(2.13)
Chevron [52]	$VBI_i = \frac{logv_i}{3 + logv_i}$	(2.14)
	$VBI_\beta = \sum x_i VBI_i$	(2.15)
	$\mu = 10^{\frac{aVBI_\beta}{1-VBI_\beta}}$	(2.16)

[a] List of symbols: μ_m, dynamic viscosity of mixture (mPa·s); μ_s, dynamic viscosity of solvent (mPa·s); μ_B, dynamic viscosity of bitumen (mPa·s); μ_i, dynamic viscosity of component i (mPa·s); x_s, volume fraction of solvent; x_B, volume fraction of bitumen; w_s, mass fraction of solvent; w_B, mass fraction of bitumen; w_i, mass fraction of component i; v_m, kinematic viscosity of mixture (cSt); v_s, kinematic viscosity of solvent (cSt); v_B, kinematic viscosity of bitumen (cSt); v_i, kinematic viscosity of component i (cSt); z, flow behavior index; VBI_i, viscosity blending index of component i; VBI_β, viscosity blending index of mixture.

Miadonye et al.'s model has also been reported to be one of the top-performing mixing rules for predicting bitumen mixtures with diverse hydrocarbon solvents, including paraffins, naphthenes, and aromatics. It predicted mixture viscosities with AARD values of approximately 30% [28]. The straightforward requirements of Miadonye et al.'s model, involving only the viscosity, density, and mass fraction of both bitumen and solvent, made it a suitable choice for use in the current thesis. The model was employed to estimate the unknown viscosity of pure bitumen based on solvent and diluted bitumen data, whenever necessary.

2.2.4.3 Thermal dependence of viscosity in bitumen/solvent mixtures

The viscosity of bitumen and light hydrocarbon solvents has a logarithmic dependence on temperature, and correlations of the type ln$\mu \times T$ are commonly reported in the literature [53]. The general form of the MacCoull equation (**Eq. 2.17**), similar to that suggested in ASTM D341 [54], can be used to examine the linear relationship between the viscosity and temperature of bitumen or bitumen-solvent mixtures. In **Eq. 2.17**, μ is the viscosity of bitumen (mPa·s), a and b are the slope and intercept of the linear regression, respectively, and T is the temperature (K).

$$ln\ (ln\,(\mu))\ =\ a\ \cdot\ ln\,(T)\ +\ b \tag{2.17}$$

The viscosity of bitumen and bitumen/*n*-pentane mixtures as a function of temperature is illustrated in **Table 2.6**. The more diluted the bitumen the less the effect of temperature on the mixture's viscosity. For a variation in temperature from 27 to 103 °C, the viscosity decreased 60 times compared to 8 times when the dilution went from 0.1:1 to 0.3:1 wt/wt. Additionally, at higher temperatures, the effect of dilution on bitumen's viscosity is lowered [43, 55]. These observations are in agreement with the fact that the viscosity vs. temperature relationship of bitumen-solvent mixtures over the total mixture range is the same as that for the viscosity vs. temperature of bitumen or solvent on its own.

The regression data, presenting the linear correlation between viscosity and temperature based on **Eq. 2.17**, is also given in **Table 2.6** [43]. The coefficient of determination was higher than 0.996 for both pure bitumen and the *n*-pentane/bitumen mixture (0.1:1 wt/wt). The slope in **Eq. 2.17** has the potential to be employed as an indicator for tracking changes in the composition of a medium. A slight increase in the slope observed when comparing pure bitumen with the *n*-pentane/bitumen mixture (0.1:1 wt/wt) – from -3.83 to -4.10 – may suggest a change in composition due to dilution. The viscosity vs. temperature data for the *n*-pentane/bitumen mixture (0.3:1 wt/wt) showed non-linearity, indicated by an R^2 value of 0.8830 (refer to **Table 2.6**). This deviation from linearity could be attributed to many possible effects, such as inconsistencies in the dataset, the occurrence of phase separation with varying temperatures, and reactive changes at elevated temperature measurements.

Table 2.6: Dependence of bitumen and diluted bitumen viscosity on temperature. Viscosity was measured at 4 MPa [43].

Viscosity (mPa·s)	Mixture		
	bitumen	*n*-pentane/bitumen (0.1:1 wt/wt)	*n*-pentane/bitumen (0.3:1 wt/wt)
27 °C	-	1384	17.1
53 °C	15900	187	7.77
103 °C	234	22.9	2.26
152 °C	33.5	6.21	1.06
190 °C	12.2	3.29	0.68
Slope	-3.83	-4.10	-10.75
R^2	0.9995	0.9964	0.8830

Bazyleva et al.[56] studied the dependence of Athabasca bitumen's viscosity on temperature in the range of -43 to 137 °C. One important finding in this study was the irreversibility of bitumen's viscosity upon heating and cooling (i.e., the viscosity measurements yielded different values at the same temperature reading when comparing the heating and cooling experiments) in the higher temperature range (67–137 °C). The measured viscosity values were higher in the cooling cycle subsequent to the heating cycle. The authors suggested that the observed irreversibility was possibly due to changes in the physicochemical properties of the asphaltenes during the heating and cooling processes. Also, asphaltenes are very reactive species, and evidence of conversion taking place in the low-temperature range (100–150 °C) has been reported before [57]. When measuring the viscosity of bitumen at elevated temperatures, it is important to account for the possibility that changes due to reactions could lead to irreversible alterations in the original bitumen's viscosity.

Comprehending the factors that influence bitumen's density and viscosity, as well as the effect of bitumen dilution using paraffinic and naphthenic solvents, provides a fundamental basis for understanding the steps required for the froth treatment that are presented in the next section.

2.3 Froth treatment

During the early stages of the oilsands mining process, bitumen needs to be extracted from the mineral matter. The extraction process is accomplished via the Clark hot water extraction. During this process, the crushed oilsands ores undergo conditioning with hot water (50–80 °C) and a minor amount of NaOH through a hydrotransport pipeline. Subsequently, aeration is applied to the slurry, leading to the separation of bitumen from the sand as it attaches to the air bubbles forming the froth. A gravity separator is then used to recover the bitumen-rich froth. This froth comprises not only bitumen but also free water, emulsified water, and suspended mineral solids [5, 9].

The separation of water and solids is achieved through the froth treatment. Water and mineral solids must be removed from the bitumen phase because they are deleterious to downstream operations. Solids clog and poison catalysts in upgrading and refining processes, whereas water contains dissolved salts (primarily sodium chloride), which can cause major corrosion issues in equipment and pipelines [9]. The separation of water and solids from bitumen is challenging for many reasons, including the high viscosity of bitumen, the slight density difference between bitumen and water, and the presence of water-in-oil emulsions in the froth, which are stabilized by natural surfactants in bitumen (e.g., asphaltenes and resins) and the fine solids [5, 9].

In this section, the composition of froth is reviewed, along with the current froth treatment approaches. Lastly, a review of the studies developed to improve the froth treatment process is presented.

2.3.1 Froth composition

The froth that originates from the hot water extraction has a composition that varies in the range of 45–65 wt% bitumen, 20–35 wt% water, and 5–15 wt% mineral solids [7]. The mineral solids and water content of bitumen froth are dependent on the process conditions employed during the hot water extraction, such as extraction shear rates, extraction temperature, and NaOH concentration [58].

The minerals found in froth are classified as clays and non-clays. Clay minerals (such as kaolinite and illite) are the major components in froth solids (40–60 wt% of the total solids), while the remaining portion is constituted by non-clay minerals such as quartz, rutile, and siderite [59–61]. The crystalline structures of some of the main minerals present in froth are shown in **Figure 2.4**.

Clay minerals are alumino-silicates, and the majority of them are composed of layers of tetrahedral silica and octahedral alumina sheets [62]. Due to their structure, clays possess both adsorptive and catalytic properties. For instance, kaolinite (**Figure 2.4a**) consists of a 1:1 layered phyllosilicate with the formula $Al_2Si_2O_5(OH)_4$, formed by many stacked layers of one silicon-based (siloxane) tetrahedral sheet bound to one aluminum-based (aluminol) octahedral sheet through hydrogen bonding and dipolar interactions. Kaolinite shows strong adsorption properties because the siloxane surfaces carry an overall negative charge while the aluminol surfaces carry an overall positive charge [63, 64].

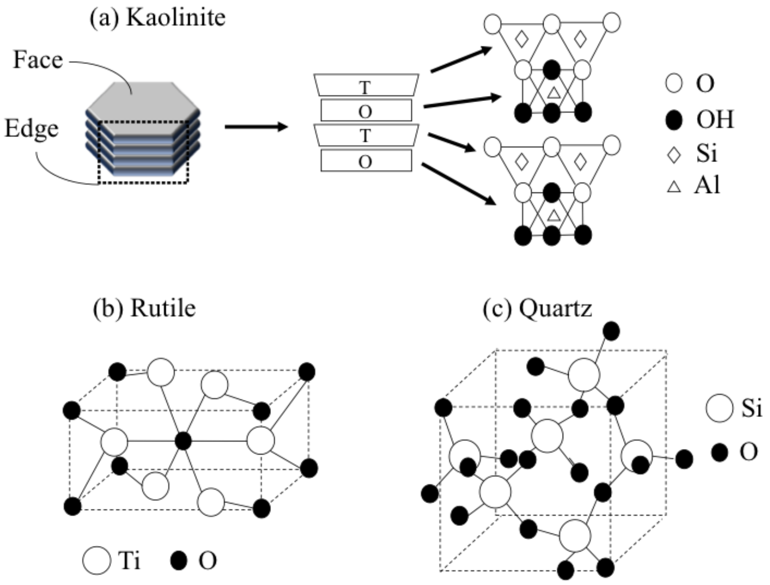

Figure 2.4: Crystalline structures of (a) Kaolinite[64], (b) Rutile[65], and (c) Quartz[66].

There are two types of acid sites on the clay's surface: Brønsted-Lowry acid sites (proton donors) and Lewis acid sites (electron pair acceptors). The hydrated and dehydrated cations in the interlayer spaces are the sources of Brønsted-Lowry and Lewis acidity [67]. As kaolinite does not present interlayer cations, its Lewis acidity arises from the coordinately unsaturated Al^{3+} ions at the edges of its external surface [67, 68], while Brønsted-Lowry acidity is developed from hydroxyl groups located between aluminum and silicon-occupied oxygen tetrahedra [69]. In kaolinite, the hydroxyl groups (-OH) are bonded to the aluminum atoms (Al) in the alumina octahedral layer. The electronegativity difference between oxygen and hydrogen is such that the oxygen atom tends to pull the shared electrons closer to itself, creating a partial positive charge on the hydrogen atom, making it susceptible to dissociation. The acidity of clays has an impact on bitumen recovery during hot water extraction. For instance, the acidity of illite clay contributed to a decrease in the bitumen flotation recovery at 25 and 35 °C [70].

The non-clay minerals found in the oilsands can be classified into different classes, including oxides (e.g., hematite, rutile, and anatase), sulfides (e.g., pyrite, bornite, and sphalerite), carbonates (e.g., siderite, calcite, dolomite, and magnesite), and silicates (e.g., quartz, garnet, and zircon) [10]. Non-clays found in froth also present acidic properties. For example, rutile (**Figure 2.4b**) presents strong Lewis acid sites while presenting very low Brønsted-Lowry acidity in its structure [71, 72].

The particle size distribution of the mineral solids in the froth was measured by Kaminsky et al.[59] The analysis revealed that almost 50% of the solid particles in the froth sample used in that study were classified as fine solids (diameter < 44 μm). Furthermore, it was observed that within this subset of fine solids, 18% consisted of extremely small particles (diameter < 2 μm). In a separate investigation conducted by Chen et al.[61], it was shown that almost 85% of the solid particles had chord lengths below 10 μm. The aforementioned studies have demonstrated that the fine solids account for a significant portion of the froth solids. The presence of these fines contributes to the challenges encountered in the separation process during froth treatment since they are known to stabilize water-in-oil emulsions.

The water composition from froth contains the major cations and anions found in the connate and process water from the oilsands extraction, such as sodium, potassium, calcium, magnesium, chloride, sulfate, phosphate, nitrite, and nitrate. Turuga and de Klerk [73] reported the composition of the water separated from the froth sample used in their study. The major ions found in the aqueous phase were sodium and chloride (concentrations of 722 μg/g and 812 mg/L, respectively). The amounts of calcium (Ca), magnesium (Mg), and iron (Fe) ranged from 5 to 10 ppm, while the remaining cations (Al, K, Ni, Ti, and V) exhibited quantities below 1 ppm. The concentration of sulfates, phosphates, nitrites, and nitrates among the anions exceeded 50 ppm. The pH of the water was approximately 8.3, indicating mild alkalinity.

Another important characteristic to take into consideration when analyzing the main characteristics of froth is the interaction between solids and water, measured by the solids' wettability (i.e., the ability of a solid surface to maintain contact with a liquid). Because solid particles have a strong inclination to remain at the water-oil interface, they modify the characteristics of the interface of emulsion droplets and create a barrier to the coalescence of droplets through steric hindrance [74, 75]. Typically, solids that exhibit a water-wet nature have a tendency to stabilize oil-in-water emulsions, while oil-wet solids tend to stabilize water-in-oil emulsions. Because the surface of the fine solids in froth is coated with organic components from bitumen, they are biwettable. Both water-in-oil and oil-in-water emulsions can be stabilized by these biwettable fine solids. Moreover, the particles adsorbed at the interface of oil and free water create a "rag" layer with asphaltenes. The "rag" layer is a middle phase located between the top organic phase and the bottom aqueous phase, which can build up with time and become a thick and viscous layer that can inhibit the separation of water droplets and solid particles [75, 76].

2.3.2 Froth treatment technologies

In the previous sections, it was highlighted the main challenges to separating water and solids from the bitumen froth, which is accomplished in the froth treatment unit. The two main froth treatment approaches are paraffinic froth treatment (PFT) and naphthenic froth treatment (NFT). Both technologies rely on froth dilution with light hydrocarbons. Naphtha is used as a diluent in the NFT to reduce bitumen's viscosity and density and allow for the separation of water and solids. A paraffinic solvent (typically C_5 and C_6) is utilized in the PFT for the same aim of bitumen's viscosity and density reduction; however, asphaltenes precipitation also takes place during the PFT, yielding a cleaner bitumen product [5]. Asphaltenes precipitation plays a critical role in enhancing separation efficiency in the PFT. Consequently, to achieve asphaltenes precipitation, the volume of solvent needed in the PFT is approximately three times greater than that required in the NFT. The precipitation of asphaltenes is not substantial until the solvent/bitumen (S/B) volume ratio reaches around 1. However, with an increase in the solvent volume up to a S/B volume ratio of 5, approximately 90% of the asphaltenes precipitate [7].

Some of the operational conditions of both PFT and NFT, as well as the quality of the final bitumen product, are summarized in **Table 2.7**. The temperatures of operation of both technologies are comparable, but the amount of solvent used in the PFT is higher than in the NFT. Because the solvent employed in the PFT has a lower density and higher volatility, it requires a higher vessel pressure than the NFT. The PFT is somehow a carbon rejection technology since some asphaltenes precipitate due to the addition of the paraffinic solvent. The precipitation of asphaltenes during the PFT yields a cleaner bitumen product (as compared to the NFT product) that does not require further separation steps but leads to a lower bitumen recovery (about 4–10% reduction in bitumen recovery) than the NFT process. Because of the higher amount of solvent necessary for the PFT and the reduced bitumen recovery throughout the treatment, the NFT is the most widely used industrial-scale process in Alberta's oilsands industry [9, 75].

Table 2.7: Summary of operational conditions used in the naphthenic (NFT) and paraffinic (PFT) froth treatment [9, 75].

Operational condition	NFT	PFT
Solvent	Naphtha	Pentane/Hexane
Solvent/Bitumen ratio (w/w)	0.6–0.8	1.5–2
Solvent density (kg/m^3)	750–800	625–670
Temperature (°C)	75–85	70–90
Operating pressure	Lower than in the PFT	Higher than in the NFT
Residual water in the bitumen product (wt%)	2–5	<0.5
Residual solids in the bitumen product (wt%)	0.5–1	<0.3
Asphaltenes precipitation	No	Yes
Further treatment required for product	Yes	No

The addition of a diluent in both NFT and PFT results in the formation of four different layers: (1) a top layer containing mostly diluted bitumen; (2) an intermediate layer at the bitumen-water interface containing stable emulsions of water and hydrocarbons with fine particles (called the "rag layer"); (3) a separated water phase; and (4) the tailing, which contains solid particles (including fine solids in both PFT and NFT and asphaltenes in the PFT), hydrocarbons, and water [75]. The undesirable stable emulsions in the "rag layer" make it a viscous and thick phase that can accumulate over time, inhibiting the settling of water droplets and solid particles, which impacts the efficiency of the process and can result in process disruptions [76].

2.3.2.1 The naphthenic froth treatment (NFT)

The simplified overview of the NFT is depicted in **Figure 2.5**. A demulsifier is added to the froth in the NFT, in addition to the diluent (naphtha), to facilitate the separation of water and solids. The demulsifier assists in breaking the water-oil emulsions that are stabilized by the asphaltenes, resins, and fine solids. The inclined plate settlers (IPS) act as a primary separation step. The IPS are gravity separation vessels with a cone bottom and internal plates that provide a large surface area for the settling of solids and water. They provide a high-quality overflow with minimal solids and water content (less than 2%). However, there is still a large amount of bitumen and naphtha in the IPS underflow, which must be treated through the centrifuge plant. The IPS underflow enters a dual-stage centrifugation system made of solid bowl scroll centrifuges and disc centrifuges. In the scroll centrifuges, coarse solids (larger than 44 μm) are removed, while most of the water and some of the fine solids are removed in the disc centrifuges. Besides the centrifuge plant, cyclones are used to assist in the clean-up of the IPS underflow. Due to the high cost associated with the operation of centrifuges, new extraction plants are opting for more IPS stages and reducing the number of centrifuges [5, 75, 77].

The residual solid content (0.5–1 wt%) and residual water content (2–5 wt%) of the bitumen product from the NFT are still too high to allow pipeline transportation. The residual water and naphtha diluent can be removed in a distillation column, but the bitumen product still contains all of the fines and any dissolved salts that were originally found in the process water. As long as the concentration of salt is not too high, the bitumen product containing the residual solids can be fed to coker-based facilities [5].

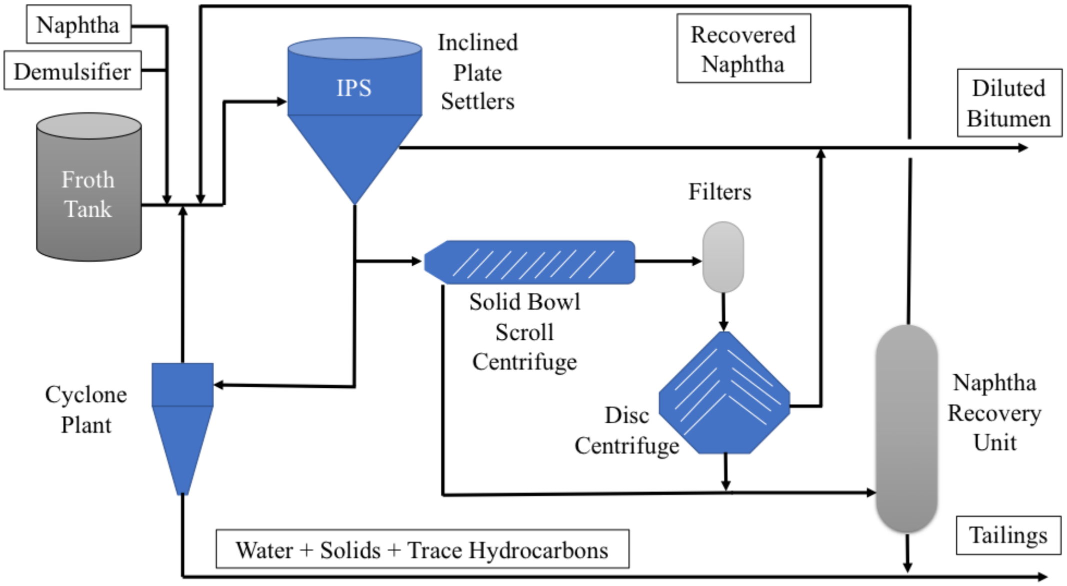

Figure 2.5: Simplified overview of the naphthenic froth treatment (NFT) [5, 75, 77].

2.3.2.2 The paraffinic froth treatment (PFT)

The simplified overview of the PFT is illustrated in **Figure 2.6**. The addition of a paraffinic solvent to the froth results in the formation of aggregates composed of water droplets, fine solids, and precipitated asphaltenes. These aggregates are separated by conventional settlers [9]. The diluted froth is sent to the first stage of gravity separation vessels (Settler). The overflow of the first-stage settler is the final bitumen product diluted with the added solvent. That stream is then sent to the solvent recovery unit (SRU), where it yields a clean bitumen product that does not need to be further purified since it contains less than 0.5 wt% of residual water and less than 0.3 wt% residual solids. However, the underflow of the first-stage settler still contains a significant amount of bitumen and water and needs to be sent to a second-stage settler. The underflow of the second settler contains almost all the solids and water from the original froth sample, the asphaltenes precipitated from bitumen (around 7–9 wt% of bitumen is precipitated as asphaltenes), and a small portion of solvent that is recovered in the tailings solvent recovery unit (TSRU) [5, 75, 78].

As a result of the extra asphaltenes component, the TSRU tailings stream has a high energy level. However, these asphaltenes are contaminated with a high concentration of solids (typically a 2:1 w/w ratio of solids to bitumen). Before the asphaltenes could be used as fuel or a gasifier feedstock, the tailings stream would need to be treated to minimize the mineral concentration [5].

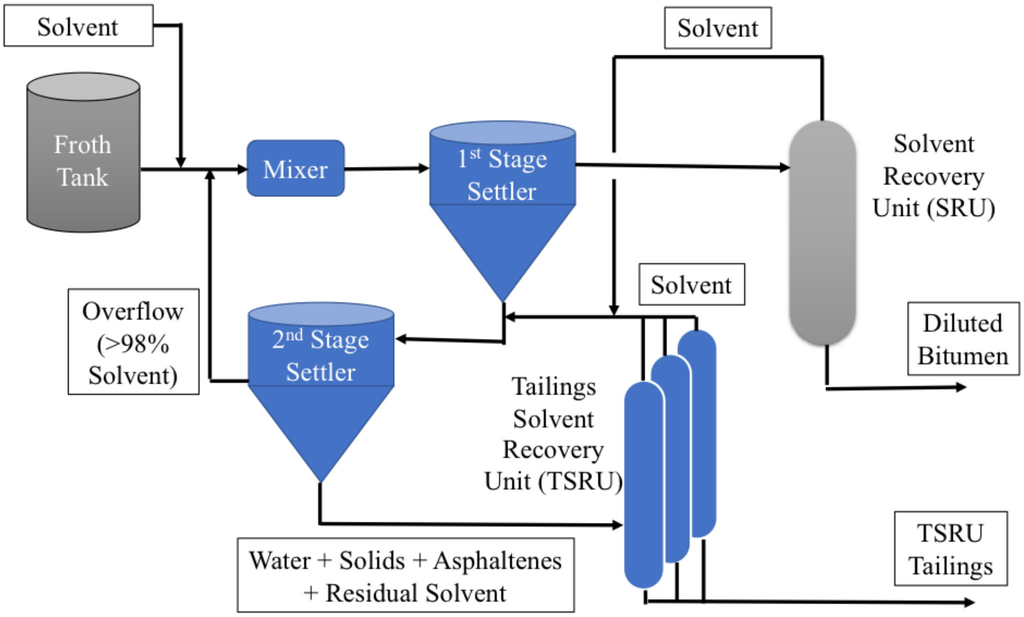

Figure 2.6: Simplified overview of the paraffinic froth treatment (PFT) [5, 75, 78].

2.3.3 Improvements to the froth treatment process

This section presents an overview of studies that have focused on improving the froth treatment process, specifically the separation efficiency of the treatment. The main objectives in these studies were to maximize bitumen recovery (i.e., less carbon rejection as asphaltenes in the PFT), maximize bitumen quality (i.e., minimize the water and fines content in the bitumen product), and at the same time minimize the energy requirements for the process [79]. Three major factors affect the efficiency of the froth treatment: temperature, solvent type/amount, and demulsifier properties. Both temperature and solvent type/amount have a direct impact on the energy requirements of the process [8, 75].

The effect of temperature on bitumen recovery and quality depends on the solvent selection for the froth treatment. Shelfantook [8] showed that an increase in temperature in the NFT from 80 to 130 °C was followed by an increase in the quality of the bitumen product but no significant change in the bitumen recovery, while the increase in temperature in the same range improved the bitumen recovery in the PFT but did not affect the product quality. However, the decision to increase the process temperature also needs to take into account the energy cost and equipment limitations.

The dilution ratio influences product recovery and quality in froth treatment. Romanov et al.[80] studied the effect of the solvent-to-bitumen (S/B) ratio during the froth treatment in the presence of an aromatic (toluene) and a paraffinic (*n*-heptane) solvent. The authors found that increasing the S/B ratio increased bitumen recovery and quality up to an optimum S/B ratio, after which increasing dilution had little effect on both processes. The optimum S/B ratio varied with solvent type, extraction temperature, oilsands quality, and extraction time. In general, the optimum S/B ratio varied within the range of 0.4–0.9 wt/wt for toluene and 1.1–1.9 wt/wt for *n*-heptane.

Some studies focused on the settling properties of aggregates during the froth treatment, which have a direct impact on the effectiveness of the process. Kosior et al.[81, 82] investigated the influence of process temperature, solvent type, and S/B ratio on the settling rates of aggregates in the PFT. Three paraffinic solvents were used in their study: isopentane, *n*-pentane, and *n*-hexane. The authors observed that an increase in temperature and S/B ratio resulted in an increase in the settling rates of the aggregates, irrespective of the solvent used. The increase in temperature from

30 to 90 °C increased the settling rates by one order of magnitude. The authors suggested that the formation of more compact aggregates at higher temperatures had a major influence on the settling rates. The effect of increased dilution on the settling rates was significant but not as pronounced as the effect of temperature. The solvent type also influenced the settling rates. When compared at the same temperature and S/B ratio, isopentane promoted the highest settling rates, while *n*-hexane promoted the lowest ones. The authors proposed that the governing factors influencing the settling rates were more likely associated with the aggregate structures, such as aggregate densities, than the density and viscosity of the oil phase.

The mixing energy input to the PFT also has an effect on the performance of the process. Zawala et al.[83] studied the effect of the mixing energy (by means of the energy input through the duration of mixing and the speed of an impeller) on the composition and settling rates of aggregates during the mixing of solvent (*n*-pentane and *n*-heptane) and froth at 80 °C in the PFT. The aggregates formed during the study consisted mainly of mineral particles and precipitated asphaltenes since the high temperature favored the coalescence of water droplets and the separation of free water. The authors found that increased mixing energy resulted in a higher concentration of mineral particles in the aggregates without affecting the aggregate's size, which resulted in an increased density of the aggregate and, consequently, increased settling rates.

Improvements related to the asphaltenes precipitation during the PFT have been investigated [84–87]. The main focus of these studies was on the application of either traditional or novel solvents during the PFT, the effect of temperature on the asphaltenes precipitation, and the optimum S/B ratio that would lead to less material rejection while yielding a high-quality bitumen product. Booran et al.[85] and Xu [86] tested the cofeed of CO_2 with traditional paraffinic solvents in the PFT and observed that the CO_2 injection resulted in the precipitation of asphaltenes at a lower paraffinic solvent to bitumen ratio, suggesting a potential decrease in the amount of paraffinic solvent required for the process. Although the exact mechanism leading to those results was unclear, the authors presented some speculations. These included the formation of carbonic acid, which lowers the pH of the aqueous medium, thus destabilizing asphaltenes at the oil/water interface and causing asphaltenes precipitation.

Xu [86] also observed a slight effect of temperature on the amount of precipitated asphaltenes using *n*-pentane, isopentane, and neopentane. The amount of precipitated asphaltenes decreased with an increase in temperature from 20 °C to 90 °C, and this effect was higher when using lower S/B ratios. No explanation was presented for the observed effect of temperature on the asphaltenes precipitation.

Lin and Pang [87] identified a correlation between settling rates of aggregates and deasphalting in the PFT using *n*-heptane: the higher the amount of precipitated asphaltenes, the higher the settling rates of the aggregates. The authors suggested that the structure and size of the aggregates were not significantly affected during the tests and that the enhanced settling rates observed with increased deasphalting were likely attributed to alterations in the density and viscosity of the oil phase.

Hristova et al.[88, 89] used a bench-scale froth treatment settling unit to investigate the effect of a solvent mixture containing naphtha and *n*-pentane at different compositions in order to couple the strengths of the NFT (i.e., no carbon rejection) and the PFT (i.e., cleaner product). The authors observed the existence of a transition region with solvent composition varying from 20 to 50 vol% naphtha, in which the bitumen product is clean (as comparable to the product from the PFT) but without bulk asphaltenes precipitation (as comparable to the NFT).

Efforts on improvements to the NFT also dedicated attention to studies on the use of commercial and newly developed demulsifiers in the process [90–93]. Improvements related to the application of demulsifiers are important contributions to the separation efficiency of the NFT, in which highly stable emulsions are formed (e.g., the "rag layer"). Kailey [90] studied the effect of three ethylene and propylene oxide copolymer demulsifiers (DMO A, DMO B, and DMO C) on the separation efficiency of the NFT. The three studied demulsifiers resulted in different removal efficiencies, with DMO C yielding the highest levels of water and solids removal and the lowest hydrocarbon rejection during the treatment.

Laplante et al.[92] investigated the effect of mixing energy and demulsifier injection concentration on the removal of water and solids from naphtha-diluted bitumen using a mixing test cell. The authors showed that the effectiveness of the demulsifier was increased by increasing mixing time and intensity. The same study also highlighted the relevance of knowing the optimum mixing conditions and injection concentration level in order to minimize the amount of demulsifier needed for water/solids separation.

Recent studies have focused on the integration of froth and thermal treatment in a single step. Chen et al.[61] investigated the thermal treatment of froth in the temperature range 300–400 °C and identified that it improved the separation of minerals from bitumen through filtration. The best filtration result was obtained after the thermal treatment at 390 °C for 30 min. The authors suggested that a change in the surface properties of the fine solids facilitated the stacking of clays, which made the filter cake more permeable and, consequently, improved the solids filtration. Turuga and de Klerk [73] evaluated the physicochemical changes in the bitumen phase during hydrothermal treatment of froth at 250 °C. Their research found that when bitumen was treated with solids and/or water, its viscosity increased compared to untreated bitumen. They also noticed changes in the H/C ratio, *n*-heptane insoluble content, and total acid number (TAN), all of which are strong indicators that minerals and water influenced the changes in the bitumen phase during the treatment.

Once bitumen is free from water and minerals, the next step in bitumen production is its upgrading, which is detailed in the following section.

2.4 Bitumen upgrading

The challenges encountered during bitumen transportation and processing are a consequence of bitumen's physicochemical properties, as highlighted in **Sections 2.2** and **2.3**. Both the quality and value of bitumen need to be improved before it is ready to be sent to its final market, the refineries. This section starts with an overview of the upgrading objectives, followed by a description of the relevant reactions that take place during the treatment. Additionally, it includes a review of the upgrading of bitumen in the presence of water and froth minerals.

2.4.1 Upgrading objectives

A number of technologies have been used for upgrading bitumen, including visbreaking, coking, catalytic cracking, hydrocracking, hydrotreating, and solvent deasphalting. These technologies have the aim of achieving one or more of the following: (1) reduce bitumen's density and viscosity;

(2) increase the H/C ratio of the bitumen product; (3) increase the amount of lighter boiling material in the product; (4) remove heteroatoms [5].

Some of the upgrading technologies aim for full upgrading of bitumen (e.g., coking), while others are selected to achieve only partial upgrading (e.g., visbreaking). Partial upgrading of bitumen is the term used for the low conversion of bitumen to improve its physicochemical properties to an extent that decreases the amount of solvent needed for bitumen dilution in order to meet pipeline specifications, given in **Table 2.2** [17]. From the properties listed in **Table 2.2**, viscosity, density, and bottom solids and water have already been discussed in the previous topics. The olefin content is not a concern when handling raw bitumen since olefins are absent in its composition; nevertheless, olefin formation during thermal treatment was claimed to pose a risk of gum formation and, consequently, clogging of pipelines and equipment. However, the fouling tendency of thermally-cracked bitumen is likely not solely due to the olefins formed during treatment but also due to their interactions with other components in bitumen [94].

The term "severity" usually employed during bitumen upgrading is related to both reaction temperature and time. The upgrading severity depends on the objective of the thermal treatment (e.g., partial or full upgrading). Visbreaking, for example, is considered a mild-severity thermal treatment since the main target is to achieve viscosity reduction while at the same time avoiding coke formation. On the other side, high severity is needed for coking, in which a high conversion of heavier material into lighter components is expected at the cost of carbon rejection through coke formation. **Table 2.8** shows the evolution of the coke, liquid, and gas yields of the thermal treatment of Cold Lake bitumen at 400 °C and varying reaction times. The higher the severity (by means of increased residence times), the higher the amount of coke formed and the lower the liquid yield [95].

Table 2.8: Coke, liquid, and gas yields during thermal treatment of Cold Lake bitumen at 400 °C and varying reaction times [95].

Residence time (min)	Yield (wt%)		
	Coke	Liquid	Gas
Feed	1.3 ± 0.1	98.7 ± 0.4	-
30	1.8 ± 0.3	97.5 ± 0.4	0.7 ± 0.3
60	1.5 ± 0.4	94.1 ± 0.3	4.1 ± 0.2
90	5.0 ± 2.1	88.8 ± 1.7	3.4 ± 2.4
180	8.0 ± 0.3	84.2 ± 1.3	7.7 ± 1.1
270	11.7 ± 0.2	81.5 ± 1.9	6.9 ± 1.7

Studies on the thermal treatment of bitumen usually report the residence time for a constant temperature defined at the design stage of the investigation. Many of these studies have frequently neglected the heating and cooling profiles of the reaction medium, which can lead to an underestimation of the actual severity of the treatment. An alternative approach for reporting a more realistic severity during the upgrading of bitumen is the use of the equivalent residence time (ERT), as defined by Yan [96]. By monitoring the temperature of the reaction media at defined time intervals, the ERT at a reference temperature can be calculated according to **Eq. 2.18**, where Δt_i are defined time intervals consisting of two recorded temperatures (T_i and T_{i+1}), T_{ref} is the reference temperature for which the ERT is being calculated, E_a = 209500 J mol^{-1}, and R = 8.314 J mol^{-1} K^{-1}.

$$ERT\,at\,T_{ref} = \sum_{i=1}^{n} \Delta t_i \times exp\left[\left(-\frac{E_a}{R}\right)\left(\frac{1}{\frac{T_i + T_{i+1}}{2}} - \frac{1}{T_{ref}}\right)\right] \tag{2.18}$$

2.4.2 Chain reactions during bitumen upgrading

Bitumen upgrading relies on the conversion of some of the vacuum residue material into lighter products. For this objective, the chemical bonds of the heavy material need to be broken, yielding lighter compounds. This can be achieved by either thermal or catalytic cracking. However, there are several other reactions that take place concurrently with cracking during bitumen upgrading.

Bitumen upgrading proceeds through the traditional steps of free radical chain reactions, including initiation, propagation, and termination. Although initiation is listed as the first step in chain reactions, it is important to highlight that bitumen naturally contains free radicals in its composition, but these species are somehow stabilized at ambient conditions (persistent free radicals). **Figure 2.7** illustrates the simplified mechanisms for each of the chain reaction steps that are detailed in the next subsections.

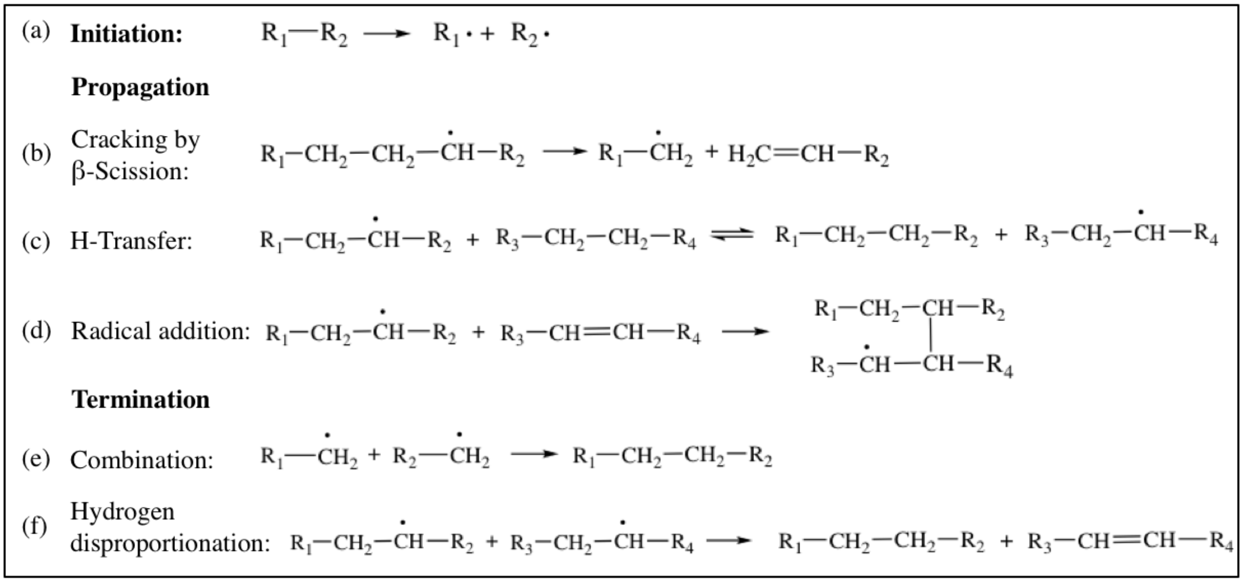

Figure 2.7: Free radical chain reaction mechanisms [97].

2.4.2.1 Free radical initiation

The lack of reactions taking place in bitumen in its natural state was explained by Acevedo et al.[15] in terms of the "caging effect", a theory in which the persistent free radicals naturally found in bitumen are "caged" by aggregates of asphaltenes. It was also suggested that mobility restrictions caused by the medium's high viscosity play a role in radical caging [98]. However, the study by Alili et al.[99] demonstrated that persistent free radicals in asphaltenes were reactive. The authors argued that free radical persistence could not be solely explained by cage effects facilitated by either steric protection or the high viscosity of the medium. While cage effects, solvent effects, steric protection, and radical stabilization collectively influence the reactivity of free radicals in bitumen, these factors alone are insufficient to explain the persistence of free radicals in bitumen. A more plausible explanation is likely to be provided by considering the dynamic equilibrium involving the dissociation and association of free radicals [100].

Therefore, the initiation of radicals (**Figure 2.7a**) is an important step to promote bitumen upgrading. This step requires high activation energy for bond dissociation. A typical example is thermally induced homolytic bond dissociation, which is a monomolecular free radical decomposition reaction. The bond dissociation energies for the main covalent bonds that are typically broken during bitumen upgrading are shown in **Table 2.9**. The weakest bonds are those between carbon and heteroatoms (S, N, and O) and those of aliphatic C–C, while aromatic C–H bonds are the strongest ones [97, 101].

Table 2.9: Bond dissociation energies for typical bonds found in bitumen composition [102].

Chemical Bond	Energy (kJ/mol)
C–C (aliphatic)	344 ± 4
C–H (primary)	411 ± 4
C–H (secondary)	398 ± 4
C–H (aromatic)	464 ± 8
C–S	307 ± 8
C–N	342 ± 8
C–O	344 ± 4

Homolytic bond dissociation plays an important role in radical initiation but cannot be seen as the only mechanism for free radical formation during upgrading. In the liquid phase, bimolecular interactions are more pronounced than in the vapor phase, and free radical initiation through molecular-induced homolysis might also take place [57, 101].

Although the initiation step is energy-intensive, once the radicals are formed, a lower activation energy is required for the free radical propagation that is discussed next [97].

2.4.2.2 Free radical propagation

The most relevant types of radical propagation during bitumen upgrading are cracking, hydrogen transfer, and free-radical addition (refer to **Figures 2.7b–d**). Details on each of these reactions are given next.

(a) Cracking by β-scission

Cracking is at the core of the bitumen upgrading processes, in which one of the main objectives is to crack heavy materials, yielding an increase in lighter fractions. Once a molecule becomes a free radical, the other bonds of the molecule are weakened, and cracking can readily take place, forming an alkene and a smaller free radical species. The process of free radical cracking occurs through the homolytic dissociation of the β-bond in relation to the free radical position. When large molecules are cracked, the formation of the most stable alkyl free radical species is favored in the following order: tertiary > secondary > primary radical [5].

Although thermal cracking yields desirable lighter species, it also produces undesirable olefinic species that can be detrimental during bitumen processing. The olefinic compounds can undergo radical addition to form a gum that can foul and clog pipelines and equipment. For this reason, the cracked products need further treatment (e.g., hydrotreating) in order to saturate the olefins and reduce the propensity for gum formation [103]. However, it is important to highlight that the olefins alone might not be responsible for the fouling tendency of cracked bitumen. It is likely that the synergetic effect of high-molecular-weight olefins and other heavy components in bitumen, such as asphaltenes, plays a role in the fouling mechanism [94].

The severity of the thermal treatment has a major influence on the extent of cracking of heavy materials into lighter ones. **Figure 2.8** contains the boiling point distribution of feed and visbroken products of a deasphalted vacuum residue sample at two different severities. As the severity of the treatment increased, the amount of the lighter fractions also increased, followed by a decrease in the residue fraction [104]. However, pushing the severity of the thermal treatment beyond coke formation can result in material rejection during the treatment.

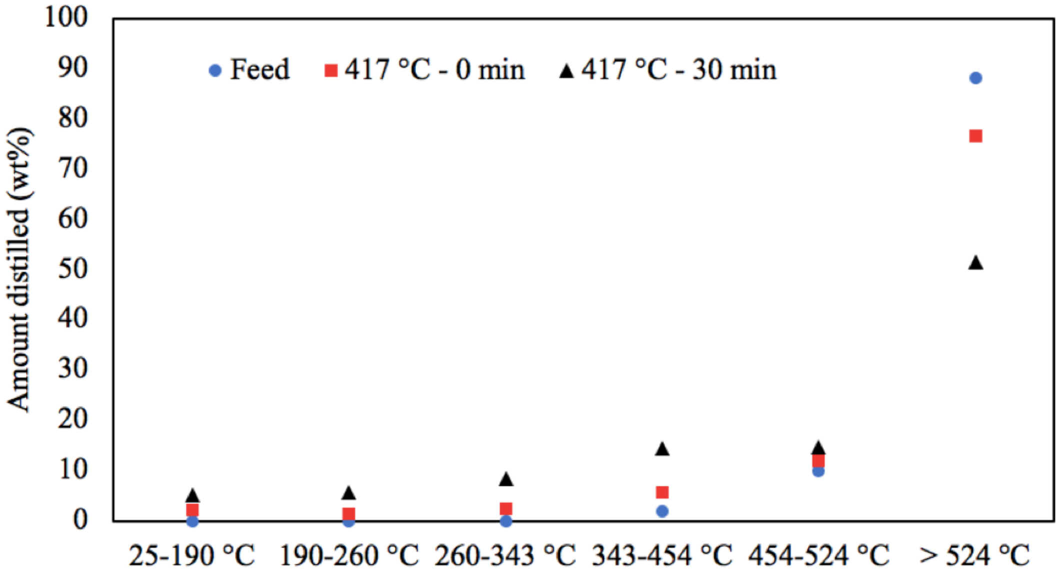

Figure 2.8: Boiling point distribution of feed and products of a deasphalted vacuum residue sample thermally treated at 417 °C for 0 and 30 min (heat-up and cool-down times are excluded) [104].

(b) Hydrogen transfer

Another relevant class of propagation reactions are those involving hydrogen transfer (refer to **Figure 2.7c**). Hydrogen transfer during bitumen upgrading enhances the probability of free radical chain transfer reactions compared to free radical addition and, consequently, influences the likelihood of heavy product formation [105]. These reactions have a major influence on the overall rate and outcome of chain reactions. The contribution of propagation reactions becomes even more pronounced below the temperature threshold of 380–400 °C, as the rate of transfer reactions increases relative to the rate of cracking as the temperature drops. This increase in the propagation rate might have a significant impact on compositional changes in bitumen because the transfer reactions produce free radical species that require less activation energy for cracking [101]. Although hydrogen transfer is more frequently mentioned in the bitumen upgrading literature, methyl transfer also takes place during both intramolecular and intermolecular transfers [105].

The relevance of hydrogen transfer reactions at temperatures below the typical operating temperatures of upgrading processes has been demonstrated in works that investigated the reactivity of bitumen-derived asphaltenes in the temperature range of 100–250 °C [57, 106]. In these studies, probe molecules were employed to evaluate the extent of hydrogen transfer in the asphaltenes. There was evidence of hydrogen transfer at temperatures as low as 120 °C. These studies highlighted the hydrogen transfer capability of the asphaltenes, which acted as both hydrogen donor and acceptor during thermal treatment.

The use of hydrogen donors in upgrading processes has been recognized for many years. Hydrogen donors are chemical compounds (with a low oxidation potential) that can easily transfer hydrogen to bitumen, which has the advantage of improving hydrogenation and, consequently, suppressing coke formation during thermal treatment. Tetralin and 9,10-dihydrophenanthrene are both good examples of hydrogen donor solvents commonly used in bitumen upgrading investigations [107].

(c) Free radical addition

Free radical addition (**Figure 2.7d**) is undesirable from the perspective of bitumen upgrading since it produces heavier compounds, which is the opposite of what is intended in the process. The addition reactions involving olefinic compounds take place at the operational temperatures of upgrading; however, addition reactions are thermodynamically favored at low temperatures [101]. Both intramolecular and intermolecular additions are possible. Intramolecular addition leads to an increase in the degree of cyclization of the product but no change in its molecular weight. On the other side, intermolecular addition results in an increase in the molecular weight and can impact the solubility of the products in the medium. In this sense, polymerization promoted by the addition of olefinic compounds can build high-molecular-weight materials that are detrimental to many of the upgrading operations [97, 101].

2.4.2.3 Free radical termination

Two typical routes are expected for free radical termination: combination (**Figure 2.7e**) and disproportionation (**Figure 2.7f**). Combination is the reverse of homolytic bond dissociation and, therefore, is exothermic. The newly combined species, although stable, might still undergo bond scission depending on the energy input of the process. Termination by disproportionation consists of the transfer of a hydrogen or methyl group from one radical species to another in such a way that both species become stable. Termination by disproportionation, likewise cracking by β-scission, produces olefins that might undergo polymerization [97, 101].

The conversion levels during bitumen upgrading are determined by the relative rates of free radical initiation, propagation, and termination. In this context, any variable that would increase the rate of termination during the process of bitumen upgrading could hinder the conversion of bitumen.

2.4.3 Influence of water during thermal treatment of bitumen and model compounds

The thermal processing of bitumen with water at different temperature levels is encountered right from the initial stages of bitumen exploration. Both surface mining and subsurface production involve, at some point, heating bitumen in the presence of water, which includes both connate and process water. This practice is observed in processes such as cyclic steam stimulation in subsurface production and hot water extraction in surface mining [3, 17]. The concomitant processing of bitumen and water is also found in upgrading operations, such as steam stripping within the fractionator of visbreaker units [108].

Research examining the influence of water in the thermal conversion of organic model compounds provides valuable insights for understanding the specific role of water in treating more complex systems, such as bitumen. For this reason, this section was divided into two subsections: the first focused on the literature on the influence of water during the thermal conversion of organic model compounds with relevance to bitumen upgrading, while the second covered studies on the effect of water during the thermal treatment of bitumen.

2.4.3.1 Influence of water during the thermal conversion of model compounds

The application of sub- and supercritical water as either a solvent or a reactant in organic reactions has been extensively reported in the literature [109–114]. As the temperature increases, changes in the physicochemical properties of water, such as the decrease in its dielectric constant and the increase in its self-dissociation constant, make it a more compatible medium for organic reactions

[110, 111]. The advantages of introducing water during the thermal conversion of organic compounds include reducing waste production by replacing conventional organic solvents, accelerating reaction rates, and enabling control over the selectivity of certain products [109]. Some of the reactions affected by high-temperature water include hydrolysis, hydration of alkenes, condensation, elimination, and addition reactions [111, 112].

In a collaborative effort, the research groups headed by Katritzky and Siskin extensively investigated the influence of hot water (encompassing temperatures ranging from 250 to 500 °C, which included both sub- and supercritical water) during the thermal conversion of organic model compounds [115–121]. Their studies primarily focused on gaining insights into the transformations involving kerogen, and the chosen model compounds included a wide range of aliphatic, carbocyclic, heterocyclic, and their substituted derivatives. These components are representative of the structures found in oil shale kerogen but are also pertinent to the field of bitumen conversion. In many of these studies, the authors compared the reactions in the presence of hot water with the same reactions carried out in cyclohexane. This comparative approach aimed to differentiate thermal (radical) chemistry from aqueous (ionic) chemistry. Some of the relevant findings to bitumen conversion from their work are summarized below:

- The presence of water during thermal conversion had a significant influence on the reaction chemistry taking place during the treatment. It had an impact not only on the reaction rates but also on the reaction pathways [115, 116]. For instance, in the study of the conversion involving benzenoid hydrocarbons and their oxygenated derivatives, there was evidence that, although radical conversion remained the primary pathway during the treatment of benzenoid hydrocarbons in the presence and absence of water, variations in product yield indicated water's ability to influence radical reactions. Also, when examining the thermal conversion of oxygen-containing benzenoids, such as cyclohexyl phenyl ether, water functioned as an acid catalyst and facilitated ionic conversion [115];

- When increasing the temperature of the reaction medium, transitioning water from a sub- to a supercritical state only affected the reaction rates and not the reaction pathways [115, 117];

- Pure water has the capacity to catalyze ionic conversions, such as hydrolysis. Nevertheless, the authors suggested that the introduction of external agents such as brine and acidic clays somehow facilitated the ionic conversion and specific acid-catalyzed reactions [117–120];

- The presence of water increased the selectivity to certain products. For example, the enhanced selectivity to products from the Diels-Alder reaction was attributed to the hydrophobic effect of water, which is the inclination of non-polar species to cluster in an aqueous solution, thereby reducing the interfacial area between hydrocarbons and water [116, 117].

In addition to the noteworthy contributions by Katritzky and Siskin, other relevant research on the conversion of model compounds in the presence of water can be found in the literature. The work by Chen et al.[122] demonstrated that when cracking a model α-olefin (1-dodecene) in the presence of water, the conversion initially decreased by 20% under subcritical conditions. However, the conversion gradually increased to levels similar to those attained in the absence of water as the water transitioned from subcritical to supercritical conditions. The authors suggested that the decreased conversion in the presence of subcritical water might be related to the cage effect of water on the bimolecular hydrogen abstraction between C radicals and 1-dodecene.

Daud et al.[123] and Arcelus-Arrilaga et al.[124] performed studies on the oxidative cracking of polycyclic aromatic hydrocarbons (PAHs) in both sub- and supercritical water. It was observed that pure water, in the absence of an oxidant, did not significantly promote the cracking of the PAHs. However, in the presence of an oxidant, higher selectivity to lighter organic-soluble products was found under supercritical conditions, whereas heavier insoluble products predominated in subcritical water. The authors attributed this phenomenon to the enhanced solubility of the PAHs in water as the water transitioned from sub- to supercritical conditions.

Most studies in the literature that investigated the influence of water in the thermal conversion of organic compounds primarily focused on the application of supercritical water during the conversion process. It is noteworthy that supercritical water requires not only high temperatures but also high pressures (i.e., $T > 374$ °C and $P > 22$ MPa), which could potentially present a limitation for practical industrial applications.

2.4.3.2 Influence of water during the thermal treatment of bitumen

Studies on the upgrading of bitumen and heavy oils in the presence of sub- and supercritical water have been frequently cited in the literature as aquathermolysis, a term used to refer to both catalytic and non-catalytic thermal treatment of bitumen in the presence of steam or hot water [125–131]. The majority of these studies focused on the kinetic modeling of the aquathermolysis process, with minor emphasis on the specific role of water during the treatment.

In this subsection, the main objective was to review the impact of water during the thermal conversion of bitumen. Therefore, this review was limited to studies that conducted hydrothermal treatment of bitumen without the use of any added catalyst.

The authors who conducted studies on the non-catalytic aquathermolysis of bitumen and heavy oils have claimed some benefits of having water in the reaction medium, such as:

- Coke suppression – Canıaz et al.[132] studied the upgrading of bitumen in supercritical water at 440 °C and 30 MPa with reaction times varying in the range of 15–120 min and noticed that the use of supercritical water during the treatment suppressed coke formation when compared to the pyrolysis of bitumen alone. Liu et al.[133] investigated the upgrading of a residual oil in the presence of sub- and supercritical water in the temperature range of 380–440 °C and water densities varying in the range of 50–200 kg/m^3. The authors observed that the reaction rates and coke formation were influenced by varying the density of water. Increasing the water density from 100 to 200 kg/m3 resulted in increased reaction rates and suppression of coke formation. These authors claimed that the dissolution of heavy components and coke precursors in supercritical water resulted in the observed coke suppression;

- Increased yield of lighter products – Wahyudiono et al.[134] conducted the upgrading of bitumen with supercritical water at 400 °C and pressures above 22.1 MPa with reaction times ranging from 5 to 120 min and observed that the conversion of heavy components into lighter ones was higher when bitumen was reacted with water. Sato et al.[135] showed that upgrading asphalt with supercritical water at 400 °C resulted in an increased yield of maltenes as compared to upgrading without water;

- Hydrogen exchange/donation – The role of water as a potential hydrogen donor solvent during bitumen upgrading has also attracted some attention but is still unclear. Some authors suggested the potential hydrogen donation from water during thermal treatment [135–138], while other studies claimed that the effect of water was not as a reactant but only as a diluent [139, 140]. Dutta et al.[138] used deuterated steam during thermal cracking of bitumen and reported hydrogen exchange between steam and hydrocarbons, preferentially at the benzylic position. Schlepp et al.[137] attributed the coke suppression and higher yield of lighter components to the potential hydrogen donation from water during aquathermolysis. However, the incorporation of deuterium into bitumen does not imply that water acts as a direct hydrogen donor. For instance, Ovalles et al.[141] provided evidence that, while hydrogen from water is transferred to bitumen, the consumption of water during the treatment is minimal (< 1 wt%). This indicated that water acted as a hydrogen transfer agent rather than a hydrogen donor under the conditions of their study.

There is also evidence in the literature indicating that water has the capacity to impact the alterations in physicochemical properties during the thermal conversion of heavy oils and bitumen. Fan et al.[142] studied the effect of water content during the thermal conversion of heavy oils at 240 °C for 48 h and reported that the presence of water resulted in a product with decreased viscosity and average molecular weight as compared to the treatment without water. On the other side, the study by Turuga and de Klerk [73], which performed thermal treatment of bitumen at 250 °C for 2 h, demonstrated that the presence of water during the treatment resulted in a bitumen product with increased viscosity as compared to the feed and to the thermal treatment of bitumen alone.

Although there is vast literature on the topic of aquathermolysis of bitumen, many of these studies did not compare the compositional changes in bitumen in the presence of water to those in the thermal treatment of bitumen alone, making it difficult to properly grasp the specific contributions of water in the aquathermolysis process. Besides, many studies combined water with other chemicals or catalysts without performing any control reactions, making it challenging to distinguish if the observed effects on bitumen properties or composition were due to water alone or to the presence of these additives. Therefore, many questions remain unanswered about the role of water in the thermal treatment of bitumen, providing ample opportunities for further research and exploration in this field.

2.4.4 Influence of minerals during thermal conversion of model compounds and bitumen

The chemical and structural properties of some minerals found in bitumen froth were discussed in **Section 2.3.1**. The catalytic properties of these minerals, frequently attributed to the presence of Brønsted-Lowry and/or Lewis acid sites in their structure, are expected to play a role during the upgrading of bitumen. In this section, some studies that presented evidence on the potential effects of minerals during the thermal treatment of organic model compounds and bitumen are reviewed.

2.4.4.1 Influence of minerals on the thermal conversion of organic model compounds

Several studies in the field of oil and natural gas geochemistry have investigated the catalytic role of minerals in the formation and transformation of hydrocarbons through thermal simulation experiments [143–146]. There is extensive literature on the impact of minerals during the thermal conversion of organic matter, with a primary focus on elucidating the mechanisms involved in the formation of kerogen from organic-rich sediments [144, 145, 147–149]. Clays have been the primary minerals of interest due to their predominance in source rocks and their recognized catalytic properties, which can promote a series of reactions during pyrolysis, including cracking, isomerization, polymerization, and heteroatom removal [143]. For instance, Smolen and Hren [150] investigated the thermal maturation of a sedimentary organic matter in the temperature range of 100–300 °C in the presence of two clays, namely kaolinite and montmorillonite. The composition of the formed *n*-alkanes was significantly affected by the type of clay, with the presence of kaolinite leading to a yield of n-C_{15}–C_{33} that was three times higher at 300 °C than in the presence of montmorillonite. Also, the conversion in kaolinite yielded more unsaturated products, whereas montmorillonite led to the formation of more branched and cyclic products. The authors suggested that the differences in the nature and concentration of acid sites on the surfaces of kaolinite and montmorillonite led to distinct mechanisms during the conversion of organic matter.

Given the intricate composition of sedimentary organic matter and kerogen, some authors have examined the influence of minerals on the thermal conversion of organic model compounds that are representative of the structures found in those more complex systems. These studies are pertinent not only for the geochemistry field but also for advancing the understanding of the potential influence of minerals during the thermal conversion of bitumen. Some of the main outcomes from the conversion of model compounds in the presence of minerals are summarized next:

- Research on the effect of clay minerals during the pyrolysis of long-chain carboxylic acids (e.g., octadecanoic acid) demonstrated that the clays influenced the reaction pathways, which consequently impacted the composition of the products. The Brønsted-Lowry acid sites of the clays promoted cationic cracking and isomerization, yielding more branched, lower-molecular-weight hydrocarbons compared to pyrolysis in the absence of clays, whereas the Lewis acid sites promoted decarboxylation [151–153];

- Clays reduced the temperature needed for the thermal decomposition of dodecanoic acid and 12-aminododecanoic acid [154–156]. Clays of varying acidity levels, including montmorillonite, kaolinite, illite, and rectorite, affected the thermal decomposition temperature to different extents. The higher the number of acid sites on the surface of the mineral, the lower the decomposition temperature, indicating that the minerals were catalytically active during the treatment [156];

- Kaolinite and illite favored addition reactions of α-methylstyrene, 1-octene, and toluene during thermal conversion at 250 °C. When pyridine was added to the reaction medium, these reactions were suppressed, indicating that even under alkaline conditions, the clays were able to promote cationic addition [157];

- The surface area of alumino-silicate clays is able to reduce the orientational freedom degree of the adsorbed species by aligning monomers along a 2-dimensional surface, facilitating reactions such as dimerization and polymerization [158]. Solomon and Rosser [159] studied the polymerization of styrene catalyzed by clays and suggested that the polymerization mechanism has the characteristics of both a free radical and an ionic mechanism. In their proposed mechanism, one electron is transferred from styrene to clay, forming a radical carbonium that rapidly dimerizes, and then propagation and termination take place by a cationic mechanism;

- Iron-containing minerals are able to catalyze various types of reactions. Yang et al.[160] demonstrated that the presence of iron-containing minerals during the hydrothermal conversion of dibenzyl ketone favored the formation of cracking and addition products when iron oxides (hematite and magnetite) were used, while the iron sulfide (troilite) mineral favored the reduction of the model ketone;

- Choudhury and Misra [161] demonstrated the application of clays as catalysts in the Friedel-Craft alkylation of benzyl chloride with toluene;
- Some authors have proposed that clay minerals could impact hydrogen and methyl transfer, but the pathways for these transformations remain unclear [162, 163].

The findings obtained from studies on the impact of minerals during the conversion of organic compounds suggest that their catalytic effects may have the potential to influence reaction rates and pathways in bitumen conversion. The following subsection addresses this topic with an emphasis on minerals found in bitumen froth.

2.4.4.2 Potential effects of minerals on the thermal conversion of bitumen

A number of studies on *in situ* upgrading (ISU) and bitumen pyrolysis have shown that minerals present in oilsands might have a catalytic effect on the compositional changes in bitumen that can influence the yield of coke and gases, as well as the distribution of the relative amounts of the different fractions produced in the liquid phase [164–168]. Many of these works consisted of kinetic studies, which reported that, in the presence of the mineral matrix, the activation energies of product formation were reduced.

Phillips et al.[164] studied the effect of the sand matrix on the thermal cracking of Athabasca bitumen from 360 to 420 °C and identified that the coke and gas yields were greater when bitumen-sand mixtures were converted as opposed to the conversion of bitumen alone. The authors also found that the mineral matter affected the yields of other pseudo-components in bitumen (defined by the authors as distillables, heavy oils, and asphaltenes for kinetic modeling purposes) and that the activation energies of cracking were lower in the presence of the sand matrix. Although some authors claimed that the acidity of clays is able to promote cracking, Rong and Xiao [169] investigated the catalytic cracking effect of clays belonging to the kaolin group (kaolinite, dickite, and halloysite) and concluded that their cracking activity was mostly influenced by their structure (surface area, pore size, and volume) rather than by their chemical composition. The specific surface area of the minerals used in their study varied in the range of 9–89 m^2/g.

The study by Zheng et al.[170] investigated the effect of montmorillonite clay on the coke formation during thermal treatment of heavy oils under an inert and oxidizing atmosphere at temperatures ranging from 300 °C to 600 °C. The authors concluded that montmorillonite shortened the induction of coking and catalyzed aromatization and polymerization under the inert atmosphere, while oxygen addition was catalyzed by the clay under the oxidizing atmosphere.

Fan et al.[142] reported that the addition of a mixture of minerals representative of reservoir rocks (including quartz, potassic feldspar, and clays) during the hydrothermal treatment of heavy oils at 240 °C and 48 h resulted in a higher viscosity reduction as compared to the hydrothermal treatment alone. However, Turuga and de Klerk [73], reported that thermal treatment of bitumen at 250 °C for 2 h in the presence of froth minerals resulted in increased viscosity and density as compared to the treatment of bitumen alone.

There is extensive literature on the aquathermolysis of bitumen and heavy oils in the presence of minerals [171–174]; however, limited attention has been directed towards the specific contributions of minerals to the observed changes in oil properties and composition during the conversion. Moreover, the frequent inclusion of additives beyond water and minerals during the experiments adds complexity, making it challenging to isolate the effects of each component in the reaction system. Therefore, the comprehension of the role played by minerals in the thermal conversion of bitumen remains an area that requires further investigation.

2.5 References

(1) *Natural Resources Canada - What are the oil sands?*, https://natural-resources.canada.ca/our-natural-resources/energy-sources-distribution/fossil-fuels/crude-oil/what-are-oil-sands/18089 (accessed 2023/2/16).

(2) IEA *World Energy Outlook*, 2022, https://www.iea.org/reports/world-energy-outlook-2022 (accessed 2023/2/10).

(3) Speight, J. G., *Heavy Oil Production Processes*; Elsevier: Waltham, MA - USA, 2013, pp 1–7.

(4) De Klerk, A. Chapter 3 - Unconventional oil: Oilsands, In *Future Energy - Improved, Sustainable and Clean Options for our Planet*, ed. by Letcher, T. M., 3rd edition, Elsevier: 2020, pp 49–65.

(5) Gray, M. R., *Upgrading oilsands bitumen and heavy oil*; Pica Pica Press - Edmonton: 2015.

(6) AER *Alberta Energy Outlook*, 2023, https://www.aer.ca/providing-information/data-and-reports/statistical-reports/st98 (accessed 2024/1/9).

(7) Czarnecki, J.; Masliyah, J.; Xu, Z.; Dobras, M., *Handbook on Theory and Practice of Bitumen Recovery from Athabasca Oil Sands - Volume 2: Industrial Practice*; Kingsley Knowledge Publishing: 2013, p 717.

(8) Shelfantook, W. E. A perspective on the selection of froth treatment processes. *Can. J. Chem. Eng.* **2004**, *82* (4), 704–709.

(9) Rao, F.; Liu, Q. Froth treatment in Athabasca oil sands bitumen recovery process: A review. *Energy Fuels* **2013**, *27* (12), 7199–7207.

(10) Strausz, O. P.; Lown, E. M., *The Chemistry of Alberta Oil Sands, Bitumens and Heavy Oils*; Alberta Energy Research Institute: Calgary, 2003, p 695.

(11) *ASTM D2007-19: Standard Test Method for Characteristic Groups in Rubber Extender and Processing Oils and Other Petroleum-Derived Oils by the Clay-Gel Absorption Chromatographic Method*; ASTM international: West Conshohocken, PA, 2019.

(12) Rhodes, A. K. Benchmark West Texas Intermediate crude assayed. *Oil andGas J.* **1994**, *92* (33), 88.

(13) Mullins, O. C.; Sheu, E. Y.; Hammami, A.; Marshall, A. G., *Asphaltenes, heavy oils, and petroleomics*; Springer: New York, 2007, p 688.

(14) Fakher, S.; Ahdaya, M.; Elturki, M.; Imqam, A. Critical review of asphaltene properties and factors impacting its stability in crude oil. *J. Pet. Explor. Prod. Technol.* **2020**, *10* (3), 1183–1200.

(15) Acevedo, S.; Escobar, G.; Ranaudo, M. A.; Pinate, J.; Amorin, A. Observations about the Structure and Dispersion of Petroleum Asphaltenes Aggregates Obtained from Dialysis Fractionation and Characterization. *Energy Fuels* **1997**, *11*, 774–778.

(16) Hart, A. A review of technologies for transporting heavy crude oil and bitumen via pipelines. *J. Pet. Explor. Prod. Technol.* **2014**, *4* (3), 327–336.

(17) Gray, M. R. Fundamentals of partial upgrading of bitumen. *Energy Fuels* **2019**, *33* (8), 6843–6856.

(18) Hristova, E.; Tchoukov, P.; Stoyanov, S. R.; McFarlane, R. Asphaltene Precipitation Onsets in Relation to the Critical Dilution of Athabasca Bitumen in Paraffinic Solvents. *Energy Fuels* **2022**, *36* (4), 1832–1841.

(19) Duran, J. A.; Casas, Y. A.; Xiang, L.; Zhang, L.; Zeng, H.; Yarranton, H. W. Nature of Asphaltene Aggregates. *Energy Fuels* **2019**, *33* (5), 3694–3710.

(20) Zhang, L.; Shi, C.; Lu, Q.; Liu, Q.; Zeng, H. Probing Molecular Interactions of Asphaltenes in Heptol Using a Surface Forces Apparatus: Implications on Stability of Water-in-Oil Emulsions. *Langmuir* **2016**, *32* (19), 4886–4895.

(21) Balestrin, L. B.; Loh, W. Recent developments on the elucidation of colloidal aspects of asphaltenes and their relevance to oilfield problems. *J. Braz. Chem. Soc.* **2020**, *31* (2), 230–243.

(22) Wakeham, W. A.; St. Cholakov, G.; Stateva, R. P. Liquid density and critical properties of hydrocarbons estimated from molecular structure. *J. Chem. Eng. Data* **2002**, *47* (3), 559–570.

(23) Gray, M. R. New technique defines the limits of upgrading heavy oils, bitumens. *Oil Gas J.* **2002**, *100* (1), 50–54.

(24) Saryazdi, F.; Motahhari, H.; Schoeggl, F. F.; Taylor, S. D.; Yarranton, H. W. Density of hydrocarbon mixtures and bitumen diluted with solvents and dissolved gases. *Energy Fuels* **2013**, *27* (7), 3666–3678.

(25) Sánchez-Lemus, M. C.; Okafor, J. C.; Ortiz, D. P.; Schoeggl, F. F.; Taylor, S. D.; Van Den Berg, F. G.; Yarranton, H. W. Improved density prediction for mixtures of native and refined heavy oil with solvents. *Energy Fuels* **2015**, *29* (5), 3052–3063.

(26) McFarlane, R. A.; Gray, M. R.; Shaw, J. M. Evaluation of co-volume mixing rules for bitumen liquid density and bubble pressure estimation. *Fluid Phase Equilib.* **2010**, *293* (1), 87–100.

(27) Guan, J. G.; Kariznovi, M.; Nourozieh, H.; Abedi, J. Density and viscosity for mixtures of Athabasca bitumen and aromatic solvents. *J. Chem. Eng. Data* **2013**, *58* (3), 611–624.

(28) Montoya Sánchez, N.; de Klerk, A. Viscosity Mixing Rules for Bitumen at 1–10 wt% Solvent Dilution When Only Viscosity and Density Are Known. *Energy Fuels* **2020**, *34* (7), 8227–8238.

(29) Nourozieh, H.; Kariznovi, M.; Abedi, J. Measurement and Prediction of Density for the Mixture of Athabasca Bitumen and Pentane at Temperatures up to 200 °C. *Energy Fuels* **2014**, *28* (5), 2874–2885.

(30) Kariznovi, M.; Nourozieh, H.; Abedi, J. Volumetric Properties of Athabasca Bitumen + n-Hexane Mixtures. *Energy Fuels* **2014**, *28*, 7418–7425.

(31) Nourozieh, H.; Kariznovi, M.; Abedi, J. Modeling and measurement of thermo-physical properties for Athabasca bitumen and n-heptane mixtures. *Fuel* **2015**, *157*, 73–81.

(32) Stewart, R. A. Beyond Viscosity - How Density, Vibration and Interfacial Tension Affect Solvent Aided Bitumen Production, PhD Thesis, University of Alberta, Edmonton, AB, 2016, p 186.

(33) Lesueur, D. The colloidal structure of bitumen: Consequences on the rheology and on the mechanisms of bitumen modification. *Adv. Colloid Interface Sci.* **2009**, *145* (1-2), 42–82.

(34) Luo, P.; Gu, Y. Effects of asphaltene content on the heavy oil viscosity at different temperatures. *Fuel* **2007**, *86* (7-8), 1069–1078.

(35) Lois, E.; Keating, E. L.; Gupta, A. K. Fuels, In *Encyclopedia of physical science and technology*, ed. by Meyers, R. A., 3rd, San Diego: Academic Press: 2002, pp 275–314.

(36) Hasan, M. A.; Shaw, J. M. Rheology of reconstituted crude oils: Artifacts and asphaltenes. *Energy Fuels* **2010**, *24* (12), 6417–6427.

(37) Pal, R. Modeling and scaling of the viscosity of suspensions of asphaltene nanoaggregates. *Energies* **2017**, *10* (6), 767.

(38) Wang, L.; Zachariah, A.; Yang, S.; Prasad, V.; De Klerk, A. Visbreaking oilsands-derived bitumen in the temperature range of 340-400 °C. *Energy Fuels* **2014**, *28* (8), 5014–5022.

(39) Roscoe, R. The viscosity of suspensions of rigid spheres. *Br. J. Appl. Phys.* **1952**, *3* (8), 267–269.

(40) Brinkman, H. C. The Viscosity of Concentrated Suspensions and Solutions. *J. Chem. Phys.* **1952**, *20* (4), 571–571.

(41) Pal, R. New Generalized Viscosity Model for Non-Colloidal Suspensions and Emulsions. *Fluids* **2020**, *5* (3), 150.

(42) Storm, D. A.; Barresi, R. J.; Sheu, E. Y. Rheological Study of Ratawi Vacuum Residue in the 298-673 K Temperature Range. *Energy Fuels* **1995**, *9* (1), 168–176.

(43) Nourozieh, H.; Kariznovi, M.; Abedi, J. Viscosity measurement and modeling for mixtures of Athabasca bitumen/n-pentane at temperatures up to 200 °C. *SPE J.* **2015**, *20* (02), 226–238.

(44) Nourozieh, H.; Kariznovi, M.; Abedi, J. Viscosity measurement and modeling for mixtures of Athabasca bitumen / hexane. *J. Pet. Sci. Eng.* **2015**, *129*, 159–167.

(45) Ramos-Pallares, F.; Schoeggl, F. F.; Taylor, S. D.; Satyro, M. A.; Yarranton, H. W. Predicting the Viscosity of Hydrocarbon Mixtures and Diluted Heavy Oils Using the Expanded Fluid Model. *Energy Fuels* **2016**, *30* (5), 3575–3595.

(46) Barnes, H. A., *A Handbook of Elementary Rheology*; University of Wales, Institute of Non-Newtonian Fluid Mechanics: 2000, p 200.

(47) Gao, J.; Okuno, R.; Li, H. A. A Phase-Behavior Study for n-Hexane/Bitumen and n-Octane/Bitumen Mixtures. *SPE J.* **2018**, *23* (01), 128–144.

(48) Wallace, D.; Henry, D.; Miadonye, A.; Puttagunta, V. R. Viscosity and Solubility of Mixtures of Bitumen and Solvent. *Fuel Sci. Technol. Int.* **1996**, *14* (3), 465–478.

(49) Miadonye, A.; Latour, N.; Puttagunta, V. R. A correlation for viscosity and solvent mass fraction of bitumen-diluent mixtures. *Pet. Sci. Technol.* **2000**, *18* (1), 1–14.

(50) Centeno, G.; Sánchez-Reyna, G.; Ancheyta, J.; Muñoz, J. A.; Cardona, N. Testing various mixing rules for calculation of viscosity of petroleum blends. *Fuel* **2011**, *90* (12), 3561–3570.

(51) Cragoe, C. S. Changes in the viscosity of liquids with temperature, pressure and composition, In *Proc. World Petrol. Congr. Lond.* 1933, pp 529–541.

(52) Riazi, M. R. Characterization and properties of petroleum fractions, In *American Society and Testing Materials, ASTM Manual Series: MNL50*, 1st ed., 2005, pp 331–338.

(53) PUTTAGUNTA, V. R.; SINGH, B.; MIADONYE, A. Correlation of Bitumen Viscosity with Temperature and Pressure. *Can. J. Chem. Eng.* **1993**, *71* (3), 447–450.

(54) *ASTM D341-20e1: Standard Practice for Viscosity Temperature Equations and Charts for Liquid Petroleum or Hydrocarbon Products*; ASTM International: West Conshohocken, PA: 2020.

(55) Argüelles-Vivas, F. J.; Babadagli, T.; Little, L.; Romaniuk, N.; Ozum, B. High temperature density, viscosity, and interfacial tension measurements of bitumen-pentane-biodiesel and process water mixtures. *J. Chem. Eng. Data* **2012**, *57* (10), 2878–2889.

(56) Bazyleva, A. B.; Hasan, A.; Fulem, M.; Becerra, M.; Shaw, J. M. Bitumen and heavy oil rheological properties: Reconciliation with viscosity measurements. *J. Chem. Eng. Data* **2010**, *55* (3), 1389–1397.

(57) Naghizada, N.; Prado, G. H. C.; de Klerk, A. Uncatalyzed hydrogen transfer during 100–250 °C conversion of asphaltenes. *Energy Fuels* **2017**, *31* (7), 6800–6811.

(58) Masliyah, J.; Zhou, Z. J.; Xu, Z.; Czarnecki, J.; Hamza, H. Understanding Water-Based Bitumen Extraction from Athabasca Oil Sands. *The Can. J. Chem. Eng.* **2008**, *82* (4), 628–654.

(59) Kaminsky, H. A.; Etsell, T. H.; Ivey, D. G.; Omotoso, O. Distribution of clay minerals in the process streams produced by the extraction of bitumen from Athabasca oil sands. *Can. J. Chem. Eng.* **2009**, *87* (1), 85–93.

(60) Zhao, J.; Liu, Q.; Gray, M. R. Characterization of fine solids in Athabasca bitumen froth before and after hydrothermal treatment. *Energy Fuels* **2016**, *30* (3), 1965–1971.

(61) Chen, Q.; Stricek, I.; Cao, M.; Gray, M. R.; Liu, Q. Influence of hydrothermal treatment on filterability of fine solids in bitumen froth. *Fuel* **2016**, *180*, 314–323.

(62) Johnston, C. T. Surface chemistry of oil-sands clay minerals, In *Introduction to Oil Sands Clays*, ed. by Hockley, D.; Omotoso, O.; Kaminsky, H., Vol. 22, Clay Minerals Society: Chantilly, VA, 2018, pp 33–60.

(63) Barton, C. D.; Karathanasis, A. D. Clay minerals, In *Encyclopedia of Soil Science*, ed. by Lal, R., 2nd, CRC Press: Boca Raton, FL, 2005, pp 187–192.

(64) Chen, Q. Organically-modified clay minerals in oil sands: Characterization and effect of hydrothermal treatment, PhD Thesis, University of Alberta, 2017.

(65) Samat, M. H.; Ali, A. M.; Taib, M. F.; Hassan, O. H.; Yahya, M. Z. Hubbard U calculations on optical properties of 3d transition metal oxide TiO2. *Results Phys.* **2016**, *6*, 891–896.

(66) Nabata, H.; Takagi, M.; Saita, K.; Maeda, S. Computational searches for crystal structures of dioxides of group 14 elements (CO2, SiO2, GeO2) under ultrahigh pressure. *RSC Adv.* **2020**, *10* (37), 22156–22163.

(67) He, M.; Wang, Z.; Moldowan, M. J.; Peters, K. Insights into catalytic effects of clay minerals on hydrocarbon composition of generated liquid products during oil cracking from laboratory pyrolysis experiments. *Org. Geochem.* **2022**, *163*, 104331.

(68) Solomon, D. Clay minerals as electron acceptors and/or electron donors in organic reactions. *Clays Clay Miner.* **1968**, *16*, 31–39.

(69) Hensen, E. J.; Poduval, D. G.; Ligthart, D. A.; Van Veen, J. A.; Rigutto, M. S. Quantification of strong brønsted acid sites in aluminosilicates. *J. Phys. Chem. C* **2010**, *114* (18), 8363–8374.

(70) Ding, X.; Repka, C.; Xu, Z.; Masliyah, J. Effect of illite clay and divalent cations on bitumen recovery. *Can. J. Chem. Eng.* **2006**, *84* (6), 643–650.

(71) Ferretto, L.; Glisenti, A. Surface acidity and basicity of a rutile powder. *Chem. Mater.* **2003**, *15* (5), 1181–1188.

(72) Li, H.; Vrinat, M.; Berhault, G.; Li, D.; Nie, H.; Afanasiev, P. Hydrothermal synthesis and acidity characterization of TiO2 polymorphs. *Mater. Res. Bull.* **2013**, *48* (9), 3374–3382.

(73) Turuga, A. S. S.; de Klerk, A. Hydrothermal Treatment of Bitumen Froth: Impact of Mineral Solids and Water on Bitumen Properties. *Energy Fuels* **2021**, *35* (21), 17536–17550.

(74) Feng, X.; Behles, J. A. Understanding the Demulsification of Water-in-Diluted Bitumen Froth Emulsions. *Energy Fuels* **2015**, *29* (7), 4616–4623.

(75) Velayati, A.; Habibi, A.; Nikrityuk, P.; Tang, T.; Zeng, H. Emulsions in Bitumen Froth Treatment and Methods for Demulsification and Fines Removal in Naphthenic Froth Treatment: Review and Perspectives. *Energy Fuels* **2022**, *36* (16), 8607–8623.

(76) Gu, G.; Zhang, L.; Xu, Z.; Masliyah, J. Novel bitumen froth cleaning device and rag layer characterization. *Energy Fuels* **2007**, *21* (6), 3462–3468.

(77) *Oil Sands Magazine - Naphthenic Froth Treatment*, www.oilsandsmagazine.com/technical/mining/froth-treatment/naphthenic (accessed 2023/4/20).

(78) *Oil Sands Magazine - Paraffinic Froth Treatment*, www.oilsandsmagazine.com/technical/mining/froth-treatment/paraffinic (accessed 2023/4/20).

(79) Romanova, U.; Valinasab, M.; Stasiuk, E.; Yarranton, H.; Schramm, L.; Shelfantook, W. The Effect of Oil Sands Bitumen Extraction Conditions on Froth Treatment Performance. *J. Can. Pet. Technol.* **2006**, *45* (9), 36–45.

(80) Romanova, U. G.; Yarranton, H. W.; Schramm, L. L.; Shelfantook, W. E. Investigation of oil sands froth treatment. *Can. J. Chem. Eng.* **2004**, *82* (4), 710–721.

(81) Kosior, D.; Ngo, E.; Xu, Y. Aggregates in Paraffinic Froth Treatment: Settling Properties and Structure. *Energy Fuels* **2018**, *32* (8), 8268–8276.

(82) Kosior, D.; Ngo, E.; Dabros, T. Determination of the Settling Rate of Aggregates Using the Ultrasound Method during Paraffinic Froth Treatment. *Energy Fuels* **2016**, *30* (10), 8192–8199.

(83) Zawala, J.; Dabros, T.; Hamza, H. A. Settling properties of aggregates in paraffinic froth treatment. *Energy Fuels* **2012**, *26* (9), 5775–5781.

(84) Saadatmand, M.; Yarranton, H. W.; Moran, K. Rag layers in oil sand froths. *Ind. Eng. Chem. Res.* **2008**, *47* (22), 8828–8839.

(85) Booran, S. K.; Wang, X.; Tan, X.; Liu, Q. Effect of carbon dioxide on paraffinic bitumen froth treatment: Asphaltene precipitation from a commercial bitumen froth sample. *ACS Omega* **2021**, *6* (18), 11918–11924.

(86) Xu, Y. Asphaltene Precipitation in Paraffinic Froth Treatment: Effects of Solvent and Temperature. *Energy Fuels* **2018**, *32* (3), 2801–2810.

(87) Lin, F.; Pang, C. J. Impact of a hybrid bitumen extraction process on the destabilization of resulting bitumen froth emulsion diluted with heptane. *Miner. Eng.* **2020**, *145*, 106069.

(88) Hristova, E.; Stoyanov, S. R. Bitumen froth treatment in the transition region between paraffinic and naphthenic process conditions. *Fuel* **2021**, *286*, 119385.

(89) Hristova, E.; Tchoukov, P.; Stoyanov, S. R. Coalescence inhibition and agglomeration initiation near the critical dilution of asphaltene precipitation. *Colloids Surfaces A: Physicochem. Eng. Asp.* **2021**, *629*, 127400.

(90) Kailey, I. Properties and Performance of Newly Developed Demulsifiers in Oil Sands Froth Treatment. *Energy Fuels* **2016**, *30* (11), 9233–9241.

(91) Wang, D.; Qiao, C.; Zhao, Z.; Yang, W.; Chen, H.; Yin, T.; Yan, Z.; Wu, M.; Mao, X.; Santander, C.; Liu, Q.; Liu, Q.; Nikrityuk, P. A.; Tang, T.; Zeng, H. Understanding the Properties of Bitumen Froth from Oil Sands Surface Mining and Treatment of Water-in-Oil Emulsions. *Energy Fuels* **2021**, *35* (24), 20079–20091.

(92) Laplante, P.; Machado, M. B.; Bhattacharya, S.; Ng, S.; Kresta, S. M. Demulsifier performance in froth treatment: Untangling the effects of mixing, bulk concentration and injection concentration using a standardized mixing test cell (CIST). *Fuel Process. Technol.* **2015**, *138*, 361–367.

(93) Stammitti-Scarpone, A.; Quraishi, S.; Bhanot, A.; Boza, A.; Ng, S.; Acosta, E. Dewatering of Naphthenic Bitumen Froth. *Energy Fuels* **2020**, *34* (9), 10688–10704.

(94) Ali, M.; Xing, T.; Alem, T.; Chen, J. Investigating the role of aliphatic olefins in fouling of thermally cracked bitumen by testing fouling tendency of model aliphatic olefin compounds in light fractions. *Fuel* **2024**, *360*, 130518.

(95) Zachariah, A. Low temperature pyrolysis and its application in bitumen processing, MSc thesis, University of Alberta, Edmonton, AB, 2014.

(96) Yan, T. Characterization of visbreaker feeds. *Fuel* **1990**, *69* (8), 1062–1064.

(97) Gray, M. R.; McCaffrey, W. C. Role of chain reactions and olefin formation in cracking, hydroconversion, and coking of petroleum and bitumen fractions. *Energy Fuels* **2002**, *16* (3), 756–766.

(98) Barry, J. T.; Berg, D. J.; Tyler, D. R. Radical Cage Effects: The Prediction of Radical Cage Pair Recombination Efficiencies Using Microviscosity Across a Range of Solvent Types. *J. Am. Chem. Soc.* **2017**, *139*, 14399–14405.

(99) Alili, A. S.; Siddiquee, M. N.; De Klerk, A. Origin of Free Radical Persistence in Asphaltenes: Cage Effect and Steric Protection. *Energy Fuels* **2020**, *34*, 348–359.

(100) Yañez Jaramillo, L. M.; Tannous, J. H.; de Klerk, A. Persistent Free Radicals in Petroleum. *Processes* **2023**, *11* (7), 2067.

(101) De Klerk, A. Thermal Conversion Modeling of Visbreaking at Temperatures below 400 °C. *Energy Fuels* **2020**, *34* (12), 15285–15298.

(102) McMillen, D. F.; Golden, D. M. Hydrocarbon bond dissociation energies. *Annu. Rev. Phys. Chem.* **1982**, (33), 493–532.

(103) Budnar Subramanya, A. S. Olefin Hydrotreating and Characterization of Olefins in Thermally Cracked Naphtha, MSc thesis, University of Alberta, Edmonton, Canada, 2020, p 170.

(104) Yan, Y. The Formation of New Asphaltenes during Visbreaking of Vacuum Residue Deasphalted Oil and the Storage Stability of Product from Visbreaking, MSc thesis, Universtiy of Alberta, Edmonton, Canada, 2020, p 117.

(105) Tannous, J. H.; de Klerk, A. Methyl and hydrogen transfer in free radical reactions. *Energy Fuels* **2020**, *34* (2), 1698–1709.

(106) Payan, F.; De Klerk, A. Hydrogen Transfer in Asphaltenes and Bitumen at 250 °C. *Energy Fuels* **2018**, *32* (9), 9340–9348.

(107) Aleman-Vazquez, L. O.; Torres-mancera, P.; Ancheyta, J.; Ramirez-salgado, J. Use of Hydrogen Donors for Partial Upgrading of Heavy Petroleum. *Energy Fuels* **2016**, *30*, 9050–9060.

(108) Raseev, S., *Thermal and Catalytic Processes in Petroleum Refining*; CRC Press: Boca Raton, 2003, p 920.

(109) Cortes-Clerget, M.; Yu, J.; Kincaid, J. R. A.; Walde, P.; Gallou, F.; Lipshutz, B. H. Water as the reaction medium in organic chemistry: from our worst enemy to our best friend. *Chem. Sci.* **2021**, *12* (12), 4237–4266.

(110) Siskin, M.; Katritzky, A. R. Reactivity of Organic Compounds in Superheated Water: General Background. *Chem. Rev.* **2001**, *101* (4), 825–836.

(111) Avola, S.; Guillot, M.; da Silva-Perez, D.; Pellet-Rostaing, S.; Kunz, W.; Goettmann, F. Organic chemistry under hydrothermal conditions. *Pure Appl. Chem.* **2012**, *85* (1), 89–103.

(112) An, J.; Bagnell, L.; Cablewski, T.; Strauss, C. R.; Trainor, R. W. Applications of high-temperature aqueous media for synthetic organic reactions. *J. Org. Chem.* **1997**, *62* (8), 2505–2511.

(113) Savage, P. E. Organic Chemical Reactions in Supercritical Water. *Chem. Rev.* **1999**, *99* (2), 603–622.

(114) Akiya, N.; Savage, P. E. Roles of Water for Chemical Reactions in High-Temperature Water. *Chem. Rev.* **2002**, *102* (8), 2725–2750.

(115) Katritzky, A. R.; Barcock, R. A.; Balasubramanian, M.; Greenhill, J. V.; Siskin, M.; Olmstead, W. N. Aqueous High-Temperature Chemistry of Carbo- and Heterocycles. 20. Reactions of Some Benzenoid Hydrocarbons and Oxygen-Containing Derivatives in Supercritical Water at 460 °C. *Energy Fuels* **1994**, *8* (2), 487–497.

(116) Katritzky, A. R.; Ignatchenko, E. S.; Allin, S. M.; Barcock, R. A.; Siskin, M.; Hudson, C. W. Aqueous High-Temperature Chemistry of Carbo- and Heterocycles. 29. Reactions of Aryl Hydrocarbons, Aryl N- Oxides, and Aryl Carbonyl Compounds in Supercritical Water at 460 °C. *Energy Fuels* **1997**, *11* (1), 160–173.

(117) Katritzky, A. R.; Allin, S. M.; Siskin, M. Aquathermolysis: Reactions of Organic Compounds with Superheated Water. *Acc. Chem. Res.* **1996**, *29* (8), 399–406.

(118) Siskin, M.; Brons, G.; Katritzky, A. R.; Balasubramanian, M. Aqueous organic chemistry. 1. Aquathermolysis: comparison with thermolysis in the reactivity of aliphatic compounds. *Energy Fuels* **1990**, *4* (5), 475–482.

(119) Siskin, M.; Brons, G.; Katritzky, A. R.; Murugan, R. Aqueous organic chemistry. 2. Crosslinked cyclohexyl phenyl compounds. *Energy Fuels* **1990**, *4* (5), 482–488.

(120) Katritzky, A. R.; Balasubramanian, M.; Siskin, M. Aqueous high-temperature chemistry of carbo- and heterocycles. 2. Monosubstituted benzenes: benzyl alcohol, benzaldehyde and benzoic acid. *Energy Fuels* **1990**, *4* (5), 499–505.

(121) Katritzky, A. R.; Luxem, F. J.; Siskin, M. Aqueous high-temperature chemistry of carbo- and heterocycles. 6. Monosubstituted benzenes with two carbon atom side chains unsubstituted or oxygenated at the alpha-position. *Energy Fuels* **1990**, *4* (5), 518–524.

(122) Chen, Y.; Wang, K.; Yang, J. Y.; Yuan, P. Q.; Cheng, Z. M.; Yuan, W. K. Dealkylation of Aromatics in Subcritical and Supercritical Water: Involvement of Carbonium Mechanism. *Ind. Eng. Chem. Res.* **2016**, *55* (36), 9578–9585.

(123) Daud, A. R. M.; Berrueco, C.; Hellgardt, K.; Millan, M.; Kandiyoti, R. Oxidative cracking of three to five-member ring polycyclic aromatic hydrocarbons in subcritical and supercritical water. *J. Supercrit. Fluids* **2021**, *167*, 105050.

(124) Arcelus-Arrillaga, P.; Hellgardt, K.; Millan, M. Effect of process conditions on the hydrothermal partial oxidation of phenanthrene as a heavy oil model structure. *Fuel* **2017**, *209*, 434–441.

(125) Kapadia, P. R.; Kallos, M. S.; Gates, I. D. A review of pyrolysis, aquathermolysis, and oxidation of Athabasca bitumen. *Fuel Process. Technol.* **2015**, *131*, 270–289.

(126) Kapadia, P. R.; Kallos, M. S.; Gates, I. D. A new reaction model for aquathermolysis of Athabasca bitumen. *Can. J. Chem. Eng.* **2013**, *91* (3), 475–482.

(127) Zhang, J.; Han, F.; Yang, Z.; Zhang, L.; Wang, X.; Zhang, X.; Jiang, Y.; Chen, K.; Pan, H.; Lin, R. Significance of aquathermolysis reaction on heavy oil recovery during the steam-assisted gravity drainage process. *Energy Fuels* **2020**, *34* (5), 5426–5435.

(128) Félix, G.; Tirado, A.; Al-Muntaser, A.; Kwofie, M.; Varfolomeev, M. A.; Yuan, C.; Ancheyta, J. SARA-based kinetic model for non-catalytic aquathermolysis of heavy crude oil. *J. Pet. Sci. Eng.* **2022**, *216*, 110845.

(129) Jia, N.; Zhao, H.; Yang, T.; Ibatullin, T.; Gao, J. Experimental measurements of bitumen–water aquathermolysis during a steam-injection process. *Energy Fuels* **2016**, *30* (7), 5291–5299.

(130) Hongfu, F.; Yongjian, L.; Liying, Z.; Xiaofei, Z. The study on composition changes of heavy oils during steam stimulation processes. *Fuel* **2002**, *81* (13), 1733–1738.

(131) Qu, X.; Zhou, G.; Lu, Y.; Li, S.; Zhang, L.; Wang, J.; Xu, H. Catalytic aquathermolysis of Mackay River bitumen with different types of Mo-based catalysts. *Fuel* **2022**, *326*, 125134.

(132) Canıaz, R. O.; Arca, S.; Yaşar, M.; Erkey, C. Refinery bitumen and domestic unconventional heavy oil upgrading in supercritical water. *J. Supercrit. Fluids* **2019**, *152*, 104569.

(133) Liu, Y.; Bai, F.; Zhu, C. C.; Yuan, P. Q.; Cheng, Z. M.; Yuan, W. K. Upgrading of residual oil in sub-and supercritical water: An experimental study. *Fuel Process. Technol.* **2013**, *106*, 281–288.

(134) Wahyudiono; Shiraishi, T.; Sasaki, M.; Goto, M. Non-catalytic liquefaction of bitumen with hydrothermal/solvothermal process. *J. Supercrit. Fluids* **2011**, *60*, 127–136.

(135) Sato, T.; Adschiri, T.; Arai, K.; Rempel, G. L.; Ng, F. T. Upgrading of asphalt with and without partial oxidation in supercritical water. *Fuel* **2003**, *82* (10), 1231–1239.

(136) Sato, T.; Trung, P. H.; Tomita, T.; Itoh, N. Effect of water density and air pressure on partial oxidation of bitumen in supercritical water. *Fuel* **2012**, *95*, 347–351.

(137) Schlepp, L.; Elie, M.; Landais, P.; Romero, M. Pyrolysis of asphalt in the presence and absence of water. *Fuel Process. Technol.* **2001**, *74* (2), 107–123.

(138) Dutta, R. P.; McCaffrey, W. C.; Gray, M. R.; Muehlenbachs, K. Thermal cracking of Athabasca bitumen: influence of steam on reaction chemistry. *Energy Fuels* **2000**, *14* (3), 671–676.

(139) Cheng, Z. M.; Ding, Y.; Zhao, L. Q.; Yuan, P. Q.; Yuan, W. K. Effects of supercritical water in vacuum residue upgrading. *Energy Fuels* **2009**, *23* (6), 3178–3183.

(140) Yuan, P. Q.; Zhu, C. C.; Liu, Y.; Bai, F.; Cheng, Z. M.; Yuan, W. K. Solvation of hydrocarbon radicals in sub-CW and SCW: An ab initio MD study. *J. Supercrit. Fluids* **2011**, *58* (1), 93–98.

(141) Ovalles, C.; Hamana, A.; Rojas, I.; Bolívar, R. A. Upgrading of extra-heavy crude oil by direct use of methane in the presence of water: deuterium-labelled experiments and mechanistic considerations. *Fuel* **1995**, *74* (8), 1162–1168.

(142) Fan, H.; Zhang, Y.; Lin, Y. The catalytic effects of minerals on aquathermolysis of heavy oils. *Fuel* **2004**, *83* (14-15), 2035–2039.

(143) Zhong, M.; Huang, H.; Xu, P.; Hu, J. Catalysis of Minerals in Pyrolysis Experiments. *Minerals* **2023**, *13* (4), 515.

(144) Wu, L. M.; Zhou, C. H.; Keeling, J.; Tong, D. S.; Yu, W. H. Towards an understanding of the role of clay minerals in crude oil formation, migration and accumulation. *Earth-Science Rev.* **2012**, *115* (4), 373–386.

(145) Tannenbaum, E.; Huizinga, B. J.; Kaplan, I. R. Role of Minerals in Thermal Alteration of Organic Matter–II: A Material Balance. *AAPG Bull.* **1986**, *70* (9), 1156–1165.

(146) Henderson, W.; Eglinton, G.; Simmonds, P.; Lovelock, J. E. Thermal Alteration as a Contributory Process to the Genesis of Petroleum. *Nature* **1968**, *219* (5158), 1012–1016.

(147) Huizinga, B. J.; Tannenbaum, E.; Kaplan, I. R. The role of minerals in the thermal alteration of organic matter - IV. Generation of n-alkanes, acyclic isoprenoids, and alkenes in laboratory experiments. *Geochim. Cosmochim. Acta* **1987**, *51* (5), 1083–1097.

(148) Eglinton, T.; Rowland, S.; Curtis, C.; Douglas, A. Kerogen-mineral reactions at raised temperatures in the presence of water. *Org. Geochem.* **1986**, *10* (4-6), 1041–1052.

(149) Dembicki, H. The effects of the mineral matrix on the determination of kinetic parameters using modified Rock Eval pyrolysis. *Org. Geochem.* **1992**, *18* (4), 531–539.

(150) Smolen, J. D.; Hren, M. T. Differential effects of clay mineralogy on thermal maturation of sedimentary n-alkanes. *Chem. Geol.* **2023**, *634*, 121572.

(151) Bu, H.; Yuan, P.; Liu, H.; Liu, D.; Liu, J.; He, H.; Zhou, J.; Song, H.; Li, Z. Effects of complexation between organic matter (OM) and clay mineral on OM pyrolysis. *Geochim. Cosmochim. Acta* **2017**, *212*, 1–15.

(152) Bu, H.; Wei, Y.; Liu, C.; Liu, D.; Tan, D.; Liu, H. Effects of illite–smectite clay minerals on the thermal evolution of aliphatic organic matter-clay complexes: a study with thermogravimetry coupled with Fourier transform infrared spectroscopy (TG-FTIR). *J. Therm. Anal. Calorim.* **2023**, *148* (3), 741–752.

(153) Zafar, R.; Watson, J. S. Adsorption of tetradecanoic acid on kaolinite minerals: Using flash pyrolysis to characterise the catalytic efficiency of clay mineral adsorbed fatty acids. *Chem. Geol.* **2017**, *471*, 111–118.

(154) Liu, H.; Yuan, P.; Liu, D.; Bu, H.; Song, H.; Qin, Z.; He, H. Pyrolysis behaviors of organic matter (OM) with the same alkyl main chain but different functional groups in the presence of clay minerals. *Appl. Clay Sci.* **2018**, *153*, 205–216.

(155) Liu, H.; Yuan, P.; Qin, Z.; Liu, D.; Tan, D.; Zhu, J.; He, H. Thermal degradation of organic matter in the interlayer clay–organic complex: A TG-FTIR study on a montmorillonite/12-aminolauric acid system. *Appl. Clay Sci.* **2013**, *80-81*, 398–406.

(156) Liu, H.; Yuan, P.; Liu, D.; Tan, D.; He, H.; Zhu, J. Effects of solid acidity of clay minerals on the thermal decomposition of 12-aminolauric acid. *J. Therm. Anal. Calorim.* **2013**, *114* (1), 125–130.

(157) Turuga, A. S. S.; de Klerk, A. Free Radical and Cationic Addition due to Clay Minerals Found in Bitumen Froth at 250 °C Probed with Use of α-Methylstyrene and 1-Octene. *Energy Fuels* **2022**, *36* (23), 14148–14162.

(158) Kleber, M.; Bourg, I. C.; Coward, E. K.; Hansel, C. M.; Myneni, S. C.; Nunan, N. Dynamic interactions at the mineral–organic matter interface. *Nat. Rev. Earth Environ.* **2021**, *2* (6), 402–421.

(159) Solomon, D. H.; Rosser, M. J. Reactions catalyzed by minerals. Part I. Polymerization of styrene. *J. Appl. Polym. Sci.* **1965**, *9* (4), 1261–1271.

(160) Yang, Z.; Gould, I. R.; Williams, L. B.; Hartnett, H. E.; Shock, E. L. Effects of iron-containing minerals on hydrothermal reactions of ketones. *Geochim. Cosmochim. Acta* **2018**, *223*, 107–126.

(161) Choudhury, T.; Misra, N. M. Role of clay as catalyst in Friedel-Craft alkylation. *Bull. Mater. Sci.* **2011**, *34* (6), 1273–1279.

(162) Ishiwatari, M. Thermal reaction of β-carotene. *J. Anal. Appl. Pyrolysis* **1981**, *2* (4), 339–351.

(163) Cai, J.; Du, J.; Song, M.; Lei, T.; Wang, X.; Li, Y. Control of clay mineral properties on hydrocarbon generation of organo-clay complexes: Evidence from high-temperature pyrolysis experiments. *Appl. Clay Sci.* **2022**, *216*, 106368.

(164) Phillips, C. R.; HAidar, N. I.; Poon, Y. C. Kinetic models for the thermal cracking of Athabasca bitumen: The effect of the sand matrix. *Fuel* **1985**, *64*, 678–691.

(165) Strausz, O. P.; Jha, K. N.; Montgomery, D. S. Chemical composition of gases in Athabasca bitumen and in low-temperature thermolysis of oil sand , asphaltene and maltene. *Fuel* **1977**, *56*, 114–120.

(166) Ovalles, C.; Vallejos, C.; Vasquez, T.; Rojas, I.; Ehrman, U.; Benitez, J. L.; Martinez, R. Downhole Upgrading of Extra-heavy Crude Oil Using Hydrogen Donors and Methane Under Steam Injection Conditions. *Pet. Sci. Technol.* **2003**, *21* (1-2), 255–274.

(167) Lechner, C. A.; Findley, M. E.; Liapis, A. I. Kinetics of the Pyrolysis of Utah Tar Sands. *Can. J. Chem. Eng.* **1987**, *65*, 487–493.

(168) Murugan, P.; Mani, T.; Mahinpey, N.; Dong, M. Pyrolysis kinetics of Athabasca bitumen using a TGA under the influence of reservoir sand. *Can. J. Chem. Eng.* **2012**, *90* (2), 315–319.

(169) Rong, T. J.; kai Xiao, J. The catalytic cracking activity of the kaolin-group minerals. *Mater. Lett.* **2002**, *57* (2), 297–301.

(170) Zheng, R.; Liu, D.; Tang, J.; Song, Q.; Yao, Q. Analysis of montmorillonite affecting coke formation during the thermal conversion of heavy oil. *Fuel* **2021**, *288*, 119687.

(171) Zhou, Z.; Slaný, M.; Kuzielová, E.; Zhang, W.; Ma, L.; Dong, S.; Zhang, J.; Chen, G. Influence of reservoir minerals and ethanol on catalytic aquathermolysis of heavy oil. *Fuel* **2022**, *307*, 121871.

(172) Sitnov, S. A.; Khelkhal, M. A.; Mukhamatdinov, I. I.; Feoktistov, D. A.; Vakhin, A. V. Iron oxide nanoparticles impact on improving reservoir rock minerals catalytic effect on heavy oil aquathermolysis. *Fuel* **2022**, *327*, 124956.

(173) Mecón Méndez, S. G.; Salas-Chia, L. M.; Martínez Vertel, J. J.; Molina Velasco, D. R.; León, A. Y.; León, P. A. Effect of Mineralogy on the Physicochemical Properties of a Heavy Crude Oil in Hybrid Steam Injection Technologies Using 1H NMR. *Energy Fuels* **2022**, *36* (17), 10315–10326.

(174) Zhang, W.; Li, Q.; Li, Y.; Dong, S.; Peng, S.; Chen, G. Viscosity Reduction and Mechanism of Aquathermolysis of Heavy Oil Co-Catalyzed by Bentonite and Transition Metal Complexes. *Catalysts* **2022**, *12* (11), 1383.

Chapter 3

Visbreaking of Bitumen Froth: Influence of Minerals, Water, and Solvent on the Physicochemical Changes in the Bitumen Phase

Abstract

Thermal treatment of oilsands bitumen froth has the goal of not only improving the separation process during froth treatment but also accomplishing bitumen upgrading. There is evidence that both water and minerals have an effect on the physicochemical transformations taking place during the treatment. However, little is known about the nature of these transformations and whether the presence of mineral solids and water can be beneficial. The current study investigated the visbreaking of froth at 400 °C with an average equivalent residence time of 30 min. The froth elements (mineral solids and water) were either separated or maintained in the mixture to assess their effects during visbreaking. Visbreaking was performed in the absence and presence of hydrocarbon solvents (*n*-hexane and kerosene). Viscosity, density, refractive index, elemental composition, persistent free radical content, and nature of hydrogen and carbon content were evaluated before and after the treatment. The products from froth visbreaking on a solvent-free bitumen basis had a kinematic viscosity in the range $1\text{–}4\times10^3$ mm^2/s at 7.5 °C and a density in the range 990–1000 kg/m^3 at 15.6 °C. When visbreaking was performed in the presence of *n*-hexane, the products had a lower increase in aromatic C, lower viscosity, and lower density on solvent-free basis compared to the products from visbreaking performed in kerosene or without a solvent. The presence of mineral solids and/or water during bitumen visbreaking consistently yielded a bitumen product with numerically higher viscosity and density compared to visbreaking of bitumen alone. Mineral solids and water affected hydrogen transfer reactions during visbreaking, which could be seen in terms of the relative change in aromatic H and C content in the products. When mineral solids were present, some products were adsorbed on the solids, which also affected the H/C and free radical content of the liquid product.

3.1 Introduction

During the early stages of bitumen production from mining operations, bitumen needs to be disengaged from the bulk of mineral matter in a process known as hot water extraction. In this process, crushed oilsands ores are mixed with warm water (50–80 °C) and pumped through hydrotransport pipelines, which promote the breakage of the oilsands lumps and facilitate the release of bitumen from the mineral matter. Then, the resulting slurry is sent to primary separation vessels, generating a mixture named froth, which consists of bitumen ($\sim$60 wt%), water ($\sim$30 wt%) and minerals ($\sim$10 wt%) [1, 2].

Water and minerals removal is achieved through the froth treatment process, in which the addition of a solvent facilitates the separation of these components by lowering the density and viscosity of bitumen [3]. Two main technologies are currently used for treating froth and are classified according to the type of solvent used during the process, namely paraffinic froth treatment (PFT) and naphthenic froth treatment (NFT). The treated bitumen product contains less than 2 wt% of water and less than 0.5 wt% of minerals [3, 4].

To produce oilsands bitumen as a marketable product, both froth treatment [3, 5, 6] and upgrading [7–9] processes have been individually investigated. However, intrigued by the possible outcomes from a synergetic perspective, the following question was posed: What would be the benefits of upgrading bitumen in the presence of froth minerals and/or water?

For instance, Chen et al.[10] investigated the direct thermal treatment of froth in the temperature range 300–400 °C and identified that it improved the separation of minerals from bitumen. The best filtration result was obtained after the thermal treatment at 390 °C for 30 min, which decreased the filtration time from infinity (non-thermally treated froth plugged the filter membrane and was not able to be filtered) to 150 s. The authors suggested that a change in the surface properties of the fine solids facilitated the minerals separation through filtration, forming a product with a lower solids content. The main findings used to corroborate the authors' claim were: a) hydrothermal treatment at 390 °C increased the coverage of organic matter on the minerals' surface, modifying the wettability of the fine solids, which became more hydrophobic; b) the changes on the minerals' surface allowed the release of bulk bitumen and ultrafine solids that were trapped inside mineral aggregates before thermal treatment; c) these ultrafine minerals got attached to the clay particles, altering the stacking of clays, making the filter cake more permeable, and, consequently, improving the solids filtration.

There is evidence that thermal treatment of bitumen in the presence of fine minerals not only improves the separation of solids but also contributes to changes in the chemical nature of the bitumen phase. For example, Sanaie et al.[11] showed that thermal treatment of bitumen at 380–400 °C in the presence of native clays reduced the coke yield by 25% compared with a mineral-free feed. Other related studies [12, 13], investigated the role of mineral solids in the kinetics of coke formation during coking of a bitumen vacuum residue at 430 °C. The authors identified that the presence of minerals suppressed coke formation compared with a solids-free feed and suggested that the decrease in the rate of coke formation was due to a stabilization mechanism in which the minerals participated as dispersant agents for coke precursors.

The upgrading of bitumen in the presence of water has also been explored. The term aquathermolysis has been cited many times in the literature, referring to both non-catalytic and catalytic thermal conversion of bitumen (or heavy oils) in the presence of steam/hot water [14–17]. Most of these studies are related to subsurface upgrading of oilsands and were performed in the temperature range of 200–350 °C for long reaction times. Qu et al.[16] studied the non-catalytic hydrothermal treatment of oilsands bitumen in the temperature range 200–350 °C with reaction times varying from 6 to 24 h. The authors found that hydrothermal treatment provided a higher viscosity reduction when compared to thermal treatment without water at the same temperature and reaction time.

It was also suggested that the mineral matrix might present a catalytic effect during hydrothermal treatment. Fan et al.[18] studied the synergetic effects of minerals and steam on the physicochemical changes of three types of heavy oils after hydrothermal treatment at 240 °C for 24 hours. The authors found out that the presence of minerals during the treatment changed the concentration of solubility classes, specifically increasing the amount of saturates and aromatics and reducing the amount of resins and asphaltenes when compared to the treatment in the absence of minerals. In other studies, the presence of minerals during hydrothermal treatment of heavy oils also had an impact on the composition of the formed gas phase [19, 20]. No direct evidence was presented in any of these studies that the effect of minerals was catalytic, although it was clear that the minerals affected the reaction. More recently, it was reported that kaolinite and illite, two clay minerals in bitumen froth, caused predominantly cationic conversion at 250 °C [21].

The present study aimed to investigate the role of water, minerals, and solvent dilution on the physicochemical changes in the bitumen phase during froth visbreaking. The main objectives of this study were: 1) to identify whether minerals and water can improve bitumen quality during upgrading by lowering its viscosity and density; and 2) to study the effect of froth dilution with a paraffinic and a naphthenic solvent on the changes in bitumen properties during visbreaking.

Initially, it was considered to combine the froth treatment and upgrading in a single step by increasing the froth treatment temperature to 250 °C (the maximum temperature achievable by steam heating without resorting to the use of a furnace). However, a previous investigation showed that this temperature was insufficient to improve the bitumen's properties [22]. Therefore, the present study is not a proposal to modify the current froth treatment technologies but rather an investigation into the effects of froth elements (minerals and water) during bitumen thermal treatment.

The current study focused on the visbreaking of non-diluted and diluted froth (and decoupled elements from froth) at 400 °C in order to evaluate the possible influences of minerals, water, and solvents on bitumen properties during thermal conversion.

3.2 Experimental Section

3.2.1 Materials

The froth used in this study was obtained from the Canadian oilsands mining industry. The characterization of the froth and froth components is reported as part of the Results section. Additional characterization of the froth components has been reported before [22]. The list of chemicals and cylinder gases used in this study is listed in **Table 3.1**.

The solids found in the froth used in this study were previously characterized [22]. The two most abundant minerals were quartz (53 wt%) and kaolinite (26 wt%).

Table 3.1: List of chemicals and cylinder gases used in the study.

Compound	Formula	CASRN[a]	Purity (%)[b]	Supplier
Chemicals				
n-Hexane	C_6H_{14}	110-54-3	95	Sigma Aldrich
Benzene	C_6H_6	71-43-2	99.8	Sigma Aldrich
Hydranal composite 5	-	-	-	Honeywell
Tetrahydrofuran	C_4H_8O	109-99-9	99.9	Fisher Scientific
Toluene	C_7H_8	108-88-3	99.9	Fisher Scientific
Chloroform-d	$CHCl_3$	865-49-6	99.8[c]	Acros Organic
2,2-diphenyl-1-picrylhydrazyl (DPPH)	$C_{18}H_{12}N_5O_6$	1898-66-4	-	Sigma Aldrich
Cylinder gas				
Nitrogen	N_2	7727-37-9	99.999[d]	Praxair

[a] Chemical Abstracts Services Registry Number (CASRN);

[b] Purity of material provided by the supplier. Material was not further purified;

[c] Atom D purity; [d] Mol% purity

A commercial naphthenic kerosene obtained from a Canadian petroleum refinery, *n*-hexane, and benzene were used to dilute the froth before the visbreaking reactions and to facilitate water and solids separation whenever necessary. The choice of *n*-hexane to represent a light paraffinic solvent as opposed to using a light straight-run naphtha (C_5–C_6 mixture) was a pragmatic decision for ease of experimental work and reduced risk of evaporative solvent loss.

The characterization of these solvents is shown in **Table 3.2**. Viscosity, density, and refractive index were measured at three different temperatures for each solvent (kerosene – 25, 40 and 60 °C; *n*-hexane and benzene – 25, 30 and 35 °C) in order to allow the correction of these properties for the bitumen/solvent mixtures after visbreaking (i.e., by removing the effect of the solvent and reporting the properties of bitumen on a solvent-free basis). The linear dependence of density and refractive index with temperature was also calculated, and the slopes ($d\rho/dT$ and dn/dT) and the coefficients of determination (R^2) are reported in **Table 3.2**. This information was useful in determining the internal consistency of the measurements.

Table 3.2: Characterization of the solvents used in the study.

Property	Solvent		
	Kerosene	*n*-Hexane	Benzene
Viscosity - μ (mPa·s)^a			
25 °C	1.3	0.29	0.60
30 °C	-	0.27	0.56
35 °C	-	0.26	0.52
40 °C	1.0	-	-
60 °C	0.78	-	-
Density - ρ (kg/m^3)			
25 °C	805.1	654.4	873.6
30 °C	-	650.3	868.2
35 °C	-	645.7	862.7
40 °C	794.2	-	-
60 °C	779.2	-	-
dρ/dT	-0.7405	-0.8700	-1.090
R^2	0.999	0.999	1
Refractive Index - *n*			
25 °C	1.4479	1.3720	1.4974
30 °C	-	1.3693	1.4942
35 °C	-	1.3665	1.4911
40 °C	1.4413	-	-
60 °C	1.4328	-	-
dη/dT	-4.3E-4	-5.5E-4	-6.3E-4
R^2	0.999	0.999	0.999
Boiling Point (°C)	199.4 – 295.3	69.0	80.1
Elemental composition (wt%)			
C	86.2	83.6^b	96.3^b
H	13.8	16.4^b	7.7^b
N	< 0.2	0^b	0^b
S	0	0^b	0^b
O	0	0^b	0^b
H Content (%)			

Continues on the next page

Property	Solvent		
	Kerosene	*n*-Hexane	Benzene
Aliphatic	95.8	100.0[b]	0[b]
Aromatic	4.2[c]	0[b]	100.0[b]
Bromine number (g Br_2/100 g)	0	0[b]	0[b]

[a] The temperature dependence of viscosity could not be fitted using the general form of the MacCoull equation used in ASTM D341[23] because it requires the viscosity, and μ (viscosity), to be higher than 1 mPa·s. Refer to **Section 3.2.4** for more details.

[b] Theoretical value, not measured by any technique. [c] Naphthene-aromatic species with hydrogen transfer ability were identified in the kerosene through gas chromatography mass spectrometry. To cite, the relative area of tetralin compared to the area of the entire chromatogram was 0.10%, while the relative area of indane was 0.06%.

3.2.2 Equipment and Procedure

3.2.2.1 Froth composition

The quantification of bitumen, water, and solids in the froth used in this study was performed using a Dean-Stark apparatus. The froth sample was contained in a 2-L jar and presented free water separated from the bitumen/solids mixture. The sub-sampling of froth proceeded by heating up the jar to 70 °C (using a water bath) to facilitate the homogenization of froth by using a spatula. Then, eight froth samples were collected for characterization through Dean-Stark extraction.

For this extraction, around 25–78 g of froth sample were placed in an empty and previously weighed thimble (filtering container). The solvent used for the extraction was toluene (200 mL), and the temperature of the heating plates was set to 225 °C (the internal temperature was determined by refluxing toluene at around 110 °C). The refluxing continued until the toluene dripping from the thimble was colorless and the water level in the trap was stable for at least 3 hours. Then, the separated water was collected from the trap into a plastic bottle and weighed. The thimble containing solids and toluene was placed in the fume hood for 3 days to evaporate the toluene.

Next, the solids weight was obtained by weighing the thimble containing the dry solids and taking the difference from the empty thimble weight. The flask containing diluted bitumen was cooled to room temperature, and its contents were transferred into a 250-mL flask. Additional toluene was added to the flask to reach the 250-mL mark. Then, 5 mL of diluted bitumen was poured over a weighed filter paper, which was left in a ventilated fume hood to evaporate the solvent. The increase in weight of the filter paper times 50 gave the mass of bitumen in the original froth sample. The composition of the eight froth samples is reported in the **Results** (**Section 3.3.1**).

3.2.2.2 Separation of water and solids from bitumen in froth and feed preparation

Four types of systems containing froth, or elements from froth, were used as feed in the reactions performed in this study: froth (B+W+S), bitumen + water (B+W), bitumen + solids (B+S) and bitumen alone (B). For this reason, bitumen, water, and solids were isolated from each other in order to allow control over the composition of the different types of feed.

The froth sample was originally contained in a 2-L jar with two separate phases: a top layer containing free water and a bottom layer containing a semi-solid mixture of bitumen, solids, and emulsified water. First, the free water was carefully collected using a glass pipette and transferred into a 500-mL jar. Then, the remaining semi-solid mixture was heated to approximately 70 °C to facilitate homogenization through the use of a spatula, and aliquots of the mixture were transferred into 25-mL jars. These aliquots were used to prepare the feed for reactions containing B+W+S and B+S.

For the preparation of the feed containing B+W and only bitumen (B), further separation steps were necessary to remove the solids and emulsified water. Three solvents were selected for this purpose (kerosene, *n*-hexane, and benzene; the solvents were individually used and not mixed together), and the type of solvent used for each feed preparation depended on the experimental group (refer to **Section 3.2.2.3** for more details) that used that specific feed.

This solvent-facilitated separation was performed by diluting bitumen with kerosene, *n*-hexane, or benzene (20 wt% of solvent in relation to bitumen when kerosene and benzene were used as diluents; 13 wt% of solvent in relation to bitumen when *n*-hexane was used as diluent), heating up the solution to 80 °C (when kerosene was used as solvent) or 50 °C (when *n*-hexane or benzene were used as solvents), and centrifuging it using an Eppendorf Centrifuge 5430 at 7000 rpm for 30 min. The samples were placed in the centrifuge while still hot, but were allowed to cool down during centrifugation. After centrifugation, three phases were visible in the centrifuge tube: a top supernatant layer containing diluted bitumen, an intermediate thin layer of water, and a bottom layer consisting of a pellet of solids. Then, the diluted bitumen in the supernatant was transferred using a pipette (avoiding touching the water phase and the solids pellet at the centrifuge tube bottom) to a filtration system built with 316 stainless steel Swagelok tubing, fittings, and a tee-type filter of 0.5 μm (**Figure A.1 in Appendix A**). The entire system was then pressurized with nitrogen up to 5 MPa, and the filtrate was collected in a 50-mL jar. This filtration was necessary to remove the fine solids that remained in suspension after the centrifugation.

A schematic diagram showing the separation of the froth elements used to prepare the feed for the visbreaking reactions containing diluted bitumen is shown in **Figure 3.1**.

For reactions containing non-diluted bitumen, benzene was the solvent used to allow water and solids separation following the abovementioned procedure. Then, non-diluted bitumen was obtained by removing benzene through rotary evaporation for 6 hours at a temperature of 65 °C and an absolute pressure of 10 kPa. The residual benzene content in the bitumen feed was measured by thermogravimetric analysis and was found to be lower than 1 wt% after the rotary evaporation.

3.2.2.3 Froth visbreaking

Visbreaking of froth and froth components was carried out using a 53-mL batch microreactor built with 316 stainless steel Swagelok tubing and fittings, equipped with a pressure gauge and a thermocouple (**Figure A.2 in Appendix A**). The feed consisted of four types of systems (**Table 3.3**) containing different elements from froth in order to decouple the effects of water and solids during the thermal treatment.

Three groups of experiments were performed for each reaction system: Group I contained bitumen diluted with kerosene as part of the reaction feed; Group II contained bitumen diluted with *n*-hexane; and Group III contained non-diluted bitumen.

For the reactions of Group I, the feed was diluted with 20 wt% of kerosene in relation to bitumen

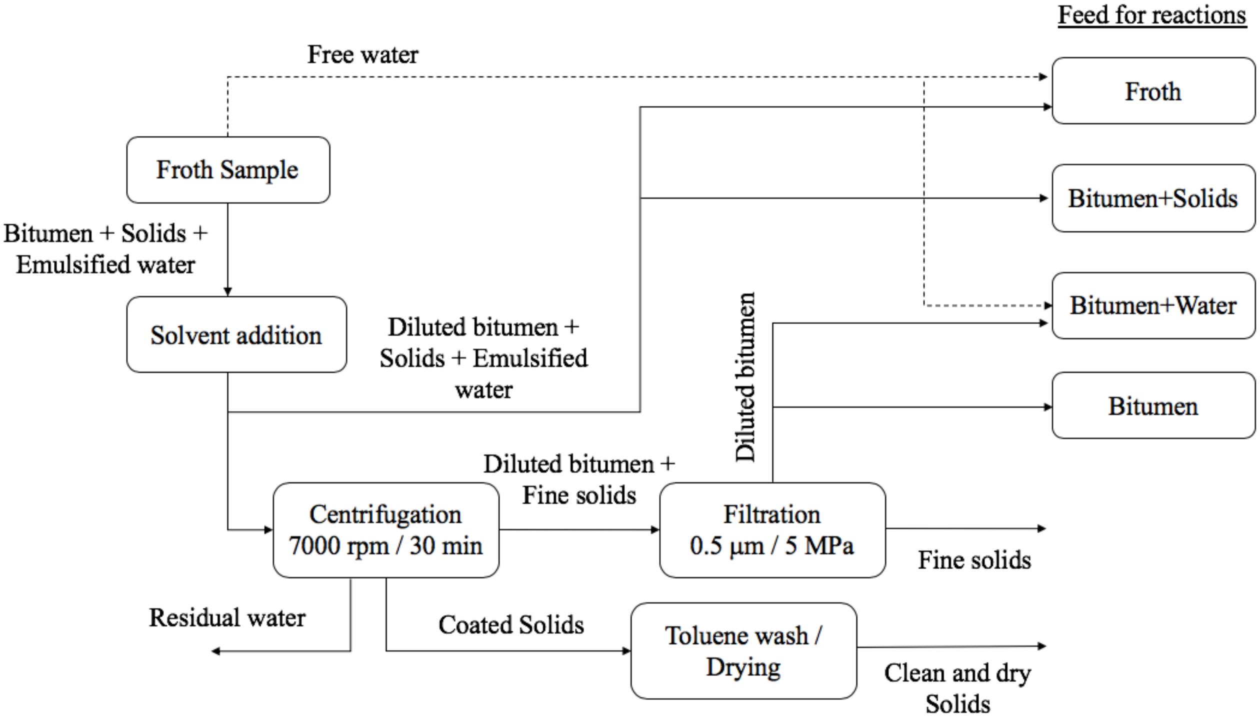

Figure 3.1: Schematic diagram of the separation of froth elements used to prepare the feed for visbreaking reactions containing diluted bitumen.

(i.e., 20 wt% of kerosene taking into account the amount of kerosene and bitumen alone). For the reactions of Group II, the feed was diluted with 13 wt% of *n*-hexane in relation to bitumen. This dilution was necessary to allow solids and water removal (the same procedure described in **Section 3.2.2.2**) for both feed and product analysis preparation. For the group of experiments containing non-diluted bitumen (Group III), 10 wt% of benzene (in relation to bitumen) was added to the untreated bitumen and products of all reaction systems after the visbreaking reaction to allow water and solids removal (whenever necessary) and for analysis preparation. In order to avoid the loss of light components that might have been formed during visbreaking, benzene was not removed from the products before further characterization.

In a typical reaction, around 24–27 g of feed was loaded into the reactor, which was then closed, purged with nitrogen, and pressurized to 1 MPa under a nitrogen atmosphere at ambient temperature. The microreactor was then inserted in a fluidized sand bath heater (Omega Fluidized Bath FSB-3), which was preheated to a temperature of 400 °C. The temperature inside the reactor was monitored throughout the reaction time using an internal thermocouple. The reaction proceeded

Table 3.3: Feed composition used in the visbreaking reactions. B – Bitumen; W – Water; S - Solids.

System	Content (wt%)		
	Diluted bitumen^a or non-diluted bitumen^b	Water	Solids
B+W+S	78	13	9
B+W	87	13	-
B+S	89	-	11
B	100	-	-

^{a}Groups I and II experiments. ^{b}Group III experiments.

for about 30 min. The reactor was then removed from the sand bath and cooled using a compressed air stream at ambient temperature.

In a typical experiment, the temperature inside the reactor varied in the range 400 ± 5 °C throughout the reaction time. The temperature profile inside the reactor during a typical experiment is shown in **Figure A.3** in **Appendix A**. In order to report a residence time that includes both the heat-up and cool-down times, and the temperature variations during the reaction period, the equivalent residence time (ERT), as defined by Yan [24], was calculated for each reaction according to **Eq. 3.1**, where Δt_i are defined time intervals consisting of two recorded temperatures (T_i and T_{i+1}), T_{ref} is the reference temperature for which the ERT is being calculated, E_a = 209500 J mol^{-1}, and R = 8.314 J mol^{-1} K^{-1}. Details on how the ERT calculation was performed are described in **Appendix A** (**Section A.4**). The ERT for each reaction is presented in the **Results** (**Section 3.3**).

$$ERT\ at\ T_{ref} = \sum_{i=1}^{n} \Delta t_i \times exp\left[\left(-\frac{E_a}{R}\right)\left(\frac{1}{\frac{T_i + T_{i+1}}{2}} - \frac{1}{T_{ref}}\right)\right] \tag{3.1}$$

After the product was collected from the reactor, minerals and water (whenever present) were removed from the bitumen before the analyses, so that the reported properties refer to the bitumen phase only. The removal of water and minerals before analysis was performed following the same steps of centrifugation, bitumen transfer, and filtration as described in **Section 3.2.2.2**.

3.2.2.4 Analyses

Viscosity measurements were performed using an Anton Paar RheolabQC viscometer. Around 4 g of sample was loaded into a concentric cylinder measuring cup (CC17/QC-LTC) with an internal diameter of 16.664 mm and a length of 24.970 mm. The temperature of the sample was controlled by a circulating heater/chiller (Julabo F25-EH) connected to the measuring cup. For the products of Group I, the measurements were performed at 25, 40, and 60 °C, with shear rates varying from 100 to 1000 s^{-1}. For the products of Groups II and III, the measurements were performed at 25, 30, and 35 °C, with shear rates varying from 100 to 600 s^{-1}, to avoid loss of solvent because of the high volatility of *n*-hexane and benzene. Next, the shear stress values were plotted against the corresponding shear rate values to confirm the Newtonian behavior of the mixture. The dynamic viscosity was then calculated by extracting the slope of the linear regression from the shear stress versus shear rate curve.

Density measurements were carried out on an Anton Paar density meter (DMA 4500M). The instrument temperature control was able to keep the temperature constant to within 0.01 °C. Around 1 ml of sample was injected in the instrument by using a syringe, and measurements were taken at 25, 40, and 60 °C for Group I experiments and 25, 30, and 35 °C for Groups II and III.

Refractive index analyses were carried out on an Anton Paar Abbemat 200. Measurements were performed at the same temperatures as the density analyses. For Group I products, the measurements did not vary with time at all measured temperatures (25, 40, and 60 °C). However, the refractive index measurements at 25, 30, and 35 °C for Groups II and III did not stabilize due to solvent evaporation. The measurement variation with time was probably caused by the high volatility of *n*-hexane and benzene, the small amount of sample used for the measurement ($\sim$0.1 mL), and the fact that the measurement cell is an open system. For this reason, the following methodology was applied for Groups II and III samples: the equipment temperature was set at 35 °C and refractive index measurements were taken every 10 min at that temperature; at the 60-min mark (when solvent evaporation ramped down), the measurements at the other temperatures (25 and 30 °C) were also taken.

Water content was determined by Karl Fischer (KF) titration using a KF titrator V20S equipped with a DM-143 SC electrode. In a typical analysis, around 5 g of sample was dissolved in 10 mL of tetrahydrofuran (THF), and the weights of both sample and solvent were noted. Next, a known amount of diluted sample was titrated with Hydranal Composite 1, and the amount of titrant at the end point was used to calculate the amount of water in the diluted sample. The amount of moisture in THF was also determined using the same method in order to determine the water content of the bitumen sample.

Elemental analysis of kerosene and bitumen samples was performed at the Analytical and Instrumentation Laboratory of the Department of Chemistry at the University of Alberta. The equipment used was a Thermo Flash 2000 Elemental Analyzer.

The olefin content of kerosene was determined by bromine number analysis, following the ASTM D1159 standard [25]. The equipment used was a Mettler Toledo titrator T70 equipped with a DM-143 SC electrode.

Thermogravimetric analysis of bitumen-coated solids was carried out using a Mettler Toledo TGA/DSC1. Around 10 mg of sample, inserted in a 70 μL alumina crucible, was used for each analysis. The temperature program was set to determine the weight loss in three regions: first, the sample was heated from 25 to 600 °C at a rate of 10 °C/min under a nitrogen atmosphere; second, the temperature was kept constant at 600 °C for 30 min under a nitrogen atmosphere; and third, the temperature was kept constant at 600 °C for 1 h under an air atmosphere.

Proton nuclear magnetic resonance (^{1}H NMR) spectra were collected using a Nananalysis 60 MHz benchtop spectrometer (NMReady-60). The analysis preparation consisted of diluting around 0.10–0.15 g of sample in 700 μL of chloroform-d and then inserting it in 5 mm NMR tubes. A total of 32 scans were collected for each sample, with a scan delay of 20.0 s and a spectral width of 12 ppm. The area in the shift range of $0.10 < \delta < 3.5$ ppm was assigned to saturated hydrogen while the area in the shift range of $6.6 < \delta < 8.3$ ppm was assigned to aromatic hydrogen. The regions outside of these ranges contained no peaks.

Carbon-13 nuclear magnetic resonance (^{13}C NMR) spectra were collected at the Analytical and Instrumentation Laboratory of the Department of Chemistry at the University of Alberta by using an Agilent/Varian Innova 400 MHz spectrometer. Samples were prepared by diluting around 0.35 mL of bitumen sample in 0.36 mL of 0.2 mM chromium (III) acetylacetonate in chloroform-d.

Once completely dissolved, the sample was transferred into a 5 mm NMR tube. The sample was scanned 2000 times within -10.0 to 270.0 ppm, with an acquisition time of 0.5 s and a relaxation time of 2 s. The area in the range of $2.5 < \delta < 60.0$ ppm was assigned to aliphatic carbon, and the area in the range of $110.0 < \delta < 160.0$ ppm was assigned to aromatic carbon.

The persistent free radical content was determined from the electron spin resonance (ESR) spectra obtained using an Active Spectrum micro-ESR. Around 20 mg of sample was diluted in 600 μL of toluene and transferred into a 5 mm-diameter PQ tube. Equipment parameters were 1.2 Gauss coil amplitude, a digital gain of 12 dB, and a microwave power of 15 mW. The spectra were obtained as the average of 7 scans with a sweep delay of 30 s. The free radical content was quantified by using a calibration curve prepared using 2,2-diphenyl-1-picrylhydrazyl in toluene.

3.3 Results

3.3.1 Froth Characterization

A total of eight froth samples were extracted using the procedure mentioned in **Section 3.2.2.1**, and the froth composition is shown in **Table 3.4**. The main challenges found during the separation of froth components are the same as those encountered during bitumen separation in an industrial froth treatment unit. First, water and bitumen are of similar densities, rendering gravity separation impracticable. Second, the high viscosity of bitumen and the presence of biwettable fine solids, which increase the stability of water-in-oil emulsions, make the separation of the froth components very difficult. The total material balance varied in the range of 91–98 wt%, meaning that some material losses were associated with the extraction procedure and content determination.

One of the possible reasons for material loss is that some drops of water might get trapped inside the condenser during the separation, resulting in a loss of water. Additionally, the methodology used to determine the bitumen content (by getting a bitumen sample, filtering it, and applying a multiplier factor to the weight of the residual material on the filter) can lead to a magnification of errors that could potentially result in an underestimation of the total bitumen content. Consequently, the uncertainty expressed in terms of the standard deviation was higher for bitumen and water than for the solids content.

Table 3.4: Composition of the froth sample used in the study. The numbers 1–8 represent the total number of extractions performed.

Froth component	Content (wt%)[a,b]									
	1	2	3	4	5	6	7	8	x	s
Bitumen	59.9	64.7	65.0	64.8	69.5	66.4	65.8	65.8	65.2	2.7
Water	22.1	24.0	24.1	19.5	17.4	21.7	21.2	17.3	20.9	2.6
Solids	8.7	8.6	9.1	8.9	6.4	8.1	8.6	8.9	8.4	0.9
Total	90.8	97.3	98.2	93.1	93.3	96.2	95.6	92.0	94.6	2.6

[a] Numbers 1–8 represent the content of each performed extraction.

[b] Average (x) and sample standard deviation (s) of the eight extractions.

3.3.2 Froth Visbreaking

3.3.2.1 Gas formation and residual water content

The gas yield and amount of water trapped in the bitumen phase after thermal conversion are reported in **Table 3.5**. As the type and concentration of solvent varied for each group of reactions, three different “untreated bitumen” samples were submitted to the same dilution as the feed used for the reactions in each group. For this reason, each experimental group has an “untreated bitumen” sample reported in **Table 3.5** and in the other results in this section. As a result, each "untreated bitumen" result provides a more solid foundation for comparing property changes in the same group before and after visbreaking. Differences among the results of the “untreated bitumen” samples of different groups are related to either the separation efficiency of water (as observed in the water content values in **Table 3.5**) or the methods used for correction of property values in order to remove the effect of dilution (as observed in the other results presented in this section).

The ERT at 400 °C was calculated for each visbreaking reaction in order to account for the residence time of the three regions shown in the time-temperature profile inside the reactors (**Figure A.3** in **Appendix A**). The time-temperature profiles were reasonably repeatable, but the variation indicated a general shortcoming with the use of fluidized sand bath heaters. Once the four reaction systems had different heating up times and also different temperature variations in the target range (400 ± 5°C), the use of the ERT provided a more reliable basis for comparison of the changes in bitumen properties after the visbreaking reactions.

Table 3.5: ERT at 400 °C of visbreaking reactions, final pressure of reactors, estimated formed gas based on the ideal gas law, and residual water content in untreated bitumen and bitumen products.

System	ERT at 400 °C (min)	Final Pressure (MPa)^{a,b}	Formed Gas (μmol of gas/g of diluted bitumen)^{c,d}	Residual Water Content (wt%)^{e}	
				x	*s*
Group I					
Solvent: kerosene					
Untreated Bitumen	-	-	-	<0.1^{f}	-
B+W+S	31.6	1.25	165	1.80	0.13
B+S	30.5	1.20	110	0.16	0.14
B+W	28.9	1.10	95	0.31	0.11
B	27.3	1.10	70	0.80	0.18
Group II					
Solvent: *n*-hexane					
Untreated Bitumen	-	-	-	1.82	0.02
B+W+S	32.0	1.40	260	0.41	0.04
B+S	30.3	1.20	70	0.86	0.06
B+W	28.4	1.20	135	0.58	0.10
B	26.6	1.20	140	0.50	0.04
Group III					
No added solvent^{g}					
Untreated Bitumen	-	-	-	0.41	0.05
B+W+S	31.0	1.40	145	0.80	0.03
B+S	31.8	1.40	200	0.40	0.02
B+W	28.5	1.40	180	1.48	0.06
B	28.0	1.30	150	0.62	0.04

[a] Starting pressure was 1 MPa for all systems. [b] Final pressure measured at room temperature. [c] Group III unit is μmol of gas/g of bitumen. [d] Bitumen diluted with 20 wt% of kerosene (Group 1) or 13 wt% of *n*-hexane (Group II). [e] Average (x) and sample standard deviation (s) of analyses in duplicate. [f] Below the detection limit of the equipment. [g] Solvent was not added prior to the reaction, but 10 wt% of benzene was added to the untreated bitumen and visbroken products prior to analyses.

Table 3.5 shows the ERT of the visbreaking reactions, which ranged from 26.6 to 32.0 min. The system containing B+W+S presented the highest ERT in Groups I and II (31.6 and 32.0 min, respectively), while the highest ERT in Group III was observed for the system B+S. For all experimental groups, the system containing only bitumen (B) had the lowest ERT (ranging from 26.6 to 28 minutes). It became clear that without the ERT calculation, the reaction time of 25 min indicated by the experimental protocol would have underreported the actual severity of the reactions.

After the visbreaking reactions, the internal pressure of the reactors was measured at room temperature and increased in the range of 0.10–0.40 MPa compared to the initial pressure of 1 MPa. This small increment in pressure is anticipated in mild thermal treatment processes, such as visbreaking, in which low-severity thermal cracking takes place, forming a low amount of gases [26]. The pressure increase was then translated into the amount of gas formed per amount of diluted bitumen by using the ideal gas law and the volume occupied by the gas inside the reactor. Although gas formation was identified after reactions, the composition of the formed gas phase was not analyzed.

When comparing the reaction systems of each group, the highest gas yield was observed in the diluted systems (Groups I and II) for the reactions containing the combination of water and solids (B+W+S). The same was not observed for the non-diluted bitumen (Group III), in which the combination of water and solids presented the lowest gas yield compared to the other systems in the same group. The reactions of Groups I and III presented an increase in the gas yield for the reactions containing only solids (B+S) and only water (B+W), compared to the systems containing only bitumen (B). This trend was not observed for reactions in Group II, in which the systems B+S and B+W presented the lowest gas yield.

Although the separation of water and solids was carefully performed as described in **Section 3.2.2.2**, some residual water was still observed in the bitumen products after separation. The residual water content of untreated and reacted bitumen was determined by Karl Fischer titration, and the results are reported in **Table 3.5**. Most of the products presented a water content below 1 wt%, except for the bitumen samples from systems B+W+S (Group I), untreated bitumen (Group II), and B+W (Group III), which presented residual water content varying between 1.48 and 1.82 wt%. The water content of each feed was not measured prior to reactions.

3.3.2.2 Elemental composition

The elemental composition of the untreated bitumen and the bitumen phase after thermal conversion is reported in **Table 3.6**. The values reported in **Table 3.6** have been corrected for solvent and water content and are reported on a solvent-free and water-free basis. The raw data is presented in **Section A.5** in **Appendix A**, together with details on how the corrections were applied. The residual mass not accounted for by the CHNS analysis was assumed to correspond to the amount of oxygen, and the values shown in the table were calculated by the difference to give a 100% mass balance. Oilsands bitumen typically has an oxygen content of around 1 wt% [27]. The calculation of the molar element ratios (H/C, N/C and S/C) was also performed and is listed in **Table 3.6**.

Changes in the H/C ratio and heteroatom content are expected when bitumen is subjected to thermal treatment, and the magnitude of these changes depends on the severity of the treatment. This is to be expected considering the low gas yield (**Table 3.5**). After visbreaking, only minor differences in the average elemental composition were observed. The H/C ratio of the majority of the reacted systems decreased after visbreaking. The highest decrease in the H/C ratio for Group I reactions was achieved by the systems B+W+S and B+W (from 1.49 to 1.40). Similarly to Group I, the system B+W in Group II reactions also presented the highest decrease in the H/C ratio (from 1.41 to 1.31). However, the same system (B+W) in Group III presented a smaller decrease in the H/C ratio (from 1.49 to 1.44) if compared to the ones obtained in groups I and II, and this decrease was equal to other systems in Group III (B+W+S and B).

When observing the H/C ratio results in the three experimental groups, there is an indication of a combined contribution of solids and water to the changes that affected that ratio. For instance, the H/C ratio of B+W+S in Group II (H/C = 1.34) was higher than that of B+W (H/C = 1.31) and similar to that of B+S (H/C = 1.33). This combined effect was also observed in the N/C ratio of Groups I and III. Changes in the S/C and the N/C ratios were very small among the systems in the same group.

3.3.2.3 Thermogravimetric analysis of bitumen-coated solids

The presence of mineral solids in bitumen can lead to the accumulation of organic matter on the surface of the mineral particles through mechanisms such as capillary retention, physisorption, and chemisorption. Previous studies showed that the amount of organic content coating mineral particles is affected by thermal treatment [22, 28] and that mineral solids are able to induce coke formation over their surface [29]. For this reason, the solids collected by centrifugation in this study, before and after reactions, were analyzed through TGA in order to get information about the relative amount of organic material that remained on the surface of mineral solids.

The TGA results (**Table 3.7**) are reported in terms of the weight loss in the three regions of the thermogram program as described in **Section 3.3.2.4**. No water separation was performed before collecting the solids for TGA analyses, and, therefore, the weight loss from 25 to 150 °C was considered to be due to water evaporation and that of residual *n*-hexane or benzene in samples from Groups II and III. The weight loss associated with the increase in temperature from 150 to 600 °C plus the loss at 600 °C for 30 min, both under a nitrogen atmosphere, was considered to be due to volatile organic matter that volatilized throughout the temperature increase in an inert atmosphere. In these regions, the volatilized material corresponded to the evaporation of light compounds plus the cracking of heavy compounds, followed by the evaporation of the formed lighter components. On the other side, the mass loss due to the constant temperature heating at 600 °C under an air atmosphere was considered to be due to fixed carbon material on the solids' surface, which went through combustion and released its combustion products. Mineral content was then calculated from the balance for non-volatilized material.

The amount of organic matter associated with the untreated froth solids after centrifugation (i.e., weight loss from 150–600 °C under a nitrogen and air atmosphere) ranged from 27.6 to 45.3 wt% in all experimental groups. The variation in these values when comparing different groups was most likely due to solids sampling for TGA analyses. The supernatant was drained after centrifugation, and the bitumen-coated solids at the bottom of the tube were mixed before the TGA sample was collected with a spatula. It is possible that the amount of bitumen that remained coating the solids after the supernatant was drained differed from group to group, which would explain the high variation of the organic matter associated with untreated solids from different groups. Furthermore, the sampling of the same systems (TGA analyses performed in triplicate) in each experimental group could have resulted in the high standard deviations observed, especially for the thermogram region of 25–600 °C/N_2.

The volatile carbon per fixed carbon ratio and the fixed carbon per mineral content ratio were calculated and are shown in **Table 3.7**. Solids from systems containing B+W+S and B+S showed an increase in both ratios when compared to untreated froth solids in all three experimental groups. The high variation when comparing volatile carbon to fixed carbon ratios could also be attributed to the aforementioned sampling challenges. It is noteworthy that the fixed carbon to mineral content ratio in the system B+W+S in Group II (1.04) was double that of the same system in Groups I and III (0.50 and 0.37, respectively).

Table 3.6: Corrected Elemental Analysis (wt%) and molar element ratios of untreated bitumen and bitumen separated from visbroken products.[a]

System	Corrected Elemental Analyses (wt%)											
	C		H		N		S		O[b]	H/C	N/C	S/C
	x	*s*	*x*	*s*	*x*	*s*	*x*	*s*		*x*	*x*	*x*
Group I												
Solvent: kerosene												
Untreated bitumen	82.89	0.48	10.38	0.14	0.53	0.01	4.76	0.03	1.44	1.49	0.0055	0.0215
B+W+S	84.55	0.34	9.93	0.07	0.60	0.01	4.62	0.09	0.31	1.40	0.0061	0.0205
B+W	83.57	0.06	9.84	0.04	0.58	0.01	4.69	0.10	1.31	1.40	0.0060	0.0210
B+S	83.86	0.08	10.11	0.02	0.55	0.01	4.55	0.04	0.94	1.44	0.0056	0.0203
B	82.62	0.34	10.00	0.03	0.56	0.02	4.69	0.23	2.13	1.44	0.0058	0.0213
Group II												
Solvent: *n*-hexane												
Untreated bitumen	83.11	0.25	9.85	0.21	0.61	0.15	5.04	0.08	1.39	1.41	0.0063	0.0227
B+W+S	84.46	0.06	9.48	0.22	0.55	0.01	4.77	0.07	0.75	1.34	0.0056	0.0211
B+W	84.73	0.14	9.32	0.18	0.58	0.01	5.17	0.17	0.20	1.31	0.0058	0.0228
B+S	84.46	0.24	9.45	0.21	0.55	0.01	4.91	0.12	0.63	1.33	0.0056	0.0218
B	84.54	0.20	9.36	0.13	0.58	0.03	4.85	0.16	0.66	1.32	0.0059	0.0215
Group III												
No added solvent[c]												
Untreated bitumen	82.34	0.64	10.29	0.05	0.52	0.02	4.97	0.03	1.89	1.49	0.0054	0.0226
B+W+S	83.58	0.09	10.13	0.29	0.56	0.01	4.66	0.04	1.08	1.44	0.0057	0.0209
B+W	84.25	0.14	10.19	0.21	0.53	0.01	4.65	0.06	0.38	1.44	0.0054	0.0207

Continues on the next page

	Corrected Elemental Analyses (wt%)											
System	C		H		N		S		O[b]	H/C	N/C	S/C
	x	*s*	*x*	*s*	*x*	*s*	*x*	*s*		*x*	*x*	*x*
B+S	83.49	0.09	10.34	0.06	0.54	0.00	4.98	0.02	0.65	1.48	0.0056	0.0223
B	83.12	0.15	10.06	0.07	0.51	0.01	4.63	0.23	1.68	1.44	0.0053	0.0209

[a] Average (*x*) and sample standard deviation (*s*) of analyses in duplicate.

[b] Oxygen amount calculated by difference. [c] Solvent was not added prior to the reaction, but 10 wt% of benzene was added to the untreated bitumen and visbroken products prior to analyses.

Table 3.7: Weight loss obtained from the TGA analysis of solids coated with bitumen and residual water.

System	Weight loss (%)[a]								Mineral Content (wt%)	Volatile Carbon/ Fixed Carbon	Fixed Carbon/ Mineral Content
	25-150 °C/ N_2		150-600 °C/ N_2		600 °C/ 30 min / N_2		600 °C/ 60 min / Air				
	x	*s*	*x*	*s*	*x*	*s*	*x*	*s*			
Group I											
Solvent: kerosene											
Untreated Froth Solids	0	-	16.1	3.3	0.9	<0.1	10.6	0.8	72.5	1.59	0.15
B+W+S	36.0	12.7	45.5	10.0	0.5	0.1	6.0	0.9	11.9	7.65	0.50
B+S	9.2	2.2	55.1	0.4	0.8	0.2	10.7	0.6	24.2	5.24	0.44
Group II											
Solvent: *n*-hexane											
Untreated Froth Solids	0	-	32.5	0.7	1.4	0.1	11.4	0.7	54.7	2.98	0.21
B+W+S	22.8	4.0	47.9	4.3	0.7	<0.1	14.6	0.6	14.0	3.32	1.04
B+S	11.5	3.8	51.1	7.8	0.7	0.1	10.4	0.4	26.3	4.98	0.40
Group III											
No added solvent[b]											
Untreated Froth Solids	0	-	21.6	5.4	1.4	0.1	9.5	0.4	67.6	2.83	0.14
B+W+S	24.0	5.7	49.1	3.3	0.7	0.1	7.0	0.4	19.2	7.46	0.37
B+S	1.2	1.4	43.7	7.2	1.0	0.1	15.8	4.6	38.3	3.23	0.41

[a] Average (*x*) and sample standard deviation (*s*) of analyses in triplicate. [b] Solvent was not added prior to the reaction, but 10 wt% of benzene was added to the untreated bitumen and visbroken products prior to analyses.

3.3.2.4 Viscosity

The first objective of this study was to identify if the presence of solid minerals and water could significantly influence changes in viscosity and density after froth visbreaking. Previous studies, mentioned in the introduction section, pointed out that both solids and water could influence the changes in these properties during upgrading. The second objective was to identify if the type of solvent (paraffinic or naphthenic) used to dilute the froth during visbreaking could influence the changes in viscosity and density as well.

The corrected viscosity values for untreated froth and reacted systems are shown in **Table 3.8**. In this table, the viscosity values were corrected for the solvent content in the untreated bitumen and reaction products. The corrected viscosity that is given in **Table 3.8** is the solvent-free viscosity of the bitumen and visbroken bitumen. The measured viscosity values and the equations used for viscosity correction are reported in **Appendix A** (**Section A.6**).

The general form of the MacCoull equation (**Eq. 3.2**), similar to that utilized in ASTM D341 [23], was used to examine the relationship between the corrected viscosity values and temperature. In **Eq. 3.2**, μ is the viscosity of bitumen (mPa·s), a and b are the slope and intercept of the linear regression, respectively, and T is the temperature (K). The slope (a), intercept (b), and coefficient of determination (R^2) of the linear regressions are also reported in **Table 3.8**. All the curves presented $R^2 \geq 0.992$, which is in accordance with the literature [1, 22]. The R^2 values are also a valuable resource to check the internal consistency of the viscosity data as a means of identifying if any event (e.g., phase separation, solvent evaporation, etc.) affected the viscosity measurements, which would consequently result in a deviation from the linear relationship.

$$ln\left(ln\left(\mu\right)\right) = a \cdot ln\left(T\right) + b \tag{3.2}$$

Before comparing the viscosity results of different systems within the same experimental group, it is important to remember that viscosity changes are dependent on the severity of visbreaking and that the ERT of the reaction systems varied, as shown in **Table 3.5**. Therefore, fair comparisons of viscosity decrease or increase from different systems must always account for the visbreaking severity measured by the ERT of each system.

Except for the system B+W in Group III, the presence of water and/or solids during visbreaking resulted in a higher viscosity compared to the system containing only bitumen (B). It is noteworthy that system B had the lowest ERT in each group (i.e., the lowest severity), making the previous comparison possible.

When the viscosity data of the systems reacted in the presence of water and/or solids in Group I were examined, the viscosity values were consistent with the severity of the treatments, i.e., $\mu_{(system\ B+W+S)} < \mu_{(system\ B+S)} < \mu_{(system\ B+W)}$ while $ERT_{(system\ B+W)} < ERT_{(system\ B+S)} < ERT_{(system\ B+W+S)}$. In other words, the lower the severity in those systems, the higher the viscosity. The same trend, however, was not observed for the same systems in Groups II and III. These findings suggest that, in addition to the severity of the treatment, the presence of water and solids also affects viscosity changes during visbreaking.

3.3.2.5 Density and refractive index

The corrected density data of untreated bitumen and visbroken products on a solvent-free basis is shown in **Table 3.9**. The raw density data and details on how these values were corrected for solvent presence are reported in **Section A.7** of the **Appendix A**.

The linear dependence of density with temperature was evaluated according to **Eq. 3.3**, where ρ is the density (kg/m^3), T is the temperature (°C), and c and d are the slope (dρ/dT) and intercept of the linear regression, respectively. The values of slope, intercept, and R^2 are also reported in **Table 3.9**. The R^2 of the linear regressions for the majority of the reacted systems was close to unity, indicating that the density varied linearly with temperature, as expected from the literature [30]. This result was also important for verifying the reliability of the density measurements, since any deviation from the linear behavior could point out inconsistent values. One inconsistent data point was observed for the system B+S in Group II reactions, which presented an R^2 of 0.987.

$$\rho = cT + d \tag{3.3}$$

Table 3.8: Corrected solvent-free viscosity of bitumen feed and bitumen separated from visbroken products at different temperatures.

System	Corrected Viscosity (Pa·s)							
	25 °C	30 °C	35 °C	40 °C	60 °C	Slope, *a*	Intercept, *b*	R^2
Group I								
Solvent: kerosene								
Untreated bitumen	78	-	-	15	3	-3.073	19.931	0.999
B+W+S	0.79	-	-	0.29	0.10	-3.302	20.709	0.999
B+W	1.2	-	-	0.49	0.14	-3.342	21.009	0.994
B+S	1.1	-	-	0.38	0.13	-3.339	20.972	1
B	0.41	-	-	0.17	0.071	-3.110	19.508	0.999
Group II								
Solvent: *n*-hexane								
Untreated bitumen	70	45	33	-	-	-2.100	14.376	0.992
B+W+S	0.42	0.34	0.28	-	-	-2.170	14.165	1
B+W	0.63	0.47	0.39	-	-	-2.400	15.535	0.992
B+S	0.29	0.23	0.19	-	-	-2.209	14.316	0.999
B	0.17	0.14	0.12	-	-	-2.049	13.303	0.998
Group III								
No added solvent[a]								
Untreated bitumen	48	29	18	-	-	-2.893	18.858	1
B+W+S	0.97	0.69	0.51	-	-	-3.020	19.133	0.999
B+W	0.61	0.46	0.36	-	-	-2.539	16.323	0.999
B+S	1.11	0.79	0.58	-	-	-2.929	18.636	0.999
B	0.62	0.47	0.35	-	-	-2.824	17.954	1

[a] Solvent was not added prior to the reaction, but 10 wt% of benzene was added to the untreated bitumen and visbroken products prior to analyses.

Table 3.9: Corrected density (ρ) of bitumen feed and bitumen separated from visbroken products at different temperatures.

System	Corrected Density (kg/m^3)							
	25 °C	30 °C	35 °C	40 °C	60 °C	Slope, *c*	Intercept, *d*	R^2
Group I								
Solvent: kerosene								
Untreated bitumen	1010.34	-	-	1000.94	988.33	-0.629	1026.09	1
B+W+S	993.37	-	-	983.31	970.10	-0.665	1009.95	1
B+W	997.71	-	-	987.69	974.50	-0.663	1014.25	1
B+S	993.28	-	-	983.21	969.99	-0.665	1009.87	1
B	988.64	-	-	978.51	965.13	-0.672	1005.41	1
Group II								
Solvent: *n*-hexane								
Untreated bitumen	1006.47	1003.49	1000.65	-	-	-0.582	1021.00	0.999
B+W+S	984.05	980.79	977.67	-	-	-0.638	999.98	0.999
B+W	981.01	977.83	974.78	-	-	-0.623	996.58	0.999
B+S	964.61	961.17	956.04	-	-	-0.857[b]	986.32	0.987
B	971.20	967.91	964.74	-	-	-0.647	987.35	0.999
Group III								
No added solvent[a]								
Untreated bitumen	1005.37	1001.50	997.64	-	-	-0.773	1024.70	1
B+W+S	988.87	984.83	980.78	-	-	-0.809	1009.10	1
B+W	982.47	978.43	974.41	-	-	-0.807	1002.64	1
B+S	989.84	985.81	981.60	-	-	-0.824	1010.47	0.999
B	985.56	981.38	976.66	-	-	-0.890	1007.91	0.999

[a] Solvent was not added prior to the reaction, but 10 wt% of benzene was added to the untreated bitumen and visbroken products prior to analyses. [b] Inconsistency in dataset.

The density of bitumen is a function of its composition [1]. As a result, changes in the derivative dρ/dT indicate compositional changes in the bitumen phase. All the products presented an increase in slope if compared to the untreated bitumen. The slope increase was near-similar for products in Group I but was more varied for products in Group II and III. System B in Group III had the greatest variation in slope (from -0.773 to -0.890). In all groups, the product from system B had the most negative slope compared to the rest of the products.

As observed in the viscosity results, the systems with solids and/or water had higher densities than the system with only bitumen (B), except for system B+W in Group III. It is important to highlight one more time that this comparison is valid once system B had the lowest ERT in all experimental groups.

The corrected refractive index of the untreated bitumen and visbroken products is reported in **Table 3.10**. The raw data and details on how the corrections were applied are reported in **Section A.8** of the **Appendix A**.

The linear dependence of refractive index with temperature was evaluated following **Eq. 3.4**, where n is the refractive index, T is the temperature (°C), and e and f are the slope and intercept of the linear regression, respectively. The values of slope (dn/dT) and R^2 for the regressions are also reported in **Table 3.10**.

$$n = eT + f \tag{3.4}$$

Table 3.10: Corrected refractive index (n) of bitumen feed and bitumen separated from visbroken products at different temperatures.

System	Corrected Refractive Index						
	25 °C	30 °C	35 °C	40 °C	60 °C	dn /dT	R^2
Group I							
Solvent: kerosene							
Untreated bitumen	1.5751	-	-	1.5695	1.5623	-3.7E-04	0.999
B+W+S	1.5793	-	-	1.5740	1.5671	-3.5E-04	0.999
B+W	1.5817	-	-	1.5761	1.5685	-3.8E-04	1
B+S	1.5763	-	-	1.5716	1.5657	-3.0E-04	0.999
B	1.5727	-	-	1.5671	1.5601	-3.6E-04	0.999
Group II							
Solvent: *n*-hexane							
Untreated bitumen	1.5854	1.5836	1.5818	-	-	-3.7E-04	0.999
B+W+S	1.6086	1.6068	1.6050	-	-	-3.6E-04	0.999
B+W	1.5942	1.5925	1.5909	-	-	-3.4E-04	0.999
B+S	1.6119	1.6102	1.6085	-	-	-3.4E-04	1
B	1.6245	1.6226	1.6210	-	-	-3.5E-04	0.997
Group III							
No added solvent[a]							
Untreated bitumen	1.5695	1.5674	1.5654	-	-	-4.1E-04	0.999
B+W+S	1.5810	1.5790	1.5770	-	-	-3.9E-04	0.999
B+W	1.5714	1.5695	1.5674	-	-	-4.0E-04	0.999
B+S	1.5686	1.5671	1.5652	-	-	-3.5E-04	0.997
B	1.5719	1.5699	1.5678	-	-	-4.1E-04	0.999

[a] Solvent was not added prior to the reaction, but 10 wt% of benzene was added to the untreated bitumen and visbroken products prior to analyses.

Previous work showed that the d*n*/dT values are correlated to the molecular weight, density, and viscosity of bitumen-derived products [31]. Thus, the values of d*n*/dT contain valuable information regarding the composition of bitumen. In the present study, only small variations of d*n*/dT were identified for the majority of systems when comparing the untreated bitumen and the reacted systems of the same group. The highest slope variations were observed for the systems B+S in Groups I and III (from -3.7×10^{-4} to -3.0×10^{-4} in Group I and from -4.1×10^{-4} to -3.5×10^{-4} in Group III). All the reacted systems presented a $R^2 \geq 0.997$, which is consistent with the linear dependence of refractive index with temperature. The least negative slope was consistently found for the B+S system. The majority of the visbroken products (B+W+S, B+W, and B+S) presented an increase in the refractive index if compared to the untreated bitumen, except for system B in Group I and B+S in Group III, which were slightly lower.

3.3.2.6 Free radicals content

Free radicals are naturally occurring species in oilsands bitumen [32]. The free radical concentration in bitumen might be affected by changes in the bulk liquid properties by means of the addition of a solvent or changes in composition due to thermal cracking [33]. In this study, electron spin resonance was used to measure the free radical content of the untreated bitumen and products of Group I only, and the corrected results are shown in **Figure 3.2**. The analyses were performed at the same analyte concentration. The raw and corrected data, as well as details on how the corrections were applied are reported in **Appendix A** (**Section A.9**). For the two reaction systems containing solids (B+W+S and B+S), a slight decrease in the free radical content was observed after visbreaking if compared to the untreated bitumen, whereas a slight increase in the radical content was identified for the reaction systems without solids (B+W and B).

3.3.2.7 Nature of hydrogen content

By monitoring the aliphatic and aromatic hydrogen content during bitumen upgrading, it is possible to get more information regarding the reaction chemistry taking place during the process. More specifically, changes in the nature of the hydrogen content after visbreaking could point out if hydrogen transfer reactions are affected or not by the presence of solids and/or water during visbreaking. In this study, proton nuclear magnetic resonance was applied to obtain the aliphatic

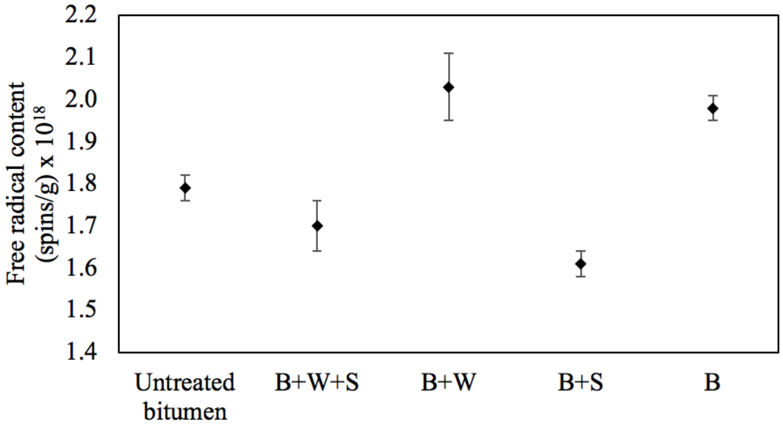

Figure 3.2: Corrected free radical content of untreated bitumen and bitumen separated from visbroken products in Group I experiments. The data points represent the average, while the error bars represent the standard deviation of analyses in triplicate.

and aromatic hydrogen content before and after visbreaking. The corrected results are shown in **Table 3.11**. Corrections to the raw data (presented in **Table A.7** in **Appendix A**) were performed by applying material balance, taking into consideration the amount of solvent in the samples and its aliphatic and aromatic hydrogen content.

The hydrogen content data indicated that in Group I reactions, the visbreaking of the systems containing water and/or solids (B+W+S, B+W, and B+S) kept the aliphatic hydrogen content unaltered within the experimental uncertainty (i.e., 92.9 ± 0.3%, 92.5 ± 0.3%, and 92.4 ± 0.3%). The aliphatic hydrogen content of all the reacted systems in Group II decreased compared to the untreated bitumen value, while no directional behavior was observed for the products of Group III. Nevertheless, within each group, the visbroken product obtained with bitumen (B) had the lowest or second lowest aliphatic hydrogen content.

Table 3.11: Corrected aliphatic and aromatic hydrogen content based on ^{1}H NMR spectra of untreated bitumen and visbroken products.

System	Aliphatic H Content (%)[a]		Aromatic H Content (%)[a]	
	x	*s*	*x*	*s*
Group I				
Solvent: kerosene				
Untreated bitumen	92.9	0.3	7.1	0.3
B+W+S	92.9	0.3	7.1	0.3
B+W	92.5	0.3	7.5	0.3
B+S	92.4	0.3	7.6	0.3
B	90.9	0.3	9.1	0.3
Group II				
Solvent: *n*-hexane				
Untreated bitumen	95.1	0.1	4.9	0.1
B+W+S	92.3	0.5	7.7	0.5
B+W	94.1	0.6	5.9	0.6
B+S	94.2	0.3	5.8	0.3
B	92.9	0.1	7.1	0.1
Group III				
No added solvent[b]				
Untreated bitumen	95.8	0.6	4.2	0.6
B+W+S	96.1	0.4	3.9	0.4
B+W	95.2	0.9	4.8	0.9
B+S	97.6	0.6	2.4	0.6
B	94.5	0.3	5.5	0.3

[a] Average (*x*) and sample standard deviation (*s*) of analyses in triplicate.

[b] Solvent was not added prior to the reaction, but 10 wt% of benzene
was added to the untreated bitumen and visbroken products prior to analyses.

3.3.2.8 Nature of carbon content

In this study, the nature of the carbon content (aliphatic and aromatic) before and after visbreaking was obtained through ^{13}C-NMR. The corrected results are shown in **Table 3.12**. Material balance was applied to correct the measured data (**Table A.8** in **Appendix A**) by taking into account the amount of solvent and its respective aliphatic and aromatic carbon content.

All the reacted systems presented an increase in their aromatic carbon content compared to the untreated bitumen. The highest variation in the aromatic carbon content was observed for the system B+W+S in the diluted bitumen experiments (from 25.4 to 35% in Group I and from 31.9 to 37.5% in Group II). These were also the two experiments with the longest ERT (**Table 3.5**) in Groups I and II. The changes in the aromatic carbon content did not follow a similar pattern compared to the changes in the aromatic hydrogen content (compare **Table 3.11** and **Table 3.12**). This finding is consistent with the literature [34].

Table 3.12: Corrected aliphatic and aromatic carbon content based on ^{1}3C NMR spectra of untreated bitumen and visbroken products.

System	Aliphatic C Content (%)^a	Aromatic C Content (%)^a
Group I		
Solvent: kerosene		
Untreated bitumen	74.6	25.4
B+W+S	65.0	35.0
B+W	67.3	32.7
B+S	67.0	33.0
B	69.3	30.7
Group II		
Solvent: *n*-hexane		
Untreated bitumen	68.1	31.9
B+W+S	62.5	37.5
B+W	67.2	32.8
B+S	66.5	33.5
B	64.7	35.3
Group III		
No added solvent^b		
Untreated bitumen	70.6	29.4
B+W+S	67.4	32.6
B+W	67.0	33.0
B+S	67.5	32.5
B	66.4	33.6

[a] Analysis performed on a single sample. [b] Solvent was not added prior to the reaction, but 10 wt% of benzene was added to the untreated bitumen and visbroken products prior to analyses.

3.4 Discussion

3.4.1 Internal consistency of data

This first topic in the discussion aimed to examine the internal consistency of the data in order to describe what types of errors might have influenced the study's results and to highlight how the data should be interpreted in light of the limitations of the methods and calculations performed.

Although the slopes of the viscosity dependence with temperature (**Table 3.8**) indicated that the viscosity measurements were consistent, the viscosity data revealed an intriguing point: the corrected viscosities at 25 °C of the untreated bitumen from the three experimental groups differed (in the range 48–78 Pa·s) when they were expected to be the same. The same holds true for all the other corrected properties in this study (e.g., density, refractive index, etc.).

The divergence in corrected property values of the untreated bitumen samples could be caused by two major sources of error: first, the handling of samples containing solvent makes them susceptible to solvent volatilization; second, the use of mixing rules for correcting some of the properties has limitations that are inherent to the particular model used for the corrections.

Because of the low boiling points of *n*-hexane and benzene (69.0 and 80.1 °C, respectively), solvent volatilization could have a greater effect on Groups II and III samples. Although every precaution was taken to reduce solvent volatilization (e.g., not leaving the sample containers open for extended periods of time, fast sampling, and product analyses as soon as possible after the reactions have been completed), some evaporation is expected when dealing with a solvent/bitumen mixture. As a result, the solvent content used to correct the analyzed properties may have been overestimated.

According to the viscosity and density data (**Table 3.8** and **Table 3.9**), the untreated bitumen in Groups II and III had the lowest values for these properties. Overestimation of solvent content in these groups could account for their lower values when compared to Group I, which was less susceptible to volatilization.

The use of mixing rules for property correction is the second possible source of error for the correction of properties. For viscosity correction, the mixing rule proposed by Miadonye et al.[35] was used in this study. It was reported that for solvent concentrations ranging from 1 to 10 wt%, this mixing rule consistently provided the best viscosity estimation with an absolute average relative deviation (AARD) that varied in the range 0–35%, depending on the solvent used [36]. In the same study, it was also observed that viscosity overestimation increased with solvent content and that, within the uncertainty of the estimation, there was no effect of the chemical nature of the solvent on viscosity prediction.

The wide AARD range presented by the mixing rule by Miadonye et al.[35] when different types of solvents are used, as well as the observation of viscosity overestimation with increased solvent content, highlight the limitations for viscosity estimation. Also, the nature of the solvent is ignored in this model, which is based solely on the viscosity and density data of the pure solvent, bitumen, and the solvent/bitumen mixture. It is, however, still one of the best options for bitumen/solvent blends. That being said, the different solvent contents in Groups I, II, and III and the chemical nature of the solvents used (i.e., kerosene – naphthenic, *n*-hexane – paraffinic and benzene – aromatic) might have affected the viscosity estimation by the mixing rule, resulting in the different corrected viscosities of the untreated bitumen samples in the current study.

Density corrections were performed using the ideal mixing assumption (i.e., no volume change upon mixing). Mixtures of bitumen and light *n*-alkanes are known to deviate from the ideal mixture assumption, as pointed out in the work of Nourozieh et al.[37] The authors found a negative volume change upon mixing for pentane/bitumen mixtures, and this deviation from an ideal mixture increased with temperature. At ambient temperature, the deviation between the density of ideal mixing and the actual density was less than 1%. This would have a minor impact on the corrections to density data from Group II experiments using *n*-hexane as the solvent. Because of the small AARD typically obtained for predicting density using the ideal mixture assumption, there is a high likelihood that deviations in the density estimation of the untreated bitumen samples were caused by solvent volatilization rather than the mixing rule's accuracy.

The density measurements in the B+S system of Group II revealed an inconsistency, with a R^2 of 0.987 for the linear dependence of density with temperature. Because the same system produced consistent values for viscosity and refractive index measurements (**Table 3.8** and **Table 3.10**, respectively), this inconsistency is most likely due to a deviation in one of the measured density points. All the other systems presented consistent values for the density measurements.

After highlighting the limitations of the density and viscosity correction methods, it is worth noting that a more reliable interpretation of the changes in viscosity and density before and after reactions should be performed within the reacted systems of a specific experimental group and the untreated bitumen of that same group. By doing so, the errors due to solvent type and solvent volatilization are comparable.

3.4.2 Physicochemical changes upon froth visbreaking

3.4.2.1 Viscosity and density changes

The main question that led to the current investigation was whether the presence of mineral solids and water in froth could somehow improve the quality of bitumen during visbreaking. Previous studies, as mentioned in the **Introduction**, suggested that the presence of these froth components could influence the viscosity and composition of bitumen during thermal treatment. As a consequence, any further viscosity and density reduction that could be promoted by the presence of solids and/or water during visbreaking would be beneficial.

The relative viscosity and density reduction that was achieved compared to the untreated bitumen is summarized in **Table 3.13**. However, conclusions cannot be drawn solely from this data without taking into account the variation in the ERT of each system across the three experimental groups (refer to **Table 3.5**). Previous research demonstrated that changes in the ERT of $\sim$0.4 min at 427 °C (i.e., $\sim$1.6 min for the ERT at 400 °C) resulted in a noticeably lower viscosity [38]. Thus, viscosity differences between reaction systems, even at small changes in the ERT, cannot be neglected.

Table 3.13: Calculated viscosity and density reduction at 25 °C compared to the untreated bitumen's viscosity and density.

System	Viscosity Reduction at 25 °C (%)[a]			Density Reduction at 25 °C (%)[a]		
	Group I	Group II	Group III	Group I	Group II	Group III
B+W+S	99.0	99.4	98.0	1.7	2.2	1.6
B+W	98.5	99.1	98.7	1.3	2.5	2.3
B+S	98.6	99.6	97.7	1.7	- b	1.5
B	99.5	99.8	98.7	2.2	3.5	2.0

[a] Viscosity and density reduction compared to the untreated bitumen values of each experimental group. [b] Inconsistency in dataset.

Ideally, the viscosity and density of the reacted systems should be adjusted to the same levels of ERT to allow a fair comparison of the viscosity and density data from different systems. However, the literature is scarce on models that predict viscosity based on the severity of visbreaking. One of the challenges is that the relationship between product viscosity and residue conversion is complex and has been shown to change after about 20% conversion [38, 39]. Marquez et al.[40] developed a model that could correlate the viscosity and density of a Western Canadian bitumen with conversion, but the same model presented large deviations when applied to a chemically different oil. Therefore, Marquez et al.'s[40] model is very specific to the bitumen specimen for which it was designed and would not be accurate for the current study.

The modeling of viscosity and density with ERT was beyond the scope of the current study, but comparisons of viscosity and density data from different systems were made, taking the severity of those systems into account. A previous study found that visbreaking bitumen at 400 °C resulted in decreased viscosity for 30 minutes, where it reached an approximately constant level but began to vary after 1 hour, achieving new maximum and minimum viscosity levels with increased severity [41]. From these observations, it was tentatively assumed that there was a consistent decrease in viscosity with severity in the current study, which presented an average ERT of 29.6 min for the reacted systems. As a result, the comparisons on viscosity and density changes assumed that the only effect of increased severity was to push viscosity and density reduction, and any deviation from that behavior was influenced by the presence or absence of water and/or solids in the reaction media.

From the viscosity reduction data shown in **Table 3.13**, two observations are immediately apparent. First, the highest viscosity reduction was achieved in all experimental groups when bitumen was reacted on its own, i.e., in the absence of water or solids. Second, the viscosity reduction achieved in Group II experiments, which contained 13 wt% *n*-hexane in the reaction mixture, was consistently greater than that found in Group I and III experiments.

All three reacted systems (B+W+S, B+W and B+S) that formed products with a higher viscosity than the system containing only bitumen (B) also presented higher ERT values than system B. Thus, from the perspective of visbreaking severity, it was expected that systems with higher ERT would achieve further viscosity reduction, but the opposite was observed, confirming that solids and/or water hindered bitumen viscosity reduction.

Low-temperature (250 °C) hydrothermal treatment of froth for 2 hours in the presence of water and/or solids resulted in increased viscosity [22]. Some potential explanations for the effects of water and/or solids on the viscosity increase included the dissolution of lighter polar compounds into water, the formation of carboxylate ions, free radical polymerization, and acid-catalyzed addition reactions. Subsequently, it was confirmed that cationic conversion due to clays, despite the slightly alkaline conditions, was definitely a contributing factor [21].

As anticipated, visbreaking is very effective at reducing viscosity, but it does not have a big impact on density changes. The density reduction after visbreaking (**Table 3.13**) reached low levels of 1.3–3.5% at 25 °C, compared to the density of the untreated bitumen. In the current study, the same trend observed for viscosity was also observed for bitumen density, i.e., the bitumen products from reactions in the presence of solids and/or water exhibited a higher density when compared to bitumen visbreaking without these components.

Because bitumen's viscosity and density are both influenced by its composition, changes in bitumen composition caused by visbreaking have a direct impact on these properties. Moreover, any potential influence of solids and water on bitumen composition during froth visbreaking would result in different levels of viscosity and density reduction, as observed in this study's results.

The addition of a light hydrocarbon solvent has a direct impact on the bulk properties of bitumen. For example, it may alter the interaction of asphaltene aggregates in the bitumen suspension, affecting the bitumen's viscosity and density. When the solvent used is paraffinic, it might result in asphaltene precipitation [42, 43]. Although the amount of *n*-hexane used in this study was significantly less than what was needed for asphaltene precipitation [44], the alterations to the aggregation levels of asphaltenes in different solvents could have interfered with how the reactive species interacted during bitumen visbreaking. However, the measurement of asphaltene content and its level of aggregation were not within the scope of this study.

Visbreaking is industrially operated in the temperature range of 430-490 °C with residence times in the range 1-30 min to avoid the onset of coke formation [45]. In comparison to industrial processes, the temperature conditions used in this study were lower.

The temperature dependence of viscosity and density can potentially be used to identify compositional changes in the bitumen phase. When compared to the slope of the untreated bitumen in each experimental group, the majority of the systems containing solids and/or water showed different slopes for viscosity and density with respect to temperature (**Table 3.8** and **Table 3.9**) after visbreaking. A change in dμ/dT and dρ/dT indicates a change in composition, as these relationships are dependent on the nature of the species in the converted product.

Although the slopes of viscosity and density provided evidence that the compositional changes of the bitumen phase are affected by water and/or solids, the chemical nature of these changes cannot be inferred from these data alone. Therefore, it was of interest to investigate the compositional changes during froth visbreaking based on refractive index, elemental analysis, and the nature of hydrogen and carbon. This is covered in **Section 3.4.2.2**. The possible influence of water and solids on the viscosity, density and aromatic content changes are discussed in **Section 3.4.3**.

3.4.2.2 Compositional changes upon froth visbreaking

The refractive index is another useful property for detecting compositional changes in bitumen after visbreaking. Because the refractive index of a mixture is affected by the molecular size and structure of the components in the mixture, compositional changes in bitumen after upgrading can be detected by comparing the refractive index values before and after the treatment [46].

The variation in the slope values of the temperature dependence of refractive index (**Table 3.10**) of the reacted systems is in agreement with the previously stated claim that the froth elements influenced how bitumen composition was changed during visbreaking.

When a medium's composition remains constant, its refractive index rises as its density increases, for example, when the temperature of the measurement decreases. Once the density and refractive index results from this study were compared, it was found that, at the same measurement temperature, most of the products (except system B in Group I and B+S in Group III) had higher refractive index values while their densities were lower when compared to the untreated bitumen values.

This counterintuitive increase in refractive index values in relation to a decrease in density was also observed in a study of partial bitumen upgrading in the temperature range 150–300°C [47].

In general, within a narrow boiling range, low refractive index values indicate the presence of more paraffinic compounds, whereas high values indicate the predominance of aromatic compounds [46]. The same conclusion is also drawn when making use of the refractivity intercept (n - 1/2 ρ), which directionally changes from low values for paraffins and polycyclic naphthenes to high values for aromatics and conjugated unsaturated species [48]. Thus, the increased refractive index results of the reacted products might suggest that these products had a higher aromatic and unsaturated species content after visbreaking.

The elemental analysis data (**Table 3.6**) was also useful to get more information regarding the compositional changes taking place during froth visbreaking. Because the formation of H-rich light ends during visbreaking contributes to a decrease in the amount of hydrogen in the bitumen product, the observed decrease in the H/C ratio for all products was already expected [49].

However, when some of the reacted systems were compared, the decrease in the H/C ratio was not always accompanied by an increase in the amount of formed gas. For instance, system B+S in Group I had a higher H/C ratio than system B+W (1.44 vs. 1.40), but the amount of gas formed in B+W (95 μmol of gas/g of diluted bitumen) was less than in B+S (110 μmol of gas/g of diluted bitumen). This is tentatively interpreted in terms of low H/C material deposited on the solids [10–12], for which supporting evidence is provided in **Table 3.7**. Other systems in the three experimental groups displayed similar behavior. As a result, it became clear that the formation of light ends is not the only factor to consider when observing changes in the H/C ratio of the reacted systems.

Another reason for the decrease in H/C ratio observed in the visbroken products is an increase in the relative amount of hydrogen-depleted species after visbreaking. In this sense, the decrease in the H/C ratio could point out an increase in the content of unsaturated species, such as olefins and polycondensed aromatic components [9].

Because olefinic compound formation is typical of thermal upgrading processes, an increase in olefins was already expected during visbreaking. One of the dominant classes of reactions taking place during bitumen upgrading is cracking by β-scission, in which large hydrocarbon molecules crack, forming smaller radical species and olefins. Consequently, the decrease in the H/C ratio in this study was clearly influenced by olefin formation during visbreaking.

Furthermore, a decrease in the H/C ratio, associated with the aforementioned increase in refractive index values, might indicate an increased aromatic content after visbreaking in the majority of the reacted systems. Additional evidence of an increased aromatic content for the reacted systems in this study was observed from the data on the nature of hydrogen (**Table 3.11**) and carbon content (**Table 3.12**). After visbreaking, all the products presented an increased aromatic carbon content, while the majority of the products presented an increased aromatic hydrogen content. Typically, the aromatic content of bitumen is an indication of the severity of thermal conversion, and therefore some increase in the aromatic content was expected upon visbreaking [50, 51].

The relative change in aromatic H and aromatic C with respect to ERT is plotted in **Figure 3.3**. At first glance, it appears that the variation in aromatic H decreases as the ERT increases (**Figure 3.3a**). However, when analyzing that data, two factors should be kept in mind: First, a fixed relationship between aromatic content and ERT during thermal treatment is not expected [34]; second, the supposed outliers represented by Group II - B+W+S and Group III - B+S suggest that other variables than ERT (i.e., the presence or absence of solids, water, and solvent) may have influenced the changes in aromatic H content during visbreaking. The latter is further supported by the scattered distribution of the variation in aromatic C with respect to ERT (**Figure 3.3b**).

The effect of water, solids, and solvent on the varying degrees of aromatization identified in the ^{13}C NMR data implies that these components may have specific contributions to hydrogen transfer reactions, which resulted in different changes to the aromatic C content. For example, when bitumen

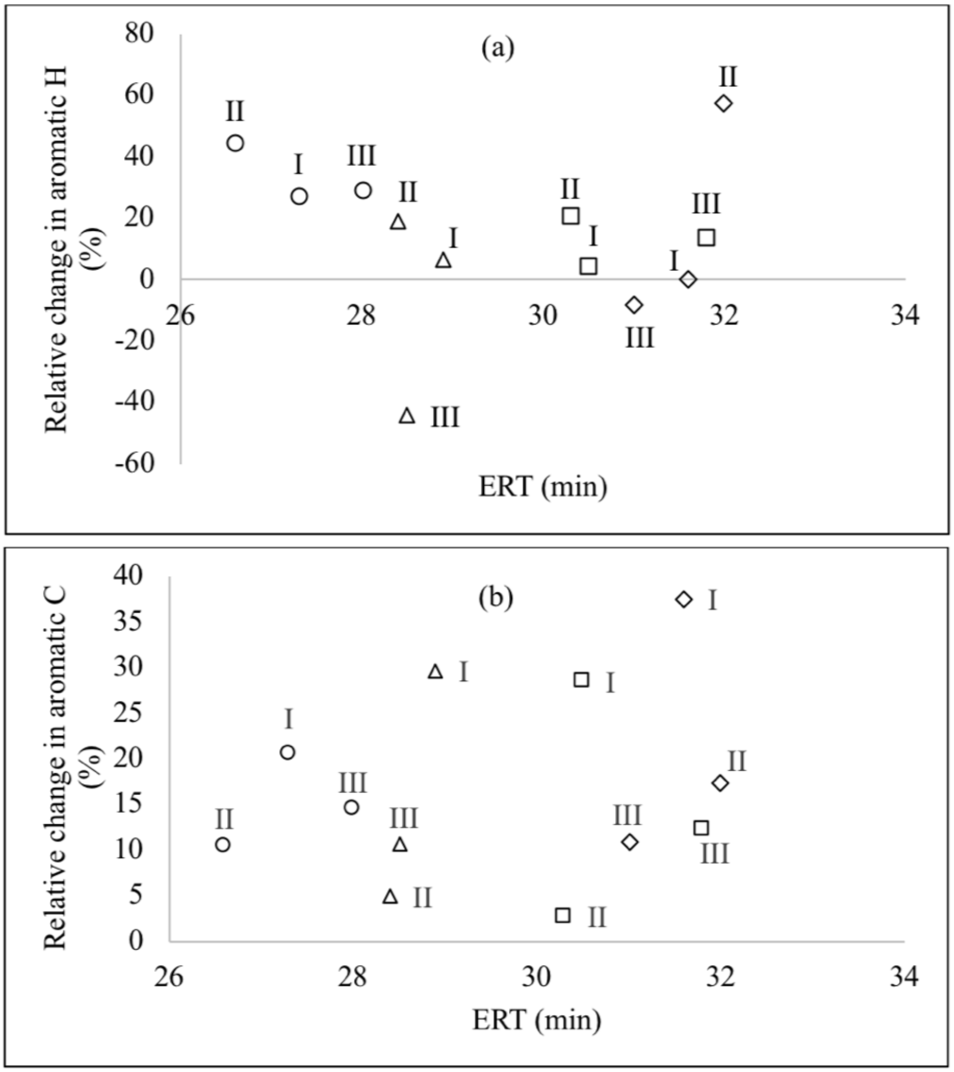

Figure 3.3: Relative change in (a) aromatic H and (b) aromatic C compared to the untreated bitumen values. The reacted systems are represented by (◊) B+W+S, (□) B+W, (△) B+S, and (○) B. Data labels refer to the type of solvent used: I – Group I experiments (kerosene), II – Group II experiments (*n*-hexane), and III – Group III experiments (no solvent).

visbreaking was performed in the presence of an organic solvent (kerosene or *n*-hexane), hydrogen transfer was increased in the combined presence of solids and water, resulting in higher aromatic content (**Figure 3.3b**). The nature of these contributions was not investigated in this study.

The data in **Figure 3.3b** also revealed that visbreaking in the presence of kerosene resulted in the largest increase in aromatic C for all the reacted systems. A tentative explanation for this finding is that the addition of kerosene to bitumen increases, among other components, the naphthene content of bitumen as compared to the addition of *n*-hexane (Group II) or the lack of solvent (Group III). The increased naphthene content in bitumen is then prone to aromatization, which could explain why the aromatic C content increased the most in the Group I experiments.

The persistent free radical results for Group I experiments provided additional evidence that water and solids influenced bitumen compositional changes during visbreaking (**Figure 3.2**). The changes in free radical content following visbreaking did not follow any trend in relation to the ERT of the reacted systems. Water and solids influenced the compositional changes in a way that resulted in different free radical concentrations after the thermal treatment. As a general observation, the free radical content in the liquid products was lower after visbreaking in the presence of solids. This is congruent with the observation that low H/C material was deposited on the solids.

3.4.3 Effect of minerals and water during bitumen visbreaking

Although it is clear that water and solids had an impact on the transformations that occurred during bitumen visbreaking, the current investigation did not provide support for any specific explanation for the nature of these effects. As a result, the topics presented in this section are just speculative but provide ideas for future studies on froth visbreaking.

3.4.3.1 Viscosity and density increase in the presence of water

As pointed out in the introduction section of this paper, a number of studies have claimed the benefits of using water during bitumen thermal treatment [15, 16]. The presence of water in the current investigation resulted in increased viscosity and density of bitumen after visbreaking when compared to the system containing only bitumen. This observation was true whether or not a solvent was added to the reaction system. The goal of this discussion is not to judge the validity of studies claiming a benefit during conversion in the presence of water or the industrial practice to co-feed steam, but to provide a counterpoint to tentatively explain the results in this study and why water can have a negative impact during bitumen visbreaking.

Three tentative explanations for the increased viscosity and density in the presence of water during visbreaking are described next:

(a) Water bridging in asphaltenes aggregates

Bitumen's viscosity reduction mechanism is based not solely on the cracking of heavy bitumen molecules into smaller species but also on the cleavage of crosslink interactions between bitumen's components forming aggregates [52]. The development of water bridges could operate as an energy barrier, preserving crosslink interactions and so hindering bitumen viscosity reduction during visbreaking [53–55].

(b) The hydrophobic effect of water on addition reactions

Despite the fact that water is a polar entity, it has been widely used as a solvent in organic synthesis, even in reaction systems containing non-polar reactants. Water, for example, has been used as a solvent in cycloaddition reactions (Diels-Alder reactions) to increase reaction rates [56, 57]. The rate acceleration observed in cycloaddition reactions in the presence of water is attributed to the hydrophobic effect, which forces the organic components in the reaction medium to aggregate, reducing their surface area and resulting in an increased reaction rate [56]. The same hydrophobic effect could have played a role during bitumen visbreaking, favouring addition reactions and resulting in the greater viscosity and density reported for the systems containing water.

(c) Vapor-liquid equilibrium

When water is present in the reaction medium, the system is thermodynamically non-ideal, and the amount of lighter products in the organic liquid phase is decreased because the partial pressure requirement for their vaporization is lowered. The decreased concentration of lighter products from the liquid phase due to water stripping changes the composition of the bulk liquid and could somehow affect the outcome of viscosity reduction. The beneficial effect of lighter organic species on suppression of coke was reported, even for species that have no hydrogen donor potential, such as naphthalene [58].

The addition of a solvent changes the bulk properties of bitumen and can influence how the reactions progress [59]. As previously stated, the Group II products (*n*-hexane–paraffinic solvent) showed the greatest levels of viscosity and density reduction (**Table 3.13**). The present study provided additional empirical evidence that indicates the beneficial effect of retaining light hydrocarbons in the organic liquid phase during thermal conversion.

3.4.3.2 Viscosity and density increase in the presence of solids

The presence of mineral solids in the current study resulted in higher viscosity and density values when compared to the visbreaking of bitumen alone. Two tentative explanations for this observation are presented next:

(a) Free radical termination on the surface of mineral solids

The termination of free radicals over the minerals surface has previously been reported in the literature [60, 61]. The extent of conversion during thermal cracking of bitumen is influenced by the relative rates of free radical initiation, propagation, and termination. In this regard, any factor that increases the rate of termination during bitumen upgrading could also hinder bitumen conversion.

In the current study, the presence of solids during bitumen visbreaking resulted in a lower free radical content (**Figure 3.2**) for the systems B+W+S (1.70×10^{18} spins/g) and B+S (1.61×10^{18} spins/g) compared to the untreated bitumen and the other reaction systems ($1.79\text{-}2.03\times10^{18}$ spins/g). This observation could point to an increase in termination reactions over the solids' surface during bitumen visbreaking, which could have resulted in a decrease in the conversion of heavy materials into lighter ones, resulting in increased density and viscosity for solid-containing systems. Termination by radical addition is also possible, which leads to the next point.

(b) Addition reactions over clay minerals

Polymerization addition reactions are reportedly enhanced in the presence of both Lewis and Brønsted-Lowry acids, which are found in clay structures such as kaolinite, which was found to be abundant in the froth used in this study [61]. It has been reported that heavier materials can be formed during thermal treatment in the presence of clays via acid-catalyzed addition reactions, including dimerization of alphamethylstyrene and 1-octene [21]. These reactions were found despite the slight alkaline nature of the froth. In this regard, acid-catalyzed addition over clays during bitumen visbreaking in the presence of mineral solids, followed by the migration of the formed heavier compounds into the bitumen phase, could be a possible explanation for the increased viscosity and density observed for the systems containing solids. Thus, irrespective of whether the formation of heavier products on the solid surface was due to radical termination or acid-catalyzed addition, some of the heavier products may still dissolve in the bulk liquid.

3.4.4 Froth visbreaking and bitumen pipeline transportation

One of the primary goals of visbreaking is to improve bitumen flowability so that it can be readily transported. Bitumen's properties make pipeline transportation extremely difficult. As a result, bitumen must be upgraded and/or diluted with a light solvent before it can be transported.

According to the Canadian pipeline specifications, bitumen must have a maximum kinematic viscosity of 350 mm^2/s at 7.5 °C (the temperature requirement during the Canadian winter) and a density of 940 kg/m^3 at 15.6 °C [39]. To determine whether the visbroken bitumen products in this study met the viscosity and density requirements for pipeline transportation, these properties were calculated at the reference temperatures, and the results are shown in **Table 3.14**. These calculations were performed by taking the corrected viscosity and density data on a solvent-free basis, and combining it with the data on the temperature dependence of these properties (**Table 3.8** and **Table 3.9**).

Table 3.14: Calculated viscosity (at 7.5 °C) and density (at 15.6 °C) of the visbroken products.

System	Calculated viscosity and density	
	Kinematic viscosity at 7.5 °C (mm^2/s)	Density at 15.6 °C (kg/m^3)
Group I		
B+W+S	3370	999.58
B+W	6293	1003.91
B+S	5310	999.50
B	1363	994.93
Group II		
B+W+S	1004	990.03
B+W	1705	986.86
B+S	644	972.95
B	326	977.26
Group III		
B+W+S	3776	996.48
B+W	1754	990.05
B+S	4306	997.62
B	2100	994.03

From the data shown in **Table 3.14**, only the product from system B in Group II met the viscosity requirement for pipeline transportation, while none of the products met the density requirement. However, the reduction in viscosity and density achieved through froth visbreaking may result in a reduction in the amount of solvent required for bitumen transportation.

3.5 Conclusions

The current study examined how water, minerals, and solvent affected the physicochemical properties of bitumen during froth visbreaking at 400 °C. There was evidence that all elements in the froth influenced to some extent the transformations taking place in the bitumen phase. The following parameters were evaluated: viscosity, density, refractive index, free radical content, elemental composition, and nature of hydrogen and carbon content.

The main outcomes from this study were:

(a) The presence of mineral solids and/or water during bitumen visbreaking consistently yielded a bitumen product with numerically higher viscosity and density when compared to the treatment of bitumen alone. Although these differences may be within experimental uncertainty, they revealed a consistent bias. Changes in dμ/dT and dρ/dT suggested that the presence of mineral solids and/or water during visbreaking resulted in compositional changes different from those in their absence. The lower viscosity and density obtained at the same severity of visbreaking in the absence of mineral solids and water were ascribed to a difference in the nature of the products formed.

(b) Mineral solids and water affected hydrogen transfer reactions during visbreaking, which could be seen in terms of the relative change in aromatic H and C content in the products.

(c) The H/C ratio of the visbroken products decreased, and the extent of the decrease in H/C at comparable severity was affected by the presence of mineral solids. Low H/C products could be adsorbed on the mineral solids, leading to a higher H/C ratio liquid product when compared to other liquid products at comparable gas yields, as well as a liquid product with lower persistent free radical content.

(d) This study tentatively found that there was benefit to performing the visbreaking in the presence of a light hydrocarbon solvent (*n*-hexane) when compared to a heavier hydrocarbon solvent (kerosene) or in the absence of a solvent, irrespective of whether mineral solids or water were also present with the bitumen. After accounting for the effect of the solvent on the properties of the product, the solvent-free bitumen product from visbreaking in *n*-hexane had a lower increase in aromatic C, a lower viscosity, and a lower density at comparable severity to the products from visbreaking in kerosene or without a solvent.

(e) Visbreaking of oilsands bitumen froth (i.e., B+W+S) at an equivalent residence time of 30 min at 400 °C resulted in products that, on a solvent-free bitumen basis, had a kinematic viscosity in the range 1–4×103 mm^2/s at 7.5 °C and a density in the range 990–1000 kg/m^3 at 15.6 °C.

3.6 References

(1) Gray, M. R., *Upgrading oilsands bitumen and heavy oil*; Pica Pica Press - Edmonton: 2015.

(2) Hong, P. K. A.; Cha, Z.; Zhao, X.; Cheng, C. J.; Duyvesteyn, W. Extraction of bitumen from oil sands with hot water and pressure cycles. *Fuel Process. Technol.* **2013**, *106*, 460–467.

(3) Rao, F.; Liu, Q. Froth treatment in Athabasca oil sands bitumen recovery process: A review. *Energy Fuels* **2013**, *27* (12), 7199–7207.

(4) Shelfantook, W. E. A perspective on the selection of froth treatment processes. *Can. J. Chem. Eng.* **2004**, *82* (4), 704–709.

(5) Gu, G.; Zhang, L.; Xu, Z.; Masliyah, J. Novel bitumen froth cleaning device and rag layer characterization. *Energy Fuels* **2007**, *21* (6), 3462–3468.

(6) Romanova, U.; Valinasab, M.; Stasiuk, E.; Yarranton, H.; Schramm, L.; Shelfantook, W. The Effect of Oil Sands Bitumen Extraction Conditions on Froth Treatment Performance. *J. Can. Pet. Technol.* **2006**, *45* (9), 36–45.

(7) Castaneda, L. C.; Munoz, J. A.; Ancheyta, J. Current situation of emerging technologies for upgrading of heavy oils. *Catal. Today* **2014**, *220*, 248–273.

(8) Sawarkar, A. N.; Pandit, A. B.; Samant, S. D.; Joshi, J. B. Petroleum residue upgrading via delayed coking: A review. *Can. J. Chem. Eng.* **2007**, *85* (1), 1–24.

(9) Joshi, J. B.; Pandit, A. B.; Kataria, K. L.; Kulkarni, R. P.; Sawarkar, A. N.; Tandon, D.; Ram, Y.; Kumar, M. M. Petroleum residue upgradation via visbreaking: A review. *Ind. Eng. Chem. Res.* **2008**, *47* (23), 8960–8988.

(10) Chen, Q.; Stricek, I.; Cao, M.; Gray, M. R.; Liu, Q. Influence of hydrothermal treatment on filterability of fine solids in bitumen froth. *Fuel* **2016**, *180*, 314–323.

(11) Sanaie, N.; Watkinson, A.; Bowen, B.; Smith, K. Effect of minerals on coke precursor formation. *Fuel* **2001**, *80* (8), 1111–1119.

(12) Tanabe, K.; Gray, M. R. Role of fine solids in the coking of vacuum residues. *Energy Fuels* **1997**, *11* (5), 1040–1043.

(13) Bi, W.; McCaffrey, W. C.; Gray, M. R. Agglomeration and deposition of coke during cracking of petroleum vacuum residue. *Energy Fuels* **2007**, *21* (3), 1205–1211.

(14) Kapadia, P. R.; Kallos, M. S.; Gates, I. D. A review of pyrolysis, aquathermolysis, and oxidation of Athabasca bitumen. *Fuel Process. Technol.* **2015**, *131*, 270–289.

(15) Wu, C.; Lei, G. L.; Yao, C. J. i.; Sun, K. J.; Gai, P. Y.; Cao, Y. B. Mechanism for reducing the viscosity of extra-heavy oil by aquathermolysis with an amphiphilic catalyst. *J. Fuel Chem. Technol.* **2010**, *38* (6), 684–690.

(16) Qu, X.; Li, Y.; Li, S.; Wang, J.; Xu, H.; Li, Z. Thermal cracking, aquathermolysis, and their upgrading effects of Mackay River oil sand. *J. Pet. Sci. Eng.* **2021**, *201*, 108473.

(17) Maity, S.; Ancheyta, J.; Marroquín, G. Catalytic aquathermolysis used for viscosity reduction of heavy crude oils: A review. *Energy Fuels* **2010**, *24* (5), 2809–2816.

(18) Fan, H. F.; Liu, Y. J.; Zhong, L. G. Studies on the synergetic effects of mineral and steam on the composition changes of heavy oils. *Energy Fuels* **2001**, *15* (6), 1475–1479.

(19) Monin, J. C.; Audibert, A. Thermal cracking of heavy-oil/mineral matrix systems. *SPE Reserv. Eng.* **1988**, *3* (4), 1243–1250.

(20) Belgrave, J. D. M.; Moore, R. G.; Ursenbach, M. G. Gas evolution from the aquathermolysis of heavy oils. *Can. J. Chem. Eng.* **1994**, *72* (3), 511–516.

(21) Turuga, A. S. S.; de Klerk, A. Free Radical and Cationic Addition due to Clay Minerals Found in Bitumen Froth at 250 °C Probed with Use of α-Methylstyrene and 1-Octene. *Energy Fuels* **2022**, *36* (23), 14148–14162.

(22) Turuga, A. S. S.; de Klerk, A. Hydrothermal Treatment of Bitumen Froth: Impact of Mineral Solids and Water on Bitumen Properties. *Energy Fuels* **2021**, *35* (21), 17536–17550.

(23) *ASTM D341-20e1: Standard Practice for Viscosity Temperature Equations and Charts for Liquid Petroleum or Hydrocarbon Products*; ASTM International: West Conshohocken, PA: 2020.

(24) Yan, T. Characterization of visbreaker feeds. *Fuel* **1990**, *69* (8), 1062–1064.

(25) *ASTM D1159-07: Standard Test Method for Bromine Numbers of Petroleum Distillates and Commercial Aliphatic Olefins by Electrometric Titration*; ASTM International: West Conshohocken, PA: 2017.

(26) Clark, P. D.; Kirk, M. J. Studies on the upgrading of bituminous oils with water and transition metal catalysts. *Energy Fuels* **1994**, *8* (2), 380–387.

(27) Speight, J. G., *The chemistry and technology of petroleum*, 5th ed.; CRC Press: Boca Raton, FL, 2014, p 188.

(28) Zhao, J.; Liu, Q.; Gray, M. R. Characterization of fine solids in Athabasca bitumen froth before and after hydrothermal treatment. *Energy Fuels* **2016**, *30* (3), 1965–1971.

(29) Zheng, R.; Liu, D.; Tang, J.; Song, Q.; Yao, Q. Analysis of montmorillonite affecting coke formation during the thermal conversion of heavy oil. *Fuel* **2021**, *288*, 119687.

(30) Nourozieh, H.; Kariznovi, M.; Abedi, J. Density and Viscosity of Athabasca Bitumen Samples at Temperatures up to 200 °C and Pressures up to 10 MPa. *SPE Reserv. Eval. Eng.* **2015**, *18* (03), 375–386.

(31) Shen, J.; Astrath, N. G.; Pedreira, P. R.; Guimarães, F. B.; Gieleciak, R.; Wen, Q.; Michaelian, K. H.; Fairbridge, C.; Malacarne, L. C.; Rohling, J. H., et al. Correlations among thermophysical properties, ignition quality, volatility, chemical composition, and kinematic viscosity of petroleum distillates. *Fuel* **2016**, *163*, 324–333.

(32) Mujica, V.; Nieto, P.; Puerta, L.; Acevedo, S. Caging of molecules by asphaltenes. A model for free radical preservation in crude oils. *Energy Fuels* **2000**, *14* (3), 632–639.

(33) Tannous, J. H.; de Klerk, A. Quantification of the free radical content of oilsands bitumen fractions. *Energy Fuels* **2019**, *33* (8), 7083–7093.

(34) Yañes Jaramillo, L. M.; Link, F.; Klerk, A. D. Relationship between aromatic hydrogen and aromatic carbon in straight run and converted oils. **2022**, *327*, 124414.

(35) Miadonye, A.; Latour, N.; Puttagunta, V. R. A correlation for viscosity and solvent mass fraction of bitumen-diluent mixtures. *Pet. Sci. Technol.* **2000**, *18* (1), 1–14.

(36) Montoya Sánchez, N.; de Klerk, A. Viscosity Mixing Rules for Bitumen at 1–10 wt% Solvent Dilution When Only Viscosity and Density Are Known. *Energy Fuels* **2020**, *34* (7), 8227–8238.

(37) Nourozieh, H.; Kariznovi, M.; Abedi, J. Measurement and Prediction of Density for the Mixture of Athabasca Bitumen and Pentane at Temperatures up to 200 °C. *Energy Fuels* **2014**, *28* (5), 2874–2885.

(38) Rahimi, P. M.; Teclemariam, A.; Taylor, E.; DeBruijn, T.; Wiehe, I. A. Thermal Processing Limits of Athabasca Bitumen during Visbreaking Using Solubility Parameters, In *Heavy hydrocarbon resources: characterization, upgrading, and utilization*, ed. by Nomura, M.; Rahimi, P. M.; Koseoglu, O. R., Vol. 895, ACS Symposium Series: 2005, pp 183–196.

(39) De Klerk, A. Processing unconventional oil: partial upgrading of oilsands bitumen. *Energy Fuels* **2021**, *35* (18), 14343–14360.

(40) Marquez, A.; Schoeggl, F.; Taylor, S.; Hay, G.; Yarranton, H. Viscosity of characterized visbroken heavy oils. *Fuel* **2020**, *271*, 117606.

(41) Zachariah, A. Low temperature pyrolysis and its application in bitumen processing, MSc thesis, University of Alberta, Edmonton, AB, 2014.

(42) Sheu, E.; De Tar, M.; Storm, D. Rheological properties of vacuum residue fractions in organic solvents. *Fuel* **1991**, *70* (10), 1151–1156.

(43) Barré, L.; Simon, S.; Palermo, T. Solution properties of asphaltenes. *Langmuir* **2008**, *24* (8), 3709–3717.

(44) Mullins, O. C.; Sheu, E. Y.; Hammami, A.; Marshall, A. G., *Asphaltenes, heavy oils, and petroleomics*; Springer: New York, 2007, p 688.

(45) Kaiser, M. J.; de Klerk, A.; Gary, J. H.; Handwerk, G. E., *Petroleum Refining: Technology, Economics, and Markets*, 6th ed.; CRC Press: Boca Raton, 2020, p 723.

(46) Strausz, O. P.; Lown, E. M., *The Chemistry of Alberta Oil Sands, Bitumens and Heavy Oils*; Alberta Energy Research Institute: Calgary, 2003, p 695.

(47) Yañez Jaramillo, L. M.; de Klerk, A. Partial upgrading of bitumen by thermal conversion at 150–300 °C. *Energy Fuels* **2018**, *32* (3), 3299–3311.

(48) Gruse, W. A.; Stevens, D. R., *Chemical Technology of Petroleum*, 3rd ed.; McGraw-Hill: New York, 1960, p 675.

(49) Ramirez-Corredores, M. M., *The science and technology of unconventional oils: finding refining opportunities*; Academic Press: London, 2017, p 778.

(50) Al-Muntaser, A. A.; Varfolomeev, M. A.; Suwaid, M. A.; Yuan, C.; Chemodanov, A. E.; Feoktistov, D. A.; Rakhmatullin, I. Z.; Abbas, M.; Domínguez-Álvarez, E.; Akhmadiyarov, A. A., et al. Hydrothermal upgrading of heavy oil in the presence of water at sub-critical, near-critical and supercritical conditions. *J. Pet. Sci. Eng.* **2020**, *184*, 106592.

(51) Liu, Y.; Bai, F.; Zhu, C. C.; Yuan, P. Q.; Cheng, Z. M.; Yuan, W. K. Upgrading of residual oil in sub-and supercritical water: An experimental study. *Fuel Process. Technol.* **2013**, *106*, 281–288.

(52) Zhang, Y.; Siskin, M.; Gray, M. R.; Walters, C. C.; Rodgers, R. P. Mechanisms of asphaltene aggregation: puzzles and a new hypothesis. *Energy Fuels* **2020**, *34* (8), 9094–9107.

(53) Andersen, S. I.; Del Rio, J. M.; Khvostitchenko, D.; Shakir, S.; Lira-Galeana, C. Interaction and solubilization of water by petroleum asphaltenes in organic solution. *Langmuir* **2001**, *17* (2), 307–313.

(54) Da Costa, L. M.; Stoyanov, S. R.; Gusarov, S.; Tan, X.; Gray, M. R.; Stryker, J. M.; Tykwinski, R.; de M. Carneiro, J. W.; Seidl, P. R.; Kovalenko, A. Density functional theory investigation of the contributions of π–π stacking and hydrogen-bonding interactions to the aggregation of model asphaltene compounds. *Energy Fuels* **2012**, *26* (5), 2727–2735.

(55) Murgich, J.; Merino-Garcia, D.; Andersen, S. I.; Manuel del Río, J.; Galeana, C. L. Molecular mechanics and microcalorimetric investigations of the effects of molecular water on the aggregation of asphaltenes in solutions. *Langmuir* **2002**, *18* (23), 9080–9086.

(56) Baire, B.; Sadhukhan, S. Chapter 3 - Cycloaddition reactions in water, In *Green Sustainable Process for Chemical and Environmental Engineering and Science*, ed. by Inamuddin; Boddula, R.; Asiri, A. M., Elsevier: 2020, pp 61–114.

(57) Adams, J. M.; Dyer, S.; Martin, K.; Matear, W. A.; McCabe, R. W. Diels-Alder reactions catalysed by cation-exchanged clay minerals. *J. Chem. Soc. Perkin Trans. 1* **1994**, (6), 761–765.

(58) Zachariah, A.; Wang, L.; Yang, S.; Prasad, V.; de Klerk, A. Suppression of coke formation during bitumen pyrolysis. *Energy Fuels* **2013**, *27* (6), 3061–3070.

(59) Amis, E. S., *Solvent effects on reaction rates and mechanisms*; Academic Press: New York, 1966, p 326.

(60) Solomon, D.; Swift, J. D. Reactions catalyzed by minerals. Part II. Chain termination in free-radical polymerizations. *J. Appl. Polym. Sci.* **1967**, *11* (12), 2567–2575.

(61) He, M.; Wang, Z.; Moldowan, M. J.; Peters, K. Insights into catalytic effects of clay minerals on hydrocarbon composition of generated liquid products during oil cracking from laboratory pyrolysis experiments. *Org. Geochem.* **2022**, *163*, 104331.

Chapter 4

Hydrothermal Treatment of Oilsands Bitumen Froth at 400 °C: Influence of Minerals and Water on Hydrogen Transfer, Cracking, and Addition Reactions

Abstract

Following prior evidence that water and mineral solids influenced the physicochemical properties of the products derived from the visbreaking of bitumen froth at 400 °C, the present study aimed to explore the effect of water and minerals on the reaction chemistry taking place during the thermal conversion of froth. The current study investigated the relative impact of water and mineral solids on hydrogen transfer, cracking, and addition reactions during the thermal treatment of froth at 400 °C. α-Methylstyrene (AMS) was employed as a probe molecule, and selected chemical species identified in the feed and thermally converted products were monitored. Water had a major effect on suppressing the conversion of AMS, whereas the hinderance of AMS conversion by mineral solids seemed to be minor. Substantial evidence of hydrogen and methyl transfer, hydration, and addition reactions was observed through the formation of specific AMS-derived products. The potential free radical and cationic pathways for the conversion of AMS were evaluated based on the product composition of the different reaction systems. There was indication that the availability of hydrogen donors also influenced the conversion pathways of AMS. Both water and mineral solids favored the extent of hydrogen transfer during the treatment. However, their specific effect on promoting transfer hydrogenation could not be determined. AMS was not a good probe for cracking under the conditions of this study. Evidence of hydration was observed in the water-containing systems. The presence of water suppressed the formation of addition products, resulting in an overall formation of these products that was half of that observed in the absence of water. The presence of minerals during the treatment seemed to have a minor impact on the selectivity profile of addition products, although it had no apparent influence on the overall formation of these products.

4.1 Introduction

The recovery of bitumen from mined oilsands bitumen ores is industrially performed with hot water, producing a bitumen froth that contains around 60 wt% bitumen, 30 wt% water, and 10 wt% mineral solids. The froth is then heated to 70–90 °C in the froth treatment unit and combined with either a naphthenic or a paraffinic solvent to facilitate the phase separation of bitumen from water and mineral solids [1–4].

The bitumen recovered in the froth treatment unit can be upgraded to improve its properties and, consequently, its value [1, 5–7]. It was suggested that it may be possible to upgrade the bitumen froth directly, which could potentially make the phase separation easier while concomitantly reducing the amount of solvent required for phase separation. Chen et al.[8] found that hydrothermal treatment of froth at 390 °C modified the wettability of the fine mineral solids to become more hydrophobic, resulting in improved solids filtration from bitumen. Thermal treatment at 250 °C was too low temperature to upgrade the bitumen, and the presence of water and minerals during the treatment resulted in a bitumen product with increased density and viscosity compared to the feed [9]. The thermal treatment of froth at 400 °C resulted in bitumen upgrading, but the presence of water and minerals during the treatment was detrimental to the quality of the final bitumen product. The treatment of bitumen with water, minerals, or a combination of both resulted in a slightly higher viscosity and density when compared to the treatment of bitumen on its own [10]. Although the physicochemical changes in the bitumen phase during thermal treatment of froth at 400 °C were explored, the influence of water and minerals on the reaction chemistry taking place during the treatment was not investigated.

The detrimental effect of water on the thermal conversion of bitumen at 400 °C was a surprising observation [10]. Steam is not only used to increase the linear velocity of oil in the coil of visbreaker units [11], but near-critical and supercritical water were also considered beneficial for thermal conversion of oil [12–17]. The presence of water during the thermal treatment of bitumen could potentially affect how the reactions progress, influencing the compositional changes in the bitumen phase [18]. It has been reported that the use of sub- and supercritical water during thermal treatment of bitumen and heavy oils influenced the product characteristics, resulting in suppressed coke formation, increased light liquid oil yield, and increased reactivity rates [19–21]. Furthermore, some studies indicated the potential hydrogen transfer from water during thermal treatment [22–24], while other studies claimed that the effect of water was not as a reactant but only as a diluent [25, 26]. The presence of water and minerals during the thermal treatment of froth at 400 °C also influenced the degree of aromatization of the bitumen product, suggesting that these components may have specific contributions to the extent of hydrogen transfer during the treatment [10].

The first objective of this study was to investigate the claim that water influenced hydrogen transfer as opposed to just being a diluent. Related to this, it was also of interest to determine if minerals from froth influenced hydrogen transfer reactions during thermal conversion. For this purpose, α-methylstyrene (AMS) was employed as a probe molecule to determine the relative extent of hydrogen transfer during thermal conversion of froth and decoupled elements from froth (i.e., water and minerals) at 400 °C. It has been demonstrated that AMS is a good hydrogen acceptor molecule, and when transferable hydrogen is available, it can be converted into cumene [27]. The froth used for the treatment was diluted with kerosene in order to resemble the dilution used during the naphthenic froth treatment and to facilitate the separation of solids and water for the experiments.

The second objective of this study was to investigate the relative contributions of water and minerals to other reactions taking place during thermal treatment of froth at 400 °C. In this study, AMS served as a probe molecule not only for hydrogen transfer but to evaluate cracking and addition reactions as well. Once cumene is formed from the hydrogenation of AMS, it can be cracked to form lighter species such as ethylbenzene and toluene [28]. Besides, AMS can readily undergo addition reactions, such as dimerization [29]. Cracking and addition can take place as free radical reactions as well as catalytic reactions.

The minerals found in froth are classified as clays and non-clays. Clays, such as kaolinite and illite, are the major components in froth solids (40–60 wt% of the total solids), while the remaining portion is constituted by non-clay minerals, such as quartz, rutile, and siderite [8, 30, 31]. These minerals have adsorptive and catalytic properties that could influence the reaction pathways during the thermal treatment of bitumen [32–34]. From the perspective of bitumen upgrading, two important classes of reactions that directly affect the physicochemical properties of bitumen are cracking and addition. The acidic properties of some minerals found in froth could influence both cracking and addition reactions [33]. During thermal conversion of froth at 250 °C, it was possible to differentiate between free radical and cationic addition, and it was reported that conversion in the presence of mineral solids was predominantly cationic despite the froth being slightly alkaline [9, 29].

In this study, selected chemical species were monitored in order to get detailed information on how water and minerals influenced hydrogen transfer, cracking, and addition reactions during thermal treatment of froth.

4.2 Experimental Section

4.2.1 Materials

The froth used in this study was obtained from a Canadian oilsands mining plant. The characterization of the bitumen phase separated from the froth is shown in **Table 4.1** [9]. The amount of bitumen, water, and solids in the froth sample was 65.2±2.7 wt%, 20.9±2.6 wt%, and 8.4±0.9 wt%, respectively [10]. The composition of the solids separated from froth has been previously reported and revealed quartz (53 wt%) and kaolinite (26 wt%) as the most abundant minerals [9]. The characterization of the water phase extracted from froth has also been reported in a prior study, revealing a slightly alkaline nature (pH = 8.3) and identifying the primary ions within its composition as Na^+ (722 μg/g) and Cl^- (812 mg/L) [9]. The simulated distillation profile of bitumen is shown in **Figure 4.1**. At the final boiling point given by the simulated distillation analysis, 80 wt% of the material had been distilled. The initial boiling point of 187 °C and the amount of non-distillable fraction (50 wt% material with an atmospheric equivalent boiling point higher than 550 °C) for the bitumen used in the study are in agreement with the distillation characteristics of bitumen [1].

A commercially produced kerosene (obtained from a Canadian refinery) was employed to resemble the dilution used during the naphthenic froth treatment and to allow the separation of mineral solids and water for the preparation of the reaction feed. The characterization of kerosene is also shown in **Table 4.1** [10]. The simulated distillation profile of kerosene is shown in **Figure 4.1**. The kerosene used in the study presented a boiling point distribution that ranged from 96 to 273 °C, and it is strictly speaking a heavy naphtha and kerosene fraction.

Table 4.1: Characterization of the kerosene and bitumen used in the study.

Property[a]	Kerosene	Bitumen
Viscosity at 25 °C (Pa·s)	1.3×10^{-3}	78
Density at 25 °C (kg/m^3)	805.1	1010.3
Refractive index at 25 °C	1.4479	1.5751
Elemental composition (wt%)		
C	86.2	82.9
H	13.8	10.4
N	< 0.2	0.5
S	0	4.8
O	0	1.4b
Aromatic H Content (%)	4.2	7.1
Aromatic C Content (%)	12.1	25.4

[a] Details on the equipment and methodology employed for obtaining each characterization property have previously been reported [10]. [b] Oxygen amount calculated by difference.

The chemicals used for feed preparation and feed and product analyses, as well as the cylinder gases used in this study, are listed in **Table 4.2**. The commercial standards used to verify the identity of species in the chromatograms are listed in **Table B.4** in **Appendix B**.

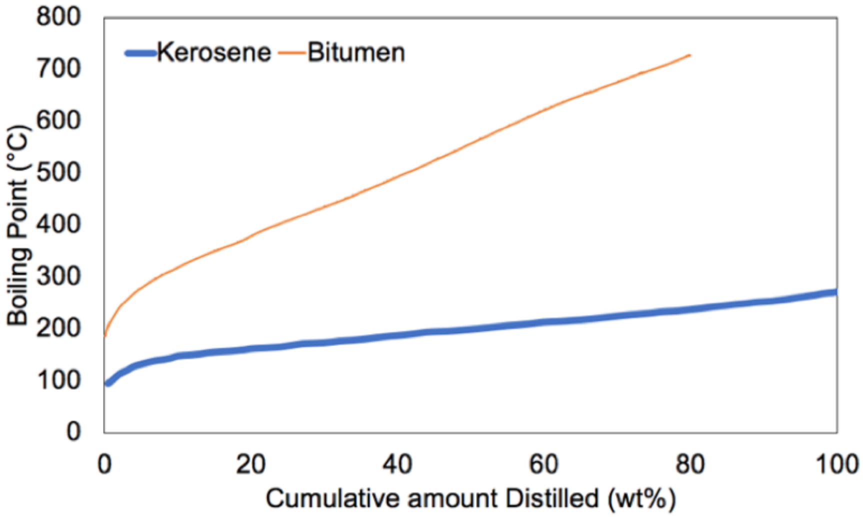

Figure 4.1: Simulated distillation profiles of bitumen and kerosene used in the study.

Table 4.2: List of chemicals and cylinder gases used in the study.

Compound	Formula	CASRN[a]	Purity (%)[b]	Supplier
Chemicals				
AMS (α-methylstyrene)	C_9H_{10}	98-83-9	99	Sigma Aldrich
biphenyl	$C_{12}H_{10}$	92-52-4	99.5	Sigma Aldrich
carbon disulfide	CS_2	75-15-0	99.99	Fisher Scientific
cumene	C_9H_{12}	98-82-8	98	Sigma Aldrich
methanol	CH_3OH	67-56-1	99.9	Fisher Scientific
Cylinder gases				
nitrogen	N_2	7727-37-9	99.999[c]	Praxair
air	O_2/N_2	132259-10-0	-	Praxair
hydrogen	H_2	1333-74-0	99.999[c]	Praxair
helium	He	7440-59-7	99[c]	Praxair

[a]Chemical Abstracts Services Registry Number (CASRN); [b]Purity of material provided by the supplier. Material was not further purified; [c]Mol% purity.

4.2.2 Equipment and Procedure

4.2.2.1 Separation of water and solids from bitumen for preparation of experiments

Water and solids separation from bitumen froth was necessary to prepare the feed for the experiments as well as the products for analysis. For this separation, it was necessary to dilute bitumen with kerosene (20 wt% of kerosene in relation to bitumen). The complete protocol for water and solids separation has been reported before [10]. The kerosene-diluted bitumen free from water and solids is referred to as diluted bitumen (DB).

Four types of reaction systems were used in the experiments for the thermal treatment: diluted bitumen + water + solids (DB+W+S), diluted bitumen + water (DB+W), diluted bitumen + solids (DB+S), and diluted bitumen alone (DB). All the products had solids and water removed prior to analyses, whereas kerosene was kept in the feed and products of all reaction systems (i.e., there was no kerosene removal before or after the reactions). The water content in the bitumen products from a prior study, which employed the same separation protocol, has been reported to be less than 1 wt% for most of the products [10].

4.2.2.2 Thermal treatment and control experiments

The thermal treatment of the samples described in **Section 4.2.2.1** was carried out using a 25-mL batch microreactor built with 316 stainless steel Swagelok tubing and fitting, equipped with a pressure gauge and an inserted thermocouple. The feeds for the four types of reaction systems investigated in this experimental setup are listed in **Table 4.3**. AMS was added to all reaction systems at a concentration of 30 wt% AMS in relation to the amount of diluted bitumen (DB), which comprised of 80 wt% bitumen and 20 wt% kerosene.

Table 4.3: Feed composition of materials used in the thermal treatment.

System[a]	Content (wt%)		
	Bitumen mixture[b]	Water	Solids
DB+W+S	83	10	7
DB+W	91	9	-
DB+S	92	-	8
DB	100	-	-

[a] DB – Diluted Bitumen (80 wt% bitumen + 20 wt% kerosene); W – Water; S – Solids. [b] 56 wt% bitumen, 14 wt% kerosene, and 30 wt% AMS.

In a typical reaction, around 14 g of feed was loaded into the reactor, which was then closed, purged three times with nitrogen (purging pressure of 5 MPa), and then pressurized to 1 MPa (the same initial pressure was used for all reaction systems). The reactor was subsequently placed in a fluidized sand bath heater (Omega Fluidized Bath FSB-3), which had been preheated to 400 °C. The reactor was kept at near-isothermal conditions for around 3 min after the reaction medium inside the reactor reached 400 °C. The reactor was then withdrawn from the sand bath and cooled using a room-temperature compressed air stream. The temperature inside the reactor was monitored throughout the entire reaction time, and the temperature was recorded every 1 minute from the moment the reactor was immersed into the sand bath until it was removed and cooled to 50 °C. The reactions were carried out in duplicate.

In order to decouple the relative contributions of bitumen and kerosene to the conversion of AMS during thermal treatment of DB, a total of four control experiments were carried out in the absence of any water or solids: bitumen + kerosene (B+K), bitumen + AMS (B+AMS), kerosene alone (K), and kerosene + AMS (K+AMS). The bitumen used in the control experiments was also obtained from the original froth sample, and separation of water and solids followed the same method mentioned in **Section 4.2.2.1**, except for the system B+AMS, in which AMS was used to dilute the bitumen and allow solids and water separation rather than kerosene.

The feeds used for the control reactions are shown in **Table 4.4**. The concentration of each component followed the same relative concentration between the components as used in the thermal treatment experiments. For instance, AMS was added to the feed of the thermal treatment experiments at a concentration of 30 wt% in relation to the amount of kerosene-diluted bitumen (20 wt%

of kerosene in relation to bitumen), which corresponded to a concentration of 35 wt% of AMS in relation to bitumen alone. One additional control experiment with bitumen and cumene (B+C) analogous to B+AMS was performed (not shown in **Table 4.4**) to determine cumene conversion. It was previously reported that cumene was a terminal product at 250 °C [35], but that was unlikely to be valid for conversion at 400 °C.

The same reactor and conditions used in the thermal treatment experiments were applied to the control experiments. The reaction systems containing B+AMS and K+AMS were performed in duplicate, while only one reaction was carried out for the systems B+K and K.

Table 4.4: Feed composition used for the control experiments.

System[a]	Content (wt%)		
	Bitumen	Kerosene	AMS
B+K	80	20	-
B+AMS	65	-	35
K	-	100	-
K+AMS	-	32	68

[a] B – Bitumen; K – Kerosene.

The quantification of AMS and cumene for the purpose of evaluating the conversion of AMS and the extent of hydrogen transfer during the thermal treatment experiments and the control experiments was performed through gas chromatography with flame ionization detection (GC-FID). The changes in bitumen composition due to the thermal treatment were evaluated through gas chromatography coupled with mass spectrometry (GC-MS).

The extraction of compounds from bitumen was performed with methanol at ambient conditions. The choice of methanol as the extraction solvent had the dual objective of minimizing the dilution of the heaviest species in bitumen and ensuring effective extraction of AMS and its products. A previous study has demonstrated the feasibility of methanol to extract AMS and its products from asphaltenes [35].

Prior to stirring for 15 min, a known amount of biphenyl was added to the product/methanol mixture as an internal standard to all the samples to be analyzed through the GC-FID. The extraction of products for GC-FID analyses was performed by diluting the product with a product-to-methanol mass ratio of 1:7.6, while the extraction for GC-MS analyses was performed by diluting the product with a product-to-methanol mass ratio of 1:3.8. Details on the extraction efficiencies are given in the Results section. Only the methanol extracts were analyzed by gas chromatography.

4.2.2.3 Analyses

Simulated distillation was carried out through gas chromatography on an Agilent 7890B with a flame ionization detector. The column used was the DB-HT-SIMDIS column (5 m × 0.53 mm × 0.15 μm). The injection volume was 0.5 μL, and helium was used as a carrier gas. The samples were prepared by dissolving 100 mg of the analyte in approximately 12 g of CS_2. The temperature program started at 50 °C with no hold time, after which the temperature was increased to 425 °C at a rate of 15 °C/min, at which temperature was kept constant for 10 min.

The instrument used for GC-FID analyses was an Agilent 7890A, and separation occurred in an Agilent J&W VF-200ms capillary column (30 m × 0.25 mm × 0.25 μm). A split/splitless injector was employed with a split ratio of 100:1 and an injection volume of 0.2 μL. The injector temperature was 250 °C. Nitrogen was used as the carrier gas with a flow rate of 1.5 mL/min. The temperature program started at 100 °C with no hold time, after which the temperature was increased to 220 °C at a rate of 10 °C/min and then increased from 220 °C to 300 °C at a rate of 5 °C/min, being held at 300 °C for 5 min. The samples obtained from the methanol extraction (refer to **Section 4.2.2.2**) were injected into the GC-FID without any further dilution. Calibration curves for AMS and cumene in methanol were built for the quantification of these compounds and are reported in **Appendix B** (**Tables B.1-B.2** and **Figures B.1-B.2**, in **Section B.1**).

The instrument used for GC-MS analyses was an Agilent 7820A coupled with a 5977E mass spectrometer, and separation was performed in a HP-PONA column (50 m × 0.20 mm × 0.5 μm), using hydrogen as carrier gas with a flow rate of 1 mL/min, an injection volume of 0.5 μL, and a split ratio of 23:1. The injector temperature was 250 °C. The temperature program started at 36 °C with a hold time of 5 min, after which the temperature was increased to 125 °C at a rate of 3 °C/min and then increased to 325 °C at a rate of 4 °C/min, being held at 325 °C for 5 min. The methanol extraction samples were injected without any additional dilution. The NIST MS Search 2.0 program was used to identify compounds in the feed and reaction products by matching their mass spectra to those found in the National Institute of Standards and Technology (NIST) mass spectral library. The identity of specific peaks suggested by the NIST library was confirmed using commercial standards that were added to some of the thermally treated products and then analyzed in the GC-MS. Confirmed identities through the use of commercial standards are indicated to distinguish those from identities based only on mass spectral assignment.

4.2.2.4 Calculations

The temperature recorded every 1 minute inside the reactor during the entire reaction period was used to calculate the equivalent residence time (ERT) at 400 °C, as specified by Yan [36] and shown in **Eq. 4.1**, where Δt_i are the 1-minute intervals containing two recorded temperatures (T_i and T_{i+1}), T_{ref} = 673.15 K (400 °C), E_a = 209500 $J\,mol^{-1}$, and R = 8.314 $J\,mol^{-1}\,K^{-1}$. The ERT for each reaction is presented in the **Results** section.

$$ERT\ at\ T_{ref} \ = \sum_{i=1}^{n} \Delta t_i \ \times \ exp\left[\left(-\frac{E_a}{R}\right)\left(\frac{1}{\frac{T_i + T_{i+1}}{2}} - \frac{1}{T_{ref}}\right)\right] \tag{4.1}$$

A quantitative indication of the extent of hydrogen transfer reactions was obtained by determining the selectivity of AMS conversion to cumene, which was calculated according to **Eq. 4.2** by using the mass (*m*, g) of cumene and AMS obtained through calibrated GC-FID quantification.

$$Selectivity\ to\ cumene\ (\%) \ = \ \frac{m_{cumene\ in\ product}}{m_{AMS\ in\ feed} \ - \ m_{AMS\ in\ product}} \times \ 100 \tag{4.2}$$

A semi-quantitative assessment of the relative amounts of compounds identified in the GC-MS chromatogram was obtained by comparing the area of the compounds to the total area of the chromatogram. The areas under the peaks were obtained by using the Agilent MassHunter Qualitative Analysis software, version B.06.00. The total area of the GC-MS chromatogram (A_{total}) was used to calculate the relative area percentage (RAP) of selected compounds from the area of each compound ($A_{compound}$) according to **Eq. 4.3**. The total area excluded the areas of methanol and biphenyl in the chromatogram because these compounds were added during the extraction (see

Section 4.2.2.2).

$$RAP(\%) = \frac{A_{compound}}{A_{total}} \times 100 \tag{4.3}$$

4.3 Results

4.3.1 Reaction severity and gas formation

The temperature profile inside the reactor during the thermal treatment and control experiments was recorded throughout the entire reaction time. The intention was to perform all the experiments at the same severity by keeping the reactor at near-isothermal conditions at 400 °C for 3 min (refer to **Section 4.2.2.2**), but practically thermal conversion starts at temperatures way below 400 °C, and the impact of heating and cooling periods had to be accounted for in terms of ERT (**eq. 4.1**). The ERT at 400 °C values calculated from the measured temperature versus time data are reported in **Table 4.5**.

Although all the reaction systems were pressurized to 1 MPa prior to the reaction, the water-containing systems were expected to reach higher pressures at the reaction temperature (400 °C). In order to report the actual pressure during the reaction in a near-isothermal condition, the pressure achieved at 400 °C for each experiment is listed in **Table 4.5**. The contribution of auto-generated pressure because of water in systems DB+W+S and DB+W increased their pressure to values that were equal to or higher than double the auto-generated pressure in systems DB+S and DB. The auto-generated pressure during the control reactions increased to similar levels (from 1 MPa to 2.5–2.8 MPa).

Gas formation is expected during the thermal treatment of bitumen and is usually noticed as an increase in reactor pressure at the end of the reaction. However, after the reaction was completed and the reactor was cooled to room temperature, no change in pressure was observed (i.e., the gauge reading indicated exactly the same initial pressure of 1 MPa). Nevertheless, the characteristic smell of hydrogen sulfide was still present in the liquid samples even after releasing the pressure from the reactors inside the fumehood, indicating the formation of gases during the thermal treatment. The not-detected increase in pressure at the end of the reactions could be a result of dissolved gases in the liquid phase at 1 MPa.

The gas phase was not analyzed to narrow the scope of the study, which primarily focused on the analysis of the liquid phase. However, the gas was quantified by subtracting the weight of the open reactor containing the products (after the reactor was cooled to room temperature and the gases were released in the fumehood) from the weight of the open reactor plus feed. The gas formation during thermal treatment and control experiments is reported in **Table 4.5**. Because of the high variability in the amount of gas formed during the thermal treatment, it was not possible to identify if the presence of water and solids had any effect on the formation of gas during the treatment. The presence of AMS in the control systems B+AMS and K+AMS resulted in a slightly higher amount of formed gas compared to the systems in the absence of AMS. The main gases expected from the AMS conversion are hydrogen, ethylene, propylene, and C_1–C_4 [37].

Table 4.5: ERT at 400 °C, maximum pressure achieved during reaction, and amount of generated gas after cooling to room temperature for the thermal treatment and control reactions.

System	ERT at 400 °C (min)[a]		Pressure at 400 °C (MPa)[b]	Gas formation (mg of formed gas/g of bitumen)[a]	
Thermal Treatment	*x*	*s*		*x*	*s*
DB+W+S	4.6	1	4	12.7	5.9
DB+W	4.9	0.1	4.5	26.7	7.8
DB+S	4.2	0.2	2	38.2	7.3
DB	3.6	0.2	2	45.4	9.8
Control Reactions					
B+K	4.7	-[c]	2.5	6.9	-[c]
B+AMS	4.9	0.2	2.5	27.4	9.3
K	4.7	-[c]	2.5	9.3[d]	-[c]
K+AMS	4.8	0.1	2.8	18.3[d]	8.4

[a] Average (*x*) and sample standard deviation (*s*) of experiments in duplicate.
[b] Initial pressure was 1 MPa for all reaction systems. [c] Only one reaction was carried out for this reaction system. [d] Unit of mg of formed gas/g of kerosene.

4.3.2 Material balance

Due to the nature of the separation of solids and water as described in **Section 4.2.2.1**, the overall material balance to account for gas, liquid (diluted bitumen and water), and solids in the product was not performed. First, the centrifuged solids at the bottom of the centrifuge tube were coated with bitumen and some trapped water (in the water-containing systems), making accurate mass measurements of different phases difficult. Second, the amount of solids and residual liquid that remained trapped inside the filtration system (including the filtration vessel, the tubing, and the tee-type filter) also made the material balance impractical. However, the lack of data on the overall material balance of the performed reactions was not detrimental to the results needed to achieve the proposed objectives of this study.

Although an overall material balance was impractical in this study, a semi-quantitative material balance on AMS in the feed and unconverted AMS + AMS-derived products was done and is reported in **Table 4.6**. This material balance was calculated based on the RAP of AMS and AMS-derived products obtained from the GC-MS results (see **Tables B.13** and **B.14** in **Appendix B**). The main AMS-derived products used for the material balance calculations were determined by monitoring variations in the RAP of feed and products of control reactions (**Table B.14** in **Appendix B**). Near-complete extraction of AMS in methanol was observed (refer to **Section B.2** in **Appendix B**).

Table 4.6: Material balance on AMS in the feed and AMS + AMS-derived products.

System	Relative area percentage (%)			AMS balance (%)[b]
	AMS in the feed	AMS in the product	Total AMS-derived products formed[a]	
Thermal Treatment				
DB+W+S	75.6	42.5	26.2	91
DB+W	75.6	34.2	31.8	87.3
DB+S	75.6	14.5	56.3	93.7
DB	75.6	12.8	56.9	92.3
Control Reactions				
B+AMS	99.4	10.6	86.2	97.4
K+AMS	78.4	41.4	39.5	103.3

[a]Total AMS derived products based on the amount of benzene, toluene, ethylbenzene, cumene, *n*-propylbenzene, *tert*-butylbenzene, *sec*-butylbenzene, *m*-cymene, *p*-cymene, 2-phenyl-2-propanol, and products with a retention time higher than 50 min. [b]The AMS balance was calculated based on the amount of total products formed plus the unconverted AMS, divided by the amount of AMS in the feed.

4.3.3 AMS conversion and cumene selectivity

Previous studies in the bitumen-related literature have already shown the suitability and application of AMS as a probe molecule to evaluate, both qualitatively and quantitatively, hydrogen transfer reactions during bitumen conversion [27, 35]. Natural hydrogen donor species are already present in bitumen, and, therefore, no external hydrogen source was added during these experiments [38]. The partitions of AMS and cumene in methanol and the bitumen phase were analyzed, and near-complete extraction was observed for both components, as shown in **Table B.3** in **Appendix B**.

The conversion of AMS and the selectivity of AMS conversion to cumene during thermal treatment are shown in **Table B.4**. The results of the control reactions containing AMS (B+AMS and K+AMS) are also reported in the same table.

Table 4.7: AMS conversion and selectivity to cumene measured by GC-FID.

System	AMS Conversion (%)[a]		Selectivity to cumene (%)[a]	
Thermal treatment[b]	x	s	x	s
DB+W+S	32	5	87	1
DB+W	47	5	73	3
DB+S	77	5	84	2
DB	84	2	65	0
Control Reactions				
B+AMS	90	3	63	2
K+AMS	52	2	8	1

[a] Average (x) and sample standard deviation (s) of experiments in duplicate. [b] AMS concentration was kept constant for all thermal treatment experiments (30 wt% of AMS in relation to the amount of diluted bitumen, which was the same as 35 wt% of AMS in relation to bitumen alone and 68 wt% of AMS in relation to kerosene alone).

The conversion of AMS (**Table 4.7**) varied in the range of 32–90%, while the severity (by measurement of the ERT at 400 °C, shown in **Table 4.5**) of the reactions varied in the range of 3.6–4.9 min. However, the increase in ERT was not necessarily followed by an increase in conversion because the systems with the lowest severities (DB+S and DB) presented the highest AMS conversions. These results indicated that the components in the reaction systems had an influence on AMS conversion, as expected.

The different components in the reaction systems had an impact not only on the conversion of AMS but also on the selectivity of AMS conversion to cumene. For instance, at a near-similar conversion, the systems DB+W and K+AMS had an order of magnitude difference in their selectivity to cumene.

4.3.4 Compositional changes in the bitumen phase

A detailed monitoring of the species formed during the thermal treatment in this study was carried out to evaluate the impact of water and mineral matter on the reaction pathways in the reaction network during the treatment.

The composition of species in the methanol extract after thermal conversion of the thermal treatment experiments and control experiments was determined by GC-MS. Out of the 83 monitored compounds, 77 had their identities confirmed using commercial standards. **Table B.4** in **Appendix B** lists the commercial standards utilized in this study by their ascending order of retention time (RT) in the GC-MS chromatograms.

The chromatograms for all the thermal treatment reactions and control experiments B+AMS and K+AMS are shown in **Figures B.3–B.18** in **Appendix B**. The monitored components were assigned peak identifiers to improve the readability of the peaks labeled in the chromatograms. Although some of the monitored compounds were not detected (ND) in the chromatograms, the peaks at the exact retention times where they would elute were labeled with their respective peak identifiers to indicate that these compounds were not present in the sample or in such a low concentration that it was below the detection limit of the GC-MS equipment.

The relative abundance of the monitored compounds was calculated before and after the treatment in terms of the relative area percentages (RAP) based on **Eq. 4.3**. Although the list of monitored components was extensive, in this section only the components relevant to the objectives of the study are presented, which will be justified in the **Discussion Section**. Complete lists of all the monitored components in the thermal treatment experiments and the control reactions are shown in **Tables B.13** and **B.14** in **Appendix B**.

The results of the RAP of selected compounds for both thermal treatment and control experiments are presented in this section. The results were divided by two regions of the chromatogram to improve the data presentation: compounds with retention times (RT) less than and higher than 50 min. The division at 50-min retention time was chosen because most compound identities were confirmed using commercial standards in the RT < 50 min region, whereas most compound identification in the RT > 50 min region was done solely by mass spectral assignment. The RAP of selected compounds with retention times lower than and higher than 50 min in the thermal treatment experiments are reported in **Tables 4.8** and **4.9**, respectively. **Tables 4.10** and **4.11** contain the RAP of selected compounds from the control experiments with RT lower than 50 min and RT higher than 50 min, respectively. **Figure 4.2** illustrates the tentative structures of the species listed in **Tables 4.9** and **4.11**. The interpretation of the mass spectra and reasoning that led to the manual structure assignments in **Figure 4.2** can be found in **Section B.5** in **Appendix B**.

There was some evidence of on-column cracking of heavier addition products [39]. For example, compounds H2 and H3 had mass spectra similar to compounds G7 and G8 (i.e., $C_{18}H_{20}$ isomers with tentative structures shown in **Figure 4.2**). The elution of the species indicated as H_2 and H_3 at higher retention times despite having mass spectra corresponding to $C_{18}H_{20}$ isomers indicated that on-column cracking was likely. While evidence of on-column cracking of heavy products was observed, the results from the B+AMS control system (refer to **Table 4.10**) indicated that there was no on-column cracking of AMS during the GC-MS analyses.

To assess the reactivity of cumene, a control experiment including the thermal treatment of bitumen with cumene (B+C) was also carried out. The cumene was mostly unconverted, although a small amount of ethylbenzene (0.1 wt%) and *n*-propylbenzene (0.2 wt%) were found in the reaction product. Given the limited number of species identified in this reaction system, the results were reported in a separate table (**Table B.15** in **Appendix B**) to improve the readability of **Table 4.10**.

Table 4.8: Abundance of selected compounds in the methanol extract from the thermal treatment experiments with a retention time lower than 50 min.

Compound	Formula	Peak identifier[a]	Retention Time (min)	Relative area percentage (%)				
				Feed	DB+W+S	DB+W	DB+S	DB
benzene	C_6H_6	A2	6.3	0.01	ND[b]	0.02	0.06	0.06
toluene	C_7H_8	A6	11.0	0.09	0.06	0.37	0.35	0.32
ethylbenzene	C_8H_{10}	B2	16.2	0.03	1.28	2.40	5.13	5.22
styrene	C_8H_8	B5	17.7	ND	ND	ND	ND	ND
cumene	C_9H_{12}	B8	20.0	0.04	19.15	22.32	38.09	38.41
n-propylbenzene	C_9H_{12}	C2	21.7	0.11	0.23	0.36	0.77	0.67
AMS	C_9H_{10}	C6	23.1	75.57	42.54	34.19	14.51	12.81
tert-butylbenzene	$C_{10}H_{14}$	C7	23.9	0.66	0.65	0.77	0.65	0.68
isobutylbenzene	$C_{10}H_{14}$	C8	24.8	ND	ND	ND	ND	ND
sec-butylbenzene	$C_{10}H_{14}$	C9	24.9	0.10	0.62	0.78	1.54	1.41
m-cymene	$C_{10}H_{14}$	C13	25.6	0.10	0.11	0.14	0.14	0.15
p-cymene	$C_{10}H_{14}$	C14	25.7	0.12	0.17	0.17	0.22	0.23
indane	C_9H_{10}	D1	26.0	0.08	0.08	0.09	0.07	0.06
indene	C_9H_8	D2	26.4	ND	ND	ND	ND	ND
o-cymene	$C_{10}H_{14}$	D3	26.5	ND	ND	ND	ND	ND
n-butylbenzene	$C_{10}H_{14}$	D8	27.3	0.09	0.09	0.12	0.14	0.14
2-phenyl-2-propanol	$C_9H_{12}O$	D11	28.4	ND	0.23	0.08	ND	ND
tetralin	$C_{10}H_{12}$	D18	32.8	0.11	0.08	0.08	0.04	0.04
naphthalene	$C_{10}H_8$	D20	33.7	ND	0.01	0.02	0.03	0.03

Continues on the next page

Compound	Formula	Peak identifier[a]	Retention Time (min)	Relative area percentage (%)				
				Feed	DB+W+S	DB+W	DB+S	DB
2-methylnaphthalene	$C_{11}H_{10}$	E3	38.8	0.15	0.22	0.25	0.22	0.23
1-methylnaphthalene	$C_{11}H_{10}$	E4	39.5	ND	0.07	0.09	0.13	0.12

[a]Peak identifier according to the labelled compounds in the chromatograms shown in **Section B.4** in **Appendix B**. [b]ND = Not detected.

Table 4.9: Abundance of compounds with retention times higher than 50 min in the methanol extract from the thermal treatment experiments.

Compound	Formula	Peak identifier[a]	RT (min)	Relative area percentage (%)				
				Feed	DB+W+S	DB+W	DB+S	DB
$C_{18}H_{20}$ – isomer[c]	$C_{18}H_{20}$	G1	53.2	ND[b]	ND	ND	ND	ND
$C_{17}H_{20}$ – isomer[c]	$C_{17}H_{20}$	G2	54.8	ND	0.09	0.13	0.28	0.26
$C_{18}H_{22}$ – isomer[c]	$C_{18}H_{22}$	G3	55.2	ND	0.66	0.76	1.35	1.43
$C_{18}H_{22}$ – isomer[c]	$C_{18}H_{22}$	G4	55.5	ND	0.67	0.76	1.39	1.49
dicumene[d]	$C_{18}H_{22}$	G5	56.0	ND	ND	ND	ND	ND
$C_{18}H_{20}$ – isomer[c]	$C_{18}H_{20}$	G6	56.6	ND	0.22	0.18	0.18	0.16
$C_{18}H_{20}$ – isomer[c]	$C_{18}H_{20}$	G7	59.2	ND	0.63	0.78	1.56	1.45
$C_{18}H_{20}$ – isomer[c]	$C_{18}H_{20}$	G8	59.4	ND	0.60	0.76	1.57	1.44
$C_{18}H_{18}$ – isomer[c]	$C_{18}H_{18}$	G9	60.0	ND	0.34	0.46	0.91	1.19
$C_{17}H_{14}$ – isomer[c]	$C_{17}H_{14}$	G10	60.1	ND	0.05	0.04	0.14	0.09
$C_{18}H_{18}$ – isomer[c]	$C_{18}H_{18}$	G11	60.6	ND	0.14	0.17	0.37	0.47

Continues on the next page

Compound	**Formula**	**Peak identifier**[a]	**RT (min)**	**Relative area percentage (%)**				
				Feed	**DB+W+S**	**DB+W**	**DB+S**	**DB**
$C_{19}H_{20}$ – isomer[c]	$C_{19}H_{20}$	H1	63.1	ND	0.02	0.02	0.04	0.04
Decomposition products consisting of $C_{18}H_{20}$ isomers [c,e]	- [e]	H2	74.8	ND	ND	ND	ND	ND
Decomposition products consisting of $C_{18}H_{20}$ isomers[c,e]	- [e]	H3	75.0	ND	ND	ND	ND	ND
Total compounds with RT between 50 and 62 min	-	-	-	ND	4.83	5.42	10.16	10.54
Total compounds with RT between 62 and 80 min	-	-	-	ND	0.18	0.19	0.4	0.52

[a] Peak identifier corresponding to the labelled peaks in the chromatograms shown in **Section B.4** in **Appendix B**.
[b] ND = Not detected. [c] Compound identification based on mass spectral assignment, and not through the use of commercial standard. [d] Commercial standard used for compound identification. [e] The MS spectra of these compounds (**Figures B.30** and **B.31** in **Appendix B**) is similar to those of $C_{18}H_{20}$ isomers but their elution at high retention times indicated that they might be product from in-column cracking of heavier species.

Table 4.10: Abundance of selected compounds in the methanol extract from the control experiments with a retention time lower than 50 min.

Compound	Formula	Peak identifier[a]	Retention Time (min)	Relative area percentage (%)							
				B+K		B+AMS		K		K+AMS	
				Feed	Product	Feed	Product	Feed	Product	Feed	Product
benzene	C_6H_6	A2	6.3	ND[b]	ND	ND	0.06	0.02	0.01	ND	0.01
toluene	C_7H_8	A6	11.0	0.98	0.97	ND	0.25	0.35	0.34	0.07	0.16
ethylbenzene	C_8H_{10}	B2	16.2	0.41	0.33	ND	6.13	0.15	0.11	0.03	2.55
styrene	C_8H_8	B5	17.7	ND	ND	ND	ND	ND	ND	ND	ND
cumene	C_9H_{12}	B8	20.0	0.19	0.18	ND	66.03	0.19	0.22	0.04	3.55
n-propylbenzene	C_9H_{12}	C2	21.7	0.54	0.48	ND	0.53	0.38	0.37	0.08	0.20
AMS	C_9H_{10}	C6	23.1	ND	ND	99.39	10.60	ND	ND	78.35	41.40
tert-butylbenzene	$C_{10}H_{14}$	C7	23.9	3.09	2.90	0.03	0.07	2.41	2.37	0.49	0.44
isobutylbenzene	$C_{10}H_{14}$	C8	24.8	ND	ND	ND	ND	ND	ND	ND	ND
sec-butylbenzene	$C_{10}H_{14}$	C9	24.9	0.41	0.36	0.03	1.45	0.46	0.45	0.09	0.26
m-cymene	$C_{10}H_{14}$	C13	25.6	0.42	0.42	ND	0.05	0.33	0.35	0.07	0.15
p-cymene	$C_{10}H_{14}$	C14	25.7	0.29	0.28	0.03	0.18	0.31	0.33	0.07	0.13
indane	C_9H_{10}	D1	26.0	0.25	0.24	ND	ND	0.17	0.18	0.06	0.02
indene	C_9H_8	D2	26.4	ND	ND	ND	ND	ND	ND	ND	ND
o-cymene	$C_{10}H_{14}$	D3	26.5	ND	ND	ND	ND	ND	ND	ND	ND
n-butylbenzene	$C_{10}H_{14}$	D8	27.3	0.25	0.36	ND	0.05	0.28	0.27	0.05	0.06
2-phenyl-2-propanol	$C_9H_{12}O$	D11	28.4	ND	ND	ND	ND	ND	ND	ND	ND
tetralin	$C_{10}H_{12}$	D18	32.8	0.52	0.42	ND	ND	0.45	0.44	0.09	0.12
naphthalene	$C_{10}H_8$	D20	33.7	ND	0.02	ND	ND	ND	ND	0.00	0.03

Continues on the next page

Compound	Formula	Peak identifier[a]	Retention Time (min)	Relative area percentage (%)							
				B+K		B+AMS		K		K+AMS	
				Feed	Product	Feed	Product	Feed	Product	Feed	Product
2-methylnaphthalene	$C_{11}H_{10}$	E3	38.8	0.68	0.71	ND	ND	0.73	0.70	0.15	0.15
1-methylnaphthalene	$C_{11}H_{10}$	E4	39.5	ND	ND	ND	ND	0.11	0.13	0.02	0.10

[a] Peak identifier according to the labeled compounds in the chromatograms shown in **Section B.4** in the **Appendix B**. [b] ND = Not detected.

Table 4.11: Abundance of compounds with retention times higher than 50 min in the methanol extract from the control experiments B+AMS and K+AMS.

Compound	Formula	Peak identifier[d]	RT (min)	Relative area percentage (%)[a]			
				B+AMS		K+AMS	
				Feed	Product	Feed	Product
$C_{18}H_{20}$ – isomer[c]	$C_{18}H_{20}$	G1	53.2	ND[b]	ND	ND	0.10
$C_{17}H_{20}$ – isomer[c]	$C_{17}H_{20}$	G2	54.8	ND	0.34	ND	0.54
$C_{18}H_{22}$ – isomer[c]	$C_{18}H_{22}$	G3	55.2	ND	1.84	ND	0.44
$C_{18}H_{22}$ – isomer[c]	$C_{18}H_{22}$	G4	55.5	ND	1.9	ND	0.52
dicumene[e]	$C_{18}H_{22}$	G5	56.0	ND	ND	ND	ND
$C_{18}H_{20}$ – isomer[c]	$C_{18}H_{20}$	G6	56.6	ND	0.16	ND	12.72
$C_{18}H_{20}$ – isomer[c]	$C_{18}H_{20}$	G7	59.2	ND	1.4	ND	4.54
$C_{18}H_{20}$ – isomer[c]	$C_{18}H_{20}$	G8	59.4	ND	1.39	ND	3.3
$C_{18}H_{18}$ – isomer[c]	$C_{18}H_{18}$	G9	60.0	ND	1.37	ND	1.78

Continues on the next page

Compound	**Formula**	**Peak identifier**[d]	**RT (min)**	**Relative area percentage (%)**[a]			
				B+AMS		**K+AMS**	
				Feed	**Product**	**Feed**	**Product**
$C_{17}H_{14}$ – isomer[c]	$C_{17}H_{14}$	G10	60.1	ND	0.16	ND	0.02
$C_{18}H_{18}$ – isomer[c]	$C_{18}H_{18}$	G11	60.6	ND	0.59	ND	1.92
$C_{19}H_{20}$ – isomer[c]	$C_{19}H_{20}$	H1	63.1	ND	0.06	ND	0.72
Decomposition product consisting of $C_{18}H_{20}$ isomers[c,f]	- [f]	H2	74.8	ND	ND	ND	0.44
Decomposition product consisting of $C_{18}H_{20}$ isomers[c,f]	- [f]	H3	75.0	ND	ND	ND	0.62
Total compounds with RT between 50 and 62 min	-	-	-	ND	11.45	ND	28.58
Total compounds with RT between 62 and 80 min	-	-	-	ND	0.7	ND	4.41

[a] None of the listed compounds were detected in the feed or products of systems B+K and K, and to improve readability, those results were omitted from the table. [b] ND = Not detected. [c] Compound identification based on mass spectral assignment only, and not through the use of commercial standard. [d] Peak identifier corresponding to the labeled peaks in the chromatograms shown in **Section B.4** in **Appendix B**. [e] Commercial standard used for compound identification. [f] The MS spectra of these compounds (**Figures B.30** and **B.31** in **Appendix B**) is similar to those of $C_{18}H_{20}$ isomers but their elution at high retention times indicated that they might be product from in-column cracking of heavier species.

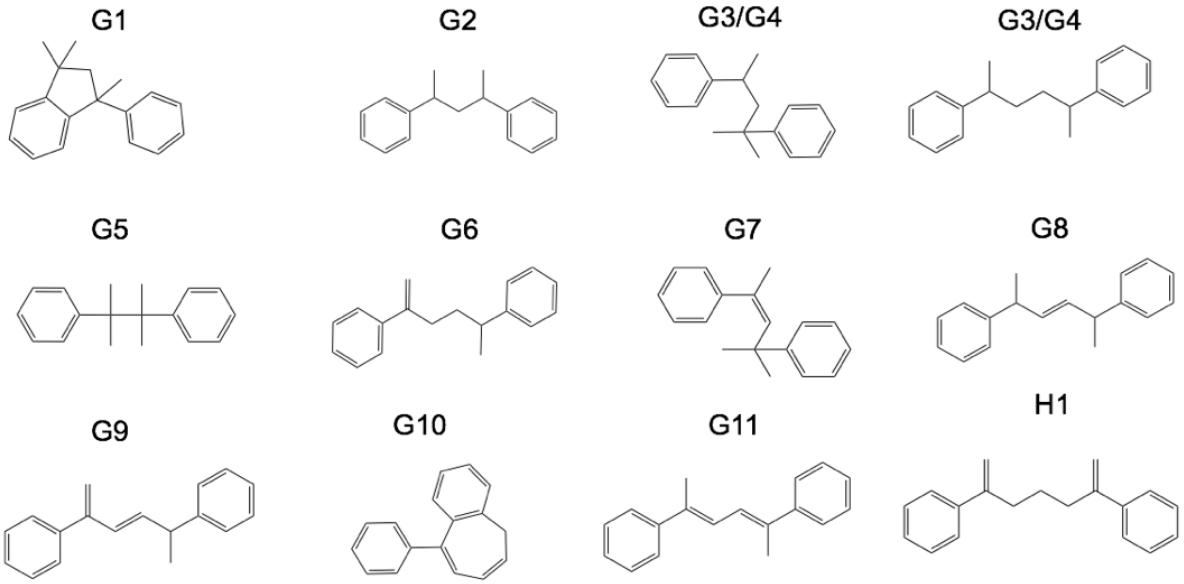

Figure 4.2: Tentative structures of species identified in regions G and H of chromatograms (**Figures B.15–B.18** in **Appendix B**). Assignment of G5 as dicumene was confirmed with a commercial standard. Structures of other species were based on mass spectra as discussed in **Sections B.7** and **B.8** in **Appendix B**.

4.4 Discussion

4.4.1 Influence of the system on AMS conversion

When comparing the AMS conversion of different reaction systems in the thermal treatment experiments **(Table 4.7)**, two observations became immediately apparent. First, the highest AMS conversion (84 ± 2%) was achieved in the absence of water and solids (i.e., system DB). This was found despite DB being the thermal treatment experiment with the shortest ERT **(Table 4.5)**. Second, the presence of water in the water-containing systems caused a major decrease in the AMS conversion while the presence of solids caused only a minor decrease in the AMS conversion.

The high AMS conversion achieved in system DB (84 ± 2%) was comparable to the one achieved in the control reaction B+AMS (90 ± 3%). It is important to remember that the system B+AMS was not diluted with kerosene. Therefore, the similar conversions between these two systems suggested that the dilution of bitumen with kerosene, as applied in all the thermal treatment experiments, did not significantly impact the overall AMS conversion. However, the conversion of AMS with kerosene (K+AMS) resulted in a lower AMS conversion (52 ± 2%) at comparable ERT than the system B+AMS. This finding suggested that, in addition to the species found in kerosene, other compounds within bitumen may have played a role in the chemical transformations involved in AMS conversion. This is further discussed in **Section 4.4.4**.

4.4.1.1 Impact of water on AMS conversion

The conversion of AMS during the thermal treatment of bitumen is expected to rise as the residence time increases [35]. However, the highest AMS conversions during the thermal treatment experiments were observed for the systems that presented the shortest residence times (i.e., DB and DB+S, with AMS conversions of 84 ± 2% and 77 ± 5%, and ERT of 3.6 ± 0.2 min and 4.2 ± 0.2 min, respectively), whereas the lowest AMS conversions (32 ± 5% and 47 ± 5%) were achieved in the water-containing systems. These results indicated that the presence of water definitely suppressed the conversion of AMS and that the lower conversions obtained in the water-containing systems were not due to the small differences in the severity of the treatment.

The results did not provide clarity on whether water had a direct effect (such as through direct chemical or physical interaction with AMS) in lowering the AMS conversion or if water had an indirect influence on other properties of the reaction medium, which subsequently led to the lower AMS conversion. Water interfered with several types of reactions taking place during the treatment. Evidence for this can be found in products that were observed only when water was present in the system. This is discussed in **Section 4.4.2.4**. Beyond this, only speculative explanations for the observed suppression of AMS conversion by water can be offered.

One potential indirect effect of water that could have influenced AMS conversion was the higher pressure in the water-containing systems. The auto-generated pressure of water during the thermal treatment **(Table 4.5)** resulted in higher pressure in the systems DB+W+S and DB+W (4.0 and 4.5 MPa, respectively) as compared to the maximum pressure achieved in the systems DB+S and DB (2 MPa). The critical temperature and pressure of AMS are 372 °C and 3.55 MPa, respectively, indicating that it became a supercritical fluid in the water-containing systems but remained subcritical in systems DB+S and DB [40]. Fluid properties such as viscosity, diffusivity, dielectric constant, and solubility are known to change drastically at supercritical conditions and can thus affect reaction rates [41, 42]. The changes in properties of AMS at supercritical conditions as compared to subcritical conditions could have resulted in a decreased conversion of AMS in the water-containing reaction systems, but further pursuit of this line of investigation was beyond the scope of this study.

4.4.1.2 Impact of mineral solids on AMS conversion

The presence of mineral solids in systems DB+S, which had similar ERT to system DB **(Table 4.5)**, did not appear to have influenced the AMS conversion (77 ± 5% in system DB+S and 84 ± 2% in system DB, **Table 4.7**). The system DB+W+S had a lower conversion than DB+W (32 ± 5% vs. 47 ± 5%), but it also had the highest standard deviation in its ERT (s = 1.0 min) when compared to the other systems, making it difficult to affirm that the lower conversion in that system was due to the presence of solids rather than the variation in its ERT. These results suggested that, if solids had any impact in suppressing AMS conversion, this impact was minor when AMS was reacted in the presence of solids alone.

One potential mechanism by which mineral solids from froth could hinder the conversion of AMS is by amplifying free radical termination by acting as radical scavengers. The primary minerals identified in the froth solids used in this study were quartz and kaolinite, constituting 53 wt% and 26 wt%, respectively (refer to **Section 4.2.1**). Clays like kaolinite are recognized for their ability to both donate and accept electrons [43]. On the other side, quartz is chemically inert and has a very stable crystalline structure [44]. Rutile and anatase, present in smaller proportions within the froth solids, are acknowledged for their ability to donate electrons [45]. If the rate of electron acceptance surpasses electron donation, free radical termination over these solids could be heightened in comparison to free radical initiation or propagation, potentially resulting in a decrease in AMS conversion. This effect is likely to be minor during thermal conversion in the presence of mineral solids.

4.4.1.3 Synergistic effect of water and mineral solids on AMS conversion

After discussing the individual impacts of water and solids on AMS conversion, there was also an interest in assessing the potential synergistic effect of both water and solids on AMS conversion. Fan et al [46]. Suggested that minerals and steam had a synergistic effect on the composition and viscosity of heavy oils during thermal treatment at 240 °C. In the current study, the observed hindrance of AMS conversion by mineral solids appeared to be somewhat more pronounced in the presence of water, even when accounting for variability in severity and conversion across other reaction systems. Minerals present in bitumen froth, including both clays like kaolinite and non-clay minerals such as rutile and calcite, can undergo hydration [47–49]. This process has the potential to alter the surface properties of these minerals and, as a result, may influence their interactions with organic matter. However, exploring the changes in the minerals properties due to hydration were not within the scope of this study.

4.4.1.4 Verification of semi-quantitative RAP data

The pattern of AMS conversion (quantitatively calculated through calibrated GC-FID data, **Table 4.7**) among the thermal treatment experiments (i.e., AMS conversion in: DB – 84% > DB+S – 77% > DB+W – 47% > DB+W+S – 32%) was consistent with the RAP (semi-quantitatively calculated from GC-MS data, **Table 4.6**) of non-converted AMS in the thermally treated products (i.e., RAP of AMS in products: DB – 12.8% < DB+S – 14.5% < DB+W – 34.2% < DB+W+S – 42.5%). This result provided an additional consistency check for the use of the RAP as a semi-quantitative assessment of the abundance of species in the methanol extract from feed and products of the experiments in this study.

The material balance on AMS and its products **(Table 4.6)** was a critical consistency check for the semi-quantitative analyses done in this study through the use of the RAP of AMS and its products. The AMS balance varied from 87.3 to 93.7% in the thermal treatment experiments and from 97.4 to 103.3% in the control experiments. The comparable AMS balance within each type of experiment was an indication that the differences in RAP of the monitored species in the feed and reaction products were due to the chemical changes during the treatment rather than poor product extraction from the bitumen phase by methanol. The products from the control reactions were nearly completely recovered, while some products from the thermal treatment experiments (around 6.3 to 12.7%) were not recovered by the methanol extraction. The unrecovered products could be the result of their partitioning between the methanol and bitumen phases, as some of these products may have remained dissolved in the bitumen phase.

4.4.2 Reaction pathways for conversion of AMS

The conversion of AMS in this study could proceed through two distinct reaction intermediates, namely free radicals [50] and, when minerals are present, cationic intermediates [29, 51]. Before discussing the specific influence of water and minerals on the conversion of AMS as a probe molecule in bitumen, it is useful to look at potential reaction pathways and evidence that the conversion of AMS proceeded through these pathways. This can then serve as a roadmap to assist with the interpretation of the results.

It is also necessary to be aware of the self-reactions of AMS. These are reactions that can take place during thermal conversion in the absence of bitumen. The main products from the thermal self-conversion of AMS could be identified by monitoring the changes in the RAP of the feed and product of the control experiment in kerosene. The kerosene (K) itself was little affected by thermal conversion. When AMS was converted in kerosene (K+AMS), the main products from the thermal conversion of AMS were ethylbenzene, cumene, and dimerization products (**Table B.14** in **Appendix B**). Minor products included toluene, *n*-propylbenzene, *sec*-butylbenzene, and cymene isomers.

4.4.2.1 Evidence of hydrogen transfer

Evidence of hydrogen transfer in this study was the conversion of AMS into cumene (**Table 4.7**). Since both free radical and cationic conversion are considered, both pathways will be discussed.

The first potential pathway is the free radical pathway for the transfer hydrogenation of AMS, which is shown in **Figure 4.3**, paths A–B. The cumyl radical might be initiated through hydrogen transfer from any of the various hydrogen donor species in bitumen to AMS (**Figure 4.3**, path A), since these species react readily with olefinic groups at high temperature [38, 50]. Initial hydrogen transfer can also take place by hydrogen disproportionation of two AMS molecules, with the result that the cumyl radical and an allylic methylstyrene radical are formed (not shown in **Figure 4.3**). Hydrogen disproportionation becomes more relevant when there are few hydrogen donor species available, for example, in the absence of bitumen, such as in the control experiment with kerosene (K+AMS). The second hydrogen transfer step to form cumene (**Figure 4.3**, path B) takes place in an analogous way.

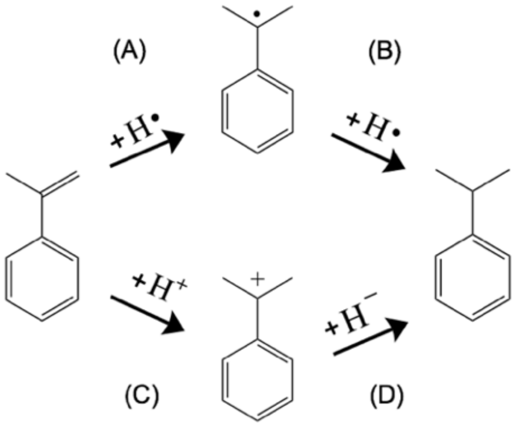

Figure 4.3: Possible pathways for the free radical and cationic transfer hydrogenation of AMS to cumene.

The second possible pathway for cumene formation is the cationic conversion of AMS into cumene (**Figure 4.3**, paths C–D). Alkenes are readily protonated by Brϕnsted-Lowry acids, forming a carbocation that can engage in various reactions, including isomerization, cracking, and addition [52]. Once the cumyl carbocation is formed by the protonation of AMS (**Figure 4.3**, path C), there are consequently many reaction possibilities. However, forming cumene is challenging because it requires a hydride ion transfer (**Figure 4.3**, path D). The hypothetical pathway shown in **Figure 4.3**, paths C–D, requires both a nucleophile and a hydride donor [53]. The importance of hydride transfer during cationic polymerization and catalytic cracking is well documented in the literature [52, 54–57], but it is usually a significant reaction pathway only under specific conditions, such as those found in aliphatic alkylation and aromatization processes.

Irrespective of the path followed, the conversion of AMS to cumene requires the transfer of two hydrogens, which means that other species in the reaction mixture become more hydrogen-depleted. This is difficult to discern in bitumen, but there was evidence for the formation of hydrogen-depleted species in the identified products. For example, the decrease in the RAP of tetralin was followed by an increase in the RAP of naphthalene in all the thermal treatment experiments and the control reaction B+K (see **Tables 4.8** and **4.10**). Also, the AMS dimerization products contained hydrogen-depleted species, which included $C_{18}H_{18}$ isomers.

4.4.2.2 Evidence of methyl transfer

Besides hydrogen transfer, the importance of intermolecular methyl transfer during the thermal conversion at 400 °C has been pointed out before [27]. This is a free radical pathway analogous to hydrogen transfer but involving a methyl radical instead of hydrogen.

Cationic methyl transfer is found in acid-catalyzed reactions such as the intramolecular isomerization of alkyl aromatics and the intermolecular methyl disproportionation of alkyl aromatics [58]. Methyl cation transfer is also involved in acid-catalyzed methylation of aromatics [59]. These reactions are limited to bond breaking and bond formation between methyl groups and an aromatic ring.

In this study, there was evidence of methyl transfer through the conversion of AMS to ethylbenzene and the formation of C_4-alkyl benzenes, such as *sec*-butylbenzene. These products are the result of reactions involving the alkyl group attached to the aromatic ring, rather than reactions between the alkyl group and the aromatic ring itself. This type of reaction can only be explained in terms of a free radical pathway, and it does not appear to have a realistic equivalent cationic pathway.

Methyl transfer can take place from species such as a cumene, or a cumyl radical, which in the present study would explain the formation of ethylbenzene (peak identifier B2 in **Tables 4.8** and **4.10**). When a methyl radical is transferred to AMS (**Figure 4.4**), it can take place first, as shown in paths A and B, or it can be transferred to a cumyl radical as a second step, as shown in paths C and D. The contributions of paths B and C in **Figure 4.4** were not expected to be significant because they result in the formation of an energetically unfavorable primary radical. It was expected that most of the reactions would proceed through paths A and D in **Figure 4.4**, because the radicals formed are in the benzylic position and resonance-stabilized by the adjacent aromatic ring.

The high increase in the RAP of *sec*-butylbenzene across all the reaction systems containing AMS, in contrast to the near constant RAP of *tert*-butylbenzene (peak identifiers C9 and C7 in **Tables 4.8** and **4.10**), indicated that path A in **Figure 4.4** was the dominant pathway. In the present investigation, evidence of methyl transfer as the initial step in the formation of *sec*-butylbenzene (**Figure 4.4**, path A) reinforced the significance of methyl transfer in promoting chain reactions.

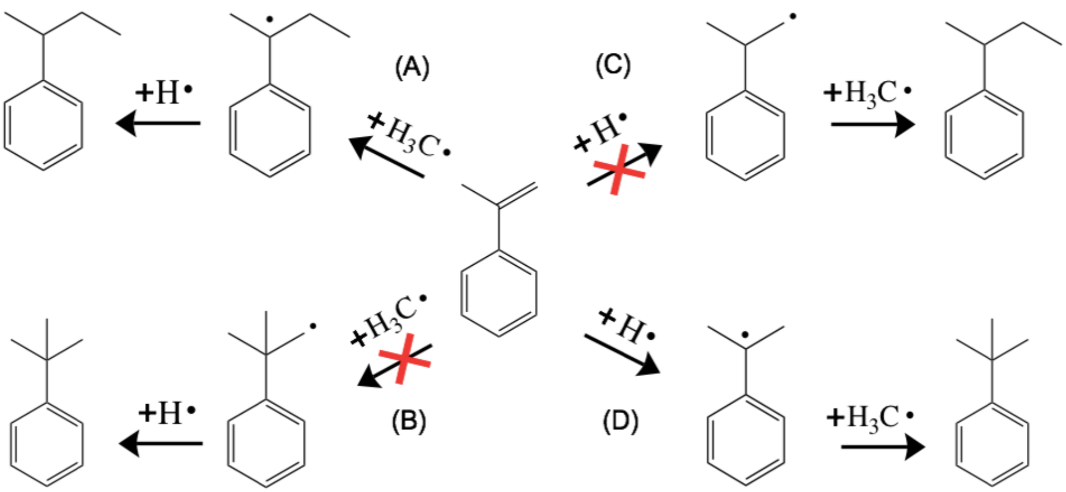

Figure 4.4: Possible free radical pathways for the conversion of AMS into *sec*-butylbenzene and *tert*-butylbenzene.

4.4.2.3 Evidence of cracking

In thermal conversion where the objective is to decrease the average molecular weight of the product compared to the feed, conditions are deliberately selected to favor free radical cracking. This type of cracking forms the basis of industrial processes such as visbreaking and is described in the literature [57, 60]. The type of free radical "cracking" that can be observed with AMS is illustrated by pathway A in **Figure 4.5**, which is a methyl transfer reaction and not free radical β-scission, which is normally associated with thermal cracking.

In the presence of mineral matter, cracking can potentially also take place through a cationic pathway involving a carbocation intermediate. This type of acid-catalyzed cracking forms the basis of industrial processes such as fluid catalytic cracking and is described in the literature [57, 61]. Acid-catalyzed conversion of AMS proceeds by protonation to yield the cumyl carbocation illustrated by pathway B in **Figure 4.5**. At 400 °C, the cumyl carbocation will not lead to cracking. Dealkylation by acid-catalyzed cracking proceeds when the carbon attached to the aromatic is not unsaturated, as illustrated by pathway C in **Figure 4.5** [62].

AMS is not a useful probe molecule for studying either free radical or acid-catalyzed cracking. Instead, what appears as "cracked" products are actually products of methyl transfer (**Section 4.4.2.2**) and not cracking by β-scission.

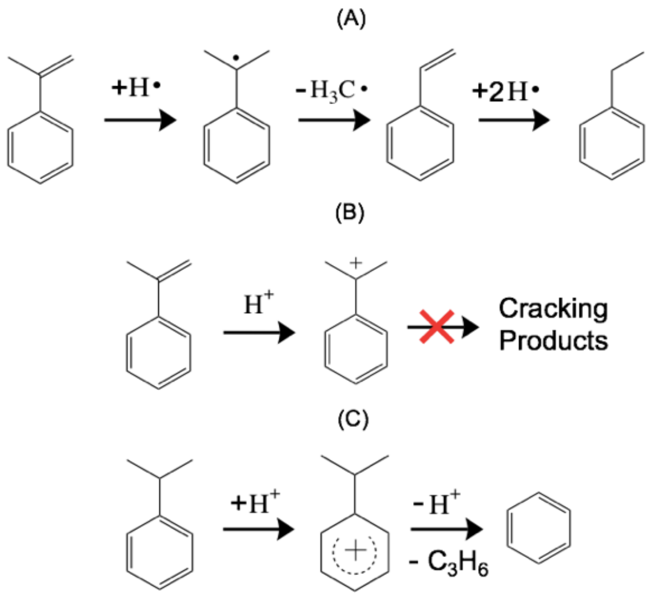

Figure 4.5: Possible pathways at 400 °C for the (A) free radical cracking of AMS to yield ethylbenzene, (B) no acid catalyzed cracking when AMS is protonated, and (C) acid catalyzed cracking of cumene to yield benzene.

4.4.2.4 Evidence of hydration

A total of 17 oxygenated compounds were monitored in this study (refer to **Tables B.13** and **B.14** in **Appendix B**), but only 2-phenyl-2-propanol was detected during the treatment. The formation of that compound was only observed in the water-containing systems (DB+W+S and DB+W). **Figure 4.6** illustrates the hydration of AMS into 2-phenyl-2-propanol.

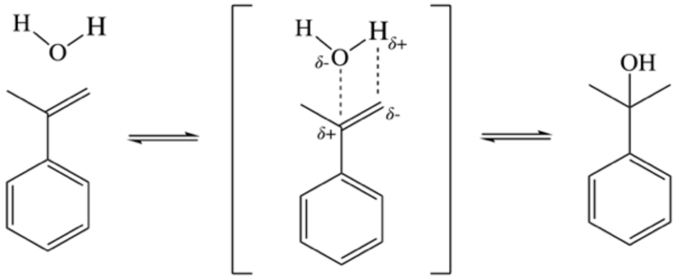

Figure 4.6: Hydration of AMS to yield 2-phenyl-2-propanol.

The hydration of olefins can take place in superheated water, even in the absence of an acid catalyst. It was reported that the equilibrium shown in **Figure 4.6** is rapidly established, and the conversion is typically low [63]. If this is indeed the case, then the difference in amount of 2-phenyl-2-propanol

(RAP of 0.08% in B+W vs. 0.23% in B+W+S, **Table 4.8**) is not meaningful and within the range of analytical uncertainty.

The addition of water to alkenes is favored by changes in the physicochemical properties of water as it approaches its critical point. As the temperature of water increases, its dissociation constant (K_w) also increases, making it an effective medium for acid- and base-catalyzed organic reactions [64]. However, in the case of hydration, which is exothermic, an increase in temperature would also imply that the equilibrium concentration of the alcohol would be lower.

4.4.2.5 Evidence of addition reactions

There was substantial evidence of addition reactions involving AMS during the thermal conversion. Most of the addition products were identified at high retention times of the chromatograms (RT > 50 min), and some of them are listed in **Tables 4.9** and **4.11**, with tentative structures shown in **Figure 4.2**. All species listed in **Tables 4.9** and **4.11** were not detected in the feed but were formed during thermal conversion.

Addition reactions involving AMS can take place by free radical and carbocation intermediates as shown in **Figure 4.7**.

There are three potential pathways for addition reactions involving AMS dimerization, all of which are illustrated in **Figure 4.7**. These are: (i) hydrogen transfer to AMS to form a cumyl free radical; (ii) a concerted reaction passing through a diradical species followed by 1,5-intramolecular hydrogen transfer; and (iii) acid-catalyzed protonation of AMS to form a cumyl carbonation.

The AMS dimers ($C_{18}H_{20}$ isomers) identified in this study were the species G1, G6, G7, and G8. Compound G1 corresponded to the cyclic AMS dimer [29, 52]. It was exclusively detected in the control system K+AMS (**Table 4.11**). The $C_{18}H_{20}$ isomers are informative because they are primary products from AMS dimerization that also provide information about the reaction pathway.

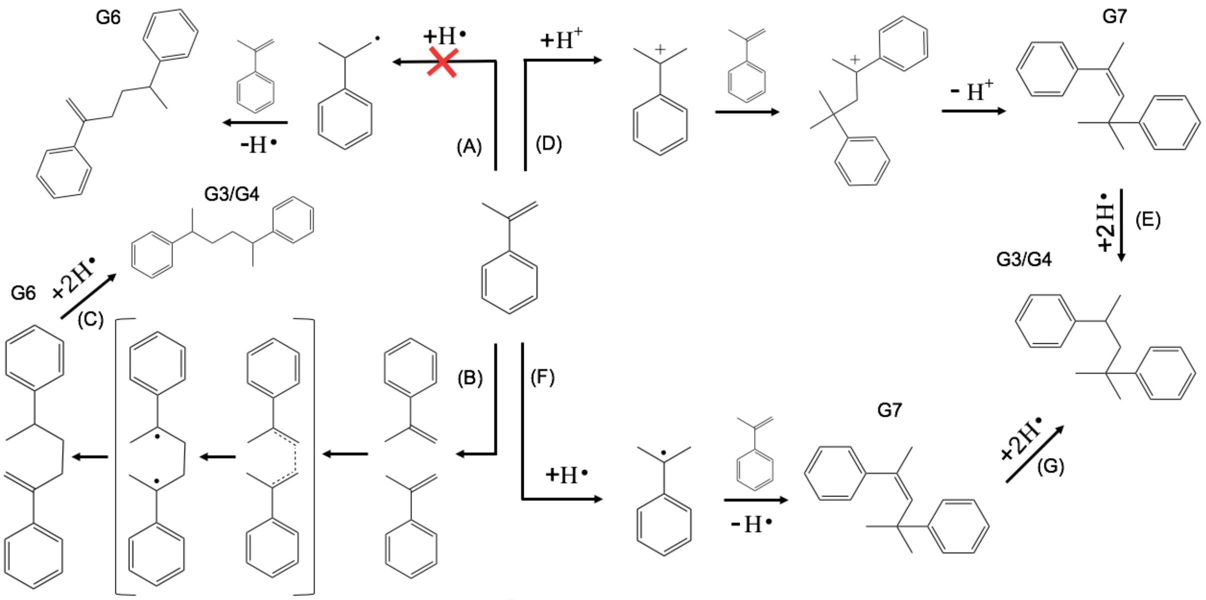

Figure 4.7: Possible free radical and cationic addition pathways for the formation of AMS dimers and their derivatives.

Hydrogen transfer to form a cumyl radical with the radical in the terminal position as opposed to the benzylic position is energetically unfavorable (pathway A in **Figure 4.7**). Although it cannot be ruled out completely, it appears more likely that terminal bond formation that forms two benzylic radicals as a diradical intermediate is more likely (pathway B in **Figure 4.7**). The diradical intermediate is an example of the general class of 1,4-diradical intermediates described in the literature [65]. There is support for such a concerted mechanism involving AMS in the work by Rüchardt et al. [66]. The concerted bimolecular reaction through path B is favored in a reaction environment low in hydrogen donors. This could be seen from **Tables 4.9** and **4.11**, where there was a higher abundance of compound G6 in the system K+AMS (RAP of 12.72%) compared to the other reaction systems containing bitumen (RAP of 0.16–0.22%).

The main difference between the formation of compound G6 through pathway B in **Figure 4.7** and that of compound G8 (not shown) is the way in which hydrogen migration takes place to form the olefinic dimer as a product. For compound G6, the process involves a 1,5-hydrogen transfer, whereas for compound G8, it requires a 1,2-hydrogen migration.

Free radical addition starting with hydrogen transfer to AMS (pathway F in **Figure 4.7**) leads to compound G7. However, this cannot be differentiated from cationic addition of AMS (pathway D in **Figure 4.7**) that leads to the same product, compound G7.

Cationic addition of AMS was reported both for acid catalysts and minerals present in bitumen froth [29, 67]. When comparing the RAP of compound G7 in the thermally converted products without solids and with solids (**Table 4.9**) there was no directional change to suggest that cationic addition contributed meaningfully to the formation of compound G7.

Hydrogen transfer to the AMS dimers (paths C, E, and G in **Figure 4.7**) leads to the formation of the corresponding saturated $C_{18}H_{22}$ isomers, compounds G3 and G4. The mass spectra of G3 and G4 (**Figures B.21** and **B.22** in **Appendix B**) were almost identical, making it challenging to specifically assign their structures. Whatever the specific assignment, the RAP in the products of all the reaction systems were comparable (**Tables 4.9** and **4.11**).

When comparing the yield of compounds G3 and G4 in the control systems B+AMS and K+AMS (**Table 4.11**), it became evident that they were formed to a greater extent in the system B+AMS, with RAP of 1.84–1.90%, in contrast to K+AMS, where their RAP was lower (0.44–0.52%). This difference was observed despite the ample availability of G6 and G7 in the K+AMS system. It is worth noting that kerosene lacks hydrogen donors, which are present in bitumen [38], and this limited availability of an effective hydrogen source might have hindered the hydrogenation of G6 and G7 into G3 and G4 in the K+AMS system. This observation also provided additional support for the assignment of compounds G3 and G4 as the hydrogenated products of AMS dimers.

4.4.3 Influence of water and mineral solids on hydrogen transfer reactions

The first objective of this study was to evaluate the effect of water and minerals on hydrogen transfer taking place during the thermal treatment of froth. From the data on the selectivity of AMS conversion to cumene (**Table 4.7**), there was substantial indication that the presence of mineral solids and water both favored hydrogen transfer during the treatment.

When comparing the systems that had comparable AMS conversions (B+AMS, DB, and DB+S), the presence of mineral solids in the system DB+S resulted in an increased selectivity to cumene of about 20% (from 63–65 ± 2% in B+AMS and DB to 84 ± 2% in DB+S). Additionally, the presence of minerals in the water-containing systems also resulted in an increased selectivity to cumene (73 ± 3% in DB+W vs. 87 ± 1% in DB+W+S).

The observed changes in selectivity could not be ascribed just to differences in conversion. For example, in comparing the system DB+S+W to the system DB+S (**Table 4.7**), the former presented lower conversion (32 ± 5% vs. 77 ± 5%), yet both systems had comparable selectivity to cumene (87 ± 1% in DB+S+W vs. 84 ± 2% in DB+S).

The effect of water in favoring hydrogen transfer during thermal treatment of bitumen has been suggested in the literature [22–24]. Some of these studies employed deuterated water to demonstrate that hydrogen is transferred from water to bitumen during hydrothermal treatment [24, 68]. Some authors have claimed that water acted as a hydrogen donor solvent, while other claimed that water acted as a hydrogen transfer agent rather than a hydrogen donor [68, 69].

In this study, it was not clear whether water and mineral solids suppressed alternative reaction pathways to favor hydrogen transfer or whether water and mineral solids increased hydrogen transfer in some way. This aspect is left unresolved.

There was no apparent synergistic effect of water and mineral solids on hydrogen transfer under the conditions of this study.

4.4.4 Influence of water and mineral solids on cracking and addition reactions

The second objective of this study was to investigate the contributions of water and solids to cracking and addition reactions during the thermal treatment of froth. In this respect, AMS was not a useful probe molecule for assessing cracking (**Section 4.4.2.3**), but it was informative as a probe molecule for assessing addition (**Section 4.4.2.5**).

When analyzing the effect of mineral solids and water on the formation of addition products (**Table 4.9**), there were two noticeable observations.

First, when comparing the thermal conversion of bitumen without solids (DB) and with mineral solids (DB+S), the latter appeared to have a slightly different selectivity profile, but there was no apparent effect on the overall formation of addition products.

Second, the presence of water during the thermal conversion suppressed the formation of AMS-derived addition products. The overall formation of addition products in the water-containing systems was about half of those obtained in the absence of water (RAP of 5.01–5.61% versus 10.20–11.06%, **Table 4.9**). This result is in agreement with previous studies which reported that water suppressed coke formation during thermal treatment of bitumen [20, 21, 24].

The RAP of most of the reported addition products listed in **Table 4.9** was lower in the system DB+W+S as compared to the system DB+W. The reduced RAP of these species in the presence of both water and solids may be attributed to their synergistic effect on AMS conversion, as discussed in **Section 4.4.1.3**.

Finally, it was noteworthy that the conversion of AMS in the control experiment K+AMS showed a substantially higher selectivity to addition products when compared to all the reaction systems in this study (the total RAP of compounds with RT between 50 and 80 min was 33%, see **Table 4.11**). Most of the compounds that eluted in region H of the K+AMS chromatogram (**Figure B.18** in **Appendix B**) were not detected for the other reaction systems (see **Tables 4.9** and **4.11**). This was an important observation because kerosene had the opposite effect on AMS selectivity to addition products than water. The reason for this difference was not determined.

4.4.5 Implications of hydrothermal treatment of froth for bitumen upgrading

The hydrothermal treatment of froth as a means of achieving bitumen upgrading in the presence of water and mineral solids was investigated in a prior study conducted at 400 °C [10]. The viscosity and density of the thermally treated bitumen in the presence of water and solids were slightly higher than in the treatment of bitumen on its own. It was expected that these macroscopic observations could be related to a decrease in hydrogen transfer activity or an increase in addition product formation in the presence of water and mineral solids. The present study provided no evidence to support that. In fact, the findings from this study indicated that the opposite was true.

It was found that water suppressed conversion somewhat (**Section 4.4.1.1**), but selectivity to products relying on hydrogen transfer increased (**Section 4.4.3**) and selectivity to addition products decreased (**Section 4.4.4**). Also, the presence of mineral solids during the treatment may have resulted in a minor decrease in conversion (**Section 4.4.1.2**), but the selectivity to products relying on hydrogen transfer increased (**Section 4.4.3**) and selectivity to addition products was unaffected (**Section 4.4.4**).

4.5 Conclusions

The present study investigated the impact of water and mineral solids on hydrogen and methyl transfer, cracking, and addition reactions taking place during hydrothermal treatment of oilsands bitumen froth at 400 °C. AMS was employed as a probe molecule, and its potential conversion pathways were discussed from the perspective of both free radical and cationic conversions. Although the products resulting from the AMS conversion provided evidence of most of the reactions of interest in this investigation, it was observed that AMS was not suitable for examining cracking under the specific experimental conditions of this study. There was substantial evidence that both water and mineral solids influenced the conversion of AMS and, consequently, the composition of the final products.

The main findings derived from this study are summarized as follows:

(a) Water hindered the AMS conversion and had an influence on various types of reactions taking place during the treatment. An example of this influence was the exclusive formation of 2-phenyl-2-propanol in the water-containing systems. Mineral solids, on the other hand, seemed to have a minor impact on lowering the AMS conversion.

(b) Three potential pathways for the free radical conversion of AMS into cumene were presented. Hydrogen transfer from hydrogen donors is a preferred route for initiating the cumyl radical in the reaction media containing bitumen, while hydrogen disproportionation between two AMS molecules would be favored in an environment low in hydrogen donors. The cationic conversion of AMS to cumene is challenging and unlikely to occur under the conditions of this study. Regardless of the pathway, the conversion of AMS to cumene was followed by the formation of hydrogen-depleted species in the product mixture.

(c) Evidence of methyl transfer as the first step in the conversion of AMS into *sec*-butylbenzene highlighted the importance of methyl transfer in promoting chain reactions.

(d) The pathways for AMS dimerization appeared to be influenced by the availability of hydrogen donors in the reaction medium. There was evidence of two potential free radical pathways: one involved a concerted bimolecular reaction between AMS molecules, which is potentially favored in a reaction medium with limited hydrogen donors, and the other involved the initiation of the cumyl radical through hydrogen transfer, which seemed to be favored in bitumen. Based on product formation, it was not possible to distinguish between free radical and cationic addition. The formation of hydrogenated products from the AMS dimers appeared to be constrained when hydrogen donors were limited.

(e) There was substantial evidence that both water and mineral solids favored hydrogen transfer during the thermal conversion. Nevertheless, it remained unclear whether this influence was a result of the suppression of alternative reaction pathways or if water and mineral solids actively promoted hydrogen transfer in some way.

(f) The presence of water hindered the formation of AMS-derived addition products, while kerosene favored the formation of those species. The presence of mineral solids appeared to have a minor effect on the selectivity profile of the addition products, but there was no apparent impact on their overall formation.

4.6 References

(1) Gray, M. R., *Upgrading oilsands bitumen and heavy oil*; Pica Pica Press - Edmonton: 2015.

(2) Masliyah, J. H.; Czarnecki, J.; Xu, Z., *Handbook on theory and practice of bitumen recovery from Athabasca oil sands - Volume 1: Theoretical basis*; Kingsley Knowledge Publishing: 2011, p 468.

(3) Rao, F.; Liu, Q. Froth treatment in Athabasca oil sands bitumen recovery process: A review. *Energy Fuels* **2013**, *27* (12), 7199–7207.

(4) Velayati, A.; Habibi, A.; Nikrityuk, P.; Tang, T.; Zeng, H. Emulsions in Bitumen Froth Treatment and Methods for Demulsification and Fines Removal in Naphthenic Froth Treatment: Review and Perspectives. *Energy Fuels* **2022**, *36* (16), 8607–8623.

(5) De Klerk, A. Processing unconventional oil: partial upgrading of oilsands bitumen. *Energy Fuels* **2021**, *35* (18), 14343–14360.

(6) Gray, M. R. Fundamentals of partial upgrading of bitumen. *Energy Fuels* **2019**, *33* (8), 6843–6856.

(7) De Klerk, A.; Gray, M. R.; Zerpa, N. Chapter 5 - Unconventional Oil and Gas: Oilsands, In *Future Energy: Improved, Sustainable and Clean Options for our Planet*, ed. by Letcher, T. M., 2nd ed., Elsevier: Amsterdam, 2014, pp 95–116.

(8) Chen, Q.; Stricek, I.; Cao, M.; Gray, M. R.; Liu, Q. Influence of hydrothermal treatment on filterability of fine solids in bitumen froth. *Fuel* **2016**, *180*, 314–323.

(9) Turuga, A. S. S.; de Klerk, A. Hydrothermal Treatment of Bitumen Froth: Impact of Mineral Solids and Water on Bitumen Properties. *Energy Fuels* **2021**, *35* (21), 17536–17550.

(10) Bassane, J. F. P.; de Klerk, A. Visbreaking of Bitumen Froth: Influence of Minerals, Water, and Solvent on the Physicochemical Changes in the Bitumen Phase. *Energy Fuels* **2023**, *37* (16), 11820–11837.

(11) LePrince, P. Visbreaking of residues, In *Petroleum Refining. Vol.3. Conversion processes*, ed. by LePrince, P., Editions Technip: Paris, 2001, pp 365–378.

(12) Kapadia, P. R.; Kallos, M. S.; Gates, I. D. A review of pyrolysis, aquathermolysis, and oxidation of Athabasca bitumen. *Fuel Process. Technol.* **2015**, *131*, 270–289.

(13) Kapadia, P. R.; Kallos, M. S.; Gates, I. D. A new reaction model for aquathermolysis of Athabasca bitumen. *Can. J. Chem. Eng.* **2013**, *91* (3), 475–482.

(14) Zhang, J.; Han, F.; Yang, Z.; Zhang, L.; Wang, X.; Zhang, X.; Jiang, Y.; Chen, K.; Pan, H.; Lin, R. Significance of aquathermolysis reaction on heavy oil recovery during the steam-assisted gravity drainage process. *Energy Fuels* **2020**, *34* (5), 5426–5435.

(15) Félix, G.; Tirado, A.; Al-Muntaser, A.; Kwofie, M.; Varfolomeev, M. A.; Yuan, C.; Ancheyta, J. SARA-based kinetic model for non-catalytic aquathermolysis of heavy crude oil. *J. Pet. Sci. Eng.* **2022**, *216*, 110845.

(16) Jia, N.; Zhao, H.; Yang, T.; Ibatullin, T.; Gao, J. Experimental measurements of bitumen–water aquathermolysis during a steam-injection process. *Energy Fuels* **2016**, *30* (7), 5291–5299.

(17) Hongfu, F.; Yongjian, L.; Liying, Z.; Xiaofei, Z. The study on composition changes of heavy oils during steam stimulation processes. *Fuel* **2002**, *81* (13), 1733–1738.

(18) Canıaz, R. O.; Erkey, C. Process intensification for heavy oil upgrading using supercritical water. *Chem. Eng. Res. Des.* **2014**, *92* (10), 1845–1863.

(19) Canıaz, R. O.; Arca, S.; Yaşar, M.; Erkey, C. Refinery bitumen and domestic unconventional heavy oil upgrading in supercritical water. *J. Supercrit. Fluids* **2019**, *152*, 104569.

(20) Watanabe, M.; Kato, S. N.; Ishizeki, S.; Inomata, H.; Smith Jr, R. L. Heavy oil upgrading in the presence of high density water: basic study. *J. Supercrit. Fluids* **2010**, *53* (1-3), 48–52.

(21) Morimoto, M.; Sugimoto, Y.; Saotome, Y.; Sato, S.; Takanohashi, T. Effect of supercritical water on upgrading reaction of oil sand bitumen. *J. Supercrit. Fluids* **2010**, *55* (1), 223–231.

(22) Sato, T.; Adschiri, T.; Arai, K.; Rempel, G. L.; Ng, F. T. Upgrading of asphalt with and without partial oxidation in supercritical water. *Fuel* **2003**, *82* (10), 1231–1239.

(23) Schlepp, L.; Elie, M.; Landais, P.; Romero, M. Pyrolysis of asphalt in the presence and absence of water. *Fuel Process. Technol.* **2001**, *74* (2), 107–123.

(24) Dutta, R. P.; McCaffrey, W. C.; Gray, M. R.; Muehlenbachs, K. Thermal cracking of Athabasca bitumen: influence of steam on reaction chemistry. *Energy Fuels* **2000**, *14* (3), 671–676.

(25) Cheng, Z. M.; Ding, Y.; Zhao, L. Q.; Yuan, P. Q.; Yuan, W. K. Effects of supercritical water in vacuum residue upgrading. *Energy Fuels* **2009**, *23* (6), 3178–3183.

(26) Yuan, P. Q.; Zhu, C. C.; Liu, Y.; Bai, F.; Cheng, Z. M.; Yuan, W. K. Solvation of hydrocarbon radicals in sub-CW and SCW: An ab initio MD study. *J. Supercrit. Fluids* **2011**, *58* (1), 93–98.

(27) Tannous, J. H.; de Klerk, A. Methyl and hydrogen transfer in free radical reactions. *Energy Fuels* **2020**, *34* (2), 1698–1709.

(28) Trejo, F.; Rana, M. S.; Ancheyta, J. Genesis of Acid- Base Support Properties with Variations of Preparation Conditions: Cumene Cracking and Its Kinetics. *Ind. Eng. Chem. Res.* **2011**, *50* (5), 2715–2725.

(29) Turuga, A. S. S.; de Klerk, A. Free Radical and Cationic Addition due to Clay Minerals Found in Bitumen Froth at 250 °C Probed with Use of α-Methylstyrene and 1-Octene. *Energy Fuels* **2022**, *36* (23), 14148–14162.

(30) Kaminsky, H. A.; Etsell, T. H.; Ivey, D. G.; Omotoso, O. Distribution of clay minerals in the process streams produced by the extraction of bitumen from Athabasca oil sands. *Can. J. Chem. Eng.* **2009**, *87* (1), 85–93.

(31) Zhao, J.; Liu, Q.; Gray, M. R. Characterization of fine solids in Athabasca bitumen froth before and after hydrothermal treatment. *Energy Fuels* **2016**, *30* (3), 1965–1971.

(32) Johnston, C. T. Surface chemistry of oil-sands clay minerals, In *Introduction to Oil Sands Clays*, ed. by Hockley, D.; Omotoso, O.; Kaminsky, H., Vol. 22, Clay Minerals Society: Chantilly, VA, 2018, pp 33–60.

(33) He, M.; Wang, Z.; Moldowan, M. J.; Peters, K. Insights into catalytic effects of clay minerals on hydrocarbon composition of generated liquid products during oil cracking from laboratory pyrolysis experiments. *Org. Geochem.* **2022**, *163*, 104331.

(34) Rahimi, P. M.; Gentzis, T. The Chemistry of Bitumen and Heavy Oil Processing, In *Practical Advances in Petroleum Processing*, ed. by Hsu, C. S.; Robinson, P. R., Vol. 2, Springer: New York, 2006, pp 149–188.

(35) Naghizada, N.; Prado, G. H. C.; de Klerk, A. Uncatalyzed hydrogen transfer during 100–250 °C conversion of asphaltenes. *Energy Fuels* **2017**, *31* (7), 6800–6811.

(36) Yan, T. Characterization of visbreaker feeds. *Fuel* **1990**, *69* (8), 1062–1064.

(37) Polovor, Y. N.; Kaminskaya, Y. G.; Vykhrestyuk, N.; Tkachenko, D. Conversions of α-methylstyrene on aluminosilicate at cracking temperatures. *Pet. Chem. U.S.S.R.* **1977**, *17* (4), 215–223.

(38) Gould, K. A.; Wiehe, I. A. Natural hydrogen donors in petroleum resids. *Energy Fuels* **2007**, *21* (3), 1199–1204.

(39) Carbognani, L.; Lubkowitz, J.; Gonzalez, M. F.; Pereira-Almao, P. High temperature simulated distillation of Athabasca vacuum residue fractions. Bimodal distributions and evidence for secondary "on-column" cracking of heavy hydrocarbons. *Energy Fuels* **2007**, *21* (5), 2831–2839.

(40) Steele, W.; Chirico, R.; Knipmeyer, S.; Nguyen, A. Vapor Pressure, Heat Capacity, and Density along the Saturation Line, Measurements for Dimethyl Isophthalate, Dimethyl Carbonate, 1, 3, 5-Triethylbenzene, Pentafluorophenol, 4-tert-Butylcatechol, α-Methylstyrene, and N, N '-Bis (2-hydroxyethyl) ethylenediamine. *J. Chem. Eng. Data* **1997**, *42* (6), 1008–1020.

(41) Savage, P. E.; Gopalan, S.; Mizan, T. I.; Martino, C. J.; Brock, E. E. Reactions at supercritical conditions: applications and fundamentals. *AIChE J.* **1995**, *41* (7), 1723–1778.

(42) Tanko, J. M.; Pacut, R. Enhanced cage effects in supercritical fluid solvents. The behavior of diffusive and geminate caged-pairs in supercritical carbon dioxide. *J. Am. Chem. Soc.* **2001**, *123* (24), 5703–5709.

(43) Solomon, D. Clay minerals as electron acceptors and/or electron donors in organic reactions. *Clays Clay Miner.* **1968**, *16*, 31–39.

(44) Pu, W. F.; Yuan, C. D.; Jin, F. Y.; Wang, L.; Qian, Z.; Li, Y. B.; Li, D.; Chen, Y. F. Low-temperature oxidation and characterization of heavy oil via thermal analysis. *Energy Fuels* **2015**, *29* (2), 1151–1159.

(45) Setvin, M.; Franchini, C.; Hao, X.; Schmid, M.; Janotti, A.; Kaltak, M.; Van de Walle, C. G.; Kresse, G.; Diebold, U. Direct View at Excess Electrons in TiO2 Rutile and Anatase. *Phys. Rev. Lett.* **2014**, *113*, 0864021–0864025.

(46) Fan, H. F.; Liu, Y. J.; Zhong, L. G. Studies on the synergetic effects of mineral and steam on the composition changes of heavy oils. *Energy Fuels* **2001**, *15* (6), 1475–1479.

(47) Nazdracheva, T.; Morozov, A.; Yavna, V.; Kochur, A. Study of hydration of kaolinite and montmorillonite mixture by IR spectroscopy. *J. Mol. Struct.* **2022**, *1250*, 131871.

(48) Erdal, S.; Kongshaug, C.; Bjørheim, T. S.; Jalarvo, N.; Haugsrud, R.; Norby, T. Hydration of rutile TiO2: Thermodynamics and effects on n-and p-type electronic conduction. *J. Phys. Chem. C* **2010**, *114* (19), 9139–9145.

(49) Yoosuk, B.; Udomsap, P.; Puttasawat, B.; Krasae, P. Modification of calcite by hydration–dehydration method for heterogeneous biodiesel production process: The effects of water on properties and activity. *Chem. Eng. J.* **2010**, *162* (1), 135–141.

(50) Gray, M. R.; McCaffrey, W. C. Role of chain reactions and olefin formation in cracking, hydroconversion, and coking of petroleum and bitumen fractions. *Energy Fuels* **2002**, *16* (3), 756–766.

(51) Emam, E. A. Clays as catalysts in petroleum refining industry. *ARPN J. Sci. Technol.* **2013**, *3* (4), 356–375.

(52) Matyjaszewski, K., *Cationic polymerizations: mechanisms, synthesis, and applications*; Marcel Dekker: New York, 1996, p 768.

(53) Boronat, M.; Viruela, P.; Corma, A. Theoretical study on the mechanism of the hydride transfer reaction between alkanes and alkylcarbenium ions. *J. Phys. Chem. B* **1997**, *101* (48), 10069–10074.

(54) Mayr, H.; Lang, G.; Ofial, A. R. Reactions of carbocations with unsaturated hydrocarbons: Electrophilic alkylation or hydride abstraction? *J. Am. Chem. Soc.* **2002**, *124* (15), 4076–4083.

(55) Corma, A.; Orchillés, A. Current views on the mechanism of catalytic cracking. *Microporous mesoporous mat.* **2000**, *35*, 21–30.

(56) Junaid, A.; Rahman, M.; Rocha, G.; Wang, W.; Kuznicki, T.; McCaffrey, W.; Kuznicki, S. On the role of water in natural-zeolite-catalyzed cracking of athabasca oilsands bitumen. *Energy Fuels* **2014**, *28* (5), 3367–3376.

(57) Raseev, S., *Thermal and Catalytic Processes in Petroleum Refining*; CRC Press: Boca Raton, 2003, p 920.

(58) Amelse, J. A. Reactions and Mechanisms of Xylene Isomerization and Related Processes. *Ind. Arene Chem. Mark. Technol. Sustain. Process. Cases Stud. Aromat. Commod.* **2023**, *1*, 403–437.

(59) Hill, I.; Malek, A.; Bhan, A. Kinetics and mechanism of benzene, toluene, and xylene methylation over H-MFI. *ACS Catal.* **2013**, *3* (9), 1992–2001.

(60) Joshi, J. B.; Pandit, A. B.; Kataria, K. L.; Kulkarni, R. P.; Sawarkar, A. N.; Tandon, D.; Ram, Y.; Kumar, M. M. Petroleum residue upgradation via visbreaking: A review. *Ind. Eng. Chem. Res.* **2008**, *47* (23), 8960–8988.

(61) Kaiser, M. J.; de Klerk, A.; Gary, J. H.; Handwerk, G. E. Fluid Catalytic Craking, In *Petroleum Refining: Technology, Economics, and Markets*, 6th ed., CRC Press: Boca Raton, 2020, pp 481–506.

(62) Corma, A.; Wojciechowski, B. The catalytic cracking of cumene. *Catal. Rev. Sci. Eng.* **1982**, *24* (1), 1–65.

(63) An, J.; Bagnell, L.; Cablewski, T.; Strauss, C. R.; Trainor, R. W. Applications of high-temperature aqueous media for synthetic organic reactions. *J. Org. Chem.* **1997**, *62* (8), 2505–2511.

(64) Savage, P. E. Organic Chemical Reactions in Supercritical Water. *Chem. Rev.* **1999**, *99* (2), 603–622.

(65) Dervan, P. B.; Dougherty, D. A. Nonconjugated diradicals as reactive intermediates, In *Diradicals*, ed. by Borden, W. T., Wiley: New York, 1982, pp 107–149.

(66) Rüchardt, C.; Gerst, M.; Nölke, M. The Uncatalyzed Transfer Hydrogenation of α-Methylstyrene by Dihydroanthracene or Xanthene - a Radical Reaction. *Angew. Chem., Int. Ed. Engl.* **1992**, *31* (11), 1523–1525.

(67) Chaudhuri, B.; Sharma, M. M. Some novel aspects of dimerization of α-methylstyrene with acidic ion-exchange resins, clays and other acidic materials as catalysts. *Ind. Eng. Chem. Res.* **1989**, *28* (12), 1757–1763.

(68) Lewan, M. D. Experiments on the role of water in petroleum formation. *Geochim. Cosmochim. Acta* **1997**, *61* (17), 3691–3723.

(69) Ovalles, C.; Hamana, A.; Rojas, I.; Bolívar, R. A. Upgrading of extra-heavy crude oil by direct use of methane in the presence of water: deuterium-labelled experiments and mechanistic considerations. *Fuel* **1995**, *74* (8), 1162–1168.

Chapter 5

Role of Water and Kaolinite on Conversion Rate and Reaction Pathways during Thermal Conversion of α-Methylstyrene at 400 °C

Abstract

Research examining the impact of water and mineral matter on the thermal conversion of crude oil has indicated that retaining these components during treatment affects cracking, hydrogen transfer, and addition reactions. However, the complex nature of a reaction medium containing crude oil poses a challenge in relating the influence of water and minerals to particular reaction pathways. To enhance understanding of the specific contributions of water and minerals to reaction chemistry during thermal conversion, a practical approach is to make use of simpler model systems to capture relevant information for petroleum processing. The current study explored the impact of water and kaolinite on the reaction rates and pathways during the thermal conversion of a model system comprising α-methylstyrene (AMS), tetralin, and *n*-pentadecane at 400 °C for 1, 5, 10, and 30 min. The effect of kaolinite at different concentrations was also compared to that of rutile and quartz during the conversion of AMS alone. Water and kaolinite, individually and collectively, affected the reaction rates. Water suppressed the AMS conversion rates, but no evidence was found that water affected reaction pathways. Kaolinite increased the conversion rates of both AMS and tetralin while also enhancing the formation rates of cumene and naphthalene. This suggested that kaolinite somehow favored hydrogen transfer during the treatment. The presence of kaolinite also increased the formation rates of benzene by dealkylation and the tricyclic AMS dimer 1,1,3-trimethyl-3-phenyl indane, indicating that kaolinite was catalytically active, influencing reaction pathways by promoting cationic conversion. The adsorption of water on the surface of kaolinite appeared to contribute to reduced reaction rates when reacting AMS in the presence of both water and kaolinite. The deposition of carbonaceous material on kaolinite suggested that the mineral is rapidly fouled during the conversion.

5.1 Introduction

Several studies have investigated the conversion of crude oil in the presence of water and/or mineral matter [1–10]. Some studies asserted that the beneficial effects of water during the conversion, such as increased liquid product yield and coke suppression, are a result of its role as a reactant, while others argued that the water influence was due to physical solvent effects [11–13]. While the impact of mineral matter during oil conversion has received less attention compared to the influence of water, some studies in the literature have explored this aspect [4–6, 14–17]. These studies have covered a range of topics, including catalytic cracking and subsurface combustion of heavy oils, thermal oxidation of oils, and the thermal treatment of bitumen froth.

Because of the complex nature of oil properties and the concurrent reactions involving several species during thermal conversion, attributing the observed impact of water and mineral matter to any specific reaction pathway involved some level of speculation. In this context, gaining a deeper understanding of how water and mineral matter contribute to the reaction chemistry during thermal conversion is pertinent to applications involving the thermal treatment of crude oil in the presence of these components.

The interpretation of the works conducted on the influence of water and mineral matter on petroleum conversion relies on insights derived from the reaction chemistry of simpler systems. For this purpose, investigators made use of model systems, which are selected in a way to elucidate specific aspects concerning the impact of water and minerals during the conversion process.

Several studies have explored the conversion of organic model compounds representative of species typically found in petroleum in the presence of water at temperatures around 350–450 °C, a range where thermal conversion becomes significant [18–27]. The collaborative research conducted by the Katritzy and Siskin groups systematically studied the reactivity of various organic compounds in the presence of sub- and supercritical water [28–34]. Some notable outcomes from their research, with relevance to petroleum conversion, were as follows: (1) The presence of water during the thermal conversion enabled additional reaction pathways as compared to the absence of water [34]. (2) Ionic reactions, such as hydrolysis, were observed in pure water but were enhanced in the presence of brine and acidic clays [28–31]; (3) Transitioning from sub- to supercritical water altered reaction rates rather than reaction pathways. While the presence of water enabled cationic pathways for certain reactions, free radical pathways still remained relevant [28, 33].

The existing body of research on the influence of minerals during the conversion of organic matter at elevated temperatures (300–450 °C) is extensive [35–38]. Most of these studies primarily centered on clay minerals such as kaolinite, illite, and montmorillonite, due to their abundance in source rocks and their recognized Brønsted-Lowry and Lewis acidity, which is known to catalyze various reactions, including cracking, isomerization, decarboxylation, and addition reactions [39–41].

Numerous studies have been conducted to explore the impact of mineral matter during the conversion of organic model compounds [42–47]. The main findings with relevance to oil conversion included the following: (1) Studies on the pyrolysis of carboxylic acids revealed that clay minerals played a significant role in influencing the reaction pathways, promoting cationic cracking and isomerization [48–50]; (2) Kaolinite and illite promoted cationic addition of α-methylstyrene (AMS) during its conversion at 250 °C [51]; (3) The presence of minerals seemed to influence hydrogen and methyl transfer during thermal conversion [52–54].

Previous studies that focused on the thermal treatment of bitumen froth evaluated the impact of water and oilsand minerals on the physicochemical properties and composition of the thermally treated products [4, 5, 54]. Thermal conversion of froth at 400 °C, employing AMS as a probe molecule, indicated that water and minerals lowered the conversion of AMS and favored hydrogen transfer. Additionally, the presence of water hindered the formation of addition products, including AMS dimers [54]. However, attributing the influence of water and minerals to specific reaction pathways during the treatment was not possible due to the complex nature of reaction systems involving bitumen, water, and a mixture of minerals. For this reason, in the present study, the thermal conversion of model systems containing AMS was carried out. This approach aimed to limit the number of species formed while at the same time capturing relevant information to understand the role of water and minerals during the thermal conversion.

The first objective of the present study was to evaluate if water and kaolinite affect the rate of AMS conversion during thermal treatment at 400 °C. There were claims in the literature that both minerals and water had an impact on the rate of product formation during the thermal conversion of oil and organic model compounds [7, 28, 55]. To investigate these claims, thermal conversion of a mixture of AMS, tetralin, and *n*-pentadecane was performed at 400 °C and reaction times of 1, 5, 10, and 30 min in the presence of water and/or kaolinite. AMS was selected as a probe molecule because its thermal conversion encompasses relevant reactions to oil conversion, as illustrated in **Figure 5.1**. Tetralin and *n*-pentadecane were added to the model system to provide a source of transferable hydrogen and alkyl groups. Kaolinite was chosen because of its prevalence in oilsands and its acidic properties, which were expected to impact the reaction pathways during AMS conversion. More specifically, the Brønsted-Lowry acidity of kaolinite was anticipated to promote cationic conversion during the treatment. Cationic conversion in the context of this study refers to conversion by H^+.

The second objective of this study was to investigate if minerals found in oilsands have a catalytic effect on the dimerization of AMS at 400 °C. Previous studies at lower temperature levels (240–250 °C) suggested that the mineral matrix had a catalytic effect on the conversion of heavy oils [7], and that kaolinite and illite promoted cationic dimerization of AMS [51]. However, when performing the thermal conversion of bitumen at 400 °C in the presence of oilsand minerals and using AMS as a probe molecule, it was not possible to differentiate between cationic and free radical conversion [54]. To investigate the claim that minerals found in oilsands have a catalytic effect during thermal conversion, self-reaction of AMS at 400 °C was carried out for 10 min in the presence of kaolinite, rutile, and quartz at two concentration levels. These minerals were selected because they are commonly found in oilsands and present different acidity characteristics. The Brønsted-Lowry acidity of kaolinite was expected to promote cationic dimerization of AMS, while the Lewis acidity of rutile and the lack of acidity of quartz were not expected to catalyze dimerization. In this sense, the thermal conversion of AMS in the presence of rutile and quartz served as control experiments to assess the potential catalytic effect of kaolinite during the conversion.

The current study aimed to advance the understanding of the influence of water and minerals on the reaction chemistry during the thermal conversion of organic compounds. A better knowledge of this field is beneficial to practical applications in crude oil exploration and processing, including the thermal treatment of bitumen froth and the subsurface (or *in situ*) upgrading of heavy oils and bitumen.

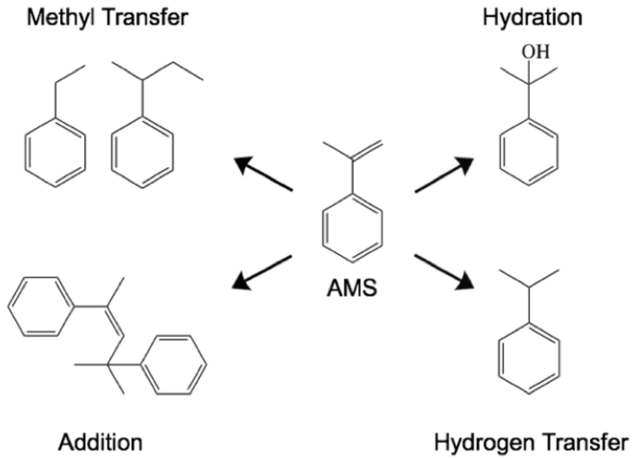

Figure 5.1: Potential AMS conversion pathways.

5.2 Experimental Section

5.2.1 Materials

The chemicals used for feed preparation and feed and product analyses, the commercially acquired minerals, and the cylinder gases used in this study are listed in **Table 5.1**. The characterization of the minerals used in this study is reported in **Table C.1** in **Appendix C**.

The water used as feed in the water-containing reaction systems consisted of both connate and process water isolated from a bitumen froth sample obtained from the Canadian oilsands production in Alberta, Canada. The choice of process water rather than deionized water was done to mimic a water environment that would be relevant to processes involving the hydrothermal treatment of petroleum. The same water sample was used as feed in a previous study, and its characterization has been reported before [4]. The water was slightly alkaline (pH = 8.3) and contained mostly Na^+ and Cl^- ions in its composition.

Table 5.1: List of chemicals, minerals, and cylinder gases used in the study.

Compound	Formula	CASRN[a]	Purity (%)[b]	Supplier
Chemicals				
AMS (α-methylstyrene)	C_9H_{10}	98-83-9	99	Sigma Aldrich
biphenyl	$C_{12}H_{10}$	92-52-4	99.5	Sigma Aldrich
methanol	CH_3OH	67-56-1	99.9	Fisher Scientific
n-pentadecane	$C_{15}H_{32}$	629-62-9	99	Acros Organics
tetralin (1,2,3,4-tetrahydronaphthalene)	$C_{10}H_{12}$	119-64-2	99	Sigma Aldrich
Minerals				
kaolinite	$Al_2O_7Si_2{\cdot}2H_2O$	1318-74-7	-	Sigma Aldrich
rutile	TiO_2	1317-80-2	99.5	Alfa Aesar
quartz	SiO_2	14808-60-7	99.99	Sigma Aldrich
Cylinder gases				
air	O_2/N_2	132259-10-0	-	Praxair
hydrogen	H_2	1333-74-0	99.999[c]	Praxair
nitrogen	N_2	7727-37-9	99.999[c]	Praxair

[a] Chemical Abstracts Services Registry Number (CASRN); [b] Purity of material provided by the supplier. Material was not further purified; [c] Mol% purity.

5.2.2 Equipment and Procedure

5.2.2.1 Thermal conversion of AMS and separation of products

Two sets of experiments involving the thermal conversion of AMS were carried out. Details on the feed, reaction time, and number of performed reactions for both sets of experiments are given in **Table 5.2**.

The first set of experiments consisted of the thermal conversion of a mixture of AMS, tetralin, and *n*-pentadecane with and without water and/or kaolinite. In the present study, this set is referred to as ATP experiments (i.e., ATP stands for AMS, Tetralin, and *n*-Pentadecane). The second set of experiments involved the thermal conversion of AMS in the presence and absence of kaolinite, rutile, quartz, and water. These experiments are referred to as AWM experiments (i.e., AWM stands for AMS, Water, and Minerals).

Table 5.2: Feed composition, planned reaction time, and number of performed experiments for the ATP and AWM experiments.

Experiment identifier	Feed[a]	Planned reaction time at 400 °C (min)	Number of performed reactions (per reaction time)
ATP experiments			
ATP	AMS (30 wt%) + tetralin (20 wt%) + *n*-pentadecane (50 wt%)	1, 5, 10 & 30	1
ATP+K	AMS (29 wt%) + tetralin (19 wt%) + *n*-pentadecane (48 wt%) + Kaolinite (4 wt%)	1, 5, 10 & 30	1
ATP+W	AMS (28 wt%) + tetralin (18 wt%) + *n*-pentadecane (46 wt%) + Water (8 wt%)	1, 5, 10 & 30	1[b]
ATP+W+K	AMS (27 wt%) + tetralin (17 wt%) + *n*-pentadecane (45 wt%) + water (7 wt%) + kaolinite (4 wt%)	1, 5, 10 & 30	1[b]
AWM experiments			
AMS	AMS (100 wt%)	10	2
AMS+K(3)	AMS (97 wt%) + kaolinite (3 wt%)	10	2
AMS+K(9)	AMS (91 wt%) + kaolinite (9 wt%)	10	2
AMS+R(5)	AMS (95 wt%) + rutile (5 wt%)	10	2
AMS+R(13)	AMS (87 wt%) + rutile (13 wt%)	10	2
AMS+Q(9)	AMS (91 wt%) + quartz (9 wt%)	10	2
AMS+Q(23)	AMS (77 wt%) + quartz (23 wt%)	10	2

[a] The relative concentration of AMS, tetralin, and *n*-pentadecane were kept constant in all the ATP experiments. [b] Duplicates of reactions were performed for the 30-min experiments only.

In all the ATP experiments, the relative amounts of AMS, tetralin, and *n*-pentadecane were kept constant (i.e., AMS : tetralin : *n*-pentadecane = 30 wt% : 20 wt% : 50 wt%). This standardization was meant to ensure that any observed differences (either in product formation or in the monitored physicochemical properties) due to the thermal conversion were primarily attributed to differences in the reaction time, or the presence or absence of water and kaolinite, rather than variations in the relative concentrations of the species in the feed among the systems. The selection of water and kaolinite concentrations in the ATP experiments was guided by a prior study that examined the influence of water and minerals during the thermal treatment of bitumen froth [54]. As the current study aimed to gain insights to enhance the understanding of phenomena observed in that previous work, it was considered beneficial to utilize similar concentrations of water and minerals as employed in that study.

Two concentration levels were tested for each mineral in the AWM experiments in order to evaluate if the presence of minerals had any catalytic effect during the dimerization of AMS.

Because of the significant number of reactions designed for the ATP experiments, duplicates were conducted only for the ATP+W and ATP+W+K experiments at 30-min reactions. This was done to provide an indication of the level of experimental variability within this specific set of experiments. Duplicates of reactions were performed for all the reaction systems in the AWM experiments.

In a typical reaction, approximately 12–14 g of feed was loaded into a 25-mL batch microreactor built using 316 stainless steel Swagelok tubing and fitting. This reactor was equipped with a pressure gauge (with a measurement range of 0–15 MPa and a precision of 0.2 MPa) and an inserted thermocouple. After loading, the reactor was sealed, purged three times with nitrogen at 5 MPa, and then pressurized to an initial pressure of 1 MPa. Next, the reactor was inserted into a fluidized sand bath heater (Omega Fluidized Bath FSB-3), which had been preheated to 400 °C. The temperature of 400 °C was chosen for this study because it has been reported that mild visbreaking of bitumen froth can be effectively conducted at this temperature level [5]. Also, previous research demonstrated that relevant reactions involved in bitumen upgrading, such as hydrogen transfer, methyl transfer, and addition reactions, were influenced by the presence of water and oilsands minerals during thermal treatment of froth at 400 °C [54]. The temperature inside the reactor was carefully monitored and recorded every 1 minute from the moment the reactor was immersed into the sand bath until it was removed and cooled to 50 °C with the assistance of a room-temperature air stream.

To ensure that the reaction times were consistent across different reaction systems with the same planned reaction time (see **Table 5.2**), it was necessary to take into account the duration of each of the thermal events during the reaction (i.e., heating up time to 400 °C, reaction time at near-isothermal conditions, and cooling down time to 50 °C). To accomplish this, the equivalent residence time (ERT) concept, which is typically used to assess the severity of the thermal conversion of oils, was applied [56]. Details on how the ERT was calculated are given in **Section 5.2.2.3**. The temperature recorded in a digital thermometer was input to the ERT equation every minute so that the reactor was removed from the sand bath with an ERT at 400 °C as close to the planned reaction time as possible. The ERT for each reaction performed in this study is reported in the **Results** section.

After the reaction was completed and the reactor had cooled to room temperature, the products of the reaction systems that contained minerals or water were placed into a 15-mL centrifuge tube and then centrifuged using an Eppendorf Centrifuge 5430 at 7000 rpm for 15 min. After centrifugation of the systems including both water and kaolinite, three distinct phases were observed: a major top layer consisting of an organic phase, a minor intermediate layer of an aqueous phase, and wet solids at the bottom of the tube. For systems including either water or minerals, two phases were found. Most of the organic layer was carefully transferred with a pipette into a 25-mL flask while avoiding contact with the water phase and solids. The organic phase transfer was conducted rapidly to minimize the loss of light components. To avoid carrying some water with the organic product, the organic phase near the aqueous-organic interface was not transferred. The aqueous product was not analyzed in this study in order to narrow the scope and maintain the focus on the conversion of the organic phase, particularly the transformations involving AMS.

The identification of species in the products of the organic liquid phase was performed through gas chromatography coupled with mass spectrometry (GC-MS), while the quantification of selected species was performed through gas chromatography with flame ionization detection (GC-FID). Around 0.5 g of product, the exact mass noted, and 0.05 g of biphenyl (added as an internal standard) were diluted in approximately 1.9 g of methanol. The mixture was then homogenized at ambient conditions by mechanical stirring for 5 min. Next, this mixture was transferred into a GC insertion vial that was used for both GC-FID and GC-MS analyses.

5.2.2.2 Analyses

The identification of reaction products by GC-MS was performed using an Agilent 7820A coupled with a 5977E mass spectrometer. The separation of components was performed in a HP-PONA column with dimensions of 50 m x 0.20 mm x 0.5 μm (length, inner diameter, and film thickness, respectively). The carrier gas was hydrogen with a flow rate of 1 mL/min, an injection volume of 0.5 μL, and a split ratio of 23:1. The injector temperature was 250 °C. The products diluted in methanol (refer to **Section 5.2.2.1**) were injected without any further dilution. The temperature program started at 36 °C with a 5-min hold, followed by an increase to 125 °C at a rate of 3 °C/min. Subsequently, the temperature was raised to 325 °C at a rate of 4 °C/min and maintained at 325 °C for 5 minutes. The NIST MS Search 2.0 software was used for compound identification in the reaction products by matching their mass spectra to those in the NIST mass spectral library. The identities of selected species with retention time (RT) lower than 50 min were confirmed by using commercial standards. The list containing the commercial standards used for identity confirmation of products is shown in **Table C.2** in **Appendix C**. The identification of species with RT higher than 50 min, particularly the AMS dimers ($C_{18}H_{22}$ isomers) and their hydrogenated derivatives ($C_{18}H_{20}$ isomers), involved substantial effort to assign tentative structures to their mass spectra. Details on the reasoning behind the tentative structure assignment of these isomers have been reported in a previous study [54].

The quantification of compounds by GC-FID was carried out on an Agilent 7890A coupled to an FID detector. The GC-FID analyses used the identical column, sample injection, and run conditions as previously reported for the GC-MS analysis. The quantification of compounds identified in the reaction products, for which commercial standards were available, was made through calibrated GC-FID data. The calibration curves for these species were built using methanol as a solvent and biphenyl as an internal standard. The concentration and area ratios between the compound to be quantified and biphenyl were used to build the calibration curves, and the regression data is reported in **Table C.3** in **Appendix C**. The semi-quantitative evaluation of species with identification based only on mass spectral assignment was performed by calculating the relative area percentage (RAP) of those species using the GC-FID data, as detailed in **Section 5.2.2.3**.

Microscope pictures of the minerals before and after reaction were taken using a Carl Zeiss Stereo-Microscope Discovery V2.0 using a plan apochromatic objective lens. Images of minerals were taken at 30x magnification.

5.2.2.3 Calculations

5.2.2.3.1 Equivalent residence time

The equivalent residence time (ERT) at 400 °C, as specified by Yan [56], was calculated according to **Eq. 5.1**, where Δt_i are 1-minute intervals consisting of two recorded temperatures (T_i and T_{i+1}), T_{ref} = 673.15 K (400 °C), E_a = 209500 J mol^{-1}, and R = 8.314 J mol^{-1} K^{-1}. The activation energy (E_a) of 209500 J/mol is typically used to evaluate the thermal conversion of oil [56]. In the current study, the same activation energy was selected not to reflect the actual activation energy of any individual compound within the model mixtures. Instead, the goal was to ensure consistent severities across different reaction systems with similar planned reaction times (see **Table 5.2**). Additionally, there is evidence in the literature that supports the use of the selected activation energy for the ERT calculation: (1) A prior investigation indicated that employing the ERT with parameters identical to those in the current study resulted in small variability of AMS conversion in bitumen for slight variations in the ERT [54]; (2) The E_a of 209500 J/mol corresponds to the activation energy of the thermal cracking of gas oils with 15 carbon atoms [56]. Since the ATP experiments made use of about 50 wt$\%$ of n-pentadecane, it seemed reasonable to use an activation energy that closely approximates the conversion of that compound.

$$ERT\ at\ T_{ref} = \sum_{i=1}^{n} \Delta t_i \times exp\left[\left(-\frac{E_a}{R}\right)\left(\frac{1}{\frac{T_i + T_{i+1}}{2}} - \frac{1}{T_{ref}}\right)\right] \tag{5.1}$$

5.2.2.3.2 Gas formation

The amount of gas formed during each reaction was determined by measuring the weight of the open reactor containing the feed and then measuring the weight of the reactor with the products after it had cooled to room temperature, its pressure had been released in the fumehood, and the reactor had been opened. The loss of gas after releasing the pressure from the reactor impacts the actual concentration of species in the products. For this reason, the recorded amount of formed gas was used to correct the concentration of the species reported in this study.

5.2.2.3.3 Concentration of species in the products

The concentration of a specific compound was determined by combining the mass of that compound, obtained through GC-FID calibrated data, with the volume of the product sample containing the compound, using the measured product density at 25 °C. The concentration of each compound was corrected to take into account the volume loss due to gas formation during the thermal treatment.

5.2.2.3.4 Rates of feed conversion and product formation

The reaction rates of selected compounds were calculated for three distinct time regions of the concentration versus ERT curve, namely the initial reaction rate (measured at the time interval 0–1 min), the reaction rate at 5 min, and the reaction rate at 10 min.

The initial reaction rate was calculated according to **Eq. 5.2**, where $\mathrm{r}_{w,0}$ is the initial reaction rate of compound *w* in kg/(m^3h), $\Delta \mathrm{C}_w$ is the variation in concentration of compound *w* in kg/m^3 between the time interval 0–1 min (i.e., the difference in concentration of compound w in the feed and at an ERT of about 1 min), and Δt is the time interval between the planned reaction time of 0–1 min, expressed in terms of the calculated ERT at 400 °C, in units of h. The concentration used for calculating the reaction rates was based on the volume of the organic phase only, excluding the volume of water and minerals.

$$r_{w,0} = \frac{dC_w}{dt} \approx \frac{\Delta C_w}{\Delta t} \tag{5.2}$$

The approach used for assessing the reaction rates at 5 min ($r_{w,5}$) and 10 min ($r_{w,10}$) involved the following steps: (i) First, the concentration of a selected species *w*, denoted as C_w, as a function of the ERT (i.e., C_w = f(t)), was determined using the Lagrange interpolating polynomial with three data points, as described by **Eq. 5.3** [57]. In this equation, C_w represents the concentration of compound *w* in kg/m^3, t is the ERT in minutes, and (x, y) denotes the measured ERT vs. concentration data points. The interpolating polynomial was built using three adjacent data points to minimize oscillation of the polynomial and better represent the concentration vs. ERT trend curve. The data points at the ERT of 1, 5, and 10 min were used to obtain the interpolating polynomial to calculate the $r_{w,5}$, while the data points at the ERT of 5, 10, and 30 min were used to obtain the polynomial to calculate the $r_{w,10}$. The coefficients of the polynomials were obtained by using the software Mathematica Online by Wolfram Research Inc. and are reported in the **Results** section; (ii) Then, the reaction rates at 5 and 10 minutes were calculated using the first derivative of the polynomial function C_w(t), as outlined in **Eq. 5.4**, where $r_{w,k}$ represents the reaction rate of species w at a specific time k (either 5 or 10 min) in units of kg/(m^3 h), and k is the ERT in units of min. The multiplying factor of 60 in **Eq. 5.4** is just a conversion factor from units of minutes to hours.

$$C_w(t) = \sum_{j=0}^{3} y_j \left(\prod_{\substack{i=0 \\ i \neq j}}^{3} \frac{t - x_i}{x_j - x_i} \right) \tag{5.3}$$

$$r_{w,k} = \left. \frac{dC_w}{dt} \right|_{t=k} \times 60 \tag{5.4}$$

5.2.2.3.5 Conversion and selectivity

The conversion reported in the present study was calculated on a mass basis. The conversion of a selected species w was calculated according to **Eq. 5.5**, where m_w represents the mass of species *w*.

$$Conversion\,of\,w\,(\%) = \frac{m_{w\,in\,product}}{m_{w\,in\,feed} - m_{w\,in\,product}} \times 100 \tag{5.5}$$

The selectivity to specific products from AMS and tetralin conversion were calculated according to **Eq. 5.6**, where z represents the target compound for which the selectivity was calculated, m_z is the mass of the target compound, and m_p is the mass of the parent molecule (either AMS or tetralin). The mass inputs in **Eq. 5.6** were calculated by using calibrated GC-FID data. The data on the calibration curves is given in **Table C.3** in **Appendix C**.

$$Selectivity\, to\, z\, (\%) \;=\; \frac{m_{z\, in\, product}}{m_{p\, in\, feed} - m_{p\, in\, product}} \times 100 \tag{5.6}$$

The relative area percentage (RAP) shown in **Eq. 5.7** was used as a semi-quantitative evaluation of products for which commercial standards were not available. The area inputs in **Eq. 5.7** correspond to the peak area of a specific compound ($A_{compound}$) in the GC-FID chromatogram and the total area under the peaks (A_{total}) of the GC-FID chromatogram, excluding the areas of the solvent (methanol) and of the standard (biphenyl).

$$RAP\, (\%) \;=\; \frac{A_{compound}}{A_{total}} \times 100 \tag{5.7}$$

5.3 Results

5.3.1 Thermal conversion during the ATP experiments

5.3.1.1 ERT and gas formation during the ATP experiments

As mentioned in **Section 5.2.2.1**, the thermal history can be divided into three periods from the moment the reactor was immersed in the sand bath until it was cooled, namely heating up time to 400 °C, reaction time at near-isothermal conditions, and cooling down time to 50 °C. The temperature profiles of the ATP experiments conducted at a reaction time of 10 min are illustrated in **Figure C.2** in **Appendix C**. The systems ATP and ATP+K achieved the reaction temperature of 400 °C in approximately 10–12 min, whereas the water-containing systems required a longer time, approximately 14–16 min, to reach the same reaction temperature. The longer time required for the water-containing systems to reach the reaction temperature was likely due to the water phase affecting the heat transfer during the experiment. The air-assisted cooling down to 50 °C required about 5–7 min in all the reaction systems. The use of the ERT concept was essential to account for the significant heating up and cooling down periods during the reactions in the present study.

The comparison between the planned reaction times versus the ERT at 400 °C for all the reaction systems in the ATP experiments is plotted in **Figure 5.2**. By taking real-time measurements of the temperature inside the reactor throughout the entire reaction time, it was possible to stop the reactions at comparable ERT among different reaction systems with the same planned reaction times. The deviation in ERT among systems with the same planned reaction times was less than 0.3 minutes. Employing this approach was important to guarantee that the evaluation of differences in reaction rates and product composition was attributed to the components in the reaction systems (i.e., water and/or kaolinite) rather than being influenced by substantial variations in reaction severities.

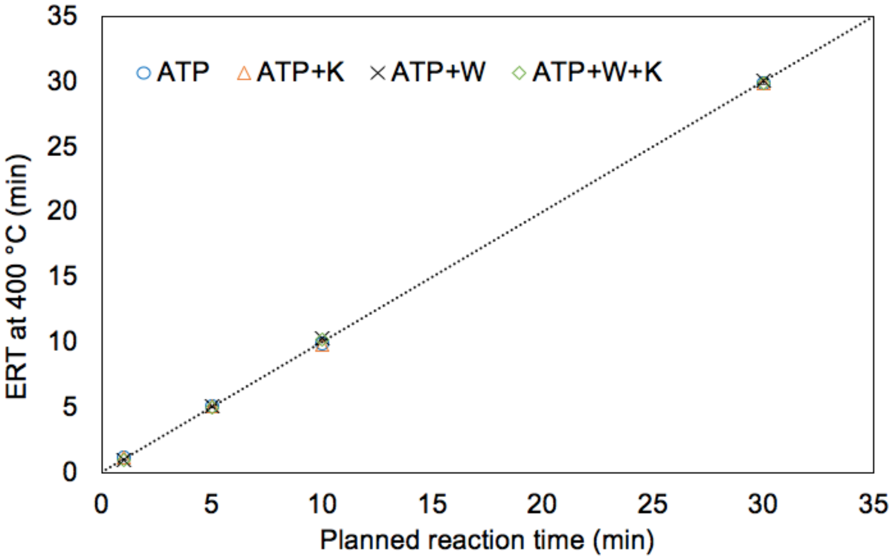

Figure 5.2: ERT at 400 °C vs. planned reaction time for the ATP experiments.

The maximum pressure achieved in each reaction system in the ATP experiments is given in **Table 5.3**. The maximum pressure was independent of the total reaction time. The auto-generated pressure due to the presence of water in the systems ATP+W and ATP+W+K raised the pressure from 1 MPa to 4.2–4.5 MPa. This range exceeds the critical point of AMS (372 °C and 3.5 MPa) [58]. In contrast, the auto-generated pressure in the remaining systems increased from 1 MPa to 2 MPa only. Once the reaction concluded and the reactor cooled to room temperature, there was no readable pressure change in the gauge (i.e., the pressure returned to 1 MPa at the end of the reactions) for all the reaction systems. This result did not imply the absence of gas formation during the treatment; rather, it suggested that the quantity of generated gas was low, and considering the precision of the gauge of 0.2 MPa, it might have not resulted in a readable pressure. Also, some of the gases may have dissolved in the liquid phase. A similar finding was reported in a prior study where bitumen froth, containing AMS as a probe molecule, underwent thermal treatment at 400 °C for about 5 min [54].

Figure 5.3 illustrates the amount of gas generated in the ATP experiments, calculated from the difference in the reactor weight containing the feed and the reactor weight containing the products after gas release (refer to **Section 5.2.2.3.2**). The measurement variability for the formed gas, derived from duplicate reactions of the systems ATP+W and ATP+W+K (both at a reaction time of 30 minutes), ranged approximately between 30 and 50 mg of formed gas per gram of ATP. Because of this high variability, it was not possible to conclusively determine if water and kaolinite had any effect on the gas formation during the ATP experiments. However, the decrease in weight across all the reaction systems indicated that gases were formed, even though there was no readable change in the reactor pressure at room temperature before and after the treatment. The gas phase was not analyzed to limit the scope of the study, which primarily concentrated on the analysis of the liquid phase.

Table 5.3: Maximum pressure achieved during reaction at near-isothermal temperature of 400 °C.

Reaction system	Pressure at 400 °C (MPa)^{a,b}
ATP	2
ATP+K	2
ATP+W	4.5
ATP+W+K	4.2

[a] Initial pressure was 1 MPa for all reaction systems.
[b] The maximum pressure achieved at 400 °C was independent of the reaction time in the ATP experiments.

The amount of gas generated in each experiment is also listed in **Table C.4** in **Appendix C** to provide the reader with the exact amount of gas used to correct the concentration of species in the liquid products of the ATP experiments.

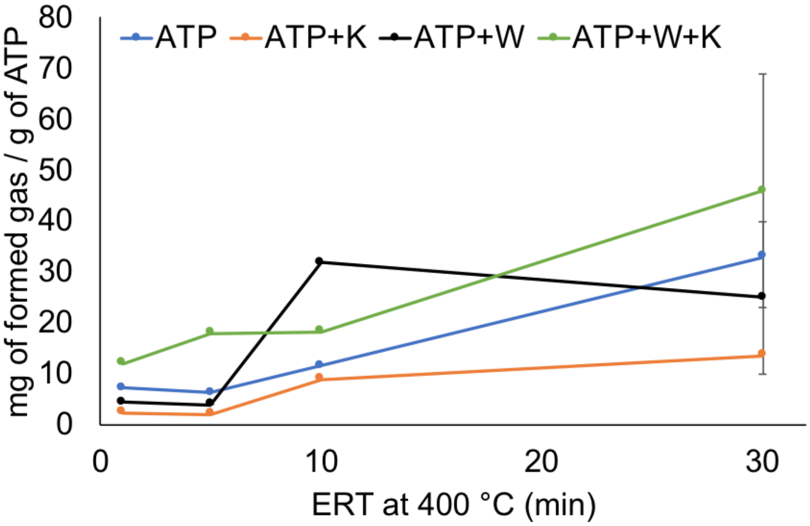

Figure 5.3: Gas formation vs. ERT at 400 °C for the ATP experiments. Error bars were included for duplicate reactions in the systems ATP+W (30 min) and ATP+W+K (30 min).

5.3.1.2 Rates of AMS, tetralin, and *n*-pentadecane conversion

The concentration and conversion of AMS, tetralin, and *n*-pentadecane (*n*-C15) versus ERT at 400 °C are plotted in **Figure 5.4**. The data used for calculating the concentration of species in the products, including the exact mass of the liquid product sample used for GC-FID quantification, the mass loss due to gas formation, the product density data at 25 °C, and the corrected volume used for calculating the concentration in each reaction system, are given in **Table C.4** in **Appendix C**. The mass fraction of AMS, tetralin, and *n*-pentadecane in the product, obtained by calibrated GC-FID quantification, and the concentration of these species in each reaction system are given in **Tables C.5–C.7** in **Appendix C**.

The conversion of AMS (**Figure 5.4B**) increased with time for all the reaction systems. The standard deviation measured for the systems ATP+W+K and ATP+W at 30-min reaction varied in a narrow range of 1.6–2.7%, suggesting that the differences observed in AMS conversion were influenced by the presence of water and/or kaolinite in the reaction medium.

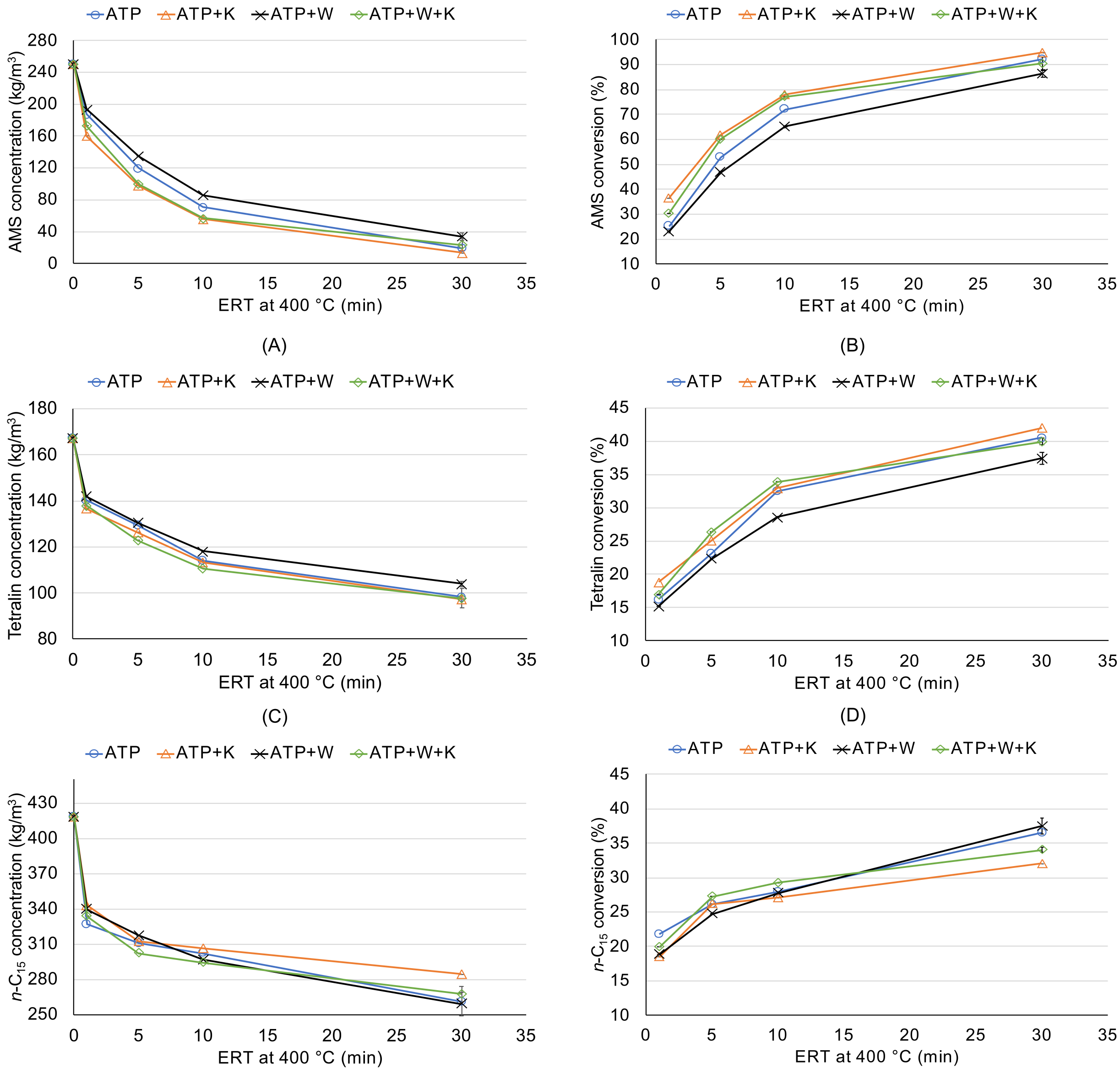

(A) (B)

(C) (D)

(E) (F)

Figure 5.4: Plots of concentration and conversion versus ERT at 400 °C of AMS (A & B), tetralin (C & D), and *n*-pentadecane (E & F). Error bars were included for the systems ATP+W (30 min) and ATP+W+K (30 min). Some of the error bars may not be visible because they are too small.

The conversions of tetralin and *n*-pentadecane (**Figures 5.4D** and **5.4F**, respectively) also increased with time for all the reaction systems. The conversion of tetralin in the systems ATP+W (30 min) and ATP+W+K (30 min), differed 0.5–0.9%. The conversion of *n*-pentadecane increased with time, with the standard deviation varying from 0.4% to 1.2% in the systems containing duplicate reactions.

The concentration versus ERT plots, illustrated in **Figures 5.4A**, **5.4C**, and **5.4E** were employed to determine the initial rate of reaction ($r_{w,0}$) and the reaction rates at 5 and 10 min ($r_{w,5}$ and $r_{w,10}$, respectively) for each component in the feed, as described in **Section 5.2.2.3**. The coefficients of the polynomials and regression plots are given in **Table C.8** and **Figures C.3–C.5** in **Appendix C**.

The rates of AMS, tetralin, and *n*-pentadecane conversion are given in **Table 5.4**. As anticipated, the highest conversion rates were noted during the 0–1 min time interval (i.e., the initial reaction rate, $r_{w,0}$). When evaluating the rates within this time frame, it is necessary to consider that, although this interval may seem brief, it actually encompassed the entire heating-up period, as detailed in **Section 5.3.1.1**.

The experiments were not designed to determine kinetic expressions for the thermal conversion of AMS, tetralin, and *n*-pentadecane. Nevertheless, plots of the natural logarithm of concentration versus time and the inverse of concentration versus time were generated. These results can be found in **Figures C.18–C.23** in **Appendix C**. The AMS conversion in the water-containing systems (i.e., ATP+W and ATP+W+K) appeared to follow a second-order reaction, as indicated by coefficients of determination exceeding 0.996 in the linear regressions of the plots depicting the inverse of AMS concentration versus time (see **Figure C.19** in **Appendix C**). The conversion of AMS in the remaining reaction systems, as well as the conversion of tetralin and *n*-pentadecane in all the reaction systems in the ATP experiments, did not exhibit characteristics indicative of either a simple first- or second-order reaction.

Table 5.4: Rates of AMS, tetralin, and *n*-pentadecane conversion during the ATP experiments.

Compound / System	Rate of conversion (kg m^{-3} h^{-1})^{a}		
	$r_{w,0}$	$r_{w,5}$	$r_{w,10}$
AMS			
ATP	-3818	-828	-500
ATP+K	-5444	-745	-424
ATP+W	-3441	-749	-499
ATP+W+K	-4671	-840	-430
tetralin			
ATP	-1621	-172	-157
ATP+K	-1835	-155	-134
ATP+W	-1507	-163	-128
ATP+W+K	-1748	-192	-125
***n*-pentadecane**			
ATP	-5467	-179	-104
ATP+K	-4506	-288	-70
ATP+W	-4703	-297	-220
ATP+W+K	-5069	-303	-93

[a] The concentration used for calculating the reaction rates was based on the volume of the organic phase only, excluding the volume of water and minerals.

5.3.1.3 Selectivity and rate of products formation during the ATP experiments

5.3.1.3.1 Formation of products with RT lower than 50 min

The GC-MS chromatograms containing the compounds with RT lower than 50 min for all the ATP experiments with a reaction time of 10 min are presented in **Figures C.24–C.27** in **Appendix C**.

The selectivity of AMS and tetralin conversion to selected compounds with RT lower than 50 min is given in **Figure 5.5**. The error bars were included for the systems ATP+W and ATP+W+K at 30-min reactions. Some of the error bars are not clearly visible in **Figure 5.5** because the standard deviation varied within a narrow range.

The selectivity of AMS conversion to benzene (**Figure 5.5A**) was consistently higher in the system ATP+K at all reaction times.

A previous study showed that the primary product of AMS conversion at 400 °C was cumene [54]. The selectivity of AMS conversion to cumene is shown in **Figure 5.5B**. It is a potential indicator of hydrogen transfer during the treatment. The systems containing kaolinite (ATP+K and ATP+W+K) presented a significant increase in selectivity to cumene of about 10% for all the reaction times over a wide range of conversion.

The selectivity of tetralin conversion to naphthalene is shown in **Figure 5.5F**. The presence of kaolinite during thermal conversion resulted in a consistent higher selectivity of tetralin conversion to naphthalene at all reaction times.

n-Pentadecane was added to the model system in the ATP experiments as a source of methyl and alkyl groups. *n*-Alkanes in the range from hexane to tetradecane were formed during the treatment (refer to **Figures C.24–C.27** in **Appendix C**), indicating that *n*-pentadecane was an effective source of alkyl groups. The total RAP of *n*-alkanes in the range from hexane to nonane is given in **Figure C.33** in **Appendix C**.

The rates of formation of benzene, toluene, ethylbenzene, *n*-propylbenzene, cumene, and naphthalene at various time intervals are given in **Table 5.5**. The coefficients of the polynomials and regression plots are given in **Table C.9** and **Figures C.6–C.11** in **Appendix C**. The formation of these compounds did not exhibit the characteristics of a simple first- or second-order reaction.

Table 5.5: Rates of formation of selected compounds with RT lower than 50 min during the ATP experiments.

Compound / System	Rate of formation (kg m^{-3} h^{-1})^{a}		
	$r_{w,0}$	$r_{w,5}$	$r_{w,10}$
benzene			
ATP	ND[b]	0.2	0.3
ATP+K	39	0.6	1.1

Continues on the next page

Compound / System	Rate of formation (kg m^{-3} h^{-1})^{a}		
	r$_{w,0}$	r$_{w,5}$	r$_{w,10}$
ATP+W	ND	ND	0.1
ATP+W+K	1.9	0.3	0.3
toluene			
ATP	12	4.4	6.3
ATP+K	3.8	4.1	4.3
ATP+W	9.3	3.5	3.4
ATP+W+K	3.5	4.9	4.5
ethylbenzene			
ATP	247	106	81
ATP+K	197	106	74
ATP+W	230	100	81
ATP+W+K	220	126	72
***n*-propylbenzene**			
ATP	12	14	13
ATP+K	12	13	11
ATP+W	11	13	13
ATP+W+K	14	14	10
cumene			
ATP	203	105	90
ATP+K	859	165	125
ATP+W	174	91	85
ATP+W+K	680	194	118
naphthalene			
ATP	51	37	39
ATP+K	205	62	55
ATP+W	49	34	39
ATP+W+K	170	83	55

[a] The concentration used for calculating the reaction rates was based on the volume of the organic phase only, excluding the volume of water and minerals. [b] ND – Not Detected

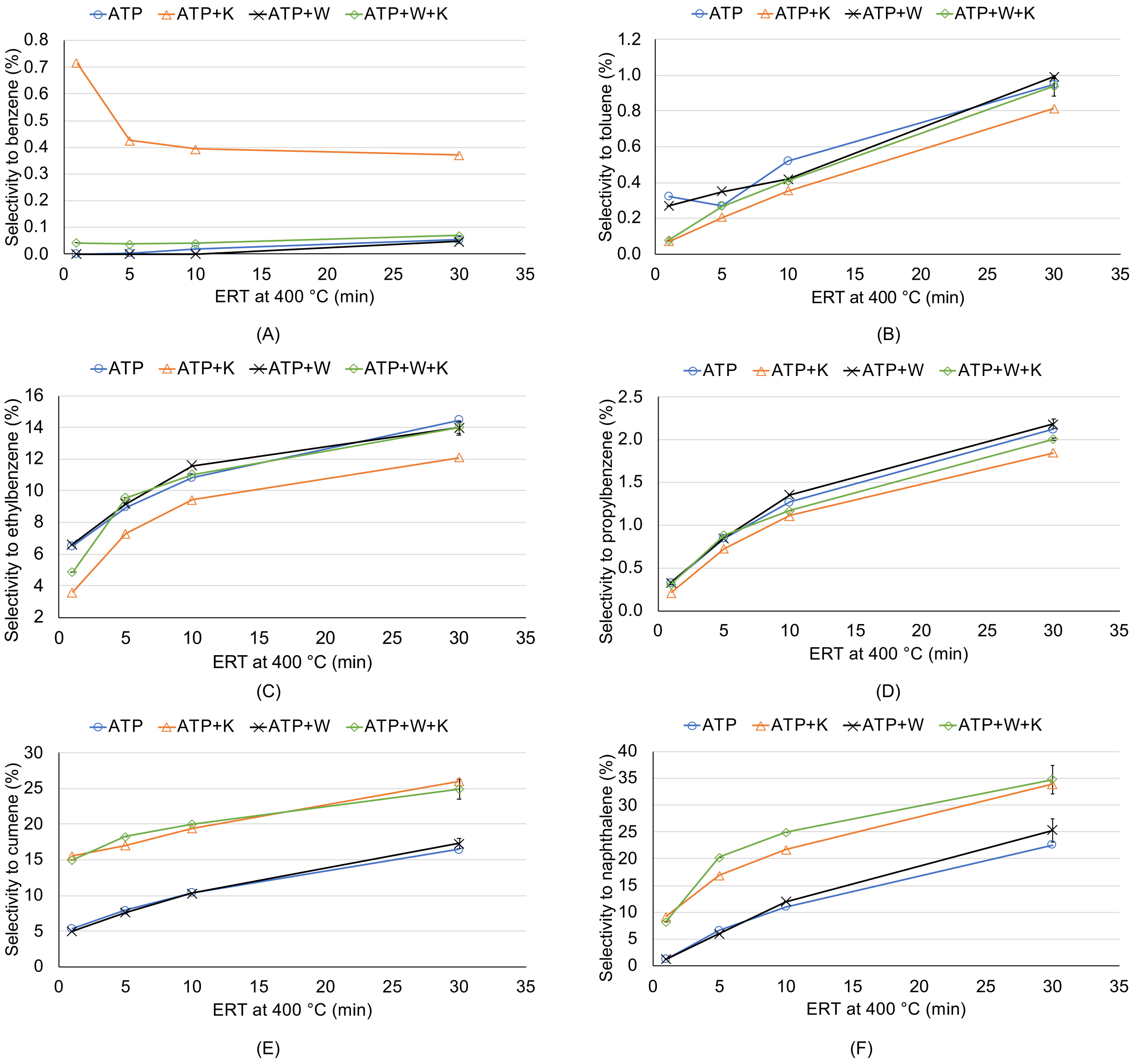

Figure 5.5: Selectivity of AMS conversion to (A) benzene, (B) toluene, (C) ethylbenzene, (D) *n*-propylbenzene, (E) cumene, and selectivity of tetralin conversion to (F) naphthalene during the ATP experiments, based on quantification using calibrated GC-FID data. Error bars were included for the systems ATP+W (30 min) and ATP+W+K (30 min). Some of the error bars may not be visible because they are too small.

5.3.1.3.2 Formation of products with RT higher than 50 min

The present study also aimed to examine how minerals and water might influence the reaction pathways of AMS dimerization. The GC-MS chromatogram containing the selected species within an RT higher than 50 min during the ATP experiments with a reaction time of 10 min is shown in **Figure C.31** in **Appendix C**. **Figure 5.6** contains the structures of the AMS dimers ($C_{18}H_{20}$ isomers) and their hydrogenated derivatives ($C_{18}H_{22}$ isomers), as identified in a previous study [54].

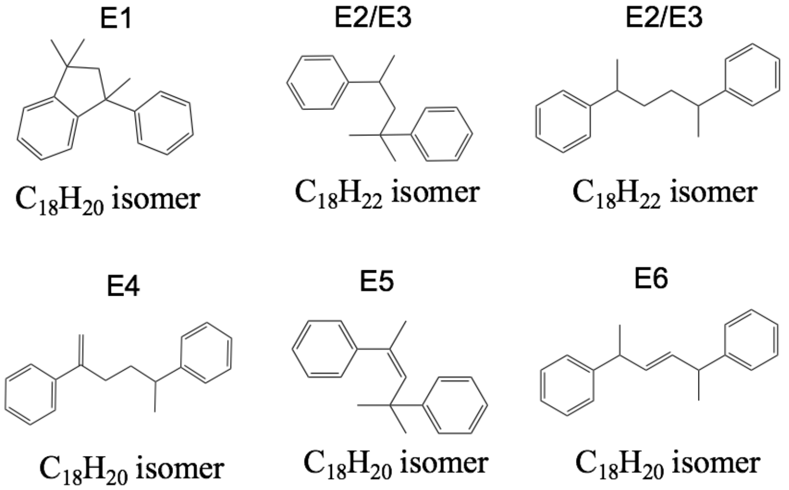

Figure 5.6: Structures of AMS dimers and their hydrogenated derivatives identified during the ATP and AWM experiments.

The change in concentration expressed as relative area percentage (RAP) with time of the species E1–E6 formed during the ATP experiments is shown in **Figure 5.7**. None of these species were detected in the reaction feed but were formed after the thermal treatment. The AMS dimer E1 (1,1,3-trimethyl-3-phenyl indane) was only identified in systems containing kaolinite. The error bars included for the systems ATP+W+K and ATP+W at 30-min reaction showed that the RAP of the selected compounds varied within a narrow range. Most of the selected compounds presented an increase in RAP with time, while the RAP of compound E4 decreased with time in all reaction systems within the range of 1–30 min.

The rates of formation and conversion of compounds E1–E6 are given in **Table 5.6**. The rates of these compounds were calculated using the same methodology as described in **Section 5.2.2.3**, but the concentration term (C_w), shown in **Eq. 5.2–5.4**, was replaced by the RAP values. The

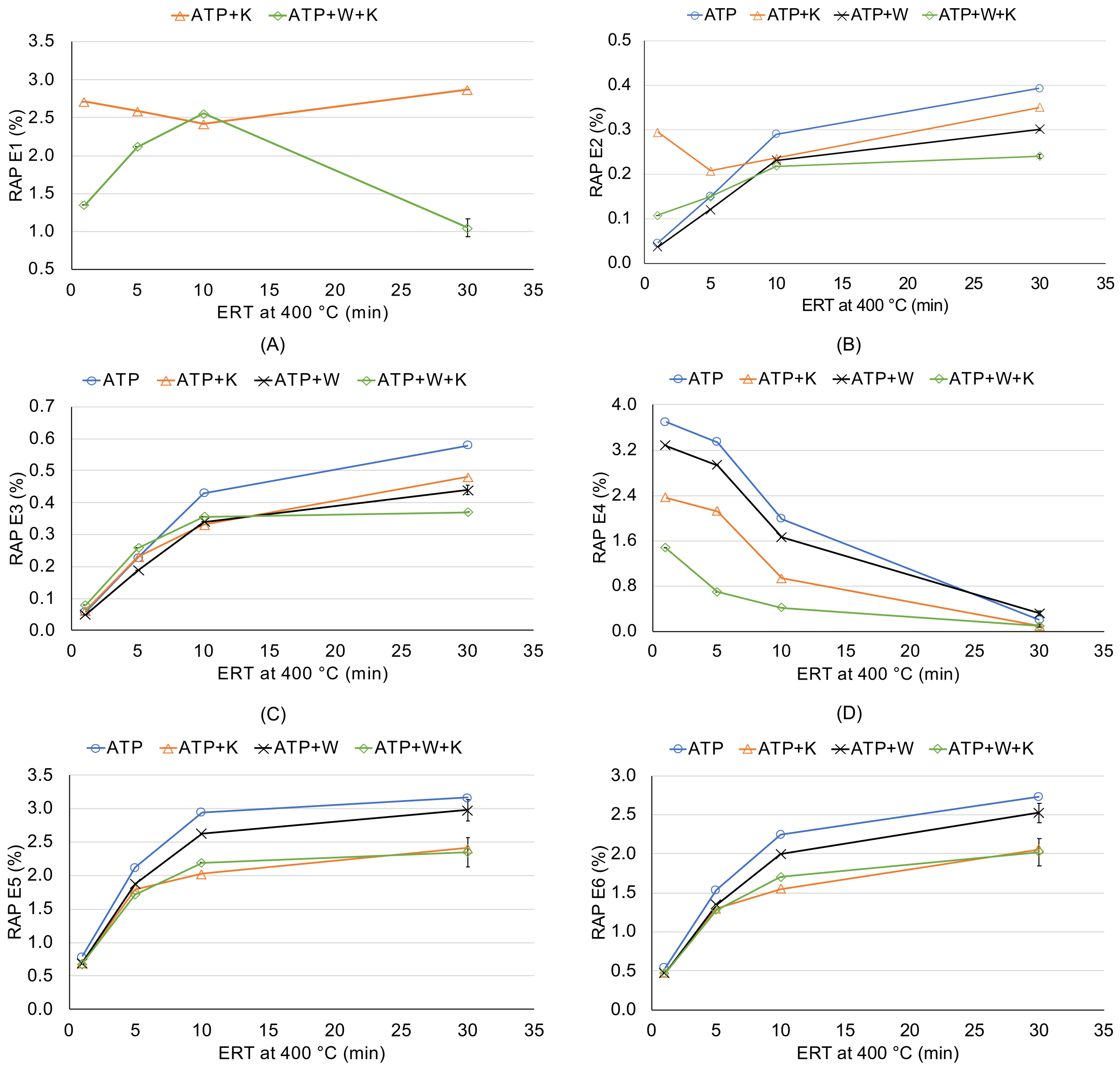

(A) (B)

(C) (D)

(E) (F)

Figure 5.7: RAP of species (A) E1, (B) E2, (C) E3, (D) E4, (E) E5, and (F) E6 formed during the ATP experiments. The structures of species E1–E6 are illustrated in **Figure 5.6**. Error bars were included for the systems ATP+W (30 min) and ATP+W+K (30 min). Some of the error bars may not be visible because they are too small.

coefficients of the polynomials and regression plots are given in **Table C.10** and **Figures C.12–C.17** in **Appendix C**. Examining the plots of the natural logarithm of concentration versus time and the inverse of concentration versus time, it was evident that the formation or conversion of compounds E1–E6 could not be described by simple first- or second-order kinetic models.

The AMS dimer E1, which was detected exclusively in the kaolinite-containing systems, and the AMS dimer E4 presented higher initial rates of formation (i.e., $r_{w,0}$ in the range of 81–222 RAP/h) compared to the AMS dimers E5 and E6 (i.e., $r_{w,0}$ in the range of 28–47 RAP/h). The species E2 exhibited a higher initial rate of formation in the system containing kaolinite in the absence of water (i.e., system ATP+K) as compared to the other reaction systems. In all reaction systems, the AMS dimer E4 exhibited the greatest initial formation rates compared to the other isomers. Despite this, the RAP of dimer E4 consistently decreased over time, as shown in **Figure 5.7D**.

Table 5.6: Rates of formation and conversion of selected compounds with RT higher than 50 min during the ATP experiments.

Compound / System	Rate of formation or conversion (RAP h^{-1})		
	$r_{w,0}$	$r_{w,5}$	$r_{w,10}$
E1			
ATP	ND[a]	ND	ND
ATP+K	163	-2.0	-1.3
ATP+W	ND	ND	ND
ATP+W+K	81	8.8	3.3
E2			
ATP	2.8	1.6	1.4
ATP+K	18	-0.6	0.3
ATP+W	2.3	1.3	1.1
ATP+W+K	6.5	0.7	0.7
E3			
ATP	3.5	2.5	2.0
ATP+K	3.7	1.9	1.1
ATP+W	2.9	2.0	1.5

Continues on the next page

Compound / System	Rate of formation or conversion (RAP h^{-1})		
	$r_{w,0}$	$r_{w,5}$	$r_{w,10}$
ATP+W+K	4.8	2.0	0.9
E4			
ATP	222	-10	-14
ATP+K	141	-8.3	-12
ATP+W	197	-9.7	-13
ATP+W+K	88	-8.0	-2.9
E5			
ATP	47	16	8.1
ATP+K	42	11	2.5
ATP+W	42	14	7.5
ATP+W+K	41	11	4.6
E6			
ATP	32	12	7.1
ATP+K	28	8.2	2.7
ATP+W	28	11	6.6
ATP+W+K	28	9.0	4.3

[a] ND – Not Detected.

5.3.1.4 Microscope images of the minerals in the ATP experiments

The microscope pictures of kaolinite after the reactions during the ATP experiments are shown in **Figure 5.8**. Notably, in the ATP+K system, the organic material deposited on kaolinite appeared to darken with increasing reaction time. In contrast, the water-containing system ATP+W+K did not exhibit the presence of dark organic matter covering kaolinite.

In order to assess the amount of organic matter deposited over the minerals' surface after reaction, the minerals in the ATP experiments were subjected to thermogravimetric analysis (TGA), and the results are shown in **Table C.19** in **Appendix C**. The fixed organic matter deposited on the minerals' surface was lower than 1 wt% across all reaction systems. Considering the low surface area of the minerals (i.e., BET surface area less than 10 m^2/g, refer to **Table C.1** in **Appendix C**) this was to be expected.

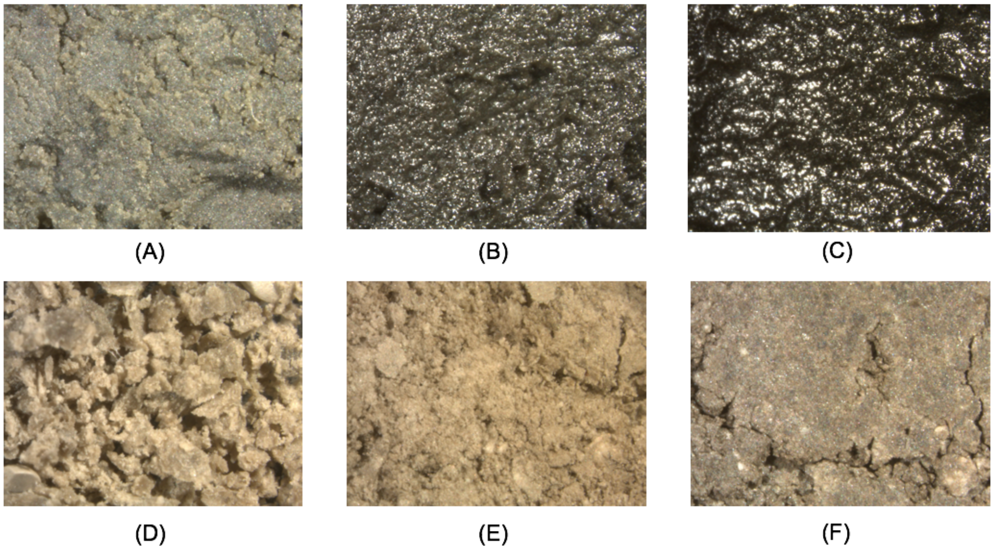

Figure 5.8: Microscope pictures at 30x magnification of kaolinite after reaction in the systems (A) ATP+K (1 min), (B) ATP+K (5 min), (C) ATP+K (30 min), (D) ATP+W+K (1 min), (E) ATP+W+K (5 min), and (F) ATP+W+K (30 min).

5.3.2 Thermal conversion during the AWM experiments

5.3.2.1 ERT at 400 °C, gas formation, and reaction pressure

The ERT at 400 °C, the gas formation per mass of AMS, and the maximum pressure achieved during reaction in the AWM experiments are listed in **Table 5.7**. The ERT at 400 °C varied in the range of 9.8–10.3 min. It was a narrow range compared to the planned reaction time of 10 min for those experiments, indicating that the reacted systems were subjected to similar thermal conversion severities. The amount of gas formed varied in the range of 6–18 mg of formed gas/g of AMS and presented a high standard deviation, making it challenging to identify any effect of minerals or water on the gas formation during the treatment. The maximum pressure achieved at isothermal conditions at 400 °C was 2.5 MPa for most of the reaction systems, except for the water-containing system (AMS+W), in which the pressure reached 5 MPa.

Table 5.7: ERT at 400 °C, gas formation, and maximum pressure achieved at 400 °C during the AWM experiments. The mineral content (wt%) is shown in parenthesis, as noted in **Table 5.2**.

System	ERT at 400 °C (min)		Gas formation (mg of formed gas / g of AMS)		Pressure at 400 °C (MPa)
	x	s	x	s	
AMS	10.3	0.1	9	8	2.5
AMS+K (3)	10.2	0.1	14	11	2.5
AMS+K (9)	10.2	0.2	5	2	2.5
AMS+R (5)	9.8	0.1	6	8	2.5
AMS+R (13)	9.8	0.1	13	1	2.5
AMS+Q (9)	9.9	0.1	15	2	2.5
AMS+Q (23)	10.2	0.3	18	9	2.5

5.3.2.2 AMS conversion and formation of compounds with RT lower than 50 min during the AWM experiments

The conversion of AMS during the AWM experiments is listed in **Table 5.8**. The AMS conversion varied in the range of 89.2–97.3%.

The chromatograms containing the compounds with RT lower than 50 min identified after the thermal conversion in the AWM experiments are shown in **Figures C.28–C.30** in **Appendix C**. The selectivity of AMS conversion to selected products with RT lower than 50 min is reported in **Table 5.8**.

5.3.2.3 Formation of compounds with RT higher than 50 min during the AWM experiments

The chromatogram containing the species with an RT higher than 50 min formed during the AWM experiments is shown in **Figure C.32** in **Appendix C**. **Table 5.9** contains the RAP of the species E1–E6, including the AMS dimers and their hydrogenated derivatives ($C_{18}H_{20}$ and $C_{18}H_{22}$ isomers, with structures shown in **Figure 5.6**). The RAP of the AMS dimer E1 was substantially higher in the reaction systems containing kaolinite as compared to the other reaction systems.

Table 5.8: AMS conversion and selectivity to compounds with retention time lower than 50 min for the AWM experiments.

	AWM experiments[a]													
	AMS		**AMS+K (3)**		**AMS+K (9)**		**AMS+R (5)**		**AMS+R (13)**		**AMS+Q (9)**		**AMS+Q (23)**	
	x	s	x	s	x	s	x	s	x	s	x	s	x	s
Conversion (%)														
AMS	89.5	0.6	90.4	0.5	92.2	0.7	90.4	0.6	91.6	1.8	89.2	0.1	91.7	0.6
Selectivity (%)														
cumene	17.1	0.2	16.6	0.1	14.2	1.1	18.6	0.1	20.0	0.4	17.1	0.5	17.4	0.4
benzene	0.06	0.01	0.25	0.00	0.46	0.05	0.06	0.00	0.06	0.01	0.05	0.00	0.06	0.01
toluene	0.65	0.14	0.44	0.00	0.80	0.58	0.57	0.05	1.17	0.85	0.53	0.02	0.59	0.18
ethylbenzene	7.1	0.1	5.9	0.2	5.1	0.1	7.8	0.1	7.3	0.7	7.1	0.2	6.4	0.6
n-propylbenzene	0.45	0.01	0.35	0.00	0.32	0.01	0.45	0.04	0.40	0.04	0.45	0.01	0.43	0.05
sec-butylbenzene	0.88	0.01	0.81	0.01	0.71	0.03	0.95	0.02	0.98	0.05	0.88	0.02	0.86	0.04

[a] Average (x) and standard deviation (s) of experiments in duplicate.

Table 5.9: RAP of selected compounds with RT higher than 50 min formed during the AWM experiments.

Compound	**RAP** (%)													
	AMS		**AMS+K (3)**		**AMS+K (9)**		**AMS+R (5)**		**AMS+R (13)**		**AMS+Q (9)**		**AMS+Q (23)**	
	x	*s*	*x*	*s*	*x*	*s*	*x*	*s*	*x*	*s*	*x*	*s*	*x*	*s*
E1	0.04	0.04	15.76	1.84	19.24	0.03	0.03	0.01	0.03	0.04	0.23	0.03	0.66	0.16
E2	2.55	0.02	1.71	0.13	1.78	0.13	2.38	0.02	2.38	0.20	2.39	0.21	2.89	0.02
E3	2.83	0.02	1.98	0.15	2.06	0.12	2.72	0.04	2.76	0.22	2.65	0.23	3.20	0.01
E4	3.80	0.28	2.57	0.38	2.37	0.43	2.92	0.13	2.62	0.66	3.82	0.18	3.33	0.48
E5	5.32	0.15	4.63	0.05	4.12	0.13	5.03	0.19	4.94	0.17	5.04	0.36	5.30	0.11
E6	4.76	0.05	4.09	0.03	3.65	0.11	4.46	0.19	4.39	0.22	4.45	0.33	4.76	0.15

5.3.2.4 Microscope images of the minerals in the AWM experiments

The microscope pictures of kaolinite, rutile, and quartz before and after the reactions in the AWM experiments are illustrated in **Figure 5.9**. Following the reactions, only kaolinite exhibited a coating of dark organic matter. The change observed in the rutile's texture was likely due to the initial microscope image capturing a dry mineral, while the post-reaction image featured a product-wet rutile. The brown color observed on quartz after the reaction corresponded to the color of the liquid product.

The fixed organic matter over the minerals' surface after reaction in the AWM experiments was lower than 1 wt%, as reported in **Table C.19** in **Appendix C**.

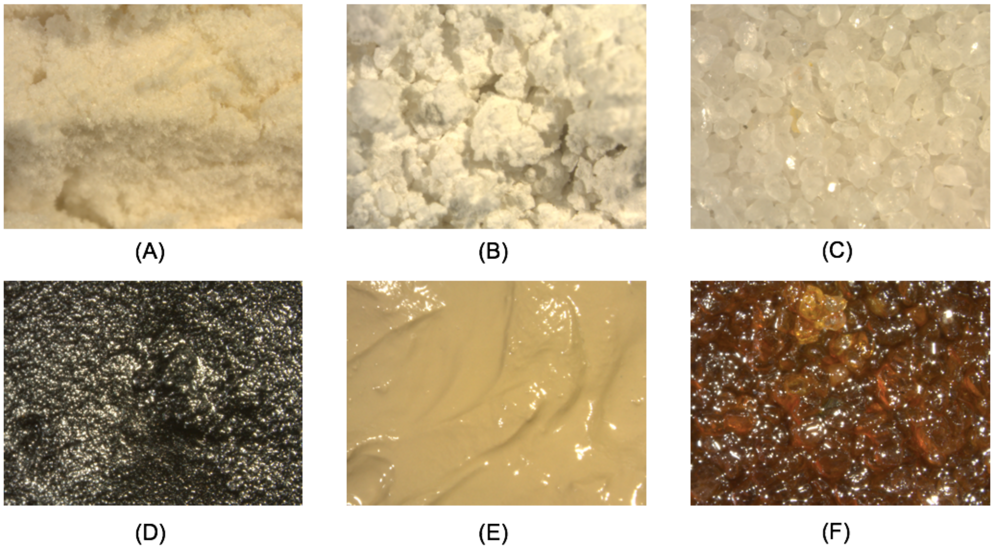

Figure 5.9: Microscope pictures at 30x magnification of (A) kaolinite, (B) rutile, and (C) quartz before reaction and (D) kaolinite, (E) rutile, and (F) quartz after reaction in the AWM experiments.

5.4 Discussion

5.4.1 Effect of water on AMS conversion

The first objective of this study was to examine how water and kaolinite affect the rate of AMS conversion. The impact of water is discussed first.

The most noticeable effect of water was its impact on AMS conversion (**Figure 5.4B**), with the system ATP+W consistently showing the lowest AMS conversions. This decreased AMS conversion in the presence of water aligns with findings from a previous study [54]. Also, Baumann and Metz [59] reported that water decreased the reactivity of AMS polymerization induced by γ-radiation. The presence of water in the system ATP+W not only led to a lower overall AMS conversion compared to the system ATP but also caused a reduction of 377 kg m^{-3} h^{-1} in the initial rate of AMS conversion (i.e., decrease in the $r_{w,0}$ from -3818 to -3441 kg m^{-3} h^{-1}; refer to **Table 5.4**) and a reduction of 79 kg m^{-3} h^{-1} in the conversion rate at 5 min (i.e., decrease in the $r_{w,5}$ from -828 to -749 kg m^{-3} h^{-1}). The AMS conversion rate at 10 min was comparable in the presence and absence of water (i.e., $r_{w,0}$ of about -500 kg m^{-3} h^{-1}).

A potential factor influencing the decreased rates of AMS conversion in this study might be the physical impact of water as a solvent. The phase behavior of mixtures containing water and hydrocarbons is complex. Brunner et al.[60] investigated the phase behavior of binary mixtures comprising various aromatic hydrocarbons with water, many of which were identified in the products of the ATP experiments, such as benzene, toluene, and polyaromatics. Based on their findings, numerous binary mixtures exhibited a single homogeneous gas phase under the temperature and pressure conditions corresponding to the reactions in the water-containing systems in the current study (i.e., 400 °C and 4.2–4.5 MPa). Therefore, it is likely that components in the ATP+W reactions, including AMS in its supercritical state, were diluted by water within a single gas phase. Dilution by water likely contributed to the observed decrease in reaction rates in that system because it decreased the concentration of the reactants. It is recognized that the ionic strength and dissolved ionic species in the water could affect the conversion, but this aspect was not investigated.

When evaluating the influence of water on the selectivity of AMS conversion to products with RT lower than 50 min (**Figure 5.5**), the presence of water in the system ATP+W yielded comparable selectivities to the ATP system for all the products listed in **Section 5.3.1.3.1**.

Importantly, there was no change in the selectivities to cumene and naphthalene (**Figures 5.5E and 5.5F**, respectively), which serve as indicators of hydrogen transfer during the treatment. Cumene can be formed via the transfer hydrogenation of AMS, while naphthalene can result from the donation of hydrogens by tetralin. In a prior study, the presence of water appeared to somehow favor the conversion of AMS into cumene, albeit within a more complex reaction system involving oilsands bitumen [54]. Nevertheless, in the current study, the same trend was not observed for the simpler model system comprising AMS, *n*-pentadecane, and tetralin. Prior studies investigating the role of water in oil conversion have suggested that water functions as a net hydrogen donor during the process [61]. However, there is also evidence suggesting that water is not consumed during the process; rather, it acts more as a hydrogen transfer agent than a hydrogen donor. In the current study, there was no evidence to indicate that water affected the reaction network and product selectivity beyond the impact of water dilution on the rate of AMS conversion. This finding provided a counterpoint to the role of water as a net hydrogen donor during the thermal conversion of oil.

The only oxygenate product identified in this study was 2-phenyl-2-propanol, exclusively identified in the water-containing systems and formed at very low concentration levels. The hydration of AMS is exothermic, and given the temperature conditions of this study, its equilibrium concentration was anticipated to be low [54]. No evidence was found to indicate that 2-phenyl-2-propanol was an intermediate product that noticeably affected the product selectivity of the hydrocarbon products.

It appears that the water dilution in the ATP+W system influenced the kinetics of AMS conversion. However, there is no evidence to suggest that water affected the reaction pathways or hydrogen transfer reactions during the treatment.

5.4.2 Effect of kaolinite on AMS conversion

The presence of Brønsted-Lowry and Lewis acid sites in the kaolinite structure is expected to facilitate additional conversion pathways for AMS, including cationic conversion [6, 62]. It was anticipated that the acid-catalyzed conversion in the presence of kaolinite could impact both reaction rates and the formation of specific products.

The first apparent impact of kaolinite was observed in the AMS conversion. The kaolinite-containing systems exhibited the highest AMS conversions (**Figure 5.4B**) across various reaction times. The inclusion of kaolinite into the reaction medium led to a 22–42$\%$ relative increase in the initial conversion rates of AMS compared to the ATP system (i.e., an increase in $r_{w,0}$ from -3818 kg m^{-3} h^{-1} in ATP to -5444 kg m^{-3} h^{-1} in ATP+K, and to -4671 kg m^{-3} h^{-1} in ATP+W+K; refer to **Table 5.4**). The initial conversion rates of tetralin were also enhanced by the presence of kaolinite, showing an increase in the range of 8–13$\%$ (i.e., an increase in $r_{w,0}$ from -1621 kg m^{-3} h^{-1} in ATP to -1835 kg m^{-3} h^{-1} in ATP+K, and to -1748 kg m^{-3} h^{-1} in ATP+W+K; refer to **Table 5.4**). These results align with prior evidence indicating that kaolinite can accelerate reaction rates during thermal conversion. Kaolinite has been reported to increase the conversion rates during the thermal oxidation of crude oils and hydrolysis of organic compounds [63–65], although the surface intermediates involved are not necessarily the same. An intriguing finding in this study was that while kaolinite enhanced the initial conversion rates of AMS and tetralin, their conversion rates at 5 and 10 min were slightly lower in the system ATP+K when compared to the system ATP. A potential explanation for this observation is discussed in Section 4.4.

The Brønsted-Lowry acidity of kaolinite not only plays a role in enhancing reaction rates during the thermal conversion of organic compounds but is also expected to influence product selectivity and reaction pathways [51, 54].

When examining the impact of kaolinite on the selectivities and reaction rates of AMS and tetralin conversion to products with RT lower than 50 min (**Figure 5.5** and **Table 5.5**), two observations became immediately apparent. First, the highest selectivities and reaction rates of AMS conversion to cumene and tetralin conversion to naphthalene were attained in the kaolinite-containing systems. Second, the presence of kaolinite in the system ATP+K resulted in increased selectivity and reaction rates of AMS conversion to benzene.

Figure 5.10 illustrates two potential pathways for the conversion of AMS into cumene. The free radical pathway (paths A–B in **Figure 5.10**) involves an initial hydrogen radical transfer to AMS, resulting in the formation of a cumyl radical, followed by a subsequent transfer of another hydrogen to produce cumene. The cationic pathway (paths C–D in **Figure 5.10**) involves the protonation of AMS, resulting in the formation of a cumyl carbocation. This first step readily takes place in the presence of Brønsted-Lowry acids. However, it also necessitates the challenging step of hydride transfer, which is unlikely under the conditions of this study [66].

The selectivities of AMS conversion to cumene (**Figure 5.5E**) were approximately 10$\%$ higher in the kaolinite-containing systems compared to the system ATP. This result suggests that kaolinite somehow enhanced the transfer hydrogenation of AMS into cumene, a finding also observed in a

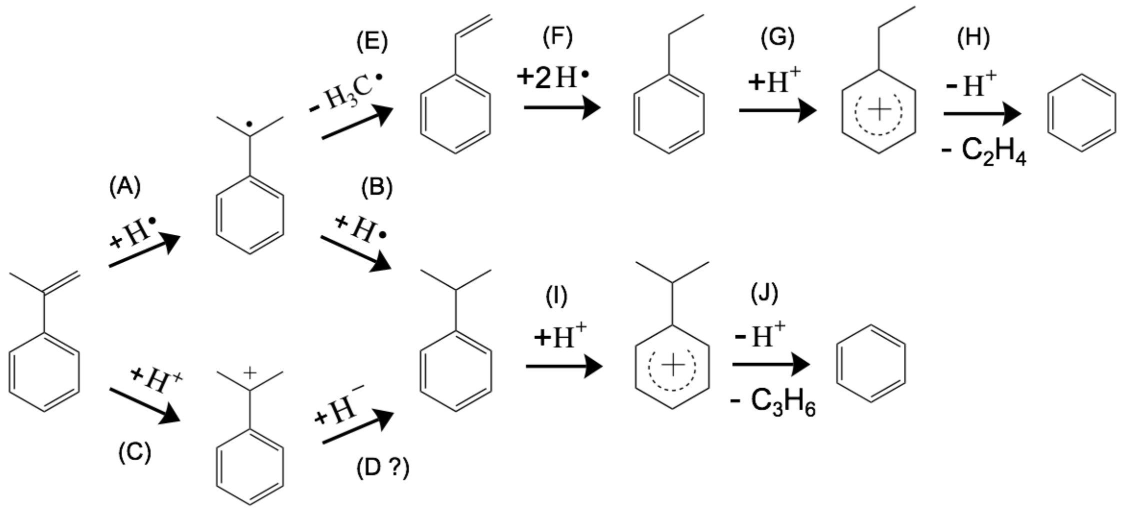

Figure 5.10: Possible reaction pathways for the (A–B) free radical transfer hydrogenation of AMS to cumene, (C–D) cationic transfer hydrogenation of AMS to cumene, (A–E–F) free radical conversion of AMS to ethylbenzene, (G–H) cationic dealkylation of ethylbenzene to yield benzene, and (I–J) cationic dealkylation of cumene to yield benzene.

previous study where AMS was thermally treated in the presence of bitumen and oilsands minerals containing kaolinite [54]. There was no apparent synergic effect of water and kaolinite on the selectivity to cumene.

Also, the initial rates of formation of cumene (**Table 5.5**) were about 3–4 times higher in the presence of kaolinite as compared to the system ATP (i.e., $r_{w,0}$ of 203 kg m^{-3} h^{-1} in ATP vs. 859 kg m^{-3} h^{-1} in ATP+K vs. 680 kg m^{-3} h^{-1} in ATP+W+K). While the formation rates of cumene at 5 and 10 min were also higher in the presence of kaolinite, the enhancement of the rates by kaolinite diminished as the reaction progressed (i.e., the initial formation rate of cumene, $r_{w,0}$, was four times higher in the presence of kaolinite, whereas $r_{w,5}$ and $r_{w,10}$ were only approximately 1.5 times higher). Other clay minerals, including smectite and illite, have been documented to impact hydrogen transfer during thermal treatment [53]. One avenue of speculation is that redox reactions on minerals are facilitating hydrogen transfer, analogous to radical ion formation found during oxidation by multivalent metals [67]. Another possible mechanism by which kaolinite might have favored hydrogen transfer during the treatment could involve the protonation of AMS by kaolinite (Figure 10, path C), followed by a hydride transfer step (Figure 10, path D). The occurrence of the hydride transfer step has been reported in works related to cationic polymerization and catalytic cracking [68, 69]. However, it is typically a relevant pathway under specific conditions, such as those found in aliphatic alkylation and aromatization. The specific mechanism by which the increase in hydrogen transfer rate occurs remains unresolved.

The selectivities of tetralin conversion to naphthalene were also higher in the presence of kaolinite, with increased selectivities to naphthalene of 10–15$\%$ in the systems ATP+K and ATP+W+K compared to the other reaction systems (see **Figure 5.5F**). Additionally, the rates of formation of naphthalene were consistently higher in the kaolinite-containing systems (see **Table 5.5**). As noted for cumene, the effect of kaolinite on enhancing the formation rates of naphthalene was more pronounced at the beginning of the conversion and decreased as the reaction progressed. Tetralin is well-recognized as a good hydrogen donor [70–72]. For every one mol of tetralin converted into naphthalene, four moles of transferable hydrogen are made available in the reaction medium, as shown in **Figure 5.11**. The increased rates of formation of naphthalene in the presence of kaolinite indicated that tetralin was an important source of hydrogen during AMS conversion.

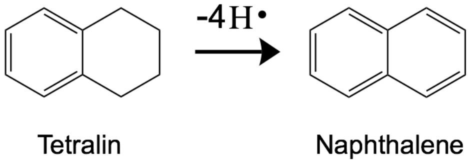

Figure 5.11: Conversion of tetralin into naphthalene.

The thermal conversion of alkyl aromatics, such as cumene, into benzene is an energy-intensive process typically requiring reaction temperatures above 600 °C [73]. Consequently, significant formation of benzene through a free radical mechanism was not expected under the temperature conditions of this study. Although benzene was not initially detected in the ATP and ATP+W systems, small amounts were formed as the reaction progressed (i.e., the formation rates of benzene at 10-min, $r_{w,10}$, varied in the range of 0.1–0.3 kg m^{-3} h^{-1} in the ATP and ATP+W systems; refer to **Table 5.5**).

However, a higher selectivity to benzene was observed in the presence of kaolinite in the ATP+K system, while the presence of water hindered the formation of benzene (refer to **Figure 5.5A**). The $r_{w,0}$ of benzene in the system ATP+K was 39 kg m^{-3} h^{-1} and in the system ATP+K+W was 1.9 kg m^{-3} h^{-1}, while benzene was not initially detected in the absence of kaolinite (see **Table 5.5**). The acid-catalyzed dealkylation of alkyl aromatics readily takes place in the presence of Brønsted-

Lowry acids at temperatures as low as 180 °C [74, 75]. The increased reaction rate of benzene in the system ATP+K was evidence that kaolinite facilitated cationic conversion during the treatment.

Figure 5.10 illustrates two potential cationic pathways for the formation of benzene in this study. The acid-catalyzed dealkylation of ethylbenzene into benzene is depicted in paths G–H, while the acid-catalyzed dealkylation of cumene into benzene is shown in paths I–J. Evidence of both pathways is documented in the literature [74, 75]. The relative contributions of cumene, ethylbenzene, or other species to the formation of benzene in the ATP+K system remain unclear. Nevertheless, an intriguing finding was that the selectivities to ethylbenzene in the system ATP+K (**Figure 5.5C**) were consistently lower than in the other systems, indicating that some ethylbenzene was possibly converted into benzene in the presence of kaolinite.

When assessing the impact of kaolinite on the dimerization of AMS by looking at products with RT > 50 min, two observations were noteworthy. First, the tricyclic AMS dimer E1 was only detected in the presence of kaolinite (see **Figure 5.7A**). Second, the presence of kaolinite resulted in consistent lower selectivity and formation rates for the AMS dimer E4 (see **Figure 5.7D** and **Table 5.6**).

Two potential pathways for the dimerization of AMS into the dimers E1 and E5 are depicted in **Figure 5.12**. The free radical pathway (**Figure 5.12**, path A) advances through the formation of an intermediate cumyl radical species, while the cationic dimerization of AMS (**Figure 5.12**, path B) proceeds through the formation of a cumyl carbocation species [76].

The exclusive detection of dimer E1 in the kaolinite-containing systems (refer to **Figure 5.7A**) provided evidence that cationic conversion promoted by kaolinite was critical for the formation of that dimer in the present study. The acid catalyzed formation of E1 from AMS was also reported for acidic resin catalysts and mordenite [77, 78]. This outcome contrasts with the findings of a study where AMS was thermally treated at 250 °C in the presence and absence of kaolinite, and the tricyclic dimer was only detected when AMS was treated in the absence of kaolinite [51]. In that study, kaolinite favored the formation of the dimer E5 (with two potential dimerization pathways illustrated in **Figure 5.12**) but hindered the formation of E1. The observed formation of E1 only in

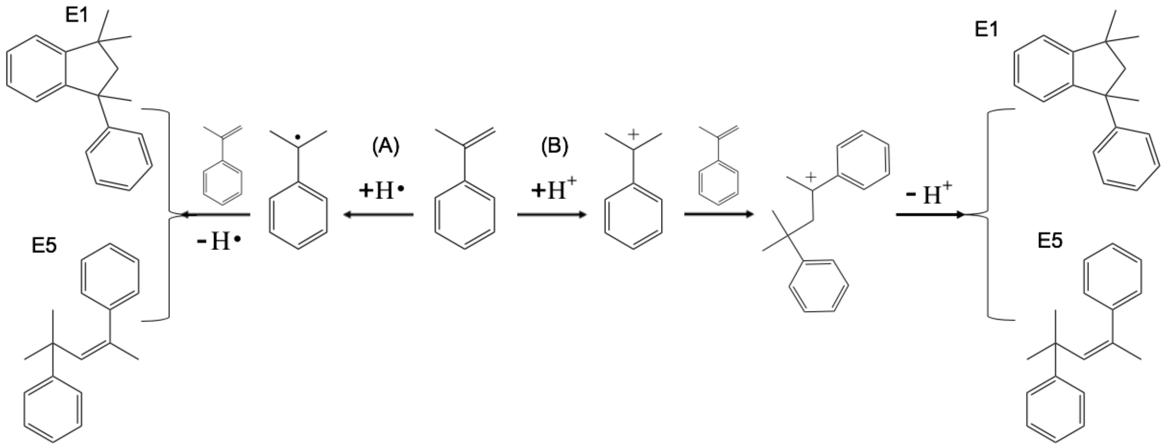

Figure 5.12: Possible (A) free radical and (B) cationic pathways for the dimerization of AMS to yield the dimers E1 and E5. The structures of the dimers E1 and E5 are given in **Figure 5.6**.

the presence of kaolinite in the current study could be a consequence of the higher temperature, 400 °C, as it has been reported that the formation of the tricyclic dimer is favored at higher temperatures [77]. Nevertheless, the formation of E1 was reported at temperatures as low as 60 °C [78].

The formation of dimer E4 is likely to proceed through the hydrogen disproportionation of two AMS molecules. A potential concerted bimolecular mechanism for the formation of E4, involving a 1,4-diradical intermediate, has been reported before [54]. Consequently, it was not anticipated that a cationic pathway promoted by kaolinite would favor the formation of this dimer. In fact, the lowest RAPs for E4 were observed in the kaolinite-containing systems (see **Figure 5.7D**). The lower initial rates of formation of E4 in the presence of kaolinite (i.e., $r_{w,0}$ of 88–141 RAP/h in the kaolinite-containing systems vs. 197–222 RAP/h in the absence of kaolinite; see **Table 5.6**) were possibly influenced by the higher rates of hydrogen transfer attained in the presence of kaolinite to form the corresponding $C_{18}H_{22}$ isomer as product.

5.4.3 Effect of kaolinite+water on AMS conversion

Based on the results discussed thus far, a noteworthy finding is that the presence of water in the system ATP+K+W consistently led to lower initial reaction rates ($r_{w,0}$) compared to the system ATP+K for the conversion of AMS and tetralin, as well as for the formation of cumene, naphthalene, and benzene (refer to **Tables 5.4** and **5.5**). There was also evidence that the presence of water in the system ATP+W+K hindered the formation of the dimers E1 and E4 (refer to **Table 5.6**).

The hindering effect of water on the reactivity of the previously mentioned compounds may be attributed to the dilution effect of water, as discussed in **Section 5.4.1**. Nevertheless, another contributing factor, such as the interaction of water with the acid sites on the kaolinite surface, could also have played a role in affecting the conversion process. The impact of water on organic reactions taking place on the surface of kaolinite has been reported before. For example, the hydrolysis rate of parathion, an organophosphate pesticide, on the surface of kaolinite decreased with an increase in water content beyond 11 wt% [79].

The surface of kaolinite exhibits both hydrophobic and hydrophilic characteristics. The strong hydrophobicity is attributed to the siloxane structures, whereas hydrophilicity arises from the hydroxyl groups on the kaolinite's surface [80]. In this context, water attached to the hydrophilic hydroxyl groups, which are also the groups responsible for the Brønsted-Lowry acidity of kaolinite, may have impeded the interaction of other chemical species in the reaction medium with kaolinite, leading to the observed lower initial reaction rates in the ATP+W+K system. Additionally, the microscope pictures of kaolinite after reactions, shown in **Figure 5.8**, revealed the presence of dark organic matter deposited over kaolinite in the ATP+K systems at all reaction times. However, the same dark organic matter was not found on the surface of kaolinite in the ATP+W+K systems. This finding suggested that water might have adhered to the surface of kaolinite, hindering the conversion of organic matter on its surface. Differently put, competitive adsorption of water on kaolinite resulted in lower AMS and tetralin conversion, as well as lower formation of carbonaceous deposits.

Another possible interaction of water and kaolinite that might have resulted in decreased conversion and reaction rates is the hydration of kaolinite [81]. This process has the potential to modify the surface properties of kaolinite, which could subsequently impact its interaction with organic matter.

5.4.4 The catalytic effect of minerals on AMS conversion

The second objective of this study was to evaluate assertions regarding the catalytic effect of minerals commonly found in oilsands during thermal conversion. Kaolinite exhibits both Brønsted-Lowry and Lewis acidity; rutile presents Lewis acidity; and quartz does not have acidity [6, 82].

The minerals employed in this study exhibited a BET surface area lower than 10 m^2/g (see **Table C.1** in **Appendix C**). As a consequence, even minimal amounts of organic matter deposition can rapidly foul the mineral, decreasing its catalytic activity. The evaluation of the catalytic effect of the minerals used in this study was conducted in light of this context.

There was no clear impact of minerals on the overall conversion of AMS at both low and high mineral concentration levels in the AWM experiments compared to the self-reaction of AMS (see **Table 5.8**). At the same time, due to the high AMS conversion, it was difficult to discern such an impact. However, in the ATP experiments, the presence of kaolinite resulted in an increase of 24–42% in the initial rates of AMS conversion (see **Table 5.4**), while the AMS conversion rates at 5- and 10-min were comparable in both the presence and absence of kaolinite.

Polovor et al.[76] reported the deposition of condensation products from the conversion of AMS, referred to by the authors as coke, on the surface of an aluminosilicate catalyst. The formation of coke-like material originating from the conversion of cumene on the surface of acid catalysts has also been reported [74, 83]. The microscope pictures of kaolinite after reaction in the ATP experiments (**Figure 5.8**) revealed the formation of dark carbonaceous material over the kaolinite's surface, which seemed to darken with increased reaction time. These findings suggest that the deposition of organic material can rapidly foul kaolinite, making its catalytic effect only apparent at the initial stages of AMS conversion. As the reaction progressed, the fouling of kaolinite could have led to the observed decreased conversion rates of AMS and tetralin at 5 and 10 min, along with the reduced enhancement in the formation rates of cumene and naphthalene at 5 and 10 min compared to the initial rates.

Additional evidence that kaolinite was catalytically active during the thermal conversion in this study was observed through the formation of benzene and the AMS dimer E1 in the AWM experiments. The selectivity of AMS conversion to benzene increased with a higher concentration of kaolinite in the reaction medium (i.e., selectivity to benzene was 0.25±0.00% in AMS+K(3) vs. 0.46±0.05% in AMS+K(9); refer to **Table 5.8**). Also, the RAP of E1 in the AWM experiments (see **Table 5.9**) was pronouncedly higher in the presence of kaolinite. However, increasing the concentration of kaolinite from 3 to 9 wt% did not result in a proportional increase in the RAP of E1.

There was no indication that either rutile or quartz were catalytically active during the AWM experiments. The selectivities to products with RT lower than 50 min (**Table 5.8**) and the RAP of the AMS dimerization products (**Table 5.9**) were comparable in the absence of minerals (i.e., system AMS) and in the presence of both rutile and quartz. Moreover, no carbonaceous material was found to be deposited on either rutile or quartz (see **Figures 5.9E** and **5.9F**, respectively) after reactions.

5.4.5 Relevance to petroleum processes

Previous investigations into petroleum conversion have suggested advantages of processing oil in the presence of water, such as increased viscosity reduction, a higher yield of light liquid products, and coke suppression [13, 84, 85]. However, many of these studies were conducted over extended reaction times (6–24 hours), under supercritical conditions, and in the presence of added catalysts. At the conditions of the current study (400 °C, 0.5 h), no beneficial impact of water was identified. In fact, the results indicated that water reduced reaction rates during thermal conversion. When considering thermal recovery methods like steam-assisted gravity drainage (SAGD) and cyclic steam stimulation (CSS) that are conducted at lower temperatures than those employed in this study and focus on extraction rather than upgrading, the findings of the present study suggest that the use of steam during extraction may not interfere with the original composition of the oil. However, from the perspective of oil upgrading, such as those found in hydrothermal treatment of oil and subsurface upgrading in the presence of water, no beneficial or deleterious effect of water could be inferred from this study.

This outcome does not invalidate previous claims about the benefits of incorporating water during thermal treatment of oil, but suggests that the positive effect of water might be dependent on other variables, such as medium composition, reaction times, and the presence or absence of catalytically active materials in the medium. This highlights that although there is extensive literature on the influence of water during the thermal treatment of oil, the precise role of water in this process remains unclear. Future studies on the relationship between the physical effect of water as a diluent during the process and its implications for the properties and composition of the final product could contribute to advancing knowledge in this field.

The results of this study suggested that the presence of kaolinite enhanced hydrogen transfer during thermal treatment when a good hydrogen donor is available in the reaction medium. This finding aligns with prior research involving the treatment of bitumen with oilsands minerals containing kaolinite [5, 54]. Increasing the rate of hydrogen transfer during oil conversion can be beneficial as it contributes to suppressing coke formation [86]. Future research on the collective impact of other clay minerals such as illite and montmorillonite (i.e., clays frequently found in oil reservoirs) during thermal oil treatment could offer valuable insights into the role of these minerals in oil conversion.

Several studies in the literature have reported the catalytic effect of kaolinite during the thermal conversion of oil, influencing reaction rates and decreasing activation energies [16, 64, 87]. In this study, there was evidence that kaolinite facilitated the cationic conversion of AMS. The enabling of additional conversion pathways by kaolinite, including cationic dealkylation to produce benzene and cationic dimerization to form the tricyclic AMS dimer 1,1,3-trimethyl-3-phenyl indane, could potentially impact the composition of the final products during oil conversion. Works regarding the *in situ* combustion of heavy oils have also reported the impact of kaolinite in enhancing reaction rates and influencing product composition [16, 88]. However, the rapid deactivation of kaolinite due to the deposition of carbonaceous material during conversion and the low surface area of kaolinite meant that the potential catalytic contribution of kaolinite was limited. Therefore, although kaolinite performed acid-catalyzed reactions, its impact on the overall conversion during petroleum processing is likely to be minor due to the fast deactivation of the mineral. At the same time, this study suggests that mineral matter may be retained in petroleum feed for thermal conversion, as long as it does not pose any risk to any equipment or process operation.

5.5 Conclusions

The current study explored the influence of water and kaolinite on reaction rates and pathways during the thermal conversion of AMS at 400 °C. Both water and kaolinite had an impact on the reaction rates, while kaolinite also influenced the pathways to the formation of specific products during the conversion process. There was evidence that kaolinite was catalytically active during the thermal treatment.

The main findings from this study are summarized as follows:

(a) The inclusion of water during the thermal treatment led to a reduction in the conversion rates of AMS. The dilution of the reaction medium by water could be a potential factor contributing to the decreased rates. Despite the impact of water on AMS conversion rates, no evidence was found to suggest that water affected reaction pathways, hydrogen transfer, or products selectivity.

(b) The presence of kaolinite resulted in increased conversion rates of both AMS and tetralin. The reaction rates and selectivities of AMS conversion to cumene and tetralin conversion to naphthalene were higher in the kaolinite-containing systems, suggesting that kaolinite somehow favored hydrogen transfer during the treatment.

(c) The higher rates of formation and selectivities of AMS conversion to benzene and the tricyclic AMS dimer E1 (1,1,3-trimethyl-3-phenyl indane), observed in the presence of kaolinite, indicated that kaolinite influenced the reaction pathways during the thermal treatment by facilitating cationic conversion.

(d) In addition to the dilution effect of water, the competitive adsorption of water on the surface of kaolinite might have played a role in decreasing the conversion rates of both AMS and tetralin, as well as the decreased formation rates of several products, including benzene and the AMS dimer E1.

(e) When comparing the impact of kaolinite to that of rutile and quartz on AMS conversion, only kaolinite was catalytically active during the treatment. However, the formation of carbonaceous deposits on the surface of kaolinite in combination with its low surface area suggests that the mineral can become rapidly fouled, making its catalytic effect apparent mainly at the initial stages of AMS conversion.

5.6 References

(1) Al-Muntaser, A. A.; Varfolomeev, M. A.; Suwaid, M. A.; Yuan, C.; Chemodanov, A. E.; Feoktistov, D. A.; Rakhmatullin, I. Z.; Abbas, M.; Domínguez-Álvarez, E.; Akhmadiyarov, A. A., et al. Hydrothermal upgrading of heavy oil in the presence of water at sub-critical, near-critical and supercritical conditions. *J. Pet. Sci. Eng.* **2020**, *184*, 106592.

(2) Liu, J.; Xing, Y.; Chen, Y. X.; Yuan, P. Q.; Cheng, Z. M.; Yuan, W. K. Visbreaking of heavy oil under supercritical water environment. *Ind. Eng. Chem. Res.* **2018**, *57* (3), 867–875.

(3) Petrukhina, N.; Kayukova, G.; Romanov, G.; Tumanyan, B.; Foss, L.; Kosachev, I.; Musin, R.; Ramazanova, A.; Vakhin, A. Conversion processes for high-viscosity heavy crude oil in catalytic and noncatalytic aquathermolysis. *Chem. Technol. Fuels Oils* **2014**, *50* (4), 315–326.

(4) Turuga, A. S. S.; de Klerk, A. Hydrothermal Treatment of Bitumen Froth: Impact of Mineral Solids and Water on Bitumen Properties. *Energy Fuels* **2021**, *35* (21), 17536–17550.

(5) Bassane, J. F. P.; de Klerk, A. Visbreaking of Bitumen Froth: Influence of Minerals, Water, and Solvent on the Physicochemical Changes in the Bitumen Phase. *Energy Fuels* **2023**, *37* (16), 11820–11837.

(6) He, M.; Wang, Z.; Moldowan, M. J.; Peters, K. Insights into catalytic effects of clay minerals on hydrocarbon composition of generated liquid products during oil cracking from laboratory pyrolysis experiments. *Org. Geochem.* **2022**, *163*, 104331.

(7) Fan, H. F.; Liu, Y. J.; Zhong, L. G. Studies on the synergetic effects of mineral and steam on the composition changes of heavy oils. *Energy Fuels* **2001**, *15* (6), 1475–1479.

(8) Li, Y. B.; Lin, X.; Luo, C.; Hu, Z. M.; Jia, H. F.; Chen, J. T.; Pu, W. F. A comprehensive investigation of the influence of clay minerals on oxidized and pyrolyzed cokes in in situ combustion for heavy oil reservoirs. *Fuel* **2021**, *302*, 121168.

(9) Zheng, R.; Liu, D.; Tang, J.; Song, Q.; Yao, Q. Analysis of montmorillonite affecting coke formation during the thermal conversion of heavy oil. *Fuel* **2021**, *288*, 119687.

(10) Zheng, R.; Pan, J.; Cai, G.; Liang, J.; Liu, D.; Song, Q.; Yao, Q. Effects of clay minerals on the low-temperature oxidation of heavy oil. *Fuel* **2019**, *254*, 115597.

(11) Ovalles, C.; Hamana, A.; Rojas, I.; Bolívar, R. A. Upgrading of extra-heavy crude oil by direct use of methane in the presence of water: deuterium-labelled experiments and mechanistic considerations. *Fuel* **1995**, *74* (8), 1162–1168.

(12) Morimoto, M.; Sugimoto, Y.; Saotome, Y.; Sato, S.; Takanohashi, T. Effect of supercritical water on upgrading reaction of oil sand bitumen. *J. Supercrit. Fluids* **2010**, *55* (1), 223–231.

(13) Dutta, R. P.; McCaffrey, W. C.; Gray, M. R.; Muehlenbachs, K. Thermal cracking of Athabasca bitumen: influence of steam on reaction chemistry. *Energy Fuels* **2000**, *14* (3), 671–676.

(14) Qi, Y.; Cai, C. F.; Sun, P.; Wang, D. W.; Zhu, H. J. Crude oil cracking in deep reservoirs: A review of the controlling factors and estimation methods. *Pet. Sci.* **2023**, *20* (4), 1978–1997.

(15) Monin, J. C.; Audibert, A. Thermal cracking of heavy-oil/mineral matrix systems. *SPE Reserv. Eng.* **1988**, *3* (4), 1243–1250.

(16) Zhang, X.; Wang, J.; Wang, L.; Li, Z.; Wang, R.; Li, H.; Luo, M.; Liu, H.; Hu, W.; Feng, Q. Effects of kaolinite and its thermal transformation on oxidation of heavy oil. *Appl. Clay Sci.* **2022**, *223*, 106507.

(17) Zheng, R.; Liao, G.; You, H.; Song, X.; Song, Q.; Yao, Q. Montmorillonite-catalyzed thermal conversion of low-asphaltene heavy oil and its main components. *J. Pet. Sci. Eng.* **2020**, *187*, 106743.

(18) Ederer, H.; Kruse, A.; Mas, C.; Ebert, K. Modelling of the pyrolysis of tert-butylbenzene in supercritical water. *J. Supercrit. Fluids* **1999**, *15* (3), 191–204.

(19) Siskin, M.; Katritzky, A. R. Reactivity of Organic Compounds in Hot Water: Geochemical and Technological Implications. *Science* **1991**, *254* (5029), 231–237.

(20) Katritzky, A. R.; Nichols, D. A.; Siskin, M.; Murugan, R.; Balasubramanian, M. Reactions in High-Temperature Aqueous Media. *Chem. Rev.* **2001**, *101* (4), 837–892.

(21) Savage, P. E. Organic Chemical Reactions in Supercritical Water. *Chem. Rev.* **1999**, *99* (2), 603–622.

(22) Arcelus-Arrillaga, P.; Hellgardt, K.; Millan, M. Effect of process conditions on the hydrothermal partial oxidation of phenanthrene as a heavy oil model structure. *Fuel* **2017**, *209*, 434–441.

(23) Arcelus-Arrillaga, P.; Pinilla, J. L.; Hellgardt, K.; Millan, M. Application of Water in Hydrothermal Conditions for Upgrading Heavy Oils: A Review. *Energy Fuels* **2017**, *31* (5), 4571–4587.

(24) Daud, A. R. M.; Berrueco, C.; Hellgardt, K.; Millan, M.; Kandiyoti, R. Oxidative cracking of three to five-member ring polycyclic aromatic hydrocarbons in subcritical and supercritical water. *J. Supercrit. Fluids* **2021**, *167*, 105050.

(25) Townsend, S. H.; Abraham, M. A.; Huppert, G. L.; Klein, M. T.; Paspek, S. C. Solvent effects during reactions in supercritical water. *Ind. Eng. Chem. Res.* **1988**, *27* (1), 143–149.

(26) Chen, Y.; Wang, K.; Yang, J. Y.; Yuan, P. Q.; Cheng, Z. M.; Yuan, W. K. Dealkylation of Aromatics in Subcritical and Supercritical Water: Involvement of Carbonium Mechanism. *Ind. Eng. Chem. Res.* **2016**, *55* (36), 9578–9585.

(27) Akiya, N.; Savage, P. E. Roles of Water for Chemical Reactions in High-Temperature Water. *Chem. Rev.* **2002**, *102* (8), 2725–2750.

(28) Katritzky, A. R.; Allin, S. M.; Siskin, M. Aquathermolysis: Reactions of Organic Compounds with Superheated Water. *Acc. Chem. Res.* **1996**, *29* (8), 399–406.

(29) Siskin, M.; Brons, G.; Katritzky, A. R.; Balasubramanian, M. Aqueous organic chemistry. 1. Aquathermolysis: comparison with thermolysis in the reactivity of aliphatic compounds. *Energy Fuels* **1990**, *4* (5), 475–482.

(30) Siskin, M.; Brons, G.; Katritzky, A. R.; Murugan, R. Aqueous organic chemistry. 2. Crosslinked cyclohexyl phenyl compounds. *Energy Fuels* **1990**, *4* (5), 482–488.

(31) Katritzky, A. R.; Balasubramanian, M.; Siskin, M. Aqueous high-temperature chemistry of carbo- and heterocycles. 2. Monosubstituted benzenes: benzyl alcohol, benzaldehyde and benzoic acid. *Energy Fuels* **1990**, *4* (5), 499–505.

(32) Katritzky, A. R.; Luxem, F. J.; Siskin, M. Aqueous high-temperature chemistry of carbo- and heterocycles. 6. Monosubstituted benzenes with two carbon atom side chains unsubstituted or oxygenated at the alpha-position. *Energy Fuels* **1990**, *4* (5), 518–524.

(33) Katritzky, A. R.; Barcock, R. A.; Balasubramanian, M.; Greenhill, J. V.; Siskin, M.; Olmstead, W. N. Aqueous High-Temperature Chemistry of Carbo- and Heterocycles. 20. Reactions of Some Benzenoid Hydrocarbons and Oxygen-Containing Derivatives in Supercritical Water at 460 °C. *Energy Fuels* **1994**, *8* (2), 487–497.

(34) Katritzky, A. R.; Ignatchenko, E. S.; Allin, S. M.; Barcock, R. A.; Siskin, M.; Hudson, C. W. Aqueous High-Temperature Chemistry of Carbo- and Heterocycles. 29. Reactions of Aryl Hydrocarbons, Aryl N- Oxides, and Aryl Carbonyl Compounds in Supercritical Water at 460 °C. *Energy Fuels* **1997**, *11* (1), 160–173.

(35) Huizinga, B. J.; Tannenbaum, E.; Kaplan, I. R. The role of minerals in the thermal alteration of organic matter - IV. Generation of n-alkanes, acyclic isoprenoids, and alkenes in laboratory experiments. *Geochim. Cosmochim. Acta* **1987**, *51* (5), 1083–1097.

(36) Eglinton, T.; Rowland, S.; Curtis, C.; Douglas, A. Kerogen-mineral reactions at raised temperatures in the presence of water. *Org. Geochem.* **1986**, *10* (4-6), 1041–1052.

(37) Wu, L. M.; Zhou, C. H.; Keeling, J.; Tong, D. S.; Yu, W. H. Towards an understanding of the role of clay minerals in crude oil formation, migration and accumulation. *Earth-Science Rev.* **2012**, *115* (4), 373–386.

(38) Tannenbaum, E.; Huizinga, B. J.; Kaplan, I. R. Role of Minerals in Thermal Alteration of Organic Matter–II: A Material Balance. *AAPG Bull.* **1986**, *70* (9), 1156–1165.

(39) Smolen, J. D.; Hren, M. T. Differential effects of clay mineralogy on thermal maturation of sedimentary n-alkanes. *Chem. Geol.* **2023**, *634*, 121572.

(40) Dembicki, H. The effects of the mineral matrix on the determination of kinetic parameters using modified Rock Eval pyrolysis. *Org. Geochem.* **1992**, *18* (4), 531–539.

(41) Rose, H. R.; Smith, D. R.; Hanna, J. V.; Palmisano, A. J.; Wilson, M. A. Comparison of the effect of minerals on aromatization reactions during kerogen pyrolysis. *Fuel* **1992**, *71* (4), 355–360.

(42) Song, H.; Liu, H.; Bu, H.; Liu, D.; Li, Y.; Du, P. Effects of montmorillonite charge reduction on the high-temperature/high-pressure pyrolysis of organic matter. *Appl. Clay Sci.* **2021**, *213*, 106243.

(43) Liu, H.; Yuan, P.; Liu, D.; Bu, H.; Song, H.; Qin, Z.; He, H. Pyrolysis behaviors of organic matter (OM) with the same alkyl main chain but different functional groups in the presence of clay minerals. *Appl. Clay Sci.* **2018**, *153*, 205–216.

(44) Liu, H.; Yuan, P.; Qin, Z.; Liu, D.; Tan, D.; Zhu, J.; He, H. Thermal degradation of organic matter in the interlayer clay–organic complex: A TG-FTIR study on a montmorillonite/12-aminolauric acid system. *Appl. Clay Sci.* **2013**, *80-81*, 398–406.

(45) Shimoyama, A.; Johns, W. D. Catalytic Conversion of Fatty Acids to Petroleum-like Paraffins and their Maturation. *Nat. Phys. Sci.* **1971**, *232* (33), 140–144.

(46) Bu, H.; Yuan, P.; Liu, H.; Liu, D.; Zhou, X. Thermal decomposition of long-chain fatty acids and its derivative in the presence of montmorillonite. *J. Therm. Anal. Calorim.* **2017**, *128* (3), 1661–1669.

(47) Liu, H.; Yuan, P.; Liu, D.; Tan, D.; He, H.; Zhu, J. Effects of solid acidity of clay minerals on the thermal decomposition of 12-aminolauric acid. *J. Therm. Anal. Calorim.* **2013**, *114* (1), 125–130.

(48) Bu, H.; Yuan, P.; Liu, H.; Liu, D.; Liu, J.; He, H.; Zhou, J.; Song, H.; Li, Z. Effects of complexation between organic matter (OM) and clay mineral on OM pyrolysis. *Geochim. Cosmochim. Acta* **2017**, *212*, 1–15.

(49) Bu, H.; Wei, Y.; Liu, C.; Liu, D.; Tan, D.; Liu, H. Effects of illite–smectite clay minerals on the thermal evolution of aliphatic organic matter-clay complexes: a study with thermogravimetry coupled with Fourier transform infrared spectroscopy (TG-FTIR). *J. Therm. Anal. Calorim.* **2023**, *148* (3), 741–752.

(50) Zafar, R.; Watson, J. S. Adsorption of tetradecanoic acid on kaolinite minerals: Using flash pyrolysis to characterise the catalytic efficiency of clay mineral adsorbed fatty acids. *Chem. Geol.* **2017**, *471*, 111–118.

(51) Turuga, A. S. S.; de Klerk, A. Free Radical and Cationic Addition due to Clay Minerals Found in Bitumen Froth at 250 °C Probed with Use of α-Methylstyrene and 1-Octene. *Energy Fuels* **2022**, *36* (23), 14148–14162.

(52) Ishiwatari, M. Thermal reaction of β-carotene. *J. Anal. Appl. Pyrolysis* **1981**, *2* (4), 339–351.

(53) Cai, J.; Du, J.; Song, M.; Lei, T.; Wang, X.; Li, Y. Control of clay mineral properties on hydrocarbon generation of organo-clay complexes: Evidence from high-temperature pyrolysis experiments. *Appl. Clay Sci.* **2022**, *216*, 106368.

(54) Bassane, J. F. P.; de Klerk, A. Hydrothermal Treatment of Oilsands Bitumen Froth at 400 °C: Influence of Minerals and Water on Hydrogen Transfer, Cracking, and Addition Reactions. *Energy Fuels* **2024**, *38* (2), 1032–1046.

(55) Tanabe, K.; Gray, M. R. Role of fine solids in the coking of vacuum residues. *Energy Fuels* **1997**, *11* (5), 1040–1043.

(56) Yan, T. Characterization of visbreaker feeds. *Fuel* **1990**, *69* (8), 1062–1064.

(57) LeVeque, R. J. Appendix B - Polynomial Interpolation and Orthogonal Polynomials, In *Finite difference methods for ordinary and partial differential equations: steady-state and time-dependent problems*, Society for Industrial and Applied Mathematics: Philadelphia, PA, 2007, p 341.

(58) Steele, W.; Chirico, R.; Knipmeyer, S.; Nguyen, A. Vapor Pressure, Heat Capacity, and Density along the Saturation Line, Measurements for Dimethyl Isophthalate, Dimethyl Carbonate, 1, 3, 5-Triethylbenzene, Pentafluorophenol, 4-tert-Butylcatechol, α-Methylstyrene, and N, N ‘-Bis (2-hydroxyethyl) ethylenediamine. *J. Chem. Eng. Data* **1997**, *42* (6), 1008–1020.

(59) Baumann, C. G.; Metz, D. J. Gamma radiation induced polymerization of alpha- methylstyrene. The effect of water on molecular weight distribution. *J. Polym. Sci.* **1962**, *62* (174), S141–S144.

(60) Brunner, E.; Thies, M. C.; Schneider, G. M. Fluid mixtures at high pressures: Phase behavior and critical phenomena for binary mixtures of water with aromatic hydrocarbons. *J. Supercrit. Fluids* **2006**, *39* (2), 160–173.

(61) Lewan, M. D. Experiments on the role of water in petroleum formation. *Geochim. Cosmochim. Acta* **1997**, *61* (17), 3691–3723.

(62) Hensen, E. J.; Poduval, D. G.; Ligthart, D. A.; Van Veen, J. A.; Rigutto, M. S. Quantification of strong brønsted acid sites in aluminosilicates. *J. Phys. Chem. C* **2010**, *114* (18), 8363–8374.

(63) Luo, C.; Liu, H.; Li, X.; Dong, X.; Zhang, Y.; Wang, H. Effects of different clay minerals on thermal conversion of oxidized and pyrolyzed oils during in situ combustion. *J. Therm. Anal. Calorim.* **2023**, *148* (22), 12629–12637.

(64) Liu, P. G.; Pu, W. F.; Ni, J. H. Catalytic effect analysis of clay minerals on low-temperature oxidation of crude oil through combined thermal analysis methods. *Pet. Sci. Technol.* **2016**, *34* (4), 343–349.

(65) Soma, Y.; Soma, M. Chemical reactions of organic compounds on clay surfaces. *Environ. Health Perspect.* **1989**, *83*, 205–214.

(66) Boronat, M.; Viruela, P.; Corma, A. Theoretical study on the mechanism of the hydride transfer reaction between alkanes and alkylcarbenium ions. *J. Phys. Chem. B* **1997**, *101* (48), 10069–10074.

(67) Sheldon, R. A.; Kochi, J. K., *Metal-catalyzed oxidations of organic compounds*; Academic Press: New York, 1981.

(68) Matyjaszewski, K., *Cationic polymerizations: mechanisms, synthesis, and applications*; Marcel Dekker: New York, 1996, p 768.

(69) Mayr, H.; Lang, G.; Ofial, A. R. Reactions of carbocations with unsaturated hydrocarbons: Electrophilic alkylation or hydride abstraction? *J. Am. Chem. Soc.* **2002**, *124* (15), 4076–4083.

(70) Alemán-Vázquez, L. O.; Cano-Domínguez, J. L.; García-Gutiérrez, J. L. Effect of tetralin, decalin and naphthalene as hydrogen donors in the upgrading of heavy oils. *Procedia Eng.* **2012**, *42*, 532–539.

(71) Ovalles, C.; Vallejos, C.; Vasquez, T.; Rojas, I.; Ehrman, U.; Benitez, J. L.; Martinez, R. Downhole Upgrading of Extra-heavy Crude Oil Using Hydrogen Donors and Methane Under Steam Injection Conditions. *Pet. Sci. Technol.* **2003**, *21* (1-2), 255–274.

(72) Aleman-Vazquez, L. O.; Torres-mancera, P.; Ancheyta, J.; Ramirez-salgado, J. Use of Hydrogen Donors for Partial Upgrading of Heavy Petroleum. *Energy Fuels* **2016**, *30*, 9050–9060.

(73) Chen, Q.; Froment, G. F. Thermal cracking of substituted aromatic hydrocarbons. I. Kinetic study of the thermal cracking of i-propylbenzene. *J. Anal. Appl. Pyrolysis* **1991**, *21* (1-2), 27–50.

(74) Best, D.; Wojciechowski, B. W. On identifying the primary and secondary products of the catalytic cracking of cumene. *J. Catal.* **1977**, *47* (1), 11–27.

(75) Mokoena, K.; Scurrell, M. S. Alkyl transfer reactions on solid acids. The disproportionation of ethylbenzene and toluene on H-mordenite and HY zeolites. *Pet. Sci. Technol.* **2018**, *36* (16), 1208–1215.

(76) Polovor, Y. N.; Kaminskaya, Y. G.; Vykhrestyuk, N.; Tkachenko, D. Conversions of α-methylstyrene on aluminosilicate at cracking temperatures. *Pet. Chem. U.S.S.R.* **1977**, *17* (4), 215–223.

(77) Chaudhuri, B.; Sharma, M. M. Some novel aspects of dimerization of α-methylstyrene with acidic ion-exchange resins, clays and other acidic materials as catalysts. *Ind. Eng. Chem. Res.* **1989**, *28* (12), 1757–1763.

(78) Rustamov, M. I.; Seidov, N. M.; Ibragimov, K. D.; Mamedbeili, E. G. Dimerization of α-methylstyrene in the presence of mordenite, aimed at preparation of transformer oils. *Russ. J. Appl. Chem.* **2009**, *82* (2), 317–322.

(79) Saltzman, S.; Mingelgrin, U.; Yaron, B. Role of Water in the Hydrolysis of Parathion and Methylparathion on Kaolinite. *J. Agrie. Food Chem.,* **1976**, *24* (4), 739–743.

(80) Zhan, W.; Yi, H.; Song, S.; Zhao, Y.; Rao, F. Hydrophobic agglomeration behaviors of clay minerals as affected by siloxane structure. *Colloids Surfaces A: Physicochem. Eng. Asp.* **2019**, *568*, 36–42.

(81) Nazdracheva, T.; Morozov, A.; Yavna, V.; Kochur, A. Study of hydration of kaolinite and montmorillonite mixture by IR spectroscopy. *J. Mol. Struct.* **2022**, *1250*, 131871.

(82) Ferretto, L.; Glisenti, A. Surface acidity and basicity of a rutile powder. *Chem. Mater.* **2003**, *15* (5), 1181–1188.

(83) Al-Khattaf, S.; de Lasa, H. Catalytic Cracking of Cumene in a Riser Simulator: A Catalyst Activity Decay Model. *Ind. Eng. Chem. Res.* **2001**, *40* (23), 5398–5404.

(84) Canıaz, R. O.; Arca, S.; Yaşar, M.; Erkey, C. Refinery bitumen and domestic unconventional heavy oil upgrading in supercritical water. *J. Supercrit. Fluids* **2019**, *152*, 104569.

(85) Kapadia, P. R.; Kallos, M. S.; Gates, I. D. A review of pyrolysis, aquathermolysis, and oxidation of Athabasca bitumen. *Fuel Process. Technol.* **2015**, *131*, 270–289.

(86) Gray, M. R.; McCaffrey, W. C. Role of chain reactions and olefin formation in cracking, hydroconversion, and coking of petroleum and bitumen fractions. *Energy Fuels* **2002**, *16* (3), 756–766.

(87) Wang, Z.; Liu, X.; Wang, Y.; Liu, L.; Wang, H.; Deng, S.; Sun, Y. Studies on the co-pyrolysis characteristics of oil shale and spent oil shale. *J. Therm. Anal. Calorim.* **2016**, *123* (2), 1707–1714.

(88) Yu, X.; Qu, Z.; Kan, C.; Zhao, X. Effect of Different Clay Minerals on Heavy Oil Oxidation during Ignition Process. *Energy Fuels* **2017**, *31* (11), 12839–12847.

Chapter 6

Conclusions

6.1 Introduction

When bitumen is recovered from mined oilsands deposits, it needs to be disengaged from the bulk of the mineral matter and recovered through a hot water extraction process. Bitumen is then recovered as a bitumen froth comprising about 60 wt% bitumen, 30 wt% water, and 10 wt% mineral solids. Separating water and minerals from bitumen presents challenges due to the comparable density of bitumen and water, as well as the high viscosity of bitumen, which hinders the separation of fines. In order to achieve this separation, a light solvent is added to the bitumen froth in the froth treatment unit. The resulting bitumen product, after solvent recovery, is still highly viscous and dense, requiring dilution and/or upgrading for transport through pipelines.

Some authors explored the potential advantages of thermally treating bitumen froth, not only aiming to enhance the separation of water and solids but also to achieve partial upgrading of bitumen. However, hydrothermal treatment of froth at 250 °C was too low temperature to yield any partial upgrading benefits, such as reduced density and viscosity of the bitumen product. Nevertheless, other studies unrelated to bitumen froth have reported advantages in thermally treating bitumen in the presence of water and minerals at temperatures exceeding 250 °C, including higher viscosity reduction and an increased yield of lighter products.

The current thesis investigated the outcomes of retaining water and minerals during the thermal treatment of bitumen froth at 400 °C. The main objective was to explore the influence of water and mineral solids on the physicochemical properties of the bitumen product and the conversion chemistry.

Following previous claims that thermally treating bitumen in the presence of water and minerals could result in benefits from the perspective of bitumen upgrading, the first study in this thesis

(**Chapter 3**) evaluated the impact of water, minerals, and solvent on the physicochemical changes of the bitumen phase during visbreaking of froth at 400 °C. It was expected that retaining water and solids during visbreaking could lead to improvements in the quality of the bitumen product, including enhanced density and viscosity reduction. Although the presence of water and minerals did not result in any partial upgrading benefits (i.e., the presence of these components resulted in increased bitumen's density and viscosity as compared to visbreaking of bitumen alone), the physicochemical changes of bitumen observed in **Chapter 3** indicated that water and minerals affected the conversion process. For instance, there was evidence that hydrogen transfer was affected by water and mineral solids.

While the findings from **Chapter 3** revealed that the presence of water and minerals in bitumen froth influenced the reactions taking place during visbreaking, that study was not designed to assess details regarding the conversion chemistry. Therefore, it was of interest to explore in **Chapter 4** the influence of water and minerals on reactions relevant to bitumen upgrading, such as cracking, hydrogen transfer, and addition reactions. This was achieved by thermally treating bitumen froth at 400 °C, a reaction medium similar to the reaction systems studied in **Chapter 3**, but including α-methylstyrene (AMS) as a probe molecule to interrogate the reaction chemistry. The thermal treatment of froth and control systems in **Chapter 4** showed evidence that both water and minerals had an impact on the reaction chemistry, specifically by influencing feed conversion and product composition.

The studies covered in **Chapters 3** and **4** indicated that water and minerals affected the reaction chemistry during the thermal treatment of froth. However, due to the complexity of the reaction medium containing bitumen, it was not possible to relate the influence of water and minerals to specific reaction pathways. In this sense, the third study presented in this thesis (**Chapter 5**) investigated the specific contributions of water and kaolinite, a common clay mineral found in oilsands, to the reaction rates and pathways during the thermal treatment of a simpler model system containing AMS, tetralin, and *n*-pentadecane.

The main findings and conclusions derived from the studies covered in this thesis are presented in the following section.

6.2 Major conclusions and insights

The first objective of this thesis was to evaluate if visbreaking of bitumen at 400 °C in the presence of water and solids from froth, with and without solvent addition, could result in partial upgrading benefits such as higher viscosity and density reduction as compared to the treatment of bitumen alone (**Chapter 3**). By design this was an applied investigation using industrially obtained materials.

As anticipated, visbreaking of bitumen froth resulted in a bitumen product with lower density and viscosity (i.e., on a solvent-free basis, the density of bitumen at 25 °C varied from 1005–1010 kg/m^3 in the feed to 964–998 kg/m^3 in the products, while the viscosity of bitumen at 25 °C varied from 48–78 Pa·s in the feed to 0.17–1.2 Pa·s in the products).

However, it was surprising that the visbreaking of bitumen in the presence of water and/or solids, with and without solvents, resulted in a bitumen product with a slight higher density and viscosity as compared to the treatment of bitumen alone (i.e., on a solvent-free basis, the density and viscosity of the bitumen product at 25 °C in systems containing water and/or solids were approximately 3–13 kg/m^3 and 0.1–0.8 Pa·s higher, respectively, compared to the bitumen product in the systems containing bitumen alone). This finding contrasts with prior literature, which indicated that the quality of the bitumen product improved with the presence of water and minerals during thermal treatment within the temperature range of 250–430 °C and prolonged reaction times (1.5–24 h).

In **Chapter 3**, the changes in the physicochemical properties of bitumen treated in the presence of water and/or mineral solids suggested that these components individually and collectively influenced the composition of the bitumen product. For instance, variations in the aliphatic and aromatic hydrogen content indicated that hydrogen transfer was affected by the presence of water and minerals. In most reaction systems containing water and/or mineral solids, the aromatic H content was 0.7–3.1$\%$ lower compared to the treatment of bitumen alone. This provided clear evidence that the reaction chemistry was influenced by both water and minerals.

There was indication of free radical termination on the surface of mineral solids during visbreaking of bitumen. This could have a direct impact on the extent of thermal conversion of bitumen since the solids might increase the rate of termination relative to initiation and propagation during visbreaking.

Regarding the effect of solvent during visbreaking of bitumen froth, the findings from **Chapter 3** suggested potential advantages of conducting visbreaking of bitumen in the presence of a lighter hydrocarbon solvent (*n*-hexane) when compared to a heavier solvent (kerosene) or visbreaking in the absence of a solvent. On a solvent-free basis, the lowest viscosity and density values when comparing the visbreaking of bitumen alone were obtained in the presence of *n*-hexane (i.e., viscosity and density at 25 °C of 0.17 Pa·s and 971 kg/m^3 in the presence of *n*-hexane vs. 0.41 Pa·s and 989 kg/m^3 in the presence of kerosene vs. 0.62 Pa·s and 986 kg/m^3 in the absence of a solvent). This finding indicated that the changes in the bulk properties of bitumen promoted by the addition of a solvent have a direct impact on the conversion chemistry during the treatment and the quality of the bitumen product. The nature of this impact was not investigated.

The results obtained in **Chapter 4** corroborated the evidence presented in **Chapter 3**, highlighting the influence of water and minerals on the reaction chemistry during the thermal treatment of froth at 400°C. In **Chapter 4**, the use of AMS as a probe molecule allowed for evaluating the impact of water and minerals on relevant reactions to bitumen upgrading, such as hydrogen transfer and addition reactions.

The presence of water in the reaction medium resulted in reduced AMS conversion and decreased formation of addition products, while at the same time favoring hydrogen transfer. Nevertheless, it remained unclear whether water directly caused these changes or if water affected other properties in the reaction medium, which in turn resulted in the observed changes. Although many authors have emphasized the beneficial effect of water in promoting hydrogen transfer and suppressing the formation of heavy products, the effect of water on the overall bitumen conversion received less attention. The decreased AMS conversion in the presence of water, noticed in **Chapter 4**, could indicate that water might have a direct impact on bitumen conversion during thermal treatment.

There was also strong evidence that mineral solids somehow favored hydrogen transfer during the treatment. This was an important contribution to the field since the literature is scarce on the effect of oilsands minerals on hydrogen transfer. Besides, the mineral solids did not seem to have any impact on the overall formation of addition products. These are beneficial aspects from the perspective of bitumen upgrading, since the enhancement of hydrogen transfer during thermal conversion can potentially suppress coke formation and increase the yield of lighter liquid products. The mechanism by which mineral solids enhanced hydrogen transfer remained unresolved.

The findings from **Chapter 4** also highlighted the impact of hydrogen donors on the suppression of addition products during the thermal treatment of bitumen. The overall formation of addition products was higher in a reaction medium with limited hydrogen donors (i.e., the control reaction using kerosene as feed) compared to a medium abundant in hydrogen donors (i.e., the reaction systems containing bitumen).

The presence of clays, such as kaolinite, in the froth solids was anticipated to facilitate cationic conversion, including cationic dimerization. While potential cationic pathways were discussed in **Chapter 4** based on the products identified from the AMS conversion, this study could not distinguish between free radical and cationic conversion. This was one of the reasons that motivated the work performed in **Chapter 5**.

The presence of water in the study presented in **Chapter 5** led to reduced conversion rates of AMS, a finding that was consistent with the suppressed AMS conversion in the presence of water within a more complex system containing bitumen (**Chapter 4**). The dilution of the reaction medium by water might have played a role in contributing to the decrease in conversion rates. This finding was supporting evidence of a potential deleterious effect of water during thermal conversion.

While water favored hydrogen transfer reactions during the thermal conversion of AMS in the presence of bitumen (**Chapter 4**), there was no evidence that it facilitated hydrogen transfer under similar reaction conditions during the thermal conversion of AMS in a simpler model system (**Chapter 5**). This result was surprising given the extensive literature claiming that water is a hydrogen donor solvent. The combined findings from **Chapters 4** and **5** provided evidence of the hydration of unsaturated compounds and the likely impact of dilution by water on decreasing the conversion rates; however, there was no evidence to support that water was a net hydrogen donor.

Kaolinite was catalytically active during the thermal treatment. There was evidence that the Brønsted-Lowry acidity of kaolinite affected reaction pathways by enabling cationic conversion, such as cationic dealkylation to form benzene and cationic dimerization of AMS to form the tricyclic dimer 1,1,3-trimethyl-3-phenyl indane. The choice of a simpler model system in **Chapter 5** enabled successful differentiation between free radical and cationic AMS conversion, which was not achievable in a system containing bitumen (**Chapter 4**).

The addition of kaolinite in the reaction media resulted in increased reaction rates and clearly favored hydrogen transfer. This finding also implies that the presence of kaolinite in the froth solids used in **Chapters 3** and **4** could have contributed to the observed increase in hydrogen transfer in those studies. However, the deposition of carbonaceous material on the surface of kaolinite suggested that while the mineral was catalytically active during treatment, it was rapidly fouled. These findings indicate that although the clays in oilsands minerals might have an important catalytic role at the early stages of thermal conversion of oil, the catalytic sites of these minerals might rapidly foul, hindering their effect during prolonged thermal conversion.

6.3 Recommended future work

6.3.1 Specific role of water during oil conversion

Despite the extensive literature on the potential impacts of water during the thermal conversion of oil, the precise role of water in this process remains unclear. While some studies suggest water's role as a hydrogen donor reactant, evidence indicates that water is not consumed during the process. Therefore, it is more likely that water serves as a hydrogen transfer agent rather than a hydrogen donor. Furthermore, the relation between the physical effect of water as a diluent during the process and its implications for the properties and composition of the final product has not been thoroughly investigated.

While numerous studies in the literature have reported the advantages of thermally treating oil in the presence of water, the studies presented in this thesis highlighted potential drawbacks associated with water during the treatment. These included increased density and viscosity during visbreaking (**Chapter 3**), reduced conversion (**Chapter 4**), and decreased reaction rates (**Chapter 5**). These outcomes do not detract from the studies that claimed the benefits of having water during the treatment but highlight that there is ample opportunity for research to advance the understanding of the role of water during the process.

The following questions are recommended for future research:

(a) How does the phase behavior of a mixture of water and oil affect the reaction chemistry during thermal conversion?

(b) What is the mechanism by which water favor hydrogen transfer during oil conversion?

(c) How does the dilution effect of water during the thermal conversion of oil differ from that of a hydrocarbon solvent in terms of the impact on the properties and composition of the thermally treated product?

(d) What is the mechanism by which water hinders the formation of addition products during the thermal conversion of oil?

6.3.2 Contribution of froth minerals to increased density and viscosity during bitumen conversion

The presence of froth minerals during thermal conversion resulted in increased density and viscosity of the bitumen product compared to the treatment of bitumen alone (**Chapter 3**). Two tentative explanations for these findings were proposed. The first involved potential free radical termination on the surface of solids, while the second suggested the potential formation of acid-catalyzed addition products in the presence of the solids. However, the results from **Chapter 4** indicated that the overall formation of addition products was not influenced by the solids. Consequently, the role of froth minerals in increasing density and viscosity remained unresolved but holds practical implications when considering the thermal treatment of oils in the presence of mineral solids.

The following questions are recommended for future research:

(a) What is the impact of froth solids on free radical quenching during the thermal conversion of oil?

(b) How does the impact of froth solids on the bitumen product composition relate to changes in density and viscosity during thermal conversion?

6.3.3 Impact of the thermal treatment of froth on the separation of solids and water

While the thermal treatment of bitumen in the presence of water and minerals did not result in partial upgrading benefits beyond what can be obtained by thermal treatment of bitumen on its own, the reduction in density and viscosity of the bitumen phase could potentially enhance the separation of solids and water in the froth treatment unit. For instance, performing visbreaking of bitumen froth could potentially reduce the amount of solvent required in the froth treatment unit. Additionally, the deposition of heavy hydrocarbons on the solids' surface could potentially facilitate their gravity separation in the froth treatment unit, resulting in a cleaner bitumen product.

The following questions are recommended for future research:

(a) What is the impact of froth visbreaking on the amount of solvent required for the separation of solids and water in the froth treatment unit?

(b) How does froth visbreaking impact the efficiency of solids and water separation in the froth treatment unit?

6.3.4 Mechanism by which froth solids and kaolinite favor hydrogen transfer

All the studies presented in this thesis indicated that the minerals found in froth somehow favored hydrogen transfer during thermal conversion at 400 °C. However, the mechanism by which this occurs remains unresolved. An exploratory path could involve investigating if froth minerals could facilitate hydride transfer, similar to mechanisms found in cationic polymerization and catalytic cracking.

The following questions are recommended for future research:

(a) Is hydride transfer a possible step during thermal conversion at 400 °C in the presence of minerals from froth?

(b) Is the Brønsted-Lowry or Lewis acidity of clays, such as kaolinite, somehow involved in favoring hydrogen transfer during thermal conversion at 400 °C?

Bibliography

Acevedo, S.; Escobar, G.; Ranaudo, M. A.; Pinate, J.; Amorin, A. Observations about the Structure and Dispersion of Petroleum Asphaltenes Aggregates Obtained from Dialysis Fractionation and Characterization. *Energy Fuels* **1997**, *11*, 774–778.

Adams, J. M.; Dyer, S.; Martin, K.; Matear, W. A.; McCabe, R. W. Diels-Alder reactions catalysed by cation-exchanged clay minerals. *J. Chem. Soc. Perkin Trans. 1* **1994**, (6), 761–765.

AER *Alberta Energy Outlook*, 2023, https://www.aer.ca/providing-information/data-and-reports/statistical-reports/st98 (accessed 2024/1/9).

Akiya, N.; Savage, P. E. Roles of Water for Chemical Reactions in High-Temperature Water. *Chem. Rev.* **2002**, *102* (8), 2725–2750.

Aleman-Vazquez, L. O.; Torres-mancera, P.; Ancheyta, J.; Ramirez-salgado, J. Use of Hydrogen Donors for Partial Upgrading of Heavy Petroleum. *Energy Fuels* **2016**, *30*, 9050–9060.

Alemán-Vázquez, L. O.; Cano-Domínguez, J. L.; García-Gutiérrez, J. L. Effect of tetralin, decalin and naphthalene as hydrogen donors in the upgrading of heavy oils. *Procedia Eng.* **2012**, *42*, 532–539.

Ali, M.; Xing, T.; Alem, T.; Chen, J. Investigating the role of aliphatic olefins in fouling of thermally cracked bitumen by testing fouling tendency of model aliphatic olefin compounds in light fractions. *Fuel* **2024**, *360*, 130518.

Alili, A. S.; Siddiquee, M. N.; De Klerk, A. Origin of Free Radical Persistence in Asphaltenes: Cage Effect and Steric Protection. *Energy Fuels* **2020**, *34*, 348–359.

Amelse, J. A. Reactions and Mechanisms of Xylene Isomerization and Related Processes. *Ind. Arene Chem. Mark. Technol. Sustain. Process. Cases Stud. Aromat. Commod.* **2023**, *1*, 403–437.

Amis, E. S., *Solvent effects on reaction rates and mechanisms*; Academic Press: New York, 1966, p 326.

An, J.; Bagnell, L.; Cablewski, T.; Strauss, C. R.; Trainor, R. W. Applications of high-temperature aqueous media for synthetic organic reactions. *J. Org. Chem.* **1997**, *62* (8), 2505–2511.

Andersen, S. I.; Del Rio, J. M.; Khvostitchenko, D.; Shakir, S.; Lira-Galeana, C. Interaction and solubilization of water by petroleum asphaltenes in organic solution. *Langmuir* **2001**, *17* (2), 307–313.

Arcelus-Arrillaga, P.; Hellgardt, K.; Millan, M. Effect of process conditions on the hydrothermal partial oxidation of phenanthrene as a heavy oil model structure. *Fuel* **2017**, *209*, 434–441.

Arcelus-Arrillaga, P.; Pinilla, J. L.; Hellgardt, K.; Millan, M. Application of Water in Hydrothermal Conditions for Upgrading Heavy Oils: A Review. *Energy Fuels* **2017**, *31* (5), 4571–4587.

Argüelles-Vivas, F. J.; Babadagli, T.; Little, L.; Romaniuk, N.; Ozum, B. High temperature density, viscosity, and interfacial tension measurements of bitumen-pentane-biodiesel and process water mixtures. *J. Chem. Eng. Data* **2012**, *57* (10), 2878–2889.

ASTM D1159-07: Standard Test Method for Bromine Numbers of Petroleum Distillates and Commercial Aliphatic Olefins by Electrometric Titration; ASTM International: West Conshohocken, PA: 2017.

ASTM D2007-19: Standard Test Method for Characteristic Groups in Rubber Extender and Processing Oils and Other Petroleum-Derived Oils by the Clay-Gel Absorption Chromatographic Method; ASTM international: West Conshohocken, PA, 2019.

ASTM D341-20e1: Standard Practice for Viscosity Temperature Equations and Charts for Liquid Petroleum or Hydrocarbon Products; ASTM International: West Conshohocken, PA: 2020.

Avola, S.; Guillot, M.; da Silva-Perez, D.; Pellet-Rostaing, S.; Kunz, W.; Goettmann, F. Organic chemistry under hydrothermal conditions. *Pure Appl. Chem.* **2012**, *85* (1), 89–103.

Baire, B.; Sadhukhan, S. Chapter 3 - Cycloaddition reactions in water, In *Green Sustainable Process for Chemical and Environmental Engineering and Science*, ed. by Inamuddin; Boddula, R.; Asiri, A. M., Elsevier: 2020, pp 61–114.

Balestrin, L. B.; Loh, W. Recent developments on the elucidation of colloidal aspects of asphaltenes and their relevance to oilfield problems. *J. Braz. Chem. Soc.* **2020**, *31* (2), 230–243.

Barnes, H. A., *A Handbook of Elementary Rheology*; University of Wales, Institute of Non-Newtonian Fluid Mechanics: 2000, p 200.

Barré, L.; Simon, S.; Palermo, T. Solution properties of asphaltenes. *Langmuir* **2008**, *24* (8), 3709–3717.

Barry, J. T.; Berg, D. J.; Tyler, D. R. Radical Cage Effects: The Prediction of Radical Cage Pair Recombination Efficiencies Using Microviscosity Across a Range of Solvent Types. *J. Am. Chem. Soc.* **2017**, *139*, 14399–14405.

Barton, C. D.; Karathanasis, A. D. Clay minerals, In *Encyclopedia of Soil Science*, ed. by Lal, R., 2nd, CRC Press: Boca Raton, FL, 2005, pp 187–192.

Bassane, J. F. P.; de Klerk, A. Hydrothermal Treatment of Oilsands Bitumen Froth at 400 °C: Influence of Minerals and Water on Hydrogen Transfer, Cracking, and Addition Reactions. *Energy Fuels* **2024**, *38* (2), 1032–1046.

Bassane, J. F. P.; de Klerk, A. Visbreaking of Bitumen Froth: Influence of Minerals, Water, and Solvent on the Physicochemical Changes in the Bitumen Phase. *Energy Fuels* **2023**, *37* (16), 11820–11837.

Baumann, C. G.; Metz, D. J. Gamma radiation induced polymerization of alpha- methylstyrene. The effect of water on molecular weight distribution. *J. Polym. Sci.* **1962**, *62* (174), S141–S144.

Bazyleva, A. B.; Hasan, A.; Fulem, M.; Becerra, M.; Shaw, J. M. Bitumen and heavy oil rheological properties: Reconciliation with viscosity measurements. *J. Chem. Eng. Data* **2010**, *55* (3), 1389–1397.

Belgrave, J. D. M.; Moore, R. G.; Ursenbach, M. G. Gas evolution from the aquathermolysis of heavy oils. *Can. J. Chem. Eng.* **1994**, *72* (3), 511–516.

Bennett, B.; Jiang, C. Oil-source and oil-oil correlations and the origin of the heavy oil and bitumen accumulations in Northern Alberta, Canada. *Org. Geochem.* **2021**, *153*, 104199.

Best, D.; Wojciechowski, B. W. On identifying the primary and secondary products of the catalytic cracking of cumene. *J. Catal.* **1977**, *47* (1), 11–27.

Bi, W.; McCaffrey, W. C.; Gray, M. R. Agglomeration and deposition of coke during cracking of petroleum vacuum residue. *Energy Fuels* **2007**, *21* (3), 1205–1211.

Booran, S. K.; Wang, X.; Tan, X.; Liu, Q. Effect of carbon dioxide on paraffinic bitumen froth treatment: Asphaltene precipitation from a commercial bitumen froth sample. *ACS Omega* **2021**, *6* (18), 11918–11924.

Boronat, M.; Viruela, P.; Corma, A. Theoretical study on the mechanism of the hydride transfer reaction between alkanes and alkylcarbenium ions. *J. Phys. Chem. B* **1997**, *101* (48), 10069–10074.

Brinkman, H. C. The Viscosity of Concentrated Suspensions and Solutions. *J. Chem. Phys.* **1952**, *20* (4), 571–571.

Brunner, E.; Thies, M. C.; Schneider, G. M. Fluid mixtures at high pressures: Phase behavior and critical phenomena for binary mixtures of water with aromatic hydrocarbons. *J. Supercrit. Fluids* **2006**, *39* (2), 160–173.

Bu, H.; Wei, Y.; Liu, C.; Liu, D.; Tan, D.; Liu, H. Effects of illite–smectite clay minerals on the thermal evolution of aliphatic organic matter-clay complexes: a study with thermogravimetry coupled with Fourier transform infrared spectroscopy (TG-FTIR). *J. Therm. Anal. Calorim.* **2023**, *148* (3), 741–752.

Bu, H.; Yuan, P.; Liu, H.; Liu, D.; Liu, J.; He, H.; Zhou, J.; Song, H.; Li, Z. Effects of complexation between organic matter (OM) and clay mineral on OM pyrolysis. *Geochim. Cosmochim. Acta* **2017**, *212*, 1–15.

Bu, H.; Yuan, P.; Liu, H.; Liu, D.; Zhou, X. Thermal decomposition of long-chain fatty acids and its derivative in the presence of montmorillonite. *J. Therm. Anal. Calorim.* **2017**, *128* (3), 1661–1669.

Budnar Subramanya, A. S. Olefin Hydrotreating and Characterization of Olefins in Thermally Cracked Naphtha, MSc thesis, University of Alberta, Edmonton, Canada, 2020, p 170.

Cai, J.; Du, J.; Song, M.; Lei, T.; Wang, X.; Li, Y. Control of clay mineral properties on hydrocarbon generation of organo-clay complexes: Evidence from high-temperature pyrolysis experiments. *Appl. Clay Sci.* **2022**, *216*, 106368.

Canıaz, R. O.; Arca, S.; Yaşar, M.; Erkey, C. Refinery bitumen and domestic unconventional heavy oil upgrading in supercritical water. *J. Supercrit. Fluids* **2019**, *152*, 104569.

Canıaz, R. O.; Erkey, C. Process intensification for heavy oil upgrading using supercritical water. *Chem. Eng. Res. Des.* **2014**, *92* (10), 1845–1863.

Carbognani, L.; Lubkowitz, J.; Gonzalez, M. F.; Pereira-Almao, P. High temperature simulated distillation of Athabasca vacuum residue fractions. Bimodal distributions and evidence for secondary "on-column" cracking of heavy hydrocarbons. *Energy Fuels* **2007**, *21* (5), 2831–2839.

Castaneda, L. C.; Munoz, J. A.; Ancheyta, J. Current situation of emerging technologies for upgrading of heavy oils. *Catal. Today* **2014**, *220*, 248–273.

Centeno, G.; Sánchez-Reyna, G.; Ancheyta, J.; Muñoz, J. A.; Cardona, N. Testing various mixing rules for calculation of viscosity of petroleum blends. *Fuel* **2011**, *90* (12), 3561–3570.

Chaudhuri, B.; Sharma, M. M. Some novel aspects of dimerization of α-methylstyrene with acidic ion-exchange resins, clays and other acidic materials as catalysts. *Ind. Eng. Chem. Res.* **1989**, *28* (12), 1757–1763.

Chen, Q.; Froment, G. F. Thermal cracking of substituted aromatic hydrocarbons. I. Kinetic study of the thermal cracking of i-propylbenzene. *J. Anal. Appl. Pyrolysis* **1991**, *21* (1-2), 27–50.

Chen, Q. Organically-modified clay minerals in oil sands: Characterization and effect of hydrothermal treatment, PhD Thesis, University of Alberta, 2017.

Chen, Q.; Stricek, I.; Cao, M.; Gray, M. R.; Liu, Q. Influence of hydrothermal treatment on filterability of fine solids in bitumen froth. *Fuel* **2016**, *180*, 314–323.

Chen, Y.; Wang, K.; Yang, J. Y.; Yuan, P. Q.; Cheng, Z. M.; Yuan, W. K. Dealkylation of Aromatics in Subcritical and Supercritical Water: Involvement of Carbonium Mechanism. *Ind. Eng. Chem. Res.* **2016**, *55* (36), 9578–9585.

Cheng, Z. M.; Ding, Y.; Zhao, L. Q.; Yuan, P. Q.; Yuan, W. K. Effects of supercritical water in vacuum residue upgrading. *Energy Fuels* **2009**, *23* (6), 3178–3183.

Choudhury, T.; Misra, N. M. Role of clay as catalyst in Friedel-Craft alkylation. *Bull. Mater. Sci.* **2011**, *34* (6), 1273–1279.

Clark, P. D.; Kirk, M. J. Studies on the upgrading of bituminous oils with water and transition metal catalysts. *Energy Fuels* **1994**, *8* (2), 380–387.

Corma, A.; Orchillés, A. Current views on the mechanism of catalytic cracking. *Microporous mesoporous mat.* **2000**, *35*, 21–30.

Corma, A.; Wojciechowski, B. The catalytic cracking of cumene. *Catal. Rev. Sci. Eng.* **1982**, *24* (1), 1–65.

Cortes-Clerget, M.; Yu, J.; Kincaid, J. R. A.; Walde, P.; Gallou, F.; Lipshutz, B. H. Water as the reaction medium in organic chemistry: from our worst enemy to our best friend. *Chem. Sci.* **2021**, *12* (12), 4237–4266.

Cragoe, C. S. Changes in the viscosity of liquids with temperature, pressure and composition, In *Proc. World Petrol. Congr. Lond.* 1933, pp 529–541.

Czarnecki, J.; Masliyah, J.; Xu, Z.; Dobras, M., *Handbook on Theory and Practice of Bitumen Recovery from Athabasca Oil Sands - Volume 2: Industrial Practice*; Kingsley Knowledge Publishing: 2013, p 717.

Da Costa, L. M.; Stoyanov, S. R.; Gusarov, S.; Tan, X.; Gray, M. R.; Stryker, J. M.; Tykwinski, R.; de M. Carneiro, J. W.; Seidl, P. R.; Kovalenko, A. Density functional theory investigation of the contributions of π–π stacking and hydrogen-bonding interactions to the aggregation of model asphaltene compounds. *Energy Fuels* **2012**, *26* (5), 2727–2735.

Daud, A. R. M.; Berrueco, C.; Hellgardt, K.; Millan, M.; Kandiyoti, R. Oxidative cracking of three to five-member ring polycyclic aromatic hydrocarbons in subcritical and supercritical water. *J. Supercrit. Fluids* **2021**, *167*, 105050.

De Klerk, A. Chapter 3 - Unconventional oil: Oilsands, In *Future Energy - Improved, Sustainable and Clean Options for our Planet*, ed. by Letcher, T. M., 3rd edition, Elsevier: 2020, pp 49–65.

De Klerk, A. Thermal Conversion Modeling of Visbreaking at Temperatures below 400 °C. *Energy Fuels* **2020**, *34* (12), 15285–15298.

De Klerk, A. Processing unconventional oil: partial upgrading of oilsands bitumen. *Energy Fuels* **2021**, *35* (18), 14343–14360.

De Klerk, A.; Gray, M. R.; Zerpa, N. Chapter 5 - Unconventional Oil and Gas: Oilsands, In *Future Energy: Improved, Sustainable and Clean Options for our Planet*, ed. by Letcher, T. M., 2nd ed., Elsevier: Amsterdam, 2014, pp 95–116.

Dembicki, H. The effects of the mineral matrix on the determination of kinetic parameters using modified Rock Eval pyrolysis. *Org. Geochem.* **1992**, *18* (4), 531–539.

Dervan, P. B.; Dougherty, D. A. Nonconjugated diradicals as reactive intermediates, In *Diradicals*, ed. by Borden, W. T., Wiley: New York, 1982, pp 107–149.

Ding, X.; Repka, C.; Xu, Z.; Masliyah, J. Effect of illite clay and divalent cations on bitumen recovery. *Can. J. Chem. Eng.* **2006**, *84* (6), 643–650.

Duran, J. A.; Casas, Y. A.; Xiang, L.; Zhang, L.; Zeng, H.; Yarranton, H. W. Nature of Asphaltene Aggregates. *Energy Fuels* **2019**, *33* (5), 3694–3710.

Dutta, R. P.; McCaffrey, W. C.; Gray, M. R.; Muehlenbachs, K. Thermal cracking of Athabasca bitumen: influence of steam on reaction chemistry. *Energy Fuels* **2000**, *14* (3), 671–676.

Ederer, H.; Kruse, A.; Mas, C.; Ebert, K. Modelling of the pyrolysis of tert-butylbenzene in supercritical water. *J. Supercrit. Fluids* **1999**, *15* (3), 191–204.

Eglinton, T.; Rowland, S.; Curtis, C.; Douglas, A. Kerogen-mineral reactions at raised temperatures in the presence of water. *Org. Geochem.* **1986**, *10* (4-6), 1041–1052.

Emam, E. A. Clays as catalysts in petroleum refining industry. *ARPN J. Sci. Technol.* **2013**, *3* (4), 356–375.

Erdal, S.; Kongshaug, C.; Bjørheim, T. S.; Jalarvo, N.; Haugsrud, R.; Norby, T. Hydration of rutile TiO2: Thermodynamics and effects on n-and p-type electronic conduction. *J. Phys. Chem. C* **2010**, *114* (19), 9139–9145.

Fakher, S.; Ahdaya, M.; Elturki, M.; Imqam, A. Critical review of asphaltene properties and factors impacting its stability in crude oil. *J. Pet. Explor. Prod. Technol.* **2020**, *10* (3), 1183–1200.

Fan, H. F.; Liu, Y. J.; Zhong, L. G. Studies on the synergetic effects of mineral and steam on the composition changes of heavy oils. *Energy Fuels* **2001**, *15* (6), 1475–1479.

Fan, H.; Zhang, Y.; Lin, Y. The catalytic effects of minerals on aquathermolysis of heavy oils. *Fuel* **2004**, *83* (14-15), 2035–2039.

Félix, G.; Tirado, A.; Al-Muntaser, A.; Kwofie, M.; Varfolomeev, M. A.; Yuan, C.; Ancheyta, J. SARA-based kinetic model for non-catalytic aquathermolysis of heavy crude oil. *J. Pet. Sci. Eng.* **2022**, *216*, 110845.

Feng, X.; Behles, J. A. Understanding the Demulsification of Water-in-Diluted Bitumen Froth Emulsions. *Energy Fuels* **2015**, *29* (7), 4616–4623.

Ferretto, L.; Glisenti, A. Surface acidity and basicity of a rutile powder. *Chem. Mater.* **2003**, *15* (5), 1181–1188.

Gao, J.; Okuno, R.; Li, H. A. A Phase-Behavior Study for n-Hexane/Bitumen and n-Octane/Bitumen Mixtures. *SPE J.* **2018**, *23* (01), 128–144.

Gould, K. A.; Wiehe, I. A. Natural hydrogen donors in petroleum resids. *Energy Fuels* **2007**, *21* (3), 1199–1204.

Gray, M. R., *Upgrading oilsands bitumen and heavy oil*; Pica Pica Press - Edmonton: 2015.

Gray, M. R. Fundamentals of partial upgrading of bitumen. *Energy Fuels* **2019**, *33* (8), 6843–6856.

Gray, M. R.; McCaffrey, W. C. Role of chain reactions and olefin formation in cracking, hydroconversion, and coking of petroleum and bitumen fractions. *Energy Fuels* **2002**, *16* (3), 756–766.

Gray, M. R. New technique defines the limits of upgrading heavy oils, bitumens. *Oil Gas J.* **2002**, *100* (1), 50–54.

Gruse, W. A.; Stevens, D. R., *Chemical Technology of Petroleum*, 3rd ed.; McGraw-Hill: New York, 1960, p 675.

Gu, G.; Zhang, L.; Xu, Z.; Masliyah, J. Novel bitumen froth cleaning device and rag layer characterization. *Energy Fuels* **2007**, *21* (6), 3462–3468.

Guan, J. G.; Kariznovi, M.; Nourozieh, H.; Abedi, J. Density and viscosity for mixtures of Athabasca bitumen and aromatic solvents. *J. Chem. Eng. Data* **2013**, *58* (3), 611–624.

Hart, A. A review of technologies for transporting heavy crude oil and bitumen via pipelines. *J. Pet. Explor. Prod. Technol.* **2014**, *4* (3), 327–336.

Hasan, M. A.; Shaw, J. M. Rheology of reconstituted crude oils: Artifacts and asphaltenes. *Energy Fuels* **2010**, *24* (12), 6417–6427.

He, M.; Wang, Z.; Moldowan, M. J.; Peters, K. Insights into catalytic effects of clay minerals on hydrocarbon composition of generated liquid products during oil cracking from laboratory pyrolysis experiments. *Org. Geochem.* **2022**, *163*, 104331.

Henderson, W.; Eglinton, G.; Simmonds, P.; Lovelock, J. E. Thermal Alteration as a Contributory Process to the Genesis of Petroleum. *Nature* **1968**, *219* (5158), 1012–1016.

Hensen, E. J.; Poduval, D. G.; Ligthart, D. A.; Van Veen, J. A.; Rigutto, M. S. Quantification of strong brønsted acid sites in aluminosilicates. *J. Phys. Chem. C* **2010**, *114* (18), 8363–8374.

Hill, I.; Malek, A.; Bhan, A. Kinetics and mechanism of benzene, toluene, and xylene methylation over H-MFI. *ACS Catal.* **2013**, *3* (9), 1992–2001.

Hong, P. K. A.; Cha, Z.; Zhao, X.; Cheng, C. J.; Duyvesteyn, W. Extraction of bitumen from oil sands with hot water and pressure cycles. *Fuel Process. Technol.* **2013**, *106*, 460–467.

Hongfu, F.; Yongjian, L.; Liying, Z.; Xiaofei, Z. The study on composition changes of heavy oils during steam stimulation processes. *Fuel* **2002**, *81* (13), 1733–1738.

Hristova, E.; Stoyanov, S. R. Bitumen froth treatment in the transition region between paraffinic and naphthenic process conditions. *Fuel* **2021**, *286*, 119385.

Hristova, E.; Tchoukov, P.; Stoyanov, S. R. Coalescence inhibition and agglomeration initiation near the critical dilution of asphaltene precipitation. *Colloids Surfaces A: Physicochem. Eng. Asp.* **2021**, *629*, 127400.

Hristova, E.; Tchoukov, P.; Stoyanov, S. R.; McFarlane, R. Asphaltene Precipitation Onsets in Relation to the Critical Dilution of Athabasca Bitumen in Paraffinic Solvents. *Energy Fuels* **2022**, *36* (4), 1832–1841.

Huizinga, B. J.; Tannenbaum, E.; Kaplan, I. R. The role of minerals in the thermal alteration of organic matter - IV. Generation of n-alkanes, acyclic isoprenoids, and alkenes in laboratory experiments. *Geochim. Cosmochim. Acta* **1987**, *51* (5), 1083–1097.

IEA *World Energy Outlook*, 2022, https://www.iea.org/reports/world-energy-outlook-2022 (accessed 2023/2/10).

Ishiwatari, M. Thermal reaction of β-carotene. *J. Anal. Appl. Pyrolysis* **1981**, *2* (4), 339–351.

Jia, N.; Zhao, H.; Yang, T.; Ibatullin, T.; Gao, J. Experimental measurements of bitumen–water aquathermolysis during a steam-injection process. *Energy Fuels* **2016**, *30* (7), 5291–5299.

Johnston, C. T. Surface chemistry of oil-sands clay minerals, In *Introduction to Oil Sands Clays*, ed. by Hockley, D.; Omotoso, O.; Kaminsky, H., Vol. 22, Clay Minerals Society: Chantilly, VA, 2018, pp 33–60.

Joshi, J. B.; Pandit, A. B.; Kataria, K. L.; Kulkarni, R. P.; Sawarkar, A. N.; Tandon, D.; Ram, Y.; Kumar, M. M. Petroleum residue upgradation via visbreaking: A review. *Ind. Eng. Chem. Res.* **2008**, *47* (23), 8960–8988.

Junaid, A.; Rahman, M.; Rocha, G.; Wang, W.; Kuznicki, T.; McCaffrey, W.; Kuznicki, S. On the role of water in natural-zeolite-catalyzed cracking of athabasca oilsands bitumen. *Energy Fuels* **2014**, *28* (5), 3367–3376.

Kailey, I. Properties and Performance of Newly Developed Demulsifiers in Oil Sands Froth Treatment. *Energy Fuels* **2016**, *30* (11), 9233–9241.

Kaiser, M. J.; de Klerk, A.; Gary, J. H.; Handwerk, G. E. Fluid Catalytic Craking, In *Petroleum Refining: Technology, Economics, and Markets*, 6th ed., CRC Press: Boca Raton, 2020, pp 481–506.

Kaiser, M. J.; de Klerk, A.; Gary, J. H.; Handwerk, G. E., *Petroleum Refining: Technology, Economics, and Markets*, 6th ed.; CRC Press: Boca Raton, 2020, p 723.

Kaminsky, H. A.; Etsell, T. H.; Ivey, D. G.; Omotoso, O. Distribution of clay minerals in the process streams produced by the extraction of bitumen from Athabasca oil sands. *Can. J. Chem. Eng.* **2009**, *87* (1), 85–93.

Kapadia, P. R.; Kallos, M. S.; Gates, I. D. A new reaction model for aquathermolysis of Athabasca bitumen. *Can. J. Chem. Eng.* **2013**, *91* (3), 475–482.

Kapadia, P. R.; Kallos, M. S.; Gates, I. D. A review of pyrolysis, aquathermolysis, and oxidation of Athabasca bitumen. *Fuel Process. Technol.* **2015**, *131*, 270–289.

Kariznovi, M.; Nourozieh, H.; Abedi, J. Volumetric Properties of Athabasca Bitumen + n-Hexane Mixtures. *Energy Fuels* **2014**, *28*, 7418–7425.

Katritzky, A. R.; Allin, S. M.; Siskin, M. Aquathermolysis: Reactions of Organic Compounds with Superheated Water. *Acc. Chem. Res.* **1996**, *29* (8), 399–406.

Katritzky, A. R.; Balasubramanian, M.; Siskin, M. Aqueous high-temperature chemistry of carbo- and heterocycles. 2. Monosubstituted benzenes: benzyl alcohol, benzaldehyde and benzoic acid. *Energy Fuels* **1990**, *4* (5), 499–505.

Katritzky, A. R.; Barcock, R. A.; Balasubramanian, M.; Greenhill, J. V.; Siskin, M.; Olmstead, W. N. Aqueous High-Temperature Chemistry of Carbo- and Heterocycles. 20. Reactions of Some Benzenoid Hydrocarbons and Oxygen-Containing Derivatives in Supercritical Water at 460 °C. *Energy Fuels* **1994**, *8* (2), 487–497.

Katritzky, A. R.; Ignatchenko, E. S.; Allin, S. M.; Barcock, R. A.; Siskin, M.; Hudson, C. W. Aqueous High-Temperature Chemistry of Carbo- and Heterocycles. 29. Reactions of Aryl Hydrocarbons, Aryl N- Oxides, and Aryl Carbonyl Compounds in Supercritical Water at 460 °C. *Energy Fuels* **1997**, *11* (1), 160–173.

Katritzky, A. R.; Luxem, F. J.; Siskin, M. Aqueous high-temperature chemistry of carbo- and heterocycles. 6. Monosubstituted benzenes with two carbon atom side chains unsubstituted or oxygenated at the alpha-position. *Energy Fuels* **1990**, *4* (5), 518–524.

Katritzky, A. R.; Nichols, D. A.; Siskin, M.; Murugan, R.; Balasubramanian, M. Reactions in High-Temperature Aqueous Media. *Chem. Rev.* **2001**, *101* (4), 837–892.

Al-Khattaf, S.; de Lasa, H. Catalytic Cracking of Cumene in a Riser Simulator: A Catalyst Activity Decay Model. *Ind. Eng. Chem. Res.* **2001**, *40* (23), 5398–5404.

Kleber, M.; Bourg, I. C.; Coward, E. K.; Hansel, C. M.; Myneni, S. C.; Nunan, N. Dynamic interactions at the mineral–organic matter interface. *Nat. Rev. Earth Environ.* **2021**, *2* (6), 402–421.

Kosior, D.; Ngo, E.; Dabros, T. Determination of the Settling Rate of Aggregates Using the Ultrasound Method during Paraffinic Froth Treatment. *Energy Fuels* **2016**, *30* (10), 8192–8199.

Kosior, D.; Ngo, E.; Xu, Y. Aggregates in Paraffinic Froth Treatment: Settling Properties and Structure. *Energy Fuels* **2018**, *32* (8), 8268–8276.

Kurnia, K. A.; Taib, M. M.; Mutalib, M. A.; Murugesan, T. Densities, refractive indices and excess molar volumes for binary mixtures of protic ionic liquids with methanol at T= 293.15 to 313.15 K. *J. Mol. Liq.* **2011**, *159* (3), 211–219.

Laplante, P.; Machado, M. B.; Bhattacharya, S.; Ng, S.; Kresta, S. M. Demulsifier performance in froth treatment: Untangling the effects of mixing, bulk concentration and injection concentration using a standardized mixing test cell (CIST). *Fuel Process. Technol.* **2015**, *138*, 361–367.

Lechner, C. A.; Findley, M. E.; Liapis, A. I. Kinetics of the Pyrolysis of Utah Tar Sands. *Can. J. Chem. Eng.* **1987**, *65*, 487–493.

LePrince, P. Visbreaking of residues, In *Petroleum Refining. Vol.3. Conversion processes*, ed. by LePrince, P., Editions Technip: Paris, 2001, pp 365–378.

Lesueur, D. The colloidal structure of bitumen: Consequences on the rheology and on the mechanisms of bitumen modification. *Adv. Colloid Interface Sci.* **2009**, *145* (1-2), 42–82.

LeVeque, R. J. Appendix B - Polynomial Interpolation and Orthogonal Polynomials, In *Finite difference methods for ordinary and partial differential equations: steady-state and time-dependent problems*, Society for Industrial and Applied Mathematics: Philadelphia, PA, 2007, p 341.

Lewan, M. D. Experiments on the role of water in petroleum formation. *Geochim. Cosmochim. Acta* **1997**, *61* (17), 3691–3723.

Li, H.; Vrinat, M.; Berhault, G.; Li, D.; Nie, H.; Afanasiev, P. Hydrothermal synthesis and acidity characterization of TiO2 polymorphs. *Mater. Res. Bull.* **2013**, *48* (9), 3374–3382.

Li, Y. B.; Lin, X.; Luo, C.; Hu, Z. M.; Jia, H. F.; Chen, J. T.; Pu, W. F. A comprehensive investigation of the influence of clay minerals on oxidized and pyrolyzed cokes in in situ combustion for heavy oil reservoirs. *Fuel* **2021**, *302*, 121168.

Lin, F.; Pang, C. J. Impact of a hybrid bitumen extraction process on the destabilization of resulting bitumen froth emulsion diluted with heptane. *Miner. Eng.* **2020**, *145*, 106069.

Liu, H.; Yuan, P.; Liu, D.; Bu, H.; Song, H.; Qin, Z.; He, H. Pyrolysis behaviors of organic matter (OM) with the same alkyl main chain but different functional groups in the presence of clay minerals. *Appl. Clay Sci.* **2018**, *153*, 205–216.

Liu, H.; Yuan, P.; Liu, D.; Tan, D.; He, H.; Zhu, J. Effects of solid acidity of clay minerals on the thermal decomposition of 12-aminolauric acid. *J. Therm. Anal. Calorim.* **2013**, *114* (1), 125–130.

Liu, H.; Yuan, P.; Qin, Z.; Liu, D.; Tan, D.; Zhu, J.; He, H. Thermal degradation of organic matter in the interlayer clay–organic complex: A TG-FTIR study on a montmorillonite/12-aminolauric acid system. *Appl. Clay Sci.* **2013**, *80-81*, 398–406.

Liu, J.; Xing, Y.; Chen, Y. X.; Yuan, P. Q.; Cheng, Z. M.; Yuan, W. K. Visbreaking of heavy oil under supercritical water environment. *Ind. Eng. Chem. Res.* **2018**, *57* (3), 867–875.

Liu, P. G.; Pu, W. F.; Ni, J. H. Catalytic effect analysis of clay minerals on low-temperature oxidation of crude oil through combined thermal analysis methods. *Pet. Sci. Technol.* **2016**, *34* (4), 343–349.

Liu, Y.; Bai, F.; Zhu, C. C.; Yuan, P. Q.; Cheng, Z. M.; Yuan, W. K. Upgrading of residual oil in sub-and supercritical water: An experimental study. *Fuel Process. Technol.* **2013**, *106*, 281–288.

Lois, E.; Keating, E. L.; Gupta, A. K. Fuels, In *Encyclopedia of physical science and technology*, ed. by Meyers, R. A., 3rd, San Diego: Academic Press: 2002, pp 275–314.

Luo, C.; Liu, H.; Li, X.; Dong, X.; Zhang, Y.; Wang, H. Effects of different clay minerals on thermal conversion of oxidized and pyrolyzed oils during in situ combustion. *J. Therm. Anal. Calorim.* **2023**, *148* (22), 12629–12637.

Luo, P.; Gu, Y. Effects of asphaltene content on the heavy oil viscosity at different temperatures. *Fuel* **2007**, *86* (7-8), 1069–1078.

Maity, S.; Ancheyta, J.; Marroquín, G. Catalytic aquathermolysis used for viscosity reduction of heavy crude oils: A review. *Energy Fuels* **2010**, *24* (5), 2809–2816.

Marquez, A.; Schoeggl, F.; Taylor, S.; Hay, G.; Yarranton, H. Viscosity of characterized visbroken heavy oils. *Fuel* **2020**, *271*, 117606.

Masliyah, J. H.; Czarnecki, J.; Xu, Z., *Handbook on theory and practice of bitumen recovery from Athabasca oil sands - Volume 1: Theoretical basis*; Kingsley Knowledge Publishing: 2011, p 468.

Masliyah, J.; Zhou, Z. J.; Xu, Z.; Czarnecki, J.; Hamza, H. Understanding Water-Based Bitumen Extraction from Athabasca Oil Sands. *The Can. J. Chem. Eng.* **2008**, *82* (4), 628–654.

Matyjaszewski, K., *Cationic polymerizations: mechanisms, synthesis, and applications*; Marcel Dekker: New York, 1996, p 768.

Mayr, H.; Lang, G.; Ofial, A. R. Reactions of carbocations with unsaturated hydrocarbons: Electrophilic alkylation or hydride abstraction? *J. Am. Chem. Soc.* **2002**, *124* (15), 4076–4083.

McFarlane, R. A.; Gray, M. R.; Shaw, J. M. Evaluation of co-volume mixing rules for bitumen liquid density and bubble pressure estimation. *Fluid Phase Equilib.* **2010**, *293* (1), 87–100.

McMillen, D. F.; Golden, D. M. Hydrocarbon bond dissociation energies. *Annu. Rev. Phys. Chem.* **1982**, (33), 493–532.

Mecón Méndez, S. G.; Salas-Chia, L. M.; Martínez Vertel, J. J.; Molina Velasco, D. R.; León, A. Y.; León, P. A. Effect of Mineralogy on the Physicochemical Properties of a Heavy Crude Oil in Hybrid Steam Injection Technologies Using 1H NMR. *Energy Fuels* **2022**, *36* (17), 10315–10326.

Miadonye, A.; Latour, N.; Puttagunta, V. R. A correlation for viscosity and solvent mass fraction of bitumen-diluent mixtures. *Pet. Sci. Technol.* **2000**, *18* (1), 1–14.

Mokoena, K.; Scurrell, M. S. Alkyl transfer reactions on solid acids. The disproportionation of ethylbenzene and toluene on H-mordenite and HY zeolites. *Pet. Sci. Technol.* **2018**, *36* (16), 1208–1215.

Monin, J. C.; Audibert, A. Thermal cracking of heavy-oil/mineral matrix systems. *SPE Reserv. Eng.* **1988**, *3* (4), 1243–1250.

Montoya Sánchez, N.; de Klerk, A. Viscosity Mixing Rules for Bitumen at 1–10 wt% Solvent Dilution When Only Viscosity and Density Are Known. *Energy Fuels* **2020**, *34* (7), 8227–8238.

Morimoto, M.; Sugimoto, Y.; Saotome, Y.; Sato, S.; Takanohashi, T. Effect of supercritical water on upgrading reaction of oil sand bitumen. *J. Supercrit. Fluids* **2010**, *55* (1), 223–231.

Mujica, V.; Nieto, P.; Puerta, L.; Acevedo, S. Caging of molecules by asphaltenes. A model for free radical preservation in crude oils. *Energy Fuels* **2000**, *14* (3), 632–639.

Mullins, O. C.; Sheu, E. Y.; Hammami, A.; Marshall, A. G., *Asphaltenes, heavy oils, and petroleomics*; Springer: New York, 2007, p 688.

Al-Muntaser, A. A.; Varfolomeev, M. A.; Suwaid, M. A.; Yuan, C.; Chemodanov, A. E.; Feoktistov, D. A.; Rakhmatullin, I. Z.; Abbas, M.; Domínguez-Álvarez, E.; Akhmadiyarov, A. A., et al. Hydrothermal upgrading of heavy oil in the presence of water at sub-critical, near-critical and supercritical conditions. *J. Pet. Sci. Eng.* **2020**, *184*, 106592.

Murgich, J.; Merino-Garcia, D.; Andersen, S. I.; Manuel del Río, J.; Galeana, C. L. Molecular mechanics and microcalorimetric investigations of the effects of molecular water on the aggregation of asphaltenes in solutions. *Langmuir* **2002**, *18* (23), 9080–9086.

Murugan, P.; Mani, T.; Mahinpey, N.; Dong, M. Pyrolysis kinetics of Athabasca bitumen using a TGA under the influence of reservoir sand. *Can. J. Chem. Eng.* **2012**, *90* (2), 315–319.

Nabata, H.; Takagi, M.; Saita, K.; Maeda, S. Computational searches for crystal structures of dioxides of group 14 elements (CO2, SiO2, GeO2) under ultrahigh pressure. *RSC Adv.* **2020**, *10* (37), 22156–22163.

Naghizada, N.; Prado, G. H. C.; de Klerk, A. Uncatalyzed hydrogen transfer during 100–250 °C conversion of asphaltenes. *Energy Fuels* **2017**, *31* (7), 6800–6811.

Natural Resources Canada - What are the oil sands?, https://natural-resources.canada.ca/our-natural-resources/energy-sources-distribution/fossil-fuels/crude-oil/what-are-oil-sands/18089 (accessed 2023/2/16).

Nazdracheva, T.; Morozov, A.; Yavna, V.; Kochur, A. Study of hydration of kaolinite and montmorillonite mixture by IR spectroscopy. *J. Mol. Struct.* **2022**, *1250*, 131871.

Nourozieh, H.; Kariznovi, M.; Abedi, J. Measurement and Prediction of Density for the Mixture of Athabasca Bitumen and Pentane at Temperatures up to 200 °C. *Energy Fuels* **2014**, *28* (5), 2874–2885.

Nourozieh, H.; Kariznovi, M.; Abedi, J. Density and Viscosity of Athabasca Bitumen Samples at Temperatures up to 200 °C and Pressures up to 10 MPa. *SPE Reserv. Eval. Eng.* **2015**, *18* (03), 375–386.

Nourozieh, H.; Kariznovi, M.; Abedi, J. Modeling and measurement of thermo-physical properties for Athabasca bitumen and n-heptane mixtures. *Fuel* **2015**, *157*, 73–81.

Nourozieh, H.; Kariznovi, M.; Abedi, J. Viscosity measurement and modeling for mixtures of Athabasca bitumen / hexane. *J. Pet. Sci. Eng.* **2015**, *129*, 159–167.

Nourozieh, H.; Kariznovi, M.; Abedi, J. Viscosity measurement and modeling for mixtures of Athabasca bitumen/n-pentane at temperatures up to 200 °C. *SPE J.* **2015**, *20* (02), 226–238.

Oil Sands Magazine - Naphthenic Froth Treatment, www.oilsandsmagazine.com/technical/mining/froth-treatment/naphthenic (accessed 2023/4/20).

Oil Sands Magazine - Paraffinic Froth Treatment, www.oilsandsmagazine.com/technical/mining/froth-treatment/paraffinic (accessed 2023/4/20).

Ovalles, C.; Hamana, A.; Rojas, I.; Bolívar, R. A. Upgrading of extra-heavy crude oil by direct use of methane in the presence of water: deuterium-labelled experiments and mechanistic considerations. *Fuel* **1995**, *74* (8), 1162–1168.

Ovalles, C.; Vallejos, C.; Vasquez, T.; Rojas, I.; Ehrman, U.; Benitez, J. L.; Martinez, R. Downhole Upgrading of Extra-heavy Crude Oil Using Hydrogen Donors and Methane Under Steam Injection Conditions. *Pet. Sci. Technol.* **2003**, *21* (1-2), 255–274.

Pal, R. Modeling and scaling of the viscosity of suspensions of asphaltene nanoaggregates. *Energies* **2017**, *10* (6), 767.

Pal, R. New Generalized Viscosity Model for Non-Colloidal Suspensions and Emulsions. *Fluids* **2020**, *5* (3), 150.

Payan, F.; De Klerk, A. Hydrogen Transfer in Asphaltenes and Bitumen at 250 °C. *Energy Fuels* **2018**, *32* (9), 9340–9348.

Petrukhina, N.; Kayukova, G.; Romanov, G.; Tumanyan, B.; Foss, L.; Kosachev, I.; Musin, R.; Ramazanova, A.; Vakhin, A. Conversion processes for high-viscosity heavy crude oil in catalytic and noncatalytic aquathermolysis. *Chem. Technol. Fuels Oils* **2014**, *50* (4), 315–326.

Phillips, C. R.; HAidar, N. I.; Poon, Y. C. Kinetic models for the thermal cracking of Athabasca bitumen: The effect of the sand matrix. *Fuel* **1985**, *64*, 678–691.

Polovor, Y. N.; Kaminskaya, Y. G.; Vykhrestyuk, N.; Tkachenko, D. Conversions of α-methylstyrene on aluminosilicate at cracking temperatures. *Pet. Chem. U.S.S.R.* **1977**, *17* (4), 215–223.

Pu, W. F.; Yuan, C. D.; Jin, F. Y.; Wang, L.; Qian, Z.; Li, Y. B.; Li, D.; Chen, Y. F. Low-temperature oxidation and characterization of heavy oil via thermal analysis. *Energy Fuels* **2015**, *29* (2), 1151–1159.

PUTTAGUNTA, V. R.; SINGH, B.; MIADONYE, A. Correlation of Bitumen Viscosity with Temperature and Pressure. *Can. J. Chem. Eng.* **1993**, *71* (3), 447–450.

Qi, Y.; Cai, C. F.; Sun, P.; Wang, D. W.; Zhu, H. J. Crude oil cracking in deep reservoirs: A review of the controlling factors and estimation methods. *Pet. Sci.* **2023**, *20* (4), 1978–1997.

Qu, X.; Li, Y.; Li, S.; Wang, J.; Xu, H.; Li, Z. Thermal cracking, aquathermolysis, and their upgrading effects of Mackay River oil sand. *J. Pet. Sci. Eng.* **2021**, *201*, 108473.

Qu, X.; Zhou, G.; Lu, Y.; Li, S.; Zhang, L.; Wang, J.; Xu, H. Catalytic aquathermolysis of Mackay River bitumen with different types of Mo-based catalysts. *Fuel* **2022**, *326*, 125134.

Rahimi, P. M.; Gentzis, T. The Chemistry of Bitumen and Heavy Oil Processing, In *Practical Advances in Petroleum Processing*, ed. by Hsu, C. S.; Robinson, P. R., Vol. 2, Springer: New York, 2006, pp 149–188.

Rahimi, P. M.; Teclemariam, A.; Taylor, E.; DeBruijn, T.; Wiehe, I. A. Thermal Processing Limits of Athabasca Bitumen during Visbreaking Using Solubility Parameters, In *Heavy hydrocarbon resources: characterization, upgrading, and utilization*, ed. by Nomura, M.; Rahimi, P. M.; Koseoglu, O. R., Vol. 895, ACS Symposium Series: 2005, pp 183–196.

Ramirez-Corredores, M. M., *The science and technology of unconventional oils: finding refining opportunities*; Academic Press: London, 2017, p 778.

Ramos-Pallares, F.; Schoeggl, F. F.; Taylor, S. D.; Satyro, M. A.; Yarranton, H. W. Predicting the Viscosity of Hydrocarbon Mixtures and Diluted Heavy Oils Using the Expanded Fluid Model. *Energy Fuels* **2016**, *30* (5), 3575–3595.

Rao, F.; Liu, Q. Froth treatment in Athabasca oil sands bitumen recovery process: A review. *Energy Fuels* **2013**, *27* (12), 7199–7207.

Raseev, S., *Thermal and Catalytic Processes in Petroleum Refining*; CRC Press: Boca Raton, 2003, p 920.

Rhodes, A. K. Benchmark West Texas Intermediate crude assayed. *Oil andGas J.* **1994**, *92* (33), 88.

Riazi, M. R. Characterization and properties of petroleum fractions, In *American Society and Testing Materials, ASTM Manual Series: MNL50*, 1st ed., 2005, pp 331–338.

Romanova, U.; Valinasab, M.; Stasiuk, E.; Yarranton, H.; Schramm, L.; Shelfantook, W. The Effect of Oil Sands Bitumen Extraction Conditions on Froth Treatment Performance. *J. Can. Pet. Technol.* **2006**, *45* (9), 36–45.

Romanova, U. G.; Yarranton, H. W.; Schramm, L. L.; Shelfantook, W. E. Investigation of oil sands froth treatment. *Can. J. Chem. Eng.* **2004**, *82* (4), 710–721.

Rong, T. J.; kai Xiao, J. The catalytic cracking activity of the kaolin-group minerals. *Mater. Lett.* **2002**, *57* (2), 297–301.

Roscoe, R. The viscosity of suspensions of rigid spheres. *Br. J. Appl. Phys.* **1952**, *3* (8), 267–269.

Rose, H. R.; Smith, D. R.; Hanna, J. V.; Palmisano, A. J.; Wilson, M. A. Comparison of the effect of minerals on aromatization reactions during kerogen pyrolysis. *Fuel* **1992**, *71* (4), 355–360.

Rüchardt, C.; Gerst, M.; Nölke, M. The Uncatalyzed Transfer Hydrogenation of α-Methylstyrene by Dihydroanthracene or Xanthene - a Radical Reaction. *Angew. Chem., Int. Ed. Engl.* **1992**, *31* (11), 1523–1525.

Rustamov, M. I.; Seidov, N. M.; Ibragimov, K. D.; Mamedbeili, E. G. Dimerization of α-methylstyrene in the presence of mordenite, aimed at preparation of transformer oils. *Russ. J. Appl. Chem.* **2009**, *82* (2), 317–322.

Saadatmand, M.; Yarranton, H. W.; Moran, K. Rag layers in oil sand froths. *Ind. Eng. Chem. Res.* **2008**, *47* (22), 8828–8839.

Saltzman, S.; Mingelgrin, U.; Yaron, B. Role of Water in the Hydrolysis of Parathion and Methylparathion on Kaolinite. *J. Agrie. Food Chem.,* **1976**, *24* (4), 739–743.

Samat, M. H.; Ali, A. M.; Taib, M. F.; Hassan, O. H.; Yahya, M. Z. Hubbard U calculations on optical properties of 3d transition metal oxide TiO2. *Results Phys.* **2016**, *6*, 891–896.

Sanaie, N.; Watkinson, A.; Bowen, B.; Smith, K. Effect of minerals on coke precursor formation. *Fuel* **2001**, *80* (8), 1111–1119.

Sánchez-Lemus, M. C.; Okafor, J. C.; Ortiz, D. P.; Schoeggl, F. F.; Taylor, S. D.; Van Den Berg, F. G.; Yarranton, H. W. Improved density prediction for mixtures of native and refined heavy oil with solvents. *Energy Fuels* **2015**, *29* (5), 3052–3063.

Saryazdi, F.; Motahhari, H.; Schoeggl, F. F.; Taylor, S. D.; Yarranton, H. W. Density of hydrocarbon mixtures and bitumen diluted with solvents and dissolved gases. *Energy Fuels* **2013**, *27* (7), 3666–3678.

Sato, T.; Adschiri, T.; Arai, K.; Rempel, G. L.; Ng, F. T. Upgrading of asphalt with and without partial oxidation in supercritical water. *Fuel* **2003**, *82* (10), 1231–1239.

Sato, T.; Trung, P. H.; Tomita, T.; Itoh, N. Effect of water density and air pressure on partial oxidation of bitumen in supercritical water. *Fuel* **2012**, *95*, 347–351.

Savage, P. E.; Gopalan, S.; Mizan, T. I.; Martino, C. J.; Brock, E. E. Reactions at supercritical conditions: applications and fundamentals. *AIChE J.* **1995**, *41* (7), 1723–1778.

Savage, P. E. Organic Chemical Reactions in Supercritical Water. *Chem. Rev.* **1999**, *99* (2), 603–622.

Sawarkar, A. N.; Pandit, A. B.; Samant, S. D.; Joshi, J. B. Petroleum residue upgrading via delayed coking: A review. *Can. J. Chem. Eng.* **2007**, *85* (1), 1–24.

Schlepp, L.; Elie, M.; Landais, P.; Romero, M. Pyrolysis of asphalt in the presence and absence of water. *Fuel Process. Technol.* **2001**, *74* (2), 107–123.

Setvin, M.; Franchini, C.; Hao, X.; Schmid, M.; Janotti, A.; Kaltak, M.; Van de Walle, C. G.; Kresse, G.; Diebold, U. Direct View at Excess Electrons in TiO2 Rutile and Anatase. *Phys. Rev. Lett.* **2014**, *113*, 0864021–0864025.

Sheldon, R. A.; Kochi, J. K., *Metal-catalyzed oxidations of organic compounds*; Academic Press: New York, 1981.

Shelfantook, W. E. A perspective on the selection of froth treatment processes. *Can. J. Chem. Eng.* **2004**, *82* (4), 704–709.

Shen, J.; Astrath, N. G.; Pedreira, P. R.; Guimarães, F. B.; Gieleciak, R.; Wen, Q.; Michaelian, K. H.; Fairbridge, C.; Malacarne, L. C.; Rohling, J. H., et al. Correlations among thermophysical properties, ignition quality, volatility, chemical composition, and kinematic viscosity of petroleum distillates. *Fuel* **2016**, *163*, 324–333.

Sheu, E.; De Tar, M.; Storm, D. Rheological properties of vacuum residue fractions in organic solvents. *Fuel* **1991**, *70* (10), 1151–1156.

Shimoyama, A.; Johns, W. D. Catalytic Conversion of Fatty Acids to Petroleum-like Paraffins and their Maturation. *Nat. Phys. Sci.* **1971**, *232* (33), 140–144.

Siskin, M.; Brons, G.; Katritzky, A. R.; Balasubramanian, M. Aqueous organic chemistry. 1. Aquathermolysis: comparison with thermolysis in the reactivity of aliphatic compounds. *Energy Fuels* **1990**, *4* (5), 475–482.

Siskin, M.; Brons, G.; Katritzky, A. R.; Murugan, R. Aqueous organic chemistry. 2. Crosslinked cyclohexyl phenyl compounds. *Energy Fuels* **1990**, *4* (5), 482–488.

Siskin, M.; Katritzky, A. R. Reactivity of Organic Compounds in Hot Water: Geochemical and Technological Implications. *Science* **1991**, *254* (5029), 231–237.

Siskin, M.; Katritzky, A. R. Reactivity of Organic Compounds in Superheated Water: General Background. *Chem. Rev.* **2001**, *101* (4), 825–836.

Sitnov, S. A.; Khelkhal, M. A.; Mukhamatdinov, I. I.; Feoktistov, D. A.; Vakhin, A. V. Iron oxide nanoparticles impact on improving reservoir rock minerals catalytic effect on heavy oil aquathermolysis. *Fuel* **2022**, *327*, 124956.

Smolen, J. D.; Hren, M. T. Differential effects of clay mineralogy on thermal maturation of sedimentary n-alkanes. *Chem. Geol.* **2023**, *634*, 121572.

Solomon, D. H.; Rosser, M. J. Reactions catalyzed by minerals. Part I. Polymerization of styrene. *J. Appl. Polym. Sci.* **1965**, *9* (4), 1261–1271.

Solomon, D.; Swift, J. D. Reactions catalyzed by minerals. Part II. Chain termination in free-radical polymerizations. *J. Appl. Polym. Sci.* **1967**, *11* (12), 2567–2575.

Solomon, D. Clay minerals as electron acceptors and/or electron donors in organic reactions. *Clays Clay Miner.* **1968**, *16*, 31–39.

Soma, Y.; Soma, M. Chemical reactions of organic compounds on clay surfaces. *Environ. Health Perspect.* **1989**, *83*, 205–214.

Song, H.; Liu, H.; Bu, H.; Liu, D.; Li, Y.; Du, P. Effects of montmorillonite charge reduction on the high-temperature/high-pressure pyrolysis of organic matter. *Appl. Clay Sci.* **2021**, *213*, 106243.

Speight, J. G., *Heavy Oil Production Processes*; Elsevier: Waltham, MA - USA, 2013, pp 1–7.

Speight, J. G., *The chemistry and technology of petroleum*, 5th ed.; CRC Press: Boca Raton, FL, 2014, p 188.

Stammitti-Scarpone, A.; Quraishi, S.; Bhanot, A.; Boza, A.; Ng, S.; Acosta, E. Dewatering of Naphthenic Bitumen Froth. *Energy Fuels* **2020**, *34* (9), 10688–10704.

Steele, W.; Chirico, R.; Knipmeyer, S.; Nguyen, A. Vapor Pressure, Heat Capacity, and Density along the Saturation Line, Measurements for Dimethyl Isophthalate, Dimethyl Carbonate, 1, 3, 5-Triethylbenzene, Pentafluorophenol, 4-tert-Butylcatechol, α-Methylstyrene, and N, N '-Bis (2-hydroxyethyl) ethylenediamine. *J. Chem. Eng. Data* **1997**, *42* (6), 1008–1020.

Stewart, R. A. Beyond Viscosity - How Density, Vibration and Interfacial Tension Affect Solvent Aided Bitumen Production, PhD Thesis, University of Alberta, Edmonton, AB, 2016, p 186.

Storm, D. A.; Barresi, R. J.; Sheu, E. Y. Rheological Study of Ratawi Vacuum Residue in the 298-673 K Temperature Range. *Energy Fuels* **1995**, *9* (1), 168–176.

Strausz, O. P.; Jha, K. N.; Montgomery, D. S. Chemical composition of gases in Athabasca bitumen and in low-temperature thermolysis of oil sand , asphaltene and maltene. *Fuel* **1977**, *56*, 114–120.

Strausz, O. P.; Lown, E. M., *The Chemistry of Alberta Oil Sands, Bitumens and Heavy Oils*; Alberta Energy Research Institute: Calgary, 2003, p 695.

Tanabe, K.; Gray, M. R. Role of fine solids in the coking of vacuum residues. *Energy Fuels* **1997**, *11* (5), 1040–1043.

Tanko, J. M.; Pacut, R. Enhanced cage effects in supercritical fluid solvents. The behavior of diffusive and geminate caged-pairs in supercritical carbon dioxide. *J. Am. Chem. Soc.* **2001**, *123* (24), 5703–5709.

Tannenbaum, E.; Huizinga, B. J.; Kaplan, I. R. Role of Minerals in Thermal Alteration of Organic Matter–II: A Material Balance. *AAPG Bull.* **1986**, *70* (9), 1156–1165.

Tannous, J. H.; de Klerk, A. Quantification of the free radical content of oilsands bitumen fractions. *Energy Fuels* **2019**, *33* (8), 7083–7093.

Tannous, J. H.; de Klerk, A. Methyl and hydrogen transfer in free radical reactions. *Energy Fuels* **2020**, *34* (2), 1698–1709.

Townsend, S. H.; Abraham, M. A.; Huppert, G. L.; Klein, M. T.; Paspek, S. C. Solvent effects during reactions in supercritical water. *Ind. Eng. Chem. Res.* **1988**, *27* (1), 143–149.

Trejo, F.; Rana, M. S.; Ancheyta, J. Genesis of Acid- Base Support Properties with Variations of Preparation Conditions: Cumene Cracking and Its Kinetics. *Ind. Eng. Chem. Res.* **2011**, *50* (5), 2715–2725.

Turuga, A. S. S.; de Klerk, A. Hydrothermal Treatment of Bitumen Froth: Impact of Mineral Solids and Water on Bitumen Properties. *Energy Fuels* **2021**, *35* (21), 17536–17550.

Turuga, A. S. S.; de Klerk, A. Free Radical and Cationic Addition due to Clay Minerals Found in Bitumen Froth at 250 °C Probed with Use of α-Methylstyrene and 1-Octene. *Energy Fuels* **2022**, *36* (23), 14148–14162.

Velayati, A.; Habibi, A.; Nikrityuk, P.; Tang, T.; Zeng, H. Emulsions in Bitumen Froth Treatment and Methods for Demulsification and Fines Removal in Naphthenic Froth Treatment: Review and Perspectives. *Energy Fuels* **2022**, *36* (16), 8607–8623.

Wahyudiono; Shiraishi, T.; Sasaki, M.; Goto, M. Non-catalytic liquefaction of bitumen with hydrothermal/solvothermal process. *J. Supercrit. Fluids* **2011**, *60*, 127–136.

Wakeham, W. A.; St. Cholakov, G.; Stateva, R. P. Liquid density and critical properties of hydrocarbons estimated from molecular structure. *J. Chem. Eng. Data* **2002**, *47* (3), 559–570.

Wallace, D.; Henry, D.; Miadonye, A.; Puttagunta, V. R. Viscosity and Solubility of Mixtures of Bitumen and Solvent. *Fuel Sci. Technol. Int.* **1996**, *14* (3), 465–478.

Wang, D.; Qiao, C.; Zhao, Z.; Yang, W.; Chen, H.; Yin, T.; Yan, Z.; Wu, M.; Mao, X.; Santander, C.; Liu, Q.; Liu, Q.; Nikrityuk, P. A.; Tang, T.; Zeng, H. Understanding the Properties of Bitumen Froth from Oil Sands Surface Mining and Treatment of Water-in-Oil Emulsions. *Energy Fuels* **2021**, *35* (24), 20079–20091.

Wang, L.; Zachariah, A.; Yang, S.; Prasad, V.; De Klerk, A. Visbreaking oilsands-derived bitumen in the temperature range of 340-400 °C. *Energy Fuels* **2014**, *28* (8), 5014–5022.

Wang, Z.; Liu, X.; Wang, Y.; Liu, L.; Wang, H.; Deng, S.; Sun, Y. Studies on the co-pyrolysis characteristics of oil shale and spent oil shale. *J. Therm. Anal. Calorim.* **2016**, *123* (2), 1707–1714.

Watanabe, M.; Kato, S. N.; Ishizeki, S.; Inomata, H.; Smith Jr, R. L. Heavy oil upgrading in the presence of high density water: basic study. *J. Supercrit. Fluids* **2010**, *53* (1-3), 48–52.

Wu, C.; Lei, G. L.; Yao, C. J. i.; Sun, K. J.; Gai, P. Y.; Cao, Y. B. Mechanism for reducing the viscosity of extra-heavy oil by aquathermolysis with an amphiphilic catalyst. *J. Fuel Chem. Technol.* **2010**, *38* (6), 684–690.

Wu, L. M.; Zhou, C. H.; Keeling, J.; Tong, D. S.; Yu, W. H. Towards an understanding of the role of clay minerals in crude oil formation, migration and accumulation. *Earth-Science Rev.* **2012**, *115* (4), 373–386.

Xu, Y. Asphaltene Precipitation in Paraffinic Froth Treatment: Effects of Solvent and Temperature. *Energy Fuels* **2018**, *32* (3), 2801–2810.

Yan, T. Characterization of visbreaker feeds. *Fuel* **1990**, *69* (8), 1062–1064.

Yan, Y. The Formation of New Asphaltenes during Visbreaking of Vacuum Residue Deasphalted Oil and the Storage Stability of Product from Visbreaking, MSc thesis, Universtiy of Alberta, Edmonton, Canada, 2020, p 117.

Yañes Jaramillo, L. M.; Link, F.; Klerk, A. D. Relationship between aromatic hydrogen and aromatic carbon in straight run and converted oils. **2022**, *327*, 124414.

Yañez Jaramillo, L. M.; Tannous, J. H.; de Klerk, A. Persistent Free Radicals in Petroleum. *Processes* **2023**, *11* (7), 2067.

Yañez Jaramillo, L. M.; de Klerk, A. Partial upgrading of bitumen by thermal conversion at 150–300 °C. *Energy Fuels* **2018**, *32* (3), 3299–3311.

Yang, Z.; Gould, I. R.; Williams, L. B.; Hartnett, H. E.; Shock, E. L. Effects of iron-containing minerals on hydrothermal reactions of ketones. *Geochim. Cosmochim. Acta* **2018**, *223*, 107–126.

Yoosuk, B.; Udomsap, P.; Puttasawat, B.; Krasae, P. Modification of calcite by hydration–dehydration method for heterogeneous biodiesel production process: The effects of water on properties and activity. *Chem. Eng. J.* **2010**, *162* (1), 135–141.

Yu, X.; Qu, Z.; Kan, C.; Zhao, X. Effect of Different Clay Minerals on Heavy Oil Oxidation during Ignition Process. *Energy Fuels* **2017**, *31* (11), 12839–12847.

Yuan, P. Q.; Zhu, C. C.; Liu, Y.; Bai, F.; Cheng, Z. M.; Yuan, W. K. Solvation of hydrocarbon radicals in sub-CW and SCW: An ab initio MD study. *J. Supercrit. Fluids* **2011**, *58* (1), 93–98.

Zachariah, A. Low temperature pyrolysis and its application in bitumen processing, MSc thesis, University of Alberta, Edmonton, AB, 2014.

Zachariah, A.; Wang, L.; Yang, S.; Prasad, V.; de Klerk, A. Suppression of coke formation during bitumen pyrolysis. *Energy Fuels* **2013**, *27* (6), 3061–3070.

Zafar, R.; Watson, J. S. Adsorption of tetradecanoic acid on kaolinite minerals: Using flash pyrolysis to characterise the catalytic efficiency of clay mineral adsorbed fatty acids. *Chem. Geol.* **2017**, *471*, 111–118.

Zawala, J.; Dabros, T.; Hamza, H. A. Settling properties of aggregates in paraffinic froth treatment. *Energy Fuels* **2012**, *26* (9), 5775–5781.

Zhan, W.; Yi, H.; Song, S.; Zhao, Y.; Rao, F. Hydrophobic agglomeration behaviors of clay minerals as affected by siloxane structure. *Colloids Surfaces A: Physicochem. Eng. Asp.* **2019**, *568*, 36–42.

Zhang, J.; Han, F.; Yang, Z.; Zhang, L.; Wang, X.; Zhang, X.; Jiang, Y.; Chen, K.; Pan, H.; Lin, R. Significance of aquathermolysis reaction on heavy oil recovery during the steam-assisted gravity drainage process. *Energy Fuels* **2020**, *34* (5), 5426–5435.

Zhang, L.; Shi, C.; Lu, Q.; Liu, Q.; Zeng, H. Probing Molecular Interactions of Asphaltenes in Heptol Using a Surface Forces Apparatus: Implications on Stability of Water-in-Oil Emulsions. *Langmuir* **2016**, *32* (19), 4886–4895.

Zhang, W.; Li, Q.; Li, Y.; Dong, S.; Peng, S.; Chen, G. Viscosity Reduction and Mechanism of Aquathermolysis of Heavy Oil Co-Catalyzed by Bentonite and Transition Metal Complexes. *Catalysts* **2022**, *12* (11), 1383.

Zhang, X.; Wang, J.; Wang, L.; Li, Z.; Wang, R.; Li, H.; Luo, M.; Liu, H.; Hu, W.; Feng, Q. Effects of kaolinite and its thermal transformation on oxidation of heavy oil. *Appl. Clay Sci.* **2022**, *223*, 106507.

Zhang, Y.; Siskin, M.; Gray, M. R.; Walters, C. C.; Rodgers, R. P. Mechanisms of asphaltene aggregation: puzzles and a new hypothesis. *Energy Fuels* **2020**, *34* (8), 9094–9107.

Zhao, J.; Liu, Q.; Gray, M. R. Characterization of fine solids in Athabasca bitumen froth before and after hydrothermal treatment. *Energy Fuels* **2016**, *30* (3), 1965–1971.

Zheng, R.; Liao, G.; You, H.; Song, X.; Song, Q.; Yao, Q. Montmorillonite-catalyzed thermal conversion of low-asphaltene heavy oil and its main components. *J. Pet. Sci. Eng.* **2020**, *187*, 106743.

Zheng, R.; Liu, D.; Tang, J.; Song, Q.; Yao, Q. Analysis of montmorillonite affecting coke formation during the thermal conversion of heavy oil. *Fuel* **2021**, *288*, 119687.

Zheng, R.; Pan, J.; Cai, G.; Liang, J.; Liu, D.; Song, Q.; Yao, Q. Effects of clay minerals on the low-temperature oxidation of heavy oil. *Fuel* **2019**, *254*, 115597.

Zhong, M.; Huang, H.; Xu, P.; Hu, J. Catalysis of Minerals in Pyrolysis Experiments. *Minerals* **2023**, *13* (4), 515.

Zhou, Z.; Slaný, M.; Kuzielová, E.; Zhang, W.; Ma, L.; Dong, S.; Zhang, J.; Chen, G. Influence of reservoir minerals and ethanol on catalytic aquathermolysis of heavy oil. *Fuel* **2022**, *307*, 121871.

Appendix A: Supporting information for Chapter 3

A.1 Filtration setup

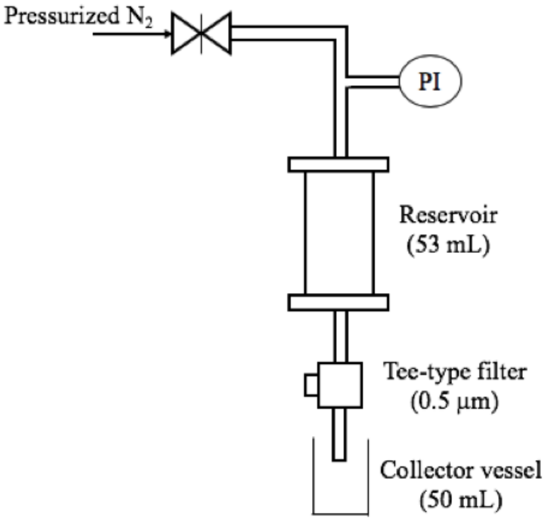

Figure A.1: Filtration setup used for solids removal.

A.2 Reactor setup for visbreaking

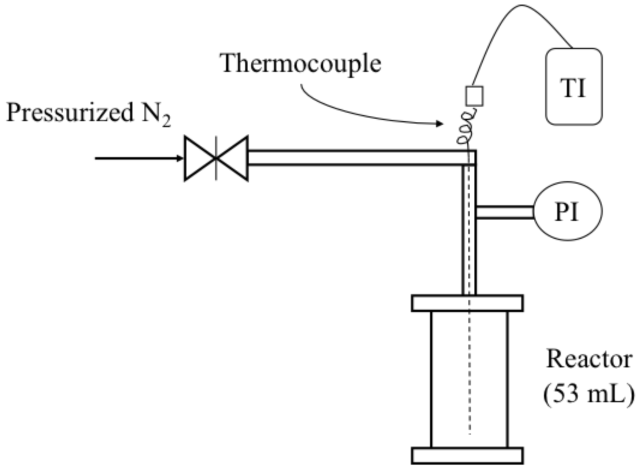

Figure A.2: Reactor setup used for visbreaking. TI – Temperature indicator; PI – Pressure indicator

A.3 Typical temperature profile inside the reactor during visbreaking

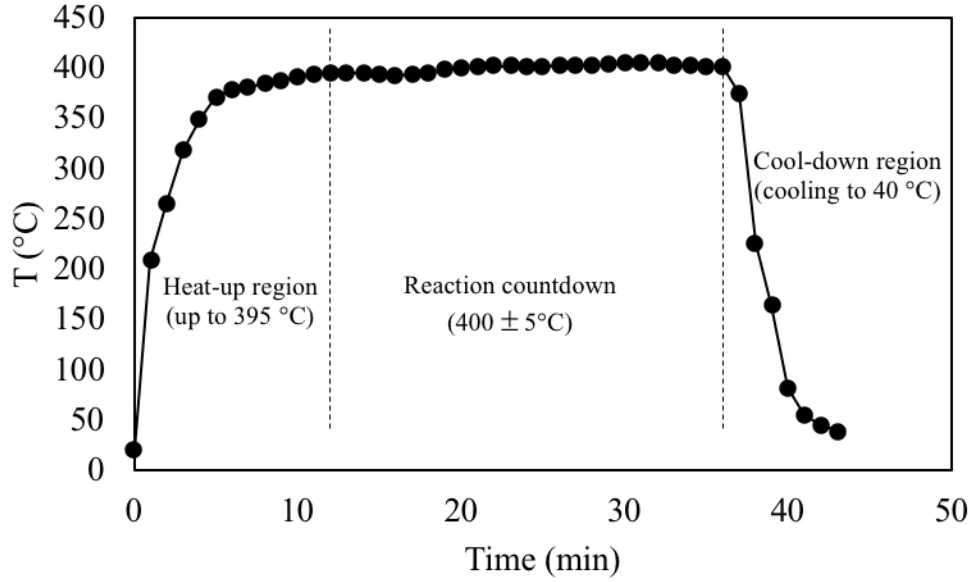

Figure A.3: Typical temperature profile inside the reactor during the visbreaking reactions.

A.4 Equivalent residence time (ERT) calculation

The ERT, as defined by Yan [3], was calculated for each time interval (1 min interval) through all the reaction times (including heat-up and cool-down times). The ERT was calculated according to equation **Eq. A.1**, where Δt_i are defined time intervals consisting of two recorded temperatures (T_i and T_{i+1}), T_{ref} is the reference temperature for which the ERT is being calculated, E_a = 209500 J mol^{-1}, and R = 8.314 J mol^{-1} K^{-1}. Then, the ERT of the reaction was obtained by adding all the ERT of each time interval.

$$ERT\, at\, T_{ref} \; = \sum_{i=1}^{n} \Delta t_i \; \times \; exp\left[\left(-\frac{E_a}{R}\right)\left(\frac{1}{\frac{T_i + T_{i+1}}{2}} - \frac{1}{T_{ref}}\right)\right] \tag{A.1}$$

A.5 Measured Elemental Analyses of bitumen samples and procedure for data correction

Table A.1 contains the measured elemental analysis of untreated bitumen and reacted systems. The analyzed bitumen samples contained solvent and residual water that had an impact over the measured results. Mass balance together with the solvents elemental composition, and the residual water content (**Table 3.6**), were used in order to correct the measured values and obtaining the elemental composition of bitumen only (**Table 3.7**).

Table A.1: Measured Elemental Analysis (wt%) and molar element ratios of untreated bitumen and bitumen separated from visbroken products. These bitumen samples reported in these results contain kerosene and residual water.[a]

System	Measured Elemental Analyses (wt%)											
	C		H		N		S		O^b	H/C	N/C	S/C
	x	*s*	*x*	*s*	*x*	*s*	*x*	*s*		*x*	*x*	*x*
Group I												
Solvent: kerosene												
Untreated bitumen	83.55	0.38	11.07	0.11	0.42	0.01	3.81	0.02	1.15	1.58	0.0043	0.0171
B+W+S	83.77	0.27	10.71	0.06	0.47	0.01	3.65	0.07	1.40	1.52	0.0048	0.0163
B+W	83.84	0.05	10.64	0.03	0.46	0.01	3.74	0.08	1.32	1.51	0.0047	0.0167
B+S	84.19	0.06	10.85	0.02	0.44	0.01	3.63	0.03	0.89	1.54	0.0045	0.0162
B	82.67	0.27	10.76	0.02	0.44	0.02	3.72	0.18	2.41	1.55	0.0046	0.0169
Group II												
Solvent: *n*-hexane												
Untreated bitumen	81.67	0.21	10.70	0.18	0.52	0.13	4.30	0.07	2.80	1.56	0.0055	0.0197
B+W+S	84.00	0.05	10.38	0.19	0.48	0.01	4.13	0.06	1.01	1.47	0.0049	0.0184

Continues on the next page

System	Measured Elemental Analyses (wt%)											
	C		H		N		S		O[b]	H/C	N/C	S/C
	x	*s*	*x*	*s*	*x*	*s*	*x*	*s*		*x*	*x*	*x*
B+W	84.10	0.12	10.24	0.16	0.50	0.01	4.47	0.15	0.69	1.45	0.0051	0.0199
B+S	83.62	0.21	10.35	0.18	0.48	0.01	4.24	0.10	1.31	1.47	0.0049	0.0190
B	84.00	0.17	10.28	0.11	0.50	0.02	4.20	0.14	1.02	1.46	0.0051	0.0187
Group III												
No added solvent[c]												
Untreated bitumen	82.34	0.64	10.29	0.05	0.52	0.02	4.97	0.03	1.89	1.44	0.0048	0.0201
B+W+S	83.58	0.09	10.13	0.29	0.56	0.01	4.66	0.04	1.08	1.41	0.0051	0.0186
B+W	84.25	0.14	10.19	0.21	0.53	0.01	4.65	0.06	0.38	1.42	0.0048	0.0184
B+S	83.49	0.09	10.34	0.06	0.54	0.00	4.98	0.02	0.65	1.43	0.0050	0.0199
B	83.12	0.15	10.06	0.07	0.51	0.01	4.63	0.23	1.68	1.40	0.0047	0.0186

[a] Average (x) and sample standard deviation (s) of analyses in duplicate. [b] Oxygen amount calculated by difference. [c] Solvent was not added prior to reaction, but 10 wt% of benzene was added to the untreated bitumen and visbroken products prior to analyses.

A.6 Measured viscosity of bitumen samples and method for viscosity correction

The dynamic viscosity of the samples was calculated by extracting the slope of the linear regression from the shear stress versus shear rate curve. All the samples presented Newtonian behavior. One example of a shear stress vs. shear rate curve from the product of the system B+S in group I experiments is shown in Figure A.4.

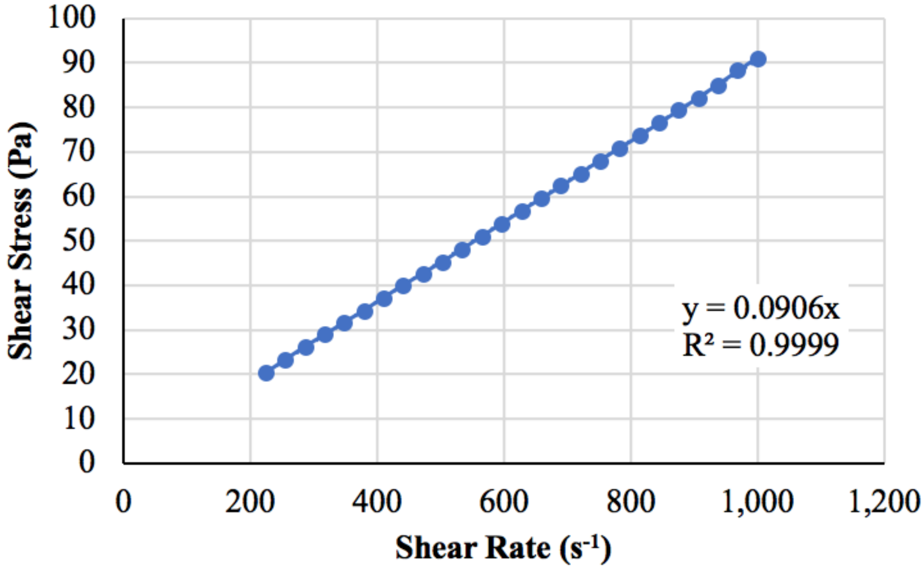

Figure A.4: Shear stress vs. shear rate curve of system B+S - Group I - measurement at 25 °C.

The measured viscosity values for the diluted bitumen samples is shown in **Table A.2**. In order to remove the dilution effect of the added solvents over the bitumen product viscosity, the correlation proposed by Miadonye et al.[2] was applied, and the results are shown as "Corrected Viscosity" in **Table 3.9**. The equations used to correct bitumen viscosity are listed in **Eq. A.2-A.4**, where v_{b+s} is the kinematic viscosity of diluted bitumen (in cSt), v_s is the kinematic viscosity of solvent (in cSt), v_b is the kinematic viscosity of bitumen (in cSt), and w_s is the mass fraction of solvent.

$$v_{b+s} = exp\ (exp\,(\alpha\,(1 - w_s^n)) + ln\,(v_s) - 1) \tag{A.2}$$

$$\alpha = ln\ (ln\,(v_b) - ln\,(v_s) + 1) \tag{A.3}$$

$$n = \frac{v_s}{0.9029v_s + 0.1351} \tag{A.4}$$

Table A.2: Measured viscosity of bitumen feed and bitumen separated from visbroken products at different temperatures.

System	Measured Viscosity (Pa·s)							
	25 °C	30 °C	35 °C	40 °C	60 °C	Slope	Intercept	R^2
Group I								
Solvent: kerosene								
Untreated bitumen	0.83	-	-	0.29	0.10	-3.416	21.370	1
B+W+S	0.076	-	-	0.037	0.017	-3.790	23.062	1
B+W	0.096	-	-	0.049	0.020	-3.799	23.176	0.995
B+S	0.091	-	-	0.043	0.019	-3.805	23.187	0.999
B	0.053	-	-	0.027	0.014	-3.664	22.253	0.999
Group II								
Solvent: *n*-hexane								
Untreated bitumen	0.49	0.35	0.27	-	-	-3.112	19.555	0.999
B+W+S	0.033	0.027	0.022	-	-	-3.454	20.926	0.999
B+W	0.041	0.032	0.027	-	-	-3.641	22.051	0.999
B+S	0.026	0.022	0.018	-	-	-3.550	21.409	0.999
B	0.019	0.016	0.014	-	-	-3.456	20.770	1
Group III								
No added solvent[a]								
Untreated bitumen	1.9	1.2	0.84	-	-	-3.455	21.708	0.999
B+W+S	0.14	0.11	0.082	-	-	-3.658	22.444	1
B+W	0.10	0.082	0.066	-	-	-3.222	19.896	0.999
B+S	0.16	0.12	0.090	-	-	-3.568	21.951	1
B	0.11	0.083	0.064	-	-	-3.492	21.436	0.999

[a] Solvent was not added prior to reaction, but 10 wt% of benzene was added to the untreated bitumen and visbroken products prior to analyses.

A.7 Measured density of bitumen samples and method for density correction

The measured density values for the diluted bitumen samples are shown in **Table A.3**. The ideal mixture rule (**Eq. A.5**) was used for correcting bitumen density by removing the solvent contribution to the density of the mixture. In **Eq.A.5**, ρ_{b+s} is the density of diluted bitumen, w_s and w_b are the mass fractions of solvent and bitumen, while ρ_s and ρ_b are the densities of solvent and bitumen, respectively.

$$\rho_{b+s} = \frac{1}{\left(\frac{w_s}{\rho_s}\right) + \left(\frac{w_b}{\rho_b}\right)} \tag{A.5}$$

Table A.3: Measured density (ρ) of bitumen feed and bitumen separated from visbroken products at different temperatures.

System	Measured Density (kg/m^3)							
	25 °C	30 °C	35 °C	40 °C	60 °C	Slope	Intercept	R^2
Group I								
Solvent: kerosene								
Untreated bitumen	961.33	-	-	951.41	937.98	-0.667	978.05	1
B+W+S	948.99	-	-	938.61	924.79	-0.691	966.27	1
B+W	952.15	-	-	941.8	927.98	-0.691	969.42	1
B+S	948.92	-	-	938.54	924.71	-0.692	966.21	1
B	945.53	-	-	935.11	921.17	-0.696	962.94	1
Group II								
Solvent: *n*-hexane								
Untreated bitumen	940.68	937.31	933.91	-	-	-0.677	957.61	1
B+W+S	923.57	920.01	916.42	-	-	-0.715	941.45	1
B+W	921.24	917.74	914.21	-	-	-0.703	938.82	1
B+S	908.62	904.93	899.82	-	-	-0.880	930.86	0.991
B						-0.719	931.68	1
Group III								
No added solvent[a]								
Untreated bitumen	990.43	987.05	983.67	-	-	-0.676	1007.33	1
B+W+S	975.99	972.45	968.89	-	-	-0.710	993.74	1
B+W	970.38	966.83	963.29	-	-	-0.709	988.10	1
B+S	976.84	973.31	969.61	-	-	-0.723	994.94	0.999
B	973.09	969.42	965.27	-	-	-0.782	992.72	0.999

[a] Solvent was not added prior to reaction, but 10 wt% of benzene was added to the untreated bitumen and visbroken products prior to analyses.

A.8 Measured refractive index of bitumen samples and method for refractive index correction

The measured refractive index (RI) values for the diluted bitumen samples are shown in **Table A.4**. As already mentioned in the experimental section of the paper, the RI measurements of group I experiments did not vary with time. However, the measurements of groups II and III experiments presented solvent evaporation, and a different procedure for taking the measurements had to be used.

In order to correct the RI values (by removing the contribution of the added solvent) from group I experiments, the Eykman correlation (**Eq. A.6**) was used [1]. In **Eq. A.6**, n_{b+s} is the refractive index of the diluted bitumen, n_b and n_s are the refractive indices of bitumen and solvent, while φ_b and φ_s are the volume fractions of bitumen and solvent, respectively. **Eq. A.7** was used to determine the volumetric fraction of the solvent in the mixture, where φ_s is the volumetric fraction of solvent, w_s and w_b are the mass fractions of solvent and bitumen, and ρ_s and ρ_b are the densities of solvent and bitumen, respectively. The values used for ρ_b were the corrected bitumen densities shown in **Table 3.11**.

$$\frac{n_{b+s}^2 - 1}{n_{b+s}^2 + 0.4} = \varphi_b \left(\frac{n_b^2 - 1}{n_b^2 + 0.4} \right) + \varphi_s \left(\frac{n_s^2 - 1}{n_s^2 + 0.4} \right) \tag{A.6}$$

$$\varphi_s = \frac{\dfrac{w_s}{\rho_s}}{\dfrac{w_s}{\rho_s} + \dfrac{w_b}{\rho_b}} \tag{A.7}$$

For groups II and III experiments, measurements were taken at 35 °C every 10 min, from 10 to 60 min. At the 60-min mark (when solvent evaporation ramped down), measurements at 25 and 30 °C were also taken. Then, the variation of the refractive index value between 10 and 60 min (at 35 °C) was used to estimate the solvent evaporation during that period. Once the loss of solvent was estimated, the residual solvent in the samples was calculated, and this value was used to find the volumetric fraction of solvent to be used in **Eq. A.6** to correct the RI values at 25, 30, and 35 °C. The estimation of the loss of solvent during the 10-60 min time period at 35 °C is detailed in the following steps:

1- The refractive index values at 10 and 60 min were input in the Eykman correlation (**Eq. A.8**), where n_{10} is the refractive index of the bitumen/solvent mixture at 35 °C after 10 min and n_{60} is the measurement after 60 min.

$$\frac{n_{10}^2 - 1}{n_{10}^2 + 0.4} = \varphi_b \left(\frac{n_{60}^2 - 1}{n_{60}^2 + 0.4} \right) + \varphi_s \left(\frac{n_s^2 - 1}{n_s^2 + 0.4} \right) \tag{A.8}$$

2- As both the refractive index and volumetric fraction of solvent varied at the same time in the 10-60 min period, the ideal mixture rule for density (**Eq. A.9**) and the volumetric fraction of solvent (**A.7**) were solved simultaneously with the Eykman correlation to give the mass fraction of solvent that evaporated in that period. The values used for the mixture density (ρ_{b+s}) in **Eq. A.9** were the measured density values shown in **Table A.3**.

$$\rho_{b+s} = \frac{1}{\dfrac{w_s}{\rho_s} + \dfrac{w_b}{\rho_b}} \tag{A.9}$$

3- The difference between the initial solvent content and the evaporated solvent was calculated and the residual solvent in the mixture was used to correct the RI values at 25, 30 and 35 °C by using **Eq. A.6** and **A.7**. The residual solvent after 60 min for each system is shown in **Table A.5**.

Table A.4: Measured refractive index (*n*) of bitumen feed and bitumen separated from visbroken products at different temperatures.

System	Measured Refractive Index						
	25 °C	30 °C	35 °C	40 °C	60 °C	d*n* /dT	R^2
Group I							
Solvent: kerosene							
Untreated bitumen	1.5423	-	-	1.5363	1.5286	-3.9E-04	0.999
B+W+S	1.5458	-	-	1.5400	1.5325	-3.8E-04	0.999
B+W	1.5474	-	-	1.5414	1.5334	-4.0E-04	1
B+S	1.5436	-	-	1.5383	1.5315	-3.5E-04	0.999
B	1.5411	-	-	1.5351	1.5276	-3.9E-04	0.999
Group II							
Solvent: *n*-hexane							
Untreated bitumen	1.5475	1.5454	1.5432	-	-	-4.3E-04	0.999
B+W+S	1.5697	1.5676	1.5655	-	-	-4.2E-04	1
B+W	1.5633	1.5613	1.5594	-	-	-3.9E-04	0.999
B+S	1.5707	1.5687	1.5667	-	-	-4.0E-04	1
B	1.5769	1.5747	1.5727	-	-	-4.2E-04	0.999
Group III							
No added solvent[a]							
Untreated bitumen	1.5650	1.5628	1.5607	-	-	-4.3E-04	0.999
B+W+S	1.5760	1.5739	1.5719	-	-	-4.2E-04	1
B+W	1.5690	1.5670	1.5649	-	-	-4.1E-04	0.999
B+S	1.5635	1.5618	1.5598	-	-	-3.7E-04	0.998
B	1.5696	1.5676	1.5654	-	-	-4.2E-04	0.999

[a] Solvent was not added prior to reaction, but 10 wt% of benzene was added to the untreated bitumen and visbroken products prior to analyses.

Table A.5: Refractive index values at 10 and 60 min and residual solvent in groups II and III.

System	Refractive Index at 35 °C		Solvent content after evaporation (wt%)
	10 min	60 min	
Group II			
Solvent: *n*-hexane			
Untreated bitumen	1.5365	1.5432	10.7
B+W+S	1.5552	1.5655	9.9
B+W	1.5450	1.5594	8.5
B+S	1.5584	1.5667	10.5
B	1.5671	1.5727	11.4
Group III			
No added solvent[a]			
Untreated bitumen	1.5567	1.5607	5.2
B+W+S	1.5671	1.5719	5.0
B+W	1.5586	1.5649	2.8
B+S	1.5566	1.5598	6.1
B	1.5589	1.5654	2.6

[a] Solvent was not added prior to reaction, but 10 wt% of benzene was added to the untreated bitumen and visbroken products prior to analyses.

A.9 Measured and corrected free radical content

The measured free radical content for the bitumen samples diluted with kerosene is shown in **Table A.6**. The kerosene added to the feed did not contain any free radicals in its composition, and, therefore, the corrected free radical content (also shown in **Table A.6**) was obtained by mass balance to report the radicals concentration per mass of bitumen only.

Table A.6: Measured and corrected free radical content of untreated bitumen and bitumen separated from visbroken products in group I experiments.

System	Measured Free Radical Content (10^{18} spins/g of diluted bitumen)[a]		Corrected Free Radical Content (10^{18} spins/g of diluted bitumen)[a]	
	x	*s*	*x*	*s*
Untreated bitumen	1.43	0.03	1.79	0.03
B+W+S	1.36	0.04	1.70	0.06
B+W	1.63	0.07	2.03	0.08
B+S	1.29	0.03	1.61	0.03
B	1.59	0.02	1.98	0.03

[a] Average (*x*) and sample standard deviation (*s*) of analyses in triplicate.

A.10 Measured aliphatic and aromatic hydrogen content

Table A.7: Measured aliphatic and aromatic hydrogen content based on ^{1}H NMR spectra of visbroken products.

System	Aliphatic H Content (%)[a]		Aromatic H Content (%)[a]	
	x	s	x	s
Group I				
Solvent: kerosene				
Untreated bitumen	93.5	0.3	6.5	0.3
B+W+S	93.5	0.3	6.5	0.3
B+W	93.2	0.3	6.8	0.3
B+S	93.1	0.2	6.9	0.2
B	91.9	0.2	8.1	0.2
Group II				
Solvent: *n*-hexane				
Untreated bitumen	95.8	0.1	4.2	0.1
B+W+S	93.3	0.4	6.7	0.4
B+W	94.9	0.5	5.1	0.5
B+S	94.9	0.2	5.1	0.2
B	93.9	0.1	6.1	0.1
Group III				
No added solvent[a]				
Untreated bitumen	86.2	0.6	13.8	0.6
B+W+S	86.5	0.3	13.5	0.3
B+W	85.6	0.8	14.4	0.8
B+S	87.9	0.5	12.1	0.5
B	85.1	0.2	14.9	0.2

[a] Solvent was not added prior to reaction, but 10 wt% of benzene was added to the untreated bitumen and visbroken products prior to analyses.

A.11 Measured aliphatic and aromatic carbon content

Table A.8: Measured aliphatic and aromatic carbon content based on ^{13}C NMR spectra of visbroken products.

System	Saturated (aliphatic) C Content (%)[a]	Aromatic C Content (%)[a]
Group I		
Solvent: kerosene		
Untreated bitumen	77.2	22.8
B+W+S	69.6	30.4
B+W	71.4	28.6
B+S	71.2	28.8
B	73.0	27.0
Group II		
Solvent: *n*-hexane		
Untreated bitumen	72.2	27.8
B+W+S	67.4	32.6
B+W	71.4	28.6
B+S	70.9	29.1
B	69.3	30.7
Group III		
No added solvent[b]		
Untreated bitumen	63.6	36.4
B+W+S	60.7	39.3
B+W	60.3	39.7
B+S	60.8	39.2
B	59.7	40.3

[a] Analysis performed on a single sample. [b] Solvent was not added prior to reaction, but 10 wt% of benzene was added to the untreated bitumen and visbroken products prior to analyses.

A.12 References

(1) Kurnia, K. A.; Taib, M. M.; Mutalib, M. A.; Murugesan, T. Densities, refractive indices and excess molar volumes for binary mixtures of protic ionic liquids with methanol at T= 293.15 to 313.15 K. *J. Mol. Liq.* **2011**, *159* (3), 211–219.

(2) Miadonye, A.; Latour, N.; Puttagunta, V. R. A correlation for viscosity and solvent mass fraction of bitumen-diluent mixtures. *Pet. Sci. Technol.* **2000**, *18* (1), 1–14.

(3) Yan, T. Characterization of visbreaker feeds. *Fuel* **1990**, *69* (8), 1062–1064.

Appendix B: Supporting information for Chapter 4

B.1 Calibration curves for AMS and cumene quantification through GC-FID

The acquired data for building the calibration curves for AMS and cumene in methanol is shown in this section. **Tables B.1** and **B.2** contain the concentration of each compound to be quantified (C_{AMS} and C_{cumene}) and the concentration of the internal standard biphenyl (C_{biph}) in the methanol extract, as well as the areas obtained under the peaks of each interest compound and biphenyl in the GC-FID chromatogram. The concentration and area ratios were calculated and used to plot the calibration curves (**Figures B.1** and **B.2**). Once the calibration curves had been plotted, linear interpolation was applied to get the equations (**Eq. B.1** and **B.2**) that were used for product quantification.

B.1.1 Calibration curve for AMS

Table B.1: Concentration and areas used for the AMS calibration curve.

C_{AMS} (wt%)	C_{biph} (wt%)	A_{AMS}	A_{biph}	C_{AMS}/C_{biph}	A_{AMS}/A_{biph}
0.00562	0.01292	142.4	353.1	0.4350	0.4033
0.01566	0.01305	394.4	351.5	1.1996	1.1220
0.03125	0.01257	742.5	320.6	2.4860	2.3160
0.05190	0.01267	1305.5	337.6	4.0951	3.8670

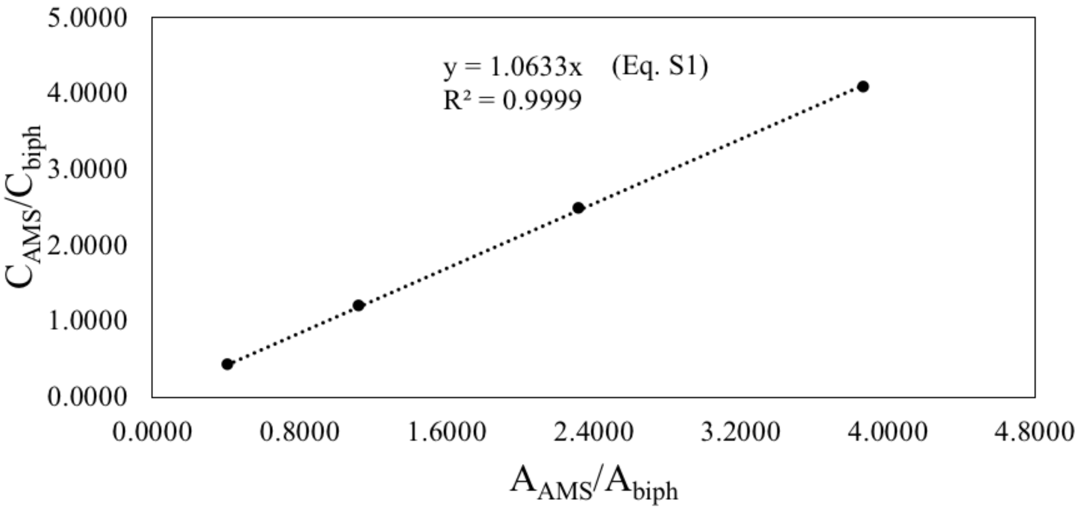

Figure B.1: Calibration curve for AMS.

$$y = 1.0633x \tag{B.1}$$

B.1.2 Calibration curve for cumene

Table B.2: Concentration and areas used for the cumene calibration curve.

C_{cumene} (wt%)	C_{biph} (wt%)	A_{cumene}	A_{biph}	C_{cumene}/C_{biph}	A_{cumene}/A_{biph}
0.0054	0.0131	140.8	362.5	0.4118	0.3884
0.0169	0.0129	440.8	361.6	1.3106	1.2190
0.0316	0.0126	776.5	331.8	2.5025	2.3403
0.0531	0.0123	1309.6	319.1	4.3210	4.1040

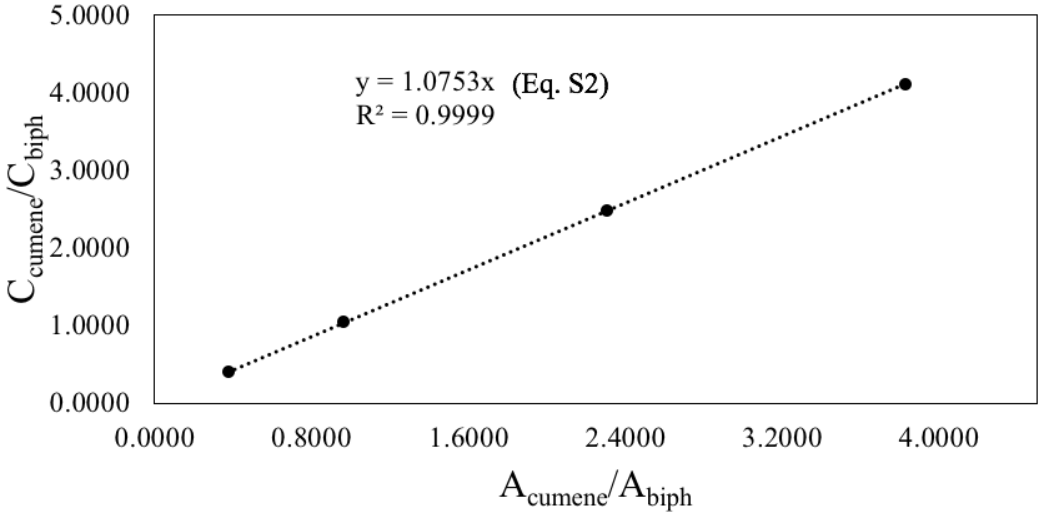

Figure B.2: Calibration curve for cumene.

$$y = 1.0753x \tag{B.2}$$

B.2 Extraction efficiency of AMS and cumene in methanol

In order to evaluate the extraction efficiency of AMS and cumene in methanol, three extractions were performed for each component following the procedure described in **Section 4.2.2.2** of the manuscript. A known amount of AMS and cumene were individually added to bitumen, extracted using methanol, and quantified through GC-FID. The results are shown in **Table B.3**.

Table B.3: Extraction efficiency of AMS and cumene in methanol.

Compound	Extraction efficiency (%)[a]				
	Extraction 1	Extraction 2	Extraction 3	*x*	*s*
AMS	107.0	105.0	103.8	105.3	1.6
cumene	105.9	104.4	102.7	104.3	1.6

[a] Average (*x*) and sample standard deviation (*s*) of three extractions.

B.3 Commercial standards used for peaks identification in the GC-MS spectra

A total of 77 commercial standards were used for compound identification in the GC-MS spectra. The list of these commercial standards, their molecular weight, and their retention times (RT) in the GC-MS spectra are shown in **Table B.4**.

Table B.4: Commercial standards used for compound identification through GC-MS.

Compound	Formula	CASRN[a]	Purity (%)[b]	Supplier	Molecular weight (g/mol)	RT (min)
hexane	C_6H_{14}	110-54-3	95	Sigma Aldrich	86.18	4.7
benzene	C_6H_6	71-43-2	99.8	Sigma Aldrich	78.11	6.3
cyclohexane	C_6H_{12}	110-82-7	99.9	Sigma Aldrich	84.16	6.6
heptane	C_7H_{16}	142-82-5	98	Fisher Scientific	100.21	8.3
methylcyclohexane	C_7H_{14}	108-87-2	99	Acros Organics	98.19	9.2
toluene	C_7H_8	108-88-3	99.9	Fisher Scientific	92.14	11.0
octane	C_8H_{18}	111-65-9	95	Fisher Scientific	114.23	13.5
ethylcyclohexane	C_8H_{16}	1678-91-7	99	Sigma Aldrich	112.21	15.2
ethylbenzene	C_8H_{10}	100-41-4	99	Sigma Aldrich	106.16	16.2
m-xylene	C_8H_{10}	108-38-3	99	Sigma Aldrich	106.17	16.7
p-xylene	C_8H_{10}	106-42-3	99	Sigma Aldrich	106.17	16.8
styrene	C_8H_8	100-42-5	99	Sigma Aldrich	104.15	17.7

Continues on the next page

Compound	Formula	CASRN[a]	Purity (%)[b]	Supplier	Molecular weight (g/mol)	RT (min)
o-xylene	C_8H_{10}	95-47-6	99	Sigma Aldrich	106.17	18.0
nonane	C_9H_{20}	111-84-2	99	Thermo Scientific	128.26	19.4
cumene	C_9H_{12}	98-82-8	98	Sigma Aldrich	120.19	20.0
isopropylcyclohexane	C_9H_{18}	696-29-7	99	TCI	126.24	20.4
propylcyclohexane	C_9H_{18}	1678-92-8	98	TCI	126.24	20.9
n-propylbenzene	C_9H_{12}	103-65-1	98	Sigma Aldrich	120.2	21.7
3-ethyltoluene	C_9H_{12}	620-14-4	98	TCI	120.2	22.1
4-ethyltoluene	C_9H_{12}	622-96-8	97	Thermo Scientific	120.2	22.2
mesitylene (1,3,5-trimethylbenzene)	C_9H_{12}	108-67-8	98	Sigma Aldrich	120.19	22.6
2-ethyltoluene	C_9H_{12}	611-14-3	99	Sigma Aldrich	120.2	23.1
AMS (alphamethylstyrene)	C_9H_{10}	98-83-9	99	Sigma Aldrich	118.18	23.1
1,2,4-trimethylbenzene	C_9H_{12}	95-63-6	98	Sigma Aldrich	120.19	23.9
tert-butylbenzene	$C_{10}H_{14}$	1998-06-06	99	Sigma Aldrich	134.22	23.9
isobutylbenzene	$C_{10}H_{14}$	538-93-2	99	Sigma Aldrich	134.22	24.8
sec-butylbenzene	$C_{10}H_{14}$	135-98-8	99	Sigma Aldrich	134.22	24.9
decane	$C_{10}H_{22}$	124-18-5	94	Sigma Aldrich	142.28	25.1
1,2,3- trimethylbenzene	C_9H_{12}	526-73-8	-[d]	Sigma Aldrich	120.19	25.4
phenylacetaldehyde	C_8H_8O	122-78-1	95	Sigma Aldrich	120.15	25.5
m-cymene	$C_{10}H_{14}$	535-77-3	99	Sigma Aldrich	134.22	25.6

Continues on the next page

Compound	Formula	CASRN[a]	Purity (%)[b]	Supplier	Molecular weight (g/mol)	RT (min)
p-cymene	$C_{10}H_{14}$	99-87-6	99	Sigma Aldrich	134.22	25.7
indane	C_9H_{10}	496-11-7	95	Acros Organics	118.18	26.0
indene	C_9H_8	95-13-6	90	Sigma Aldrich	116.16	26.4
o-cymene	$C_{10}H_{14}$	527-84-4	98	Sigma Aldrich	134.22	26.5
acetophenone	C_8H_8O	98-86-2	98	Sigma Aldrich	120.15	26.9
1-phenylethanol	$C_8H_{10}O$	98-85-1	98	Sigma Aldrich	122.16	27.1
3-propyltoluene	$C_{10}H_{14}$	1074-43-7	99	TCI	134.22	27.2
4-propyltoluene	$C_{10}H_{14}$	1074-55-1	99	TCI	134.22	27.3
n-butylbenzene	$C_{10}H_{14}$	104-51-8	99	Sigma Aldrich	134.22	27.3
decalin (decahydronaphthalene (cis/trans))	$C_{10}H_{18}$	91-17-8	99	Sigma Aldrich	138.25	27.9 & 30.1
2-propyltoluene	$C_{10}H_{14}$	1074-17-5	98	TCI	134.22	28.1
2-phenyl-2-propanol	$C_9H_{12}O$	617-94-7	98	TCI	136.19	28.4
2-phenylpropionaldehyde	$C_9H_{10}O$	93-53-8	95	Sigma Aldrich	134.18	29.1
2-phenylethanol	$C_8H_{10}O$	1960-12-08	98	Thermo Scientific	122.17	29.8
undecane	$C_{11}H_{24}$	1120-21-4	99	Sigma Aldrich	156.31	30.6
1-phenyl-2-propanol	$C_9H_{12}O$	698-87-3	98	Sigma Aldrich	136.19	30.9
3-phenylpropionaldehyde	$C_9H_{10}O$	104-53-0	95	Thermo Scientific	134.18	31.9
propiophenone	$C_9H_{10}O$	93-55-0	99	Sigma Aldrich	134.18	32.3
tetralin (1,2,3,4-tetrahydronaphthalene)	$C_{10}H_{12}$	119-64-2	99	Sigma Aldrich	132.2	32.8

Continues on the next page

Compound	Formula	CASRN[a]	Purity (%)[b]	Supplier	Molecular weight (g/mol)	RT (min)
n-pentylbenzene	$C_{11}H_{16}$	538-68-1	96	Alfa Aesar	148.24	32.9
naphthalene	$C_{10}H_8$	91-20-3	99	Sigma Aldrich	128.17	33.7
3-phenyl-1-propanol	$C_9H_{12}O$	122-97-4	98	Sigma Aldrich	136.19	35.6
dodecane	$C_{12}H_{26}$	112-40-30	99	Honeywell	170.33	35.7
2-methylnaphthalene	$C_{11}H_{10}$	91-57-6	97	Alfa Aesar	142.2	38.8
1-methylnaphthalene	$C_{11}H_{10}$	90-12-0	96	Alfa Aesar	142.2	39.5
tridecane	$C_{13}H_{28}$	629-50-5	99	Acros Organics	184.37	39.9
cis-decahydro-1-naphthol	$C_{10}H_{18}O$	207127-50-2	99	Sigma Aldrich	154.25	40.4
β-tetralone	$C_{10}H_{10}O$	530-93-8	98	Sigma Aldrich	146.19	40.8
1,5-dimethyltetralin	$C_{12}H_{16}$	21564-91-0	90	Sigma Aldrich	160.26	41.5
α-tetralone	$C_{10}H_{10}O$	529-34-0	97	Sigma Aldrich	146.19	41.5
biphenyl	$C_{12}H_{10}$	92-52-4	99.5	Sigma Aldrich	154.21	42.1
2,6-dimethylnaphthalene	$C_{12}H_{12}$	581-42-0	99	Sigma Aldrich	156.22	43.2
2,7-dimethylnaphthalene	$C_{12}H_{12}$	582-16-1	99	Sigma Aldrich	156.23	43.3
tetradecane	$C_{14}H_30$	629-59-4	99	Alfa Aesar	198.39	43.9
5,6,7,8-tetrahydro-1-naphthol	$C_{10}H_{12}O$	529-35-1	98	TCI	148.21	44.4
1,4-dimethylnaphthalene	$C_{12}H_{12}$	571-58-4	95	Sigma Aldrich	156.23	44.4
5,6,7,8-tetrahydro-2-naphthol	$C_{10}H_{12}O$	1125-78-6	98	Thermo Scientific	148.2	45.0
1,8-dimethylnaphthalene	$C_{12}H_{12}$	569-41-5	95	Sigma Aldrich	156.22	45.5

Continues on the next page

Compound	Formula	CASRN[a]	Purity (%)[b]	Supplier	Molecular weight (g/mol)	RT (min)
1-naphtol	$C_{10}H_8O$	90-15-3	-[d]	Sigma Aldrich	144.17	46.2
2-naphthol	$C_{10}H_8O$	135-19-3	98	Sigma Aldrich	144.17	46.6
pentadecane	$C_{15}H_{32}$	629-62-9	99	Acros Organics	212.42	47.2
2,4-diphenyl-4-methyl-1-Pentene	$C_{18}H_{20}$	6362-80-7	97	Sigma Aldrich	236.35	55.2
dicumene ((1,1,2-trimethyl-2-phenylpropyl)benzene)	$C_{18}H_{12}$	1889-67-4	-[d]	Sigma Aldrich	238.38	56.0
1-phenylnaphthalene	$C_{16}H_{12}$	605-02-7	97	Thermo Scientific	204.27	56.6
1-benzylnaphthalene	$C_{17}H_{14}$	611-45-0	-[d]	Sigma Aldrich	218.3	60.0
2-benzylnaphthalene	$C_{17}H_{14}$	613-59-2	-[d]	Sigma Aldrich	218.3	60.6

[a] Chemical Abstracts Services Registry Number (CASRN). [b] Purity of material provided by the supplier. Material was not further purified. [c] Mol% purity. [d] The supplier does not guarantee purity.

B.4 GC-MS chromatograms from thermal treatment experiments and control experiments B+AMS and K+AMS

To improve clarity for peak reading and labeling, the chromatograms obtained by GC-MS from the thermal treatment and the control experiments B+AMS and K+AMS were split into eight sections (A to H). The chromatograms for each region with an RT between 4.2 and 80 minutes are shown in the next subsections. The peaks were assigned peak identifier codes, which are listed in the tables in each of the following subsections.

B.4.1 Region A – RT between 4.2 and 14.5 min

Table B.5: Peak identifier and RT of compounds identified in the region A of the GC-MS chromatograms.

Compound	Peak identifier	RT (min)
hexane	A1	4.7
benzene	A2	6.3
cyclohexane	A3	6.6
heptane	A4	8.3
methylcyclohexane	A5	9.2
toluene	A6	11.0
octane	A7	13.5

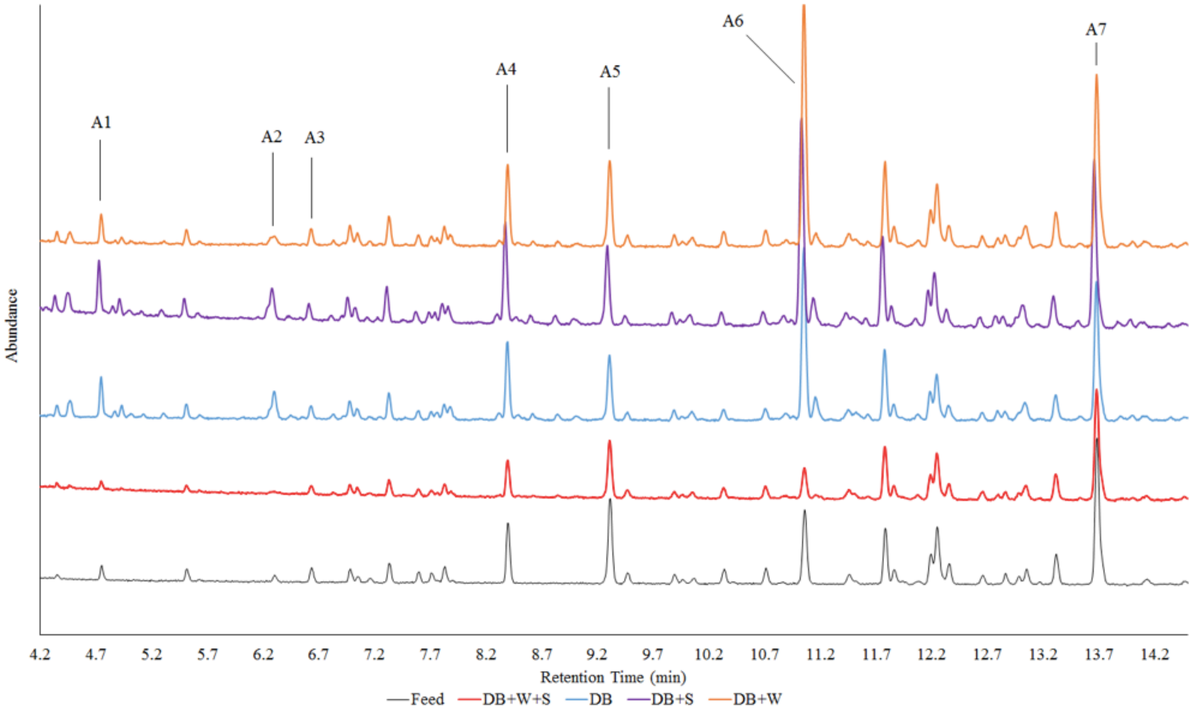

Figure B.3: GC-MS chromatograms from thermal treatment experiments - Region A (RT between 4.2 and 14.5 min).

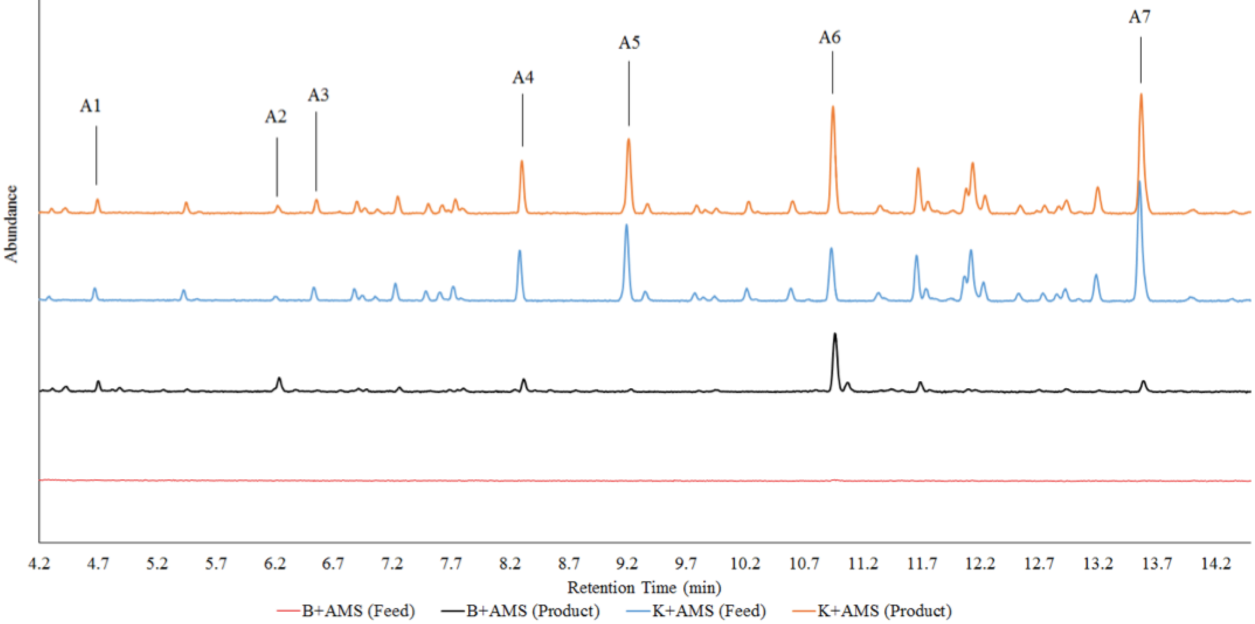

Figure B.4: GC-MS chromatograms from control experiments B+AMS and B+K - Region A (RT between 4.2 and 14.5 min).

B.4.2 Region B – RT between 14.5 and 20.5 min

Table B.6: Peak identifier and RT of compounds identified in the region B of the GC-MS chromatograms.

Compound	**Peak identifier**	**RT (min)**
ethylcyclohexane	B1	15.2
ethylbenzene	B2	16.2
m-xylene	B3	16.7
p-xylene	B4	16.8
styrene	B5	17.7
o-xylene	B6	18.0
nonane	B7	19.4
cumene	B8	20.0
isopropylcyclohexane	B9	20.4

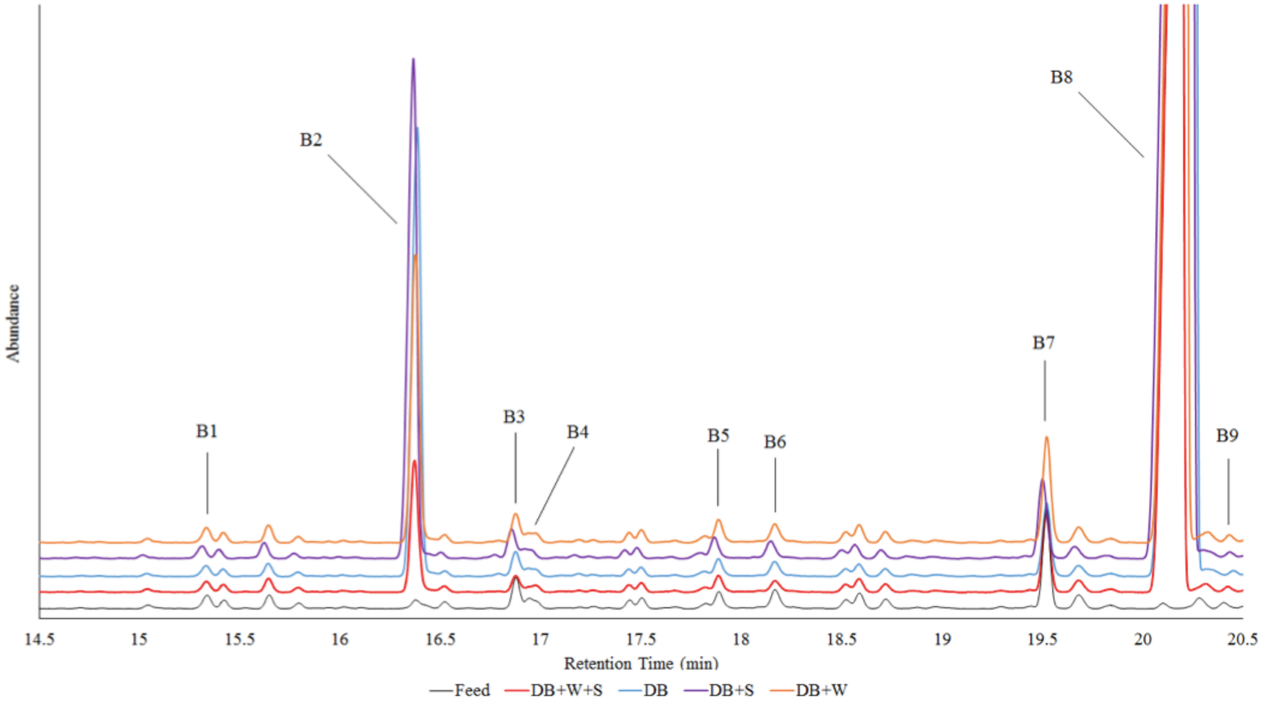

Figure B.5: GC-MS chromatograms from thermal treatment experiments - Region B (RT between 14.5 and 20.5 min).

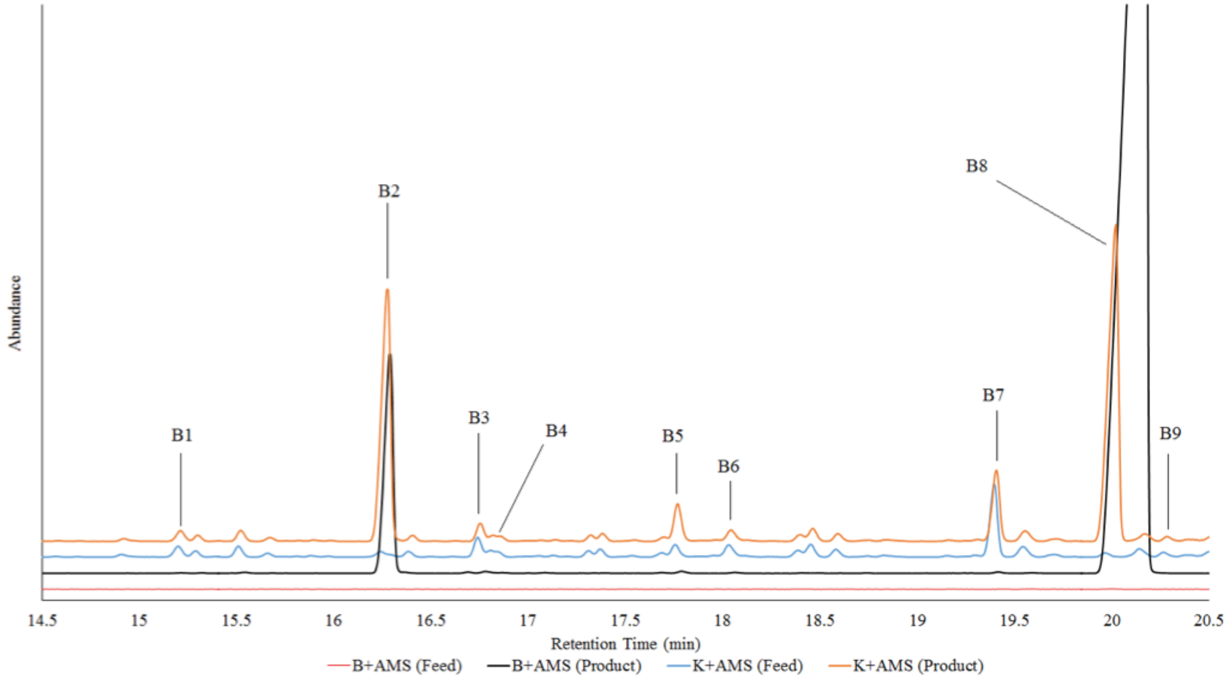

Figure B.6: GC-MS chromatograms from control experiments B+AMS and B+K - Region B (RT between 14.5 and 20.5 min).

B.4.3 Region C – RT between 20.5 and 26 min

Table B.7: Peak identifier and RT of compounds identified in the region B of the GC-MS chromatograms.

Compound	Peak identifier	RT (min)
propylcyclohexane	C1	20.9
n-propylbenzene	C2	21.7
3-ethyltoluene	C3	22.1
4-ethyltoluene	C4	22.2
mesitylene (1,3,5-trimethylbenzene)	C5	22.6
AMS & 2-ethyltoluene	C6	23.1
tert-butylbenzene & 1,2,4-trimethylbenzene	C7	23.9
isobutylbenzene	C8	24.8
sec-butylbenzene	C9	24.9
decane	C10	25.1
1,2,3- trimethylbenzene	C11	25.4
phenylacetaldehyde	C12	25.5
m-cymene	C13	25.6
p-cymene	C14	25.7

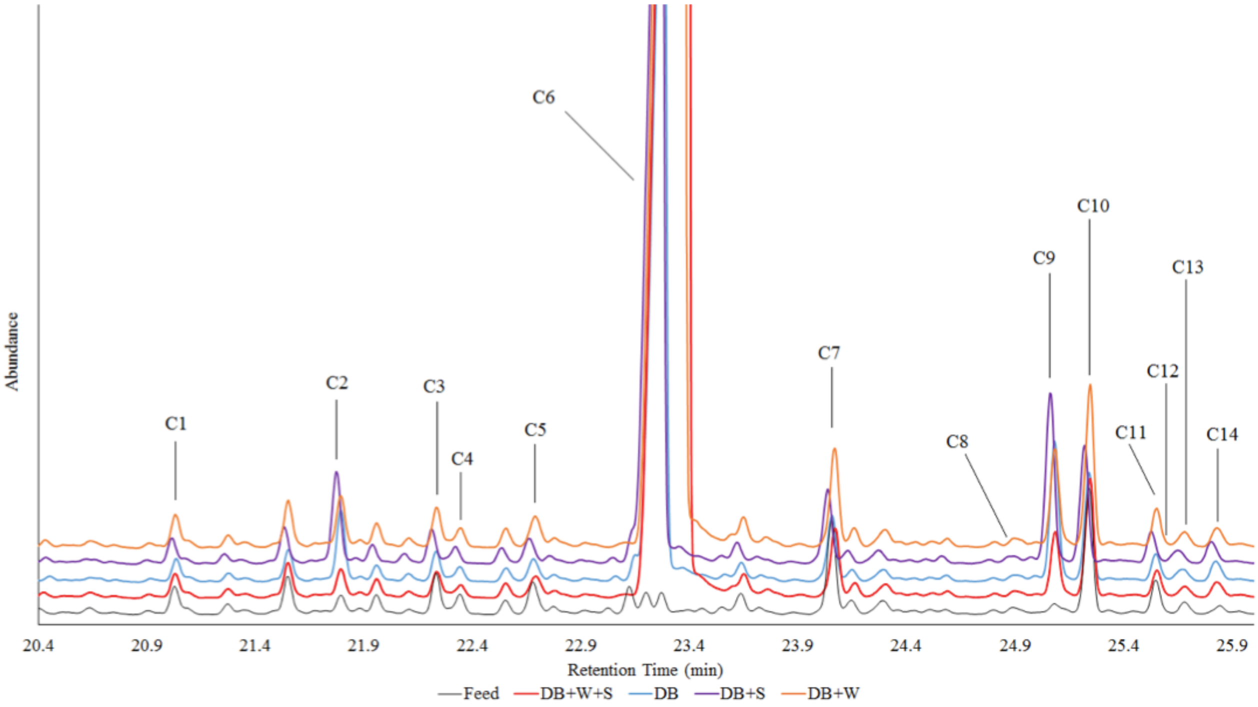

Figure B.7: GC-MS chromatograms from thermal treatment experiments - Region C (RT between 20.5 and 26 min).

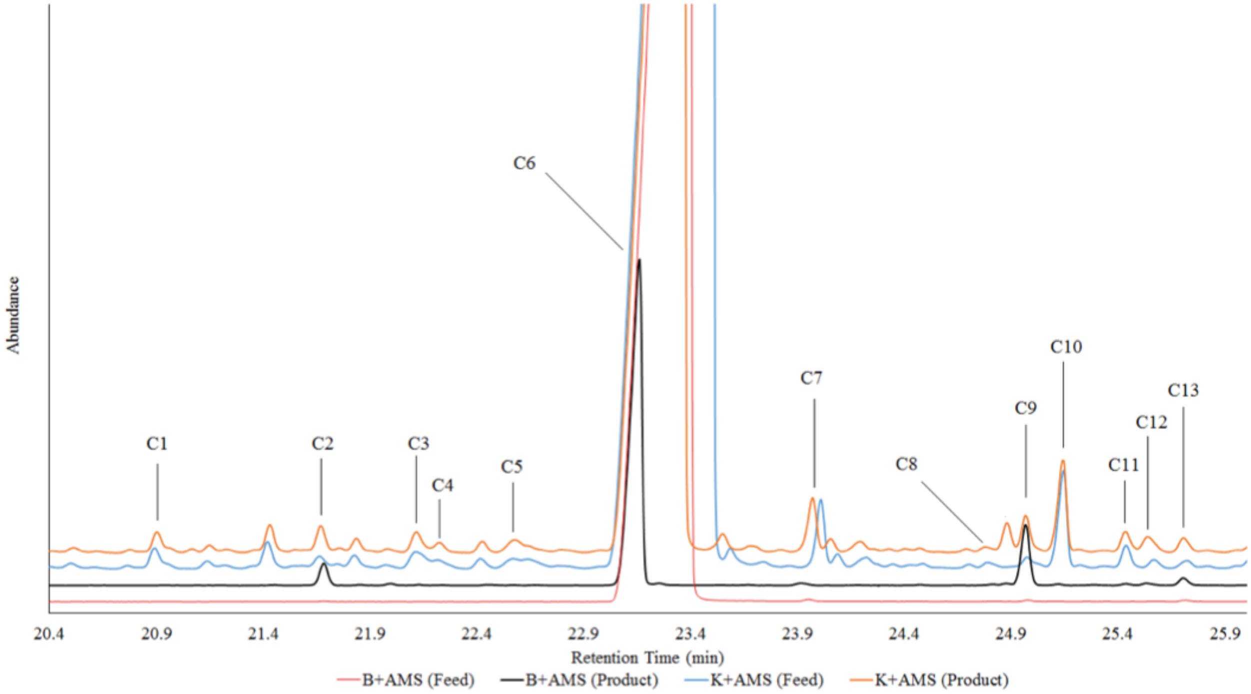

Figure B.8: GC-MS chromatograms from control experiments B+AMS and B+K - Region C (RT between 20.5 and 26 min).

B.4.4 Region D – RT between 26 and 34.5 min

Table B.8: Peak identifier and RT of compounds identified in the region D of the GC-MS chromatograms.

Compound	**Peak identifier**	**RT (min)**
indane	D1	26.0
indene	D2	26.4
o-cymene	D3	26.5
acetophenone	D4	26.9
1-phenylethanol	D5	27.1
3-propyltoluene	D6	27.2
4-propyltoluened	D7	27.3
n-butylbenzened	D8	27.3
decalin (decahydronaphthalene (cis/trans))	D9	27.9 & 30.1
2-propyltoluene	D10	28.1
2-phenyl-2-propanol	D11	28.4
2-phenylpropionaldehyde	D12	29.1
2-phenylethanol	D13	29.8
undecane	D14	30.6
1-phenyl-2-propanol	D15	30.9
3-phenylpropionaldehyde	D16	31.9
propiophenone	D17	32.3
tetralin (1,2,3,4-tetrahydronaphthalene)	D18	32.8
n-pentylbenzene	D19	32.9
naphthalene	D20	33.7

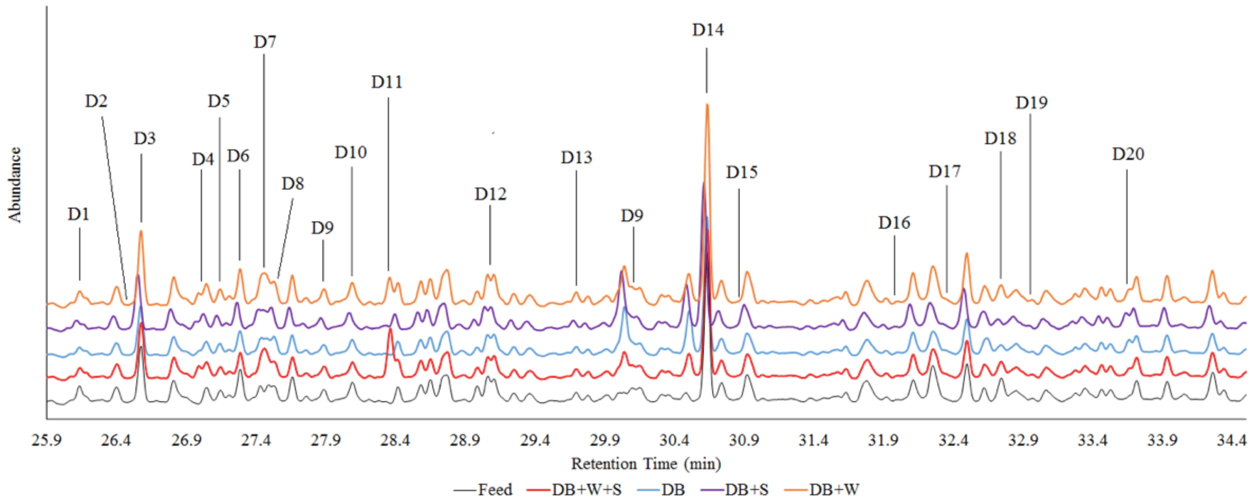

Figure B.9: GC-MS chromatograms from thermal treatment experiments - Region D (RT between 26 and 34.5 min).

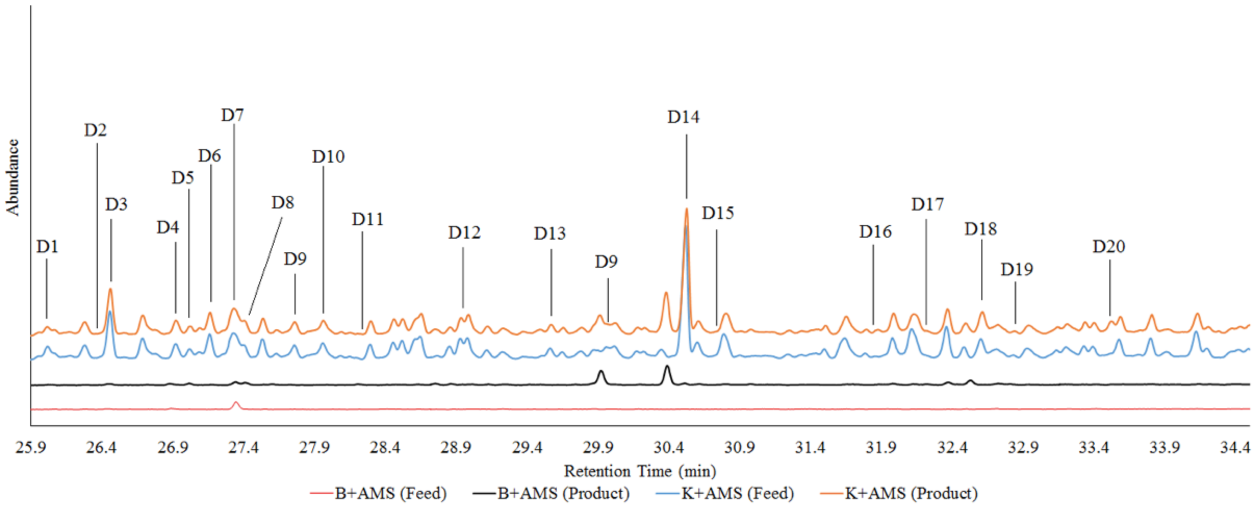

Figure B.10: GC-MS chromatograms from control experiments B+AMS and B+K - Region D (RT between 26 and 34.5 min).

B.4.5 Region E – RT between 34.5 and 42 min

Table B.9: Peak identifier and RT of compounds identified in the region E of the GC-MS chromatograms.

Compound	Peak identifier	RT (min)
3-phenyl-1-propanol	E1	35.6
dodecane	E2	35.7
2-methylnaphthalene	E3	38.8
1-methylnaphthalene	E4	39.5
tridecane	E5	39.9
cis-decahydro-1-naphthol	E6	40.4
β-tetralone	E7	40.8
1,5-dimethyltetralin + α-tetralone	E8	41.5

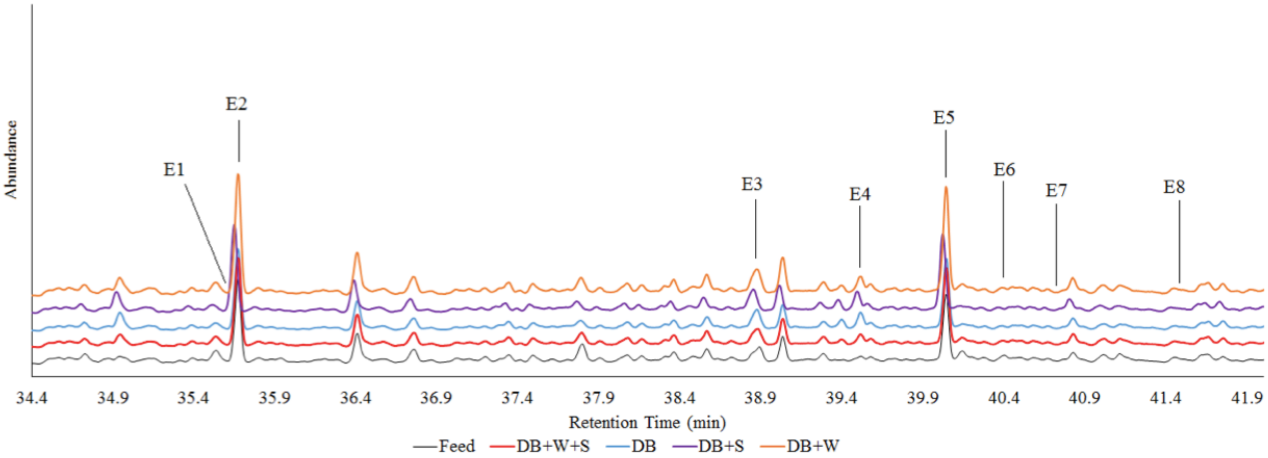

Figure B.11: GC-MS chromatograms from thermal treatment experiments - Region E (RT between 34.5 and 42 min).

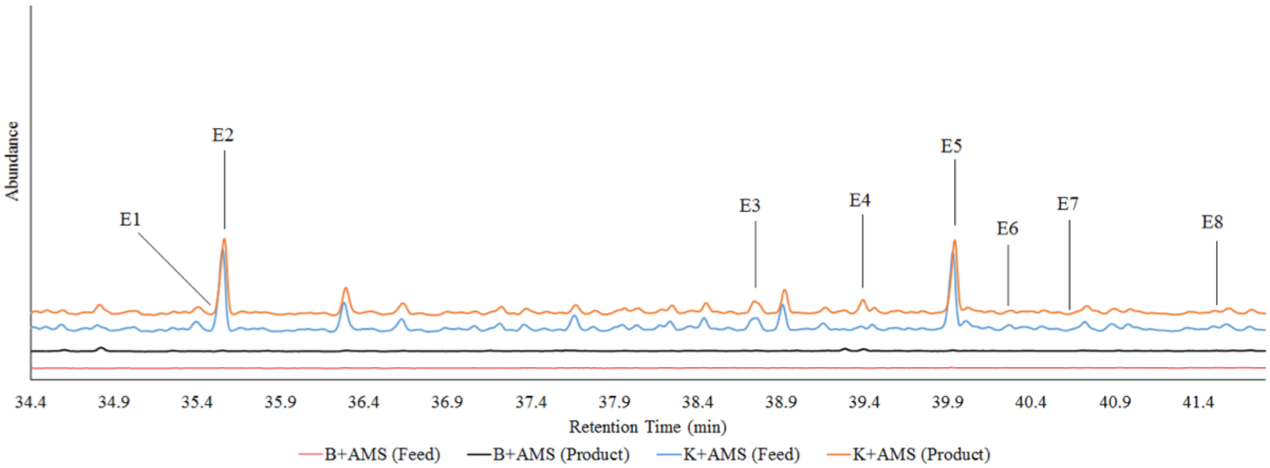

Figure B.12: GC-MS chromatograms from control experiments B+AMS and B+K - Region E (RT between 34.5 and 42 min).

B.4.6 Region F – RT between 42 and 50 min

The chromatograms in the region F for the thermal treatment of froth and the control experiments B+AMS and K+AMS are shown in **Figures B.13** and **B.14**, respectively. For the froth experiments, biphenyl was included as an internal standard only for the GC-FID analyses, and for this reason, the peak for biphenyl is not shown in **Figure B.13**. For the control experiments, biphenyl was added for both the GC-MS and GC-FID analyses, and for this reason, the peak for biphenyl is shown in **Figure B.14**. However, the peak area of biphenyl was not included for the calculation of RAP in the control experiments.

Table B.10: Peak identifier and RT of compounds identified in the region F of the GC-MS chromatograms.

Compound	Peak identifier	RT (min)
biphenyl	F1	42.1
2,6-dimethylnaphthalene	F2	43.2
2,7-dimethylnaphthalene	F3	43.3
tetradecane	F4	43.9
5,6,7,8-tetrahydro-1-naphthol	F5	44.4
1,4-dimethylnaphthalene	F6	44.4
5,6,7,8-tetrahydro-2-naphthol	F7	45.0
1,8-dimethylnaphthalene	F8	45.5
1-naphthol	F9	46.2
2-naphthol	F10	46.6
pentadecane	F11	47.2

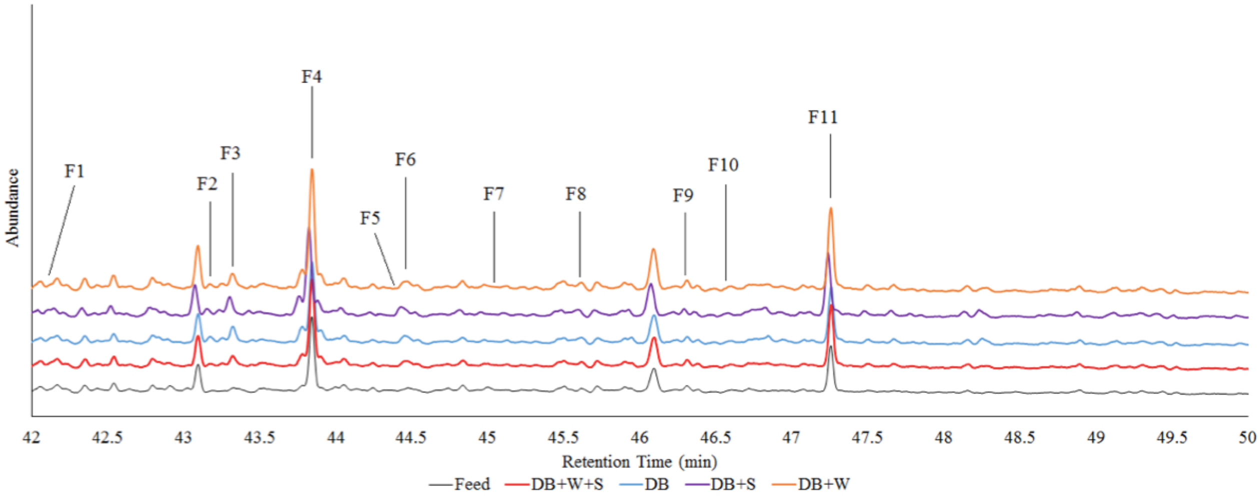

Figure B.13: GC-MS chromatograms from thermal treatment experiments - Region F (RT between 42 and 50 min).

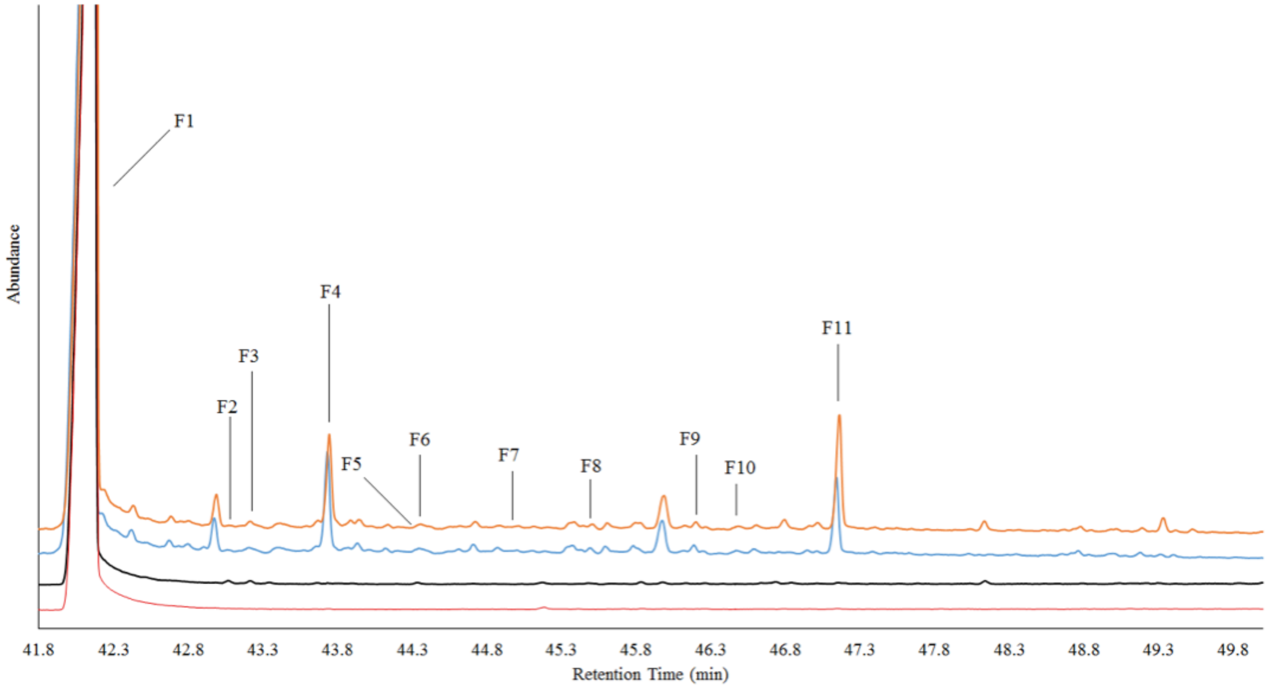

Figure B.14: GC-MS chromatograms from control experiments B+AMS and B+K - Region F (RT between 42 and 50 min).

B.4.7 Region G – RT between 50 and 62 min

The compounds identified in the RT between 50 and 62 min are listed in **Table B-11**. From that list, compounds G3, G5, G6, G9, and G11 had their identities confirmed through the use of commercial standards, while the others were obtained by suggestion from the GC-MS library.

Table B.11: Peak identifier and RT of compounds identified in the region G of the GC-MS chromatograms.

Compound	Formula	Peak identifier	RT (min)	Tentative structure[d]
$C_{18}H_{20}$ – isomer[a]	$C_{18}H_{20}$	G1	53.2	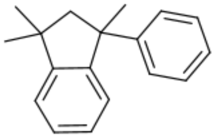
$C_{17}H_{20}$ – isomer[a]	$C_{18}H_{20}$	G2	54.8	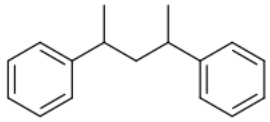
2,4-diphenyl-4-methyl-1-pentene[b,c]	$C_{18}H_{20}$	G3	55.2	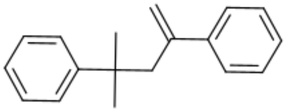
$C_{18}H_{22}$ – isomer[a]	$C_{18}H_{22}$	G3[e]	55.2	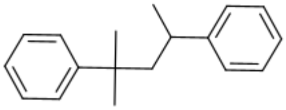 or
$C_{18}H_{22}$ – isomer[a]	$C_{18}H_{22}$	G4[e]	55.5	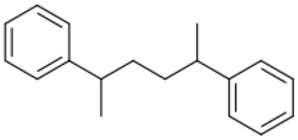
dicumene[b]	$C_{18}H_{22}$	G5	56.0	

Continues on the next page

Compound	Formula	Peak identifier	RT (min)	Tentative structure[d]
1-phenylnaphthalene[b,c]	$C_{16}H_{12}$	G6	56.6	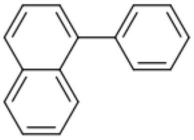
$C_{18}H_{20}$ – isomer[a]	$C_{18}H_{20}$	G6	56.6	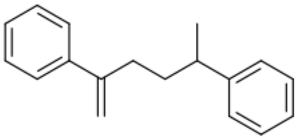
$C_{18}H_{20}$ – isomer[a]	$C_{18}H_{20}$	G7	59.2	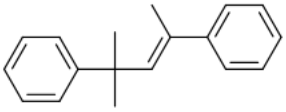
$C_{18}H_{20}$ – isomer[a]	$C_{18}H_{20}$	G8	59.4	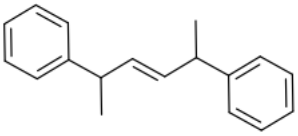
1-benzylnaphthalene[b,c]	$C_{17}H_{14}$	G9	60.0	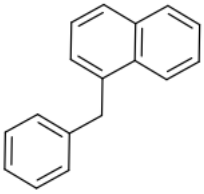
$C_{18}H_{18}$ – isomer[a]	$C_{18}H_{18}$	G9	60.0	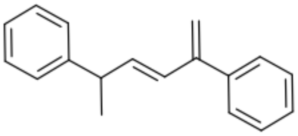

Continues on the next page

Compound	Formula	Peak identifier	RT (min)	Tentative structure[d]
$C_{17}H_{14}$ – isomer[a]	$C_{17}H_{14}$	G10	60.1	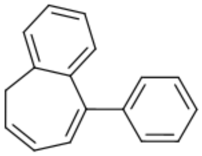
2-benzylnaphthalene[b,c]	$C_{17}H_{14}$	G11	60.6	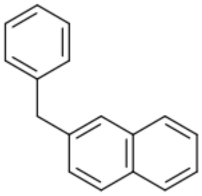
$C_{18}H_{18}$ – isomer[a]	$C_{18}H_{18}$	G11	60.6	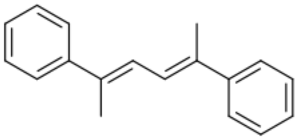

[a]Compound identification based on mass spectral assignment only, and not through the use of commercial standard. Refer to **Section B.5**. [b]Commercial standard used for compound identification. [c]Although there is a peak at the same retention time for this component, the MS spectra did not indicate its presence. [d]Structure of confirmed compounds by using commercial standards and tentative structures for unconfirmed compounds based on mass spectra assignment. [e]The mass spectra of G3 and G4 were almost identical, and their structure assignment corresponded to both isomers depicted in their tentative structures.

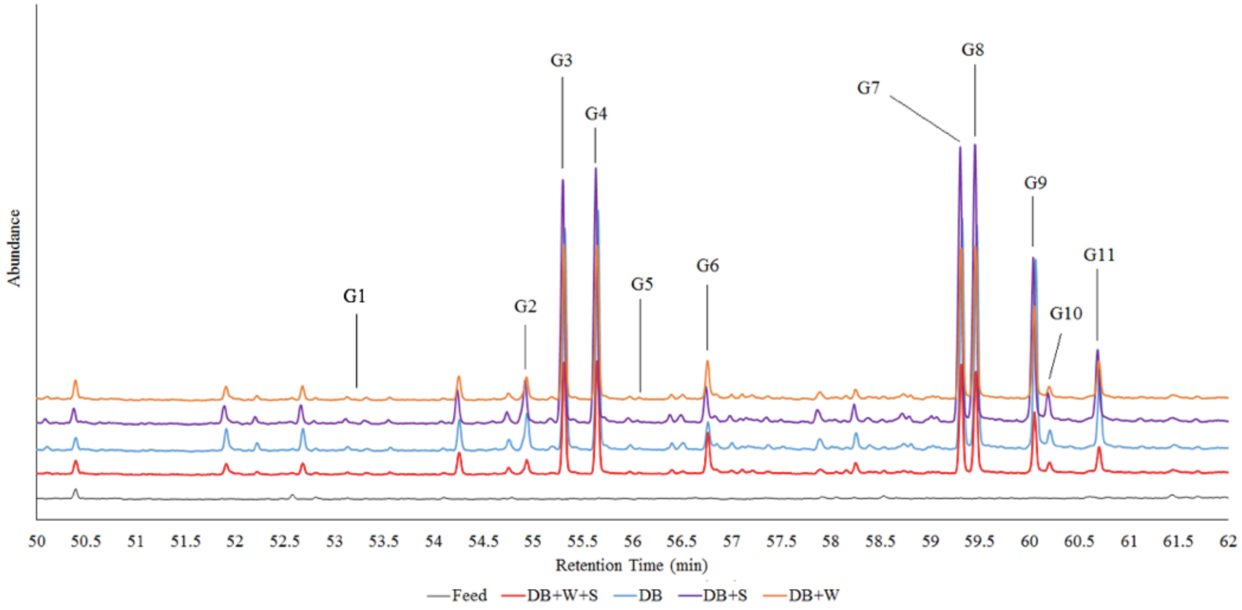

Figure B.15: GC-MS chromatograms from thermal treatment experiments - Region G (RT between 50 and 62 min).

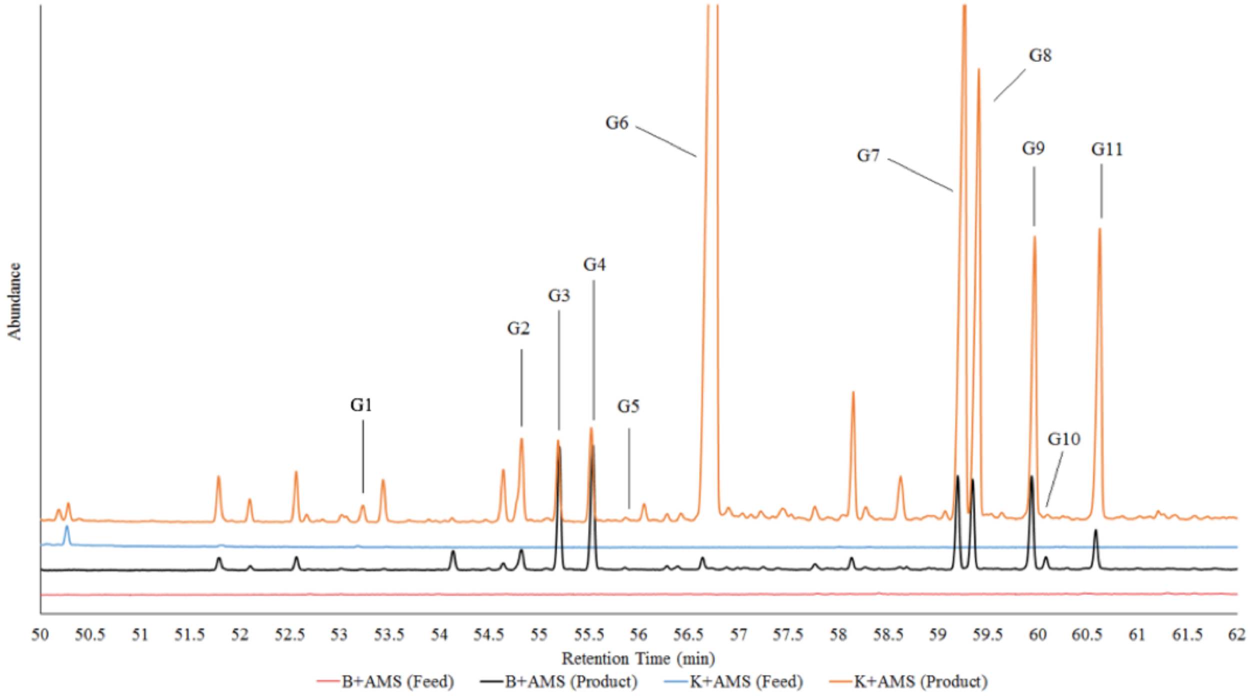

Figure B.16: GC-MS chromatograms from control experiments B+AMS and B+K - Region G (RT between 50 and 62 min).

B.4.8 Region H – RT between 62 and 80 min

The compounds identified in the RT between 62 and 80 min are listed in **Table B.12**. The identification of all the compounds in that list was based on mass spectral assignment only.

Table B.12: Peak identifier and RT of compounds identified in the region H of the GC-MS chromatograms.

Compound	**Formula**	**Peak identifier**	**RT (min)**	**Tentative structure**
$C_{19}H_{20}$ – isomer[a]	$C_{19}H_{20}$	H1	63.1	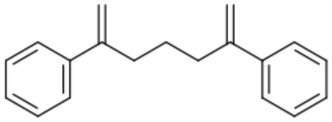
Decomposition product consisting of $C_{18}H_{20}$ isomers[a,b]	-[b]	H2	74.8	-
Decomposition product consisting of $C_{18}H_{20}$ isomers[a,b]	-[b]	H3	75.0	-

[a] Compound identification based on mass spectral assignment only, and not through the use of commercial standard. Refer to **Section B.5**. [b] The MS spectra of these compounds (**Figures B.30** and **B.31**) is similar to those of $C_{18}H_{20}$ isomers but their elution at high retention times indicated that they might be product from in-column cracking of heavier species.

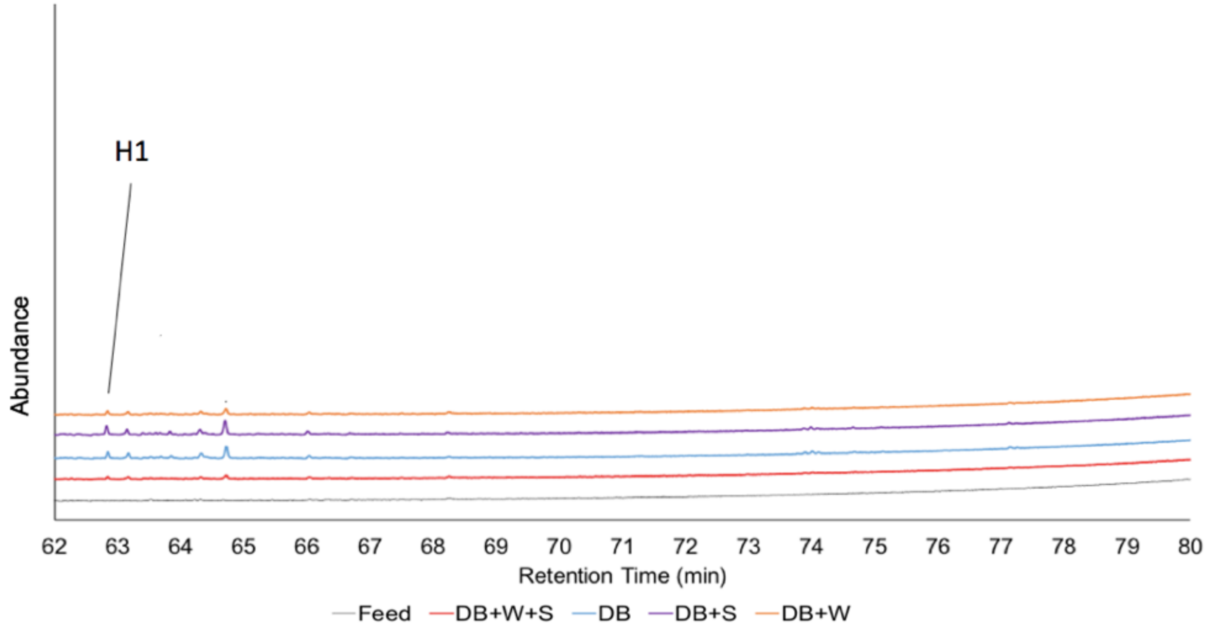

Figure B.17: GC-MS chromatograms from thermal treatment experiments - Region H (RT between 62 and 80 min).

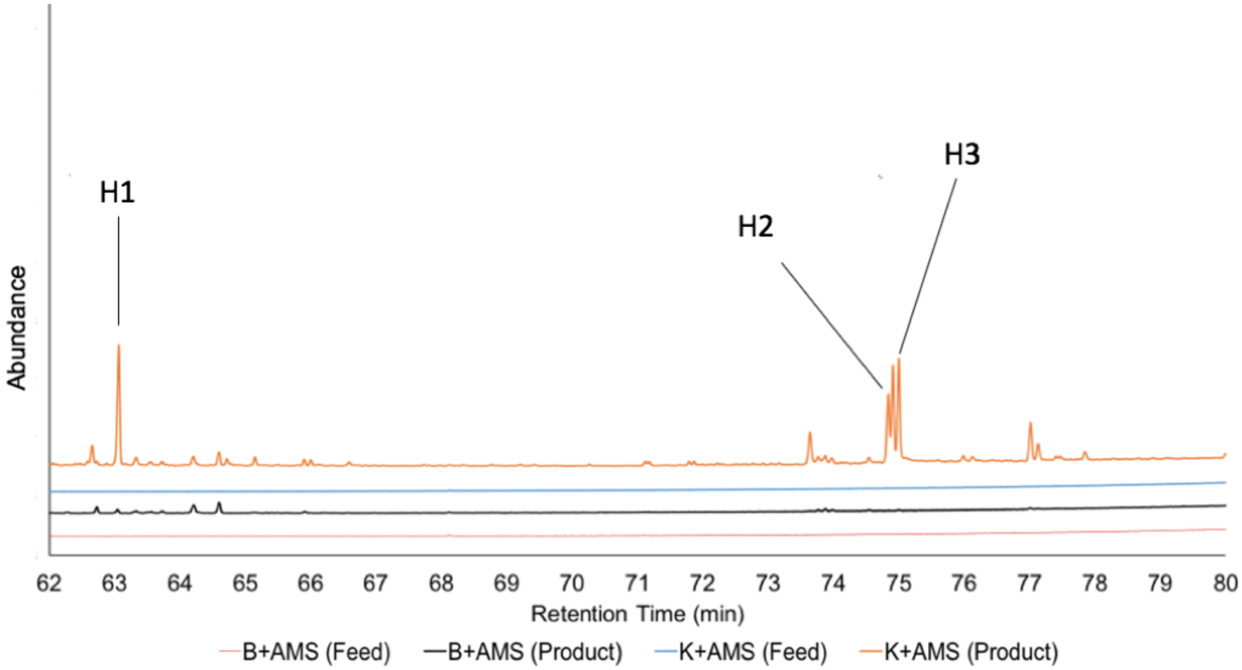

Figure B.18: GC-MS chromatograms from control experiments B+AMS and B+K - Region H (RT between 62 and 80 min).

B.5 Relative area percentages (RAP) of the monitored compounds

The relative area percentages (RAP) of the monitored compound from the thermal treatment and control experiments are shown in **Tables B-13** and **B-14**, respectively.

Table B.13: RAP of monitored compounds during the thermal treatment experiments.

Compound	Peak identifier	RT (min)	RAP (%)				
			Feed	**DB+W+S**	**DB+W**	**DB+S**	**DB**
hexane	A1	4.7	0.01	0.01	0.03	0.06	0.05
benzene	A2	6.3	0.01	0.00	0.02	0.06	0.06
cyclohexane	A3	6.6	0.02	0.01	0.02	0.02	0.02
heptane	A4	8.3	0.07	0.06	0.10	0.14	0.13
methylcyclohexane	A5	9.2	0.12	0.10	0.13	0.12	0.12
toluene	A6	11.0	0.09	0.06	0.37	0.35	0.32
octane	A7	13.5	0.23	0.22	0.29	0.31	0.29
ethylcyclohexane	B1	15.2	0.10	0.10	0.11	0.11	0.11
ethylbenzene	B2	16.2	0.03	1.28	2.40	5.13	5.22
m-xylene	B3	16.7	0.16	0.12	0.17	0.20	0.20
p-xylene	B4	16.8	0.05	0.05	0.05	0.04	0.05
styrene	B5	17.7	ND[c]	ND	ND	ND	ND
o-xylene	B6	18.0	0.12	0.11	0.15	0.16	0.16
nonane	B7	19.4	0.72	0.75	0.87	0.76	0.78
cumene	B8	20.0	0.04	19.15	22.32	38.09	38.41

Continues on the next page

Compound	**Peak identifier**	**RT (min)**	**RAP** (%)				
			Feed	**DB+W+S**	**DB+W**	**DB+S**	**DB**
isopropylcyclohexane	B9	20.4	0.04	0.04	0.05	0.04	0.04
propylcyclohexane	C1	20.9	0.17	0.18	0.20	0.18	0.18
n-propylbenzene	C2	21.7	0.11	0.23	0.36	0.77	0.67
3-ethyltoluene	C3	22.1	0.24	0.21	0.27	0.26	0.26
4-ethyltoluene	C4	22.2	0.09	0.09	0.11	0.12	0.12
mesitylene (1,3,5-trimethylbenzene)	C5	22.6	0.18	0.22	0.26	0.23	0.24
AMS[a]	C6	23.1	75.57	42.54	34.19	14.51	12.81
2-ethyltoluene[a]	C6	23.1	ND	ND	ND	ND	ND
tert-butylbenzene[b]	C7	23.9	0.66	0.65	0.77	0.65	0.68
1,2,4-trimethylbenzeneb	C7	23.9	ND	ND	ND	ND	ND
isobutylbenzene	C8	24.8	ND	ND	ND	ND	ND
sec-butylbenzene	C9	24.9	0.10	0.62	0.78	1.54	1.41
decane	C10	25.1	0.97	1.09	1.22	1.03	1.07
1,2,3- trimethylbenzene	C11	25.4	0.22	0.25	0.29	0.27	0.27
phenylacetaldehyde	C12	25.5	ND	ND	ND	ND	ND
m-cymene	C13	25.6	0.10	0.11	0.14	0.14	0.15
p-cymene	C14	25.7	0.12	0.17	0.17	0.22	0.23
indane	D1	26.0	0.08	0.08	0.09	0.07	0.06
indene	D2	26.4	ND	ND	ND	ND	ND
o-cymene	D3	26.5	ND	ND	ND	ND	ND
acetophenone	D4	26.9	ND	ND	ND	ND	ND
1-phenylethanol	D5	27.1	ND	ND	ND	ND	ND
3-propyltoluene	D6	27.2	0.05	0.13	0.16	0.14	0.15

Continues on the next page

Compound	**Peak identifier**	**RT (min)**	**RAP** (%)				
			Feed	**DB+W+S**	**DB+W**	**DB+S**	**DB**
4-propyltoluene[d]	D7	27.3	0.16	0.31	0.29	0.22	0.21
n-butylbenzene[d]	D8	27.3	0.09	0.09	0.12	0.14	0.14
decalin (decahydronaphthalene (cis/trans))	D9	27.9 & 30.1	0.07	0.09	0.07	0.08	0.07
2-propyltoluene	D10	28.1	0.09	0.10	0.12	0.10	0.10
2-phenyl-2-propanol	D11	28.4	ND	0.23	0.08	ND	ND
2-phenylpropionaldehyde	D12	29.1	ND	ND	ND	ND	ND
2-phenylethanol	D13	29.8	ND	ND	ND	ND	ND
undecane	D14	30.6	0.77	0.93	1.05	0.86	0.89
1-phenyl-2-propanol	D15	30.9	ND	ND	ND	ND	ND
3-phenylpropionaldehyde	D16	31.9	ND	ND	ND	ND	ND
propiophenone	D17	32.3	ND	ND	ND	ND	ND
tetralin (1,2,3,4-tetrahydronaphthalene)	D18	32.8	0.11	0.08	0.08	0.04	0.04
n-pentylbenzene	D19	32.9	ND	ND	ND	ND	ND
naphthalene	D20	33.7	ND	0.01	0.02	0.03	0.03
3-phenyl-1-propanol	E1	35.6	ND	ND	ND	ND	ND
dodecane	E2	35.7	0.64	0.81	0.91	0.74	0.78
2-methylnaphthalene	E3	38.8	0.15	0.22	0.25	0.22	0.23
1-methylnaphthalene	E4	39.5	ND	0.07	0.09	0.13	0.12
tridecane	E5	39.9	0.51	0.65	0.74	0.60	0.63
cis-decahydro-1-naphthol	E6	40.4	ND	ND	ND	ND	ND
β-tetralone	E7	40.8	ND	ND	ND	ND	ND
1,5-dimethyltetralin + α-tetralone	E8	41.5	ND	ND	ND	ND	ND
biphenyl	F1	42.1	-[h]	-[h]	-[h]	-[h]	-[h]

Continues on the next page

Compound	**Peak identifier**	**RT (min)**	**RAP (%)**				
			Feed	**DB+W+S**	**DB+W**	**DB+S**	**DB**
2,6-dimethylnaphthalene	F2	43.2	ND	ND	ND	ND	ND
2,7-dimethylnaphthalene	F3	43.3	ND	ND	ND	ND	ND
tetradecane	F4	43.9	0.35	0.40	0.45	0.34	0.37
5,6,7,8-tetrahydro-1-naphthol	F5	44.4	ND	ND	ND	ND	ND
1,4-dimethylnaphthalene	F6	44.4	ND	ND	ND	ND	ND
5,6,7,8-tetrahydro-2-naphthol	F7	45.0	ND	ND	ND	ND	ND
1,8-dimethylnaphthalene	F8	45.5	ND	ND	ND	ND	ND
1-naphthol	F9	46.2	ND	ND	ND	ND	ND
2-naphthol	F10	46.6	ND	ND	ND	ND	ND
pentadecane	F11	47.2	0.25	0.32	0.40	0.30	0.31
$C_{18}H_{20}$ – isomer^{e}	G1	54.1	ND	ND	ND	ND	ND
$C_{17}H_{20}$ – isomer^{e}	G2	54.8	ND	0.09	0.13	0.28	0.26
2,4-diphenyl-4-methyl-1-pentene^{f,g}	G3	55.2	ND	ND	ND	ND	ND
$C_{18}H_{22}$ – isomer^{e}	G3	55.2	ND	0.66	0.76	1.35	1.43
$C_{18}H_{22}$ – isomere	G4	55.5	ND	0.67	0.76	1.39	1.49
dicumene^{f}	G5	56.0	ND	ND	ND	ND	ND
1-phenylnaphthalene^{f,g}	G6	56.6	ND	ND	ND	ND	ND
$C_{18}H_{20}$ – isomer^{e}	G6	56.6	ND	0.22	0.18	0.18	0.16
$C_{18}H_{20}$ – isomer^{e}	G7	59.2	ND	0.63	0.78	1.56	1.45
$C_{18}H_{20}$ – isomer^{e}	G8	59.4	ND	0.60	0.76	1.57	1.44
$C_{18}H_{18}$ isomer^{e}	G9	60.0	ND	0.34	0.46	0.91	1.19
1-benzylnaphthalene^{f,i}	G9	60.0	ND	ND	ND	ND	ND
$C_{17}H_{14}$ – isomer^{e}	G10	60.1	ND	0.05	0.04	0.14	0.09

Continues on the next page

Compound	**Peak identifier**	**RT (min)**	**RAP** (%)				
			Feed	**DB+W+S**	**DB+W**	**DB+S**	**DB**
$C_{18}H_{18}$ isomer[e]	G11	60.6	ND	0.14	0.17	0.37	0.47
2-benzylnaphthalene[f,j]	G11	60.6	ND	ND	ND	ND	ND
$C_{19}H_{20}$ – isomer[e]	H1	63.1	ND	0.02	0.02	0.04	0.04
Decomposition product consisting of $C_{18}H_{20}$ isomers[e,k]	H2	74.8	ND	ND	ND	ND	ND
Decomposition product consisting of $C_{18}H_{20}$ isomers[e,k]	H3	75.0	ND	ND	ND	ND	ND
Compounds with RT between 50 and 62 min	-	50-62	ND	4.83	5.42	10.16	10.54
Compounds with RT between 62 and 80 min	-	62-80	ND	0.18	0.19	0.40	0.52

[a] AMS and 2-ethyltoluene eluted at the same RT, but only AMS was detected in the MS spectra. [b] 1,2,4-trimethylbenzene and *tert*-butylbenzene eluted at the same RT, however only *tert*-butylbenzene was detected in the MS spectra. [c] ND = Not Detected. [d] merged peaks: 4-propyltoluene on the left and *n*-butylbenzene on the right. [e] Compound identification based on mass spectral assignment only (**Figures B.19–B.31**). [f] Commercial standard used for compound identification. [g] Although there is a peak at the same retention time for this component, the MS spectra did not indicate its presence. [h] The area of biphenyl was not included in the total area used for the calculation of RAP. [i] The peak at the same retention time corresponded to $C_{18}H_{18}$ isomers and not 1-benzylnaphthalene. [j] The peak at the same retention time corresponded to $C_{18}H_{18}$ isomers and not 2-benzylnaphthalene. [k] The MS spectra of these compounds (**Figures B.30** and **B.31**) is similar to those of $C_{18}H_{20}$ isomers but their elution at high retention times indicated that they might be product from in-column cracking of heavier species.

Table B.14: RAP of monitored compounds during the control experiments.

Compound	**Peak identifier**	**RT (min)**	**RAP** (%)							
			B+K		**B+AMS**		**K**		**K+AMS**	
			Feed	**Product**	**Feed**	**Product**	**Feed**	**Product**	**Feed**	**Product**
hexane	A1	4.7	0.13	0.16	ND[c]	0.03	0.04	0.05	0.01	0.01
benzene	A2	6.3	ND	ND	ND	0.06	0.02	0.01	0.00	0.01
cyclohexane	A3	6.6	0.06	0.06	ND	ND	0.06	0.06	0.01	0.02
heptane	A4	8.3	1.41	0.31	ND	0.04	0.54	0.30	0.06	0.07
methylcyclohexane	A5	9.2	0.49	0.44	ND	0.01	0.47	0.47	0.10	0.11
toluene	A6	11.0	0.98	0.97	ND	0.25	0.35	0.34	0.07	0.16
octane	A7	13.5	0.92	0.89	ND	0.04	0.88	0.87	0.18	0.20
ethylcyclohexane	B1	15.2	0.42	0.42	ND	ND	0.42	0.40	0.08	0.09
ethylbenzene	B2	16.2	0.41	0.33	ND	6.13	0.15	0.11	0.03	2.55
m-xylene	B3	16.7	0.79	0.79	ND	0.02	0.60	0.59	0.12	0.11
p-xylene	B4	16.8	0.17	0.18	ND	0.04	0.12	0.16	0.04	0.04
styrene	B5	17.7	ND	ND	ND	ND	ND	ND	ND	ND
o-xylene	B6	18.0	0.64	0.64	ND	0.02	0.47	0.47	0.09	0.09
nonane	B7	19.4	2.82	2.67	ND	0.03	2.81	2.77	0.56	0.60
cumene	B8	20.0	0.19	0.18	ND	66.03	0.19	0.22	0.04	3.55
isopropylcyclohexane	B9	20.4	0.07	0.06	ND	ND	0.17	0.18	0.04	0.04
propylcyclohexane	C1	20.9	0.67	0.60	ND	ND	0.67	0.65	0.13	0.13
n-propylbenzene	C2	21.7	0.54	0.48	ND	0.53	0.38	0.37	0.08	0.20

Continues on the next page

Compound	**Peak identifier**	**RT (min)**	**RAP** (%)							
			B+K		**B+AMS**		**K**		**K+AMS**	
			Feed	**Product**	**Feed**	**Product**	**Feed**	**Product**	**Feed**	**Product**
3-ethyltoluene	C3	22.1	1.25	1.22	ND	ND	0.71	0.74	0.15	0.18
4-ethyltoluene	C4	22.2	0.53	0.53	ND	ND	0.14	0.10	0.02	0.06
mesitylene (1,3,5-trimethylbenzene)	C5	22.6	1.09	1.04	ND	ND	1.04	1.06	0.21	0.24
AMS[a]	C6	23.1	ND	ND	99.39	10.60	ND	ND	78.35	41.40
2-ethyltoluenea	C6	23.1	ND	ND	ND	ND	ND	ND	ND	ND
tert-butylbenzene[b]	C7	23.9	3.09	2.90	0.03	0.07	2.41	2.37	0.49	0.44
1,2,4-trimethylbenzene[b]	C7	23.9	ND	ND	ND	ND	ND	ND	ND	ND
isobutylbenzene	C8	24.8	ND	ND	ND	ND	ND	ND	ND	ND
sec-butylbenzene	C9	24.9	0.41	0.36	0.03	1.45	0.46	0.45	0.09	0.26
decane	C10	25.1	3.63	3.42	ND	0.03	3.76	3.73	0.76	0.79
1,2,3- trimethylbenzene	C11	25.4	1.12	1.10	ND	0.04	0.85	0.87	0.17	0.16
phenylacetaldehyde	C12	25.5	ND	ND	ND	ND	ND	ND	ND	ND
m-cymene	C13	25.6	0.42	0.42	ND	0.05	0.33	0.35	0.07	0.15
p-cymene	C14	25.7	0.29	0.28	0.03	0.18	0.31	0.33	0.07	0.13
indane	D1	26.0	0.25	0.24	ND	ND	0.17	0.18	0.06	0.02
indene	D2	26.4	ND	ND	ND	ND	ND	ND	ND	ND
o-cymene	D3	26.5	ND	ND	ND	ND	ND	ND	ND	ND
acetophenone	D4	26.9	ND	ND	ND	ND	ND	ND	ND	ND
1-phenylethanol	D5	27.0	ND	ND	ND	ND	ND	ND	ND	ND

Continues on the next page

Compound	Peak identifier	RT (min)	RAP (%)							
			B+K		B+AMS		K		K+AMS	
			Feed	**Product**	**Feed**	**Product**	**Feed**	**Product**	**Feed**	**Product**
3-propyltoluene	D6	27.2	0.68	0.63	ND	ND	0.51	0.49	0.10	0.10
4-propyltoluene[d]	D7	27.4	0.45	0.39	ND	ND	1.09	1.07	0.22	0.24
n-butylbenzene[d]	D8	27.4	0.25	0.36	ND	0.05	0.28	0.27	0.05	0.06
decalin (decahydronaphthalene (cis/trans))	D9	27.9 & 30.1	0.30	0.28	ND	ND	0.36	0.35	0.07	0.07
2-propyltoluene	D10	28.0	0.48	0.45	ND	ND	0.62	0.57	0.11	0.13
2-phenyl-2-propanol	D11	28.3	ND	ND	ND	ND	ND	ND	ND	ND
2-phenylpropionaldehyde	D12	29.0	ND	ND	ND	ND	ND	ND	ND	ND
2-phenylethanol	D13	29.6	ND	ND	ND	ND	ND	ND	ND	ND
undecane	D14	30.5	2.83	2.69	ND	ND	3.28	3.24	0.66	0.68
1-phenyl-2-propanol	D15	30.9	ND	ND	ND	ND	ND	ND	ND	ND
3-phenylpropionaldehyde	D16	31.9	ND	ND	ND	ND	ND	ND	ND	ND
propiophenone	D17	32.3	ND	ND	ND	ND	ND	ND	ND	ND
tetralin (1,2,3,4-tetrahydronaphthalene)	D18	32.6	0.52	0.42	ND	ND	0.45	0.44	0.09	0.11
n-pentylbenzene	D19	32.7	ND	ND	ND	ND	ND	ND	ND	ND
naphthalene	D20	33.7	ND	0.02	ND	ND	ND	ND	ND	0.03
3-phenyl-1-propanol	E1	35.6	ND	ND	ND	ND	ND	ND	ND	ND
dodecane	E2	35.7	2.33	2.16	ND	ND	3.09	3.06	0.62	0.63
2-methylnaphthalene	E3	38.8	0.68	0.71	ND	ND	0.73	0.70	0.15	0.14

Continues on the next page

Compound	Peak identifier	RT (min)	RAP (%)							
			B+K		B+AMS		K		K+AMS	
			Feed	Product	Feed	Product	Feed	Product	Feed	Product
1-methylnaphthalene	E4	39.5	ND	ND	ND	ND	0.11	0.13	0.02	0.09
tridecane	E5	39.9	1.70	1.64	ND	ND	2.61	2.55	0.53	0.53
cis-decahydro-1-naphthol	E6	40.4	ND	ND	ND	ND	ND	ND	ND	ND
β-tetralone	E7	40.8	ND	ND	ND	ND	ND	ND	ND	ND
1,5-dimethyltetralin & α-tetralone	E8	41.5	ND	ND	ND	ND	ND	ND	ND	ND
biphenyl	F1	42.1	-[h]	-[h]	-[h]	-[h]	-[h]	-[h]	-[h]	-[h]
2,6-dimethylnaphthalene	F2	43.2	ND	ND	ND	ND	ND	ND	ND	ND
2,7-dimethylnaphthalene	F3	43.3	ND	ND	ND	ND	ND	ND	ND	ND
tetradecane	F4	43.7	1.06	0.96	ND	ND	2.08	2.00	0.44	0.39
5,6,7,8-tetrahydro-1-naphthol	F5	44.4	ND	ND	ND	ND	ND	ND	ND	ND
1,4-dimethylnaphthalene	F6	44.4	ND	ND	ND	ND	ND	ND	ND	ND
5,6,7,8-tetrahydro-2-naphthol	F7	45.0	ND	ND	ND	ND	ND	ND	ND	ND
1,8-dimethylnaphthalene	F8	45.5	ND	ND	ND	ND	ND	ND	ND	ND
1-naphthol	F9	46.2	ND	ND	ND	ND	ND	ND	ND	ND
2-naphthol	F10	46.6	ND	ND	ND	ND	ND	ND	ND	ND
pentadecane	F11	47.2	0.80	0.81	ND	ND	1.70	1.67	0.35	0.57
$C_{18}H_{20}$ – isomer[e]	G1	53.2	ND	ND	ND	ND	ND	ND	ND	0.10
$C_{17}H_{20}$ – isomer[e]	G2	54.8	ND	ND	ND	0.34	ND	ND	ND	0.51

Continues on the next page

Compound	Peak identifier	RT (min)	RAP (%)							
			B+K		B+AMS		K		K+AMS	
			Feed	Product	Feed	Product	Feed	Product	Feed	Product
2,4-diphenyl-4-methyl-1-pentene[f,g]	G3	55.2	ND	ND	ND	ND	ND	ND	ND	ND
$C_{18}H_{22}$ – isomer[e]	G3	55.2	ND	ND	ND	1.84	ND	ND	ND	0.42
$C_{18}H_{22}$ – isomer[e]	G4	55.5	ND	ND	ND	1.90	ND	ND	ND	0.50
dicumene[f]	G5	56.0	ND	ND	ND	ND	ND	ND	ND	ND
1-phenylnaphthalene[f,g]	G6	56.6	ND	ND	ND	ND	ND	ND	ND	ND
$C_{18}H_{20}$ – isomer[e]	G6	56.6	ND	ND	ND	0.16	ND	ND	ND	12.16
$C_{18}H_{20}$ – isomer[e]	G7	59.2	ND	ND	ND	1.40	ND	ND	ND	4.34
$C_{18}H_{20}$ – isomer[e]	G8	59.4	ND	ND	ND	1.39	ND	ND	ND	3.16
$C_{18}H_{18}$ isomers[e]	G9	60.0	ND	ND	ND	1.37	ND	ND	ND	1.71
1-benzylnaphthalene[f,i]	G9	60.0	ND	ND	ND	ND	ND	ND	ND	ND
$C_{17}H_{14}$ – isomer[e]	G10	60.08	ND	ND	ND	0.16	ND	ND	ND	0.02
$C_{18}H_{18}$ isomers[e]	G11	60.6	ND	ND	ND	0.59	ND	ND	ND	1.84
2-benzylnaphthalene[f,j]	-	60.6	ND	ND	ND	ND	ND	ND	ND	ND
$C_{19}H_{20}$ – isomer[e]	H1	63.1	ND	ND	ND	0.06	ND	ND	ND	0.72
Decomposition product consisting of $C_{18}H_{20}$ isomers[e,k]	H2	74.8	ND	ND	ND	ND	ND	ND	ND	0.44
Decomposition product consisting of $C_{18}H_{20}$ isomers[e,k]	H3	75.0	ND	ND	ND	ND	ND	ND	ND	0.62

Continues on the next page

Compound	**Peak identifier**	**RT (min)**	**RAP** (%)							
			B+K		**B+AMS**		**K**		**K+AMS**	
			Feed	**Product**	**Feed**	**Product**	**Feed**	**Product**	**Feed**	**Product**
Compounds with RT between 50 and 62 min	-	50-62	ND	ND	ND	11.45	ND	ND	ND	28.58
Compounds with RT between 62 and 80 min	-	62-80	ND	ND	ND	0.70	ND	ND	ND	4.41

[a] Both compounds eluted at the same RT, but only AMS was detected in the MS Spectra. [b] Both compounds eluted at the same RT, however only *tert*-butylbenzene was detected in the MS spectra. [c] ND = Not Detected. [d] merged peaks: 4-propyltoluene on the left and *n*-butylbenzene on the right. [e] Compound identification based on mass spectral assignment only (**Figures B.19–B.31**). [f] Commercial standard used for compound identification. [g] Although there is a peak at the same retention time for this component, the MS spectra did not indicate its presence. [h] The area of biphenyl was not included in the total area used for the calculation of RAP. [i] The peak at the same retention time corresponded to $C_{18}H_{18}$ isomers and not 1-benzylnaphthalene. [j] The peak at the same retention time corresponded to $C_{18}H_{18}$ isomers and not 2-benzylnaphthalene. [k] The MS spectra of these compounds (**Figures B.30** and **B.31**) is similar to those of $C_{18}H_{20}$ isomers but their elution at high retention times indicated that they might be product from in-column cracking of heavier species.

B.6 Reactivity of cumene during thermal treatment of bitumen

The thermal treatment of bitumen with cumene (B+C) was an important control reaction to evaluate if cumene could be converted into other products (including AMS) during the conditions of this study. Because the amount of species in the products was limited, the results of that control reaction were reported in a separate table (**Table B.15**) instead of **Table B.14**.

Table B.15: RAP of the thermal treatment of cumene with bitumen (B+C).

Compound^a	**Peak identifier**	**RT (min)**	**RAP** (%)	
			B+C	
			Feed	**Product**
toluene	A6	11.0	0.65	0.65
ethylbenzene	B2	16.2	ND	0.08
cumene	B8	20.0	97.89	98.23
n-propylbenzene	C2	21.7	ND	0.21
AMS	C6	23.1	1.44	0.62

^{a}These compounds were the only species identified in system B+C.

B.7 Mass spectra of selected species from regions G and H of the chromatograms

This section contains the mass spectra of selected species from regions G and H. The tentative structures for those species are illustrated in **Figure 4.2** in the manuscript.

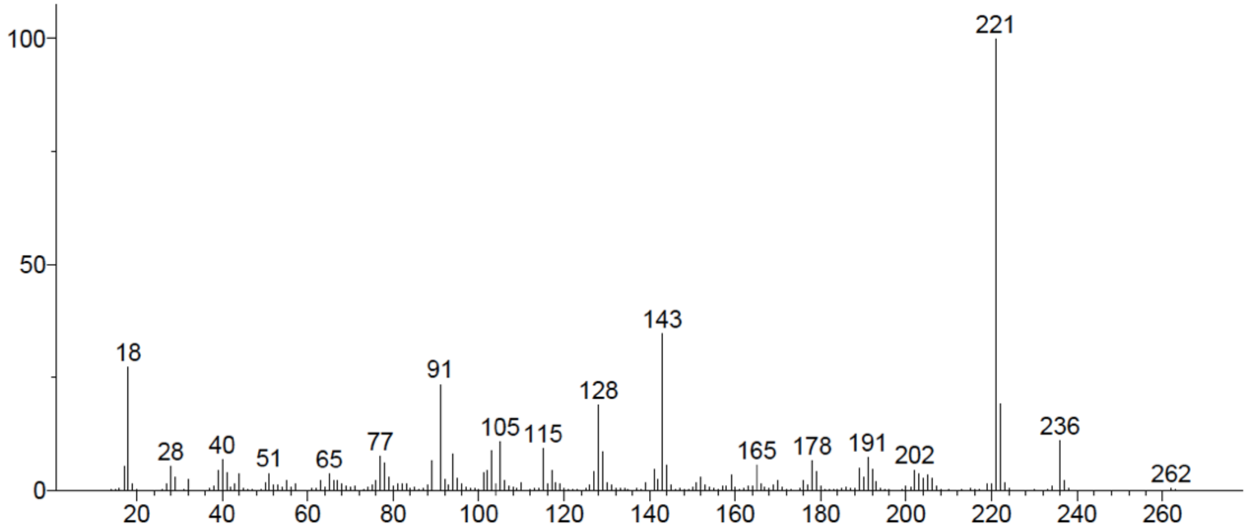

Figure B.19: Mass spectrum of compound G1.

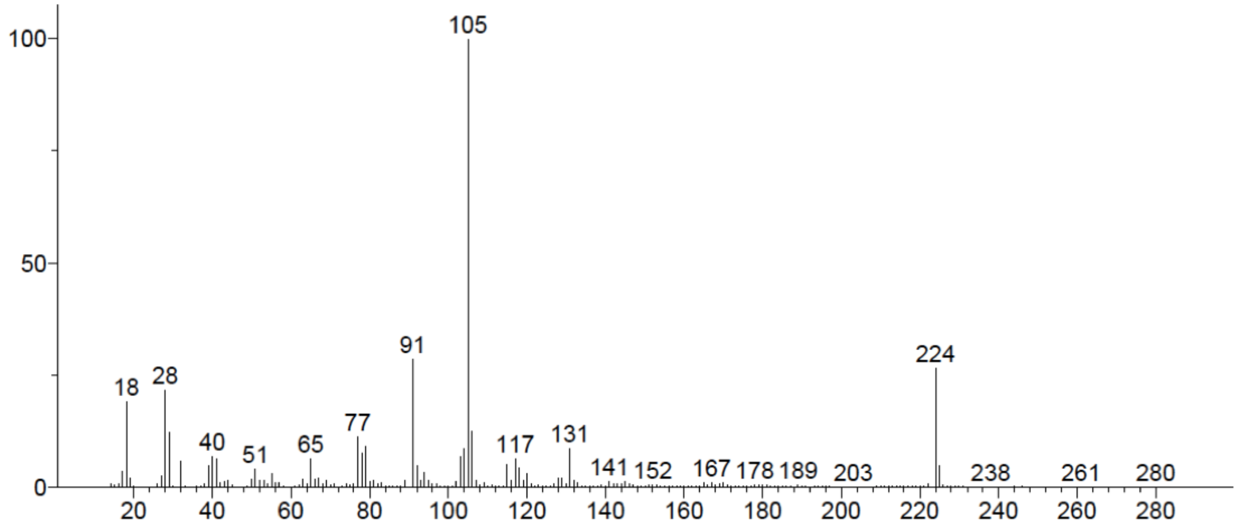

Figure B.20: Mass spectrum of compound G2.

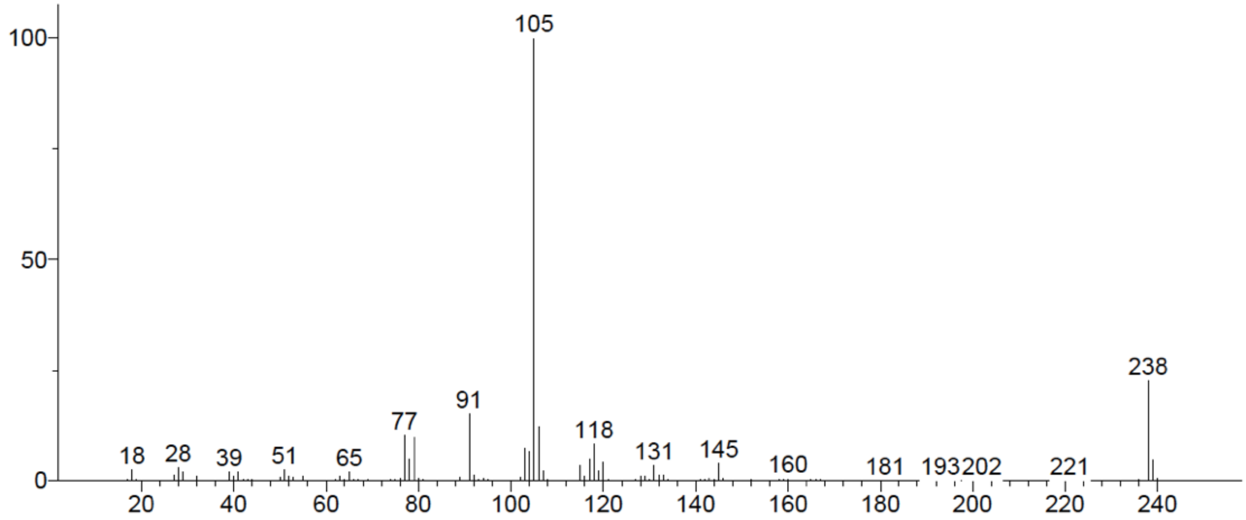

Figure B.21: Mass spectrum of compound G3.

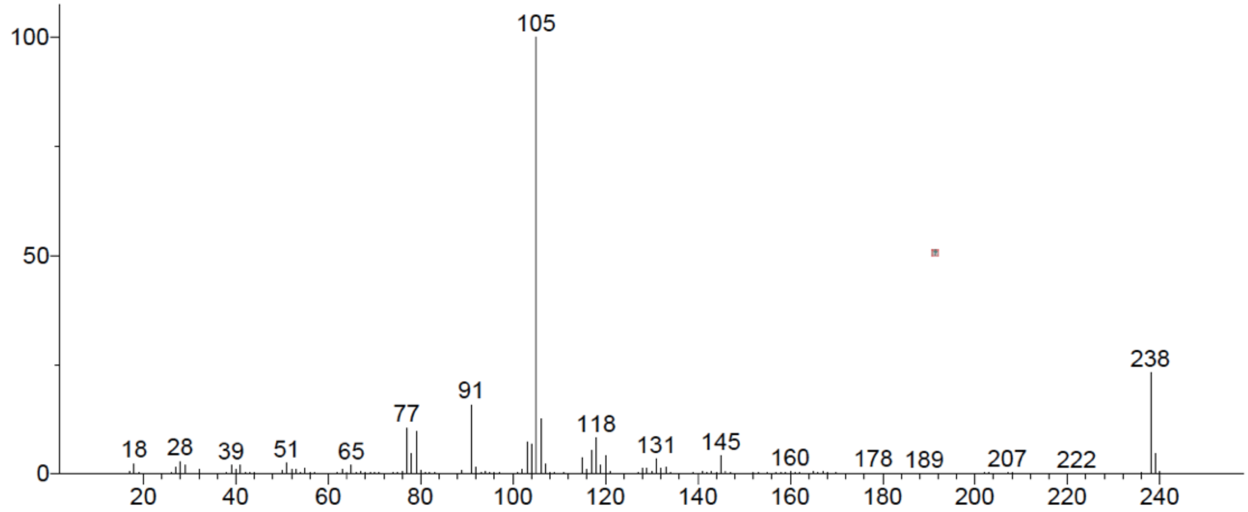

Figure B.22: Mass spectrum of compound G4.

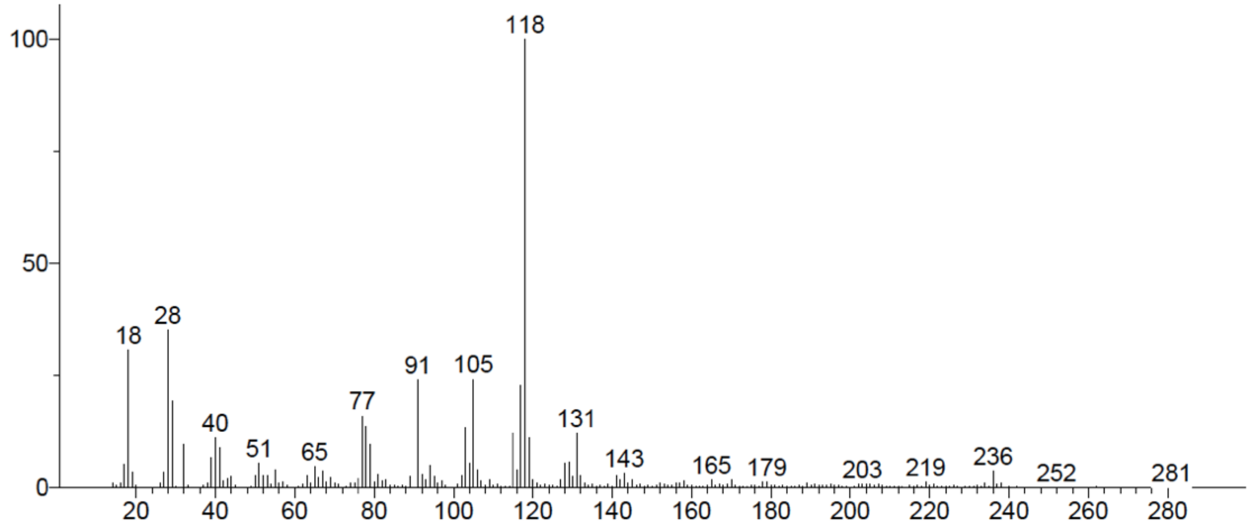

Figure B.23: Mass spectrum of compound G6.

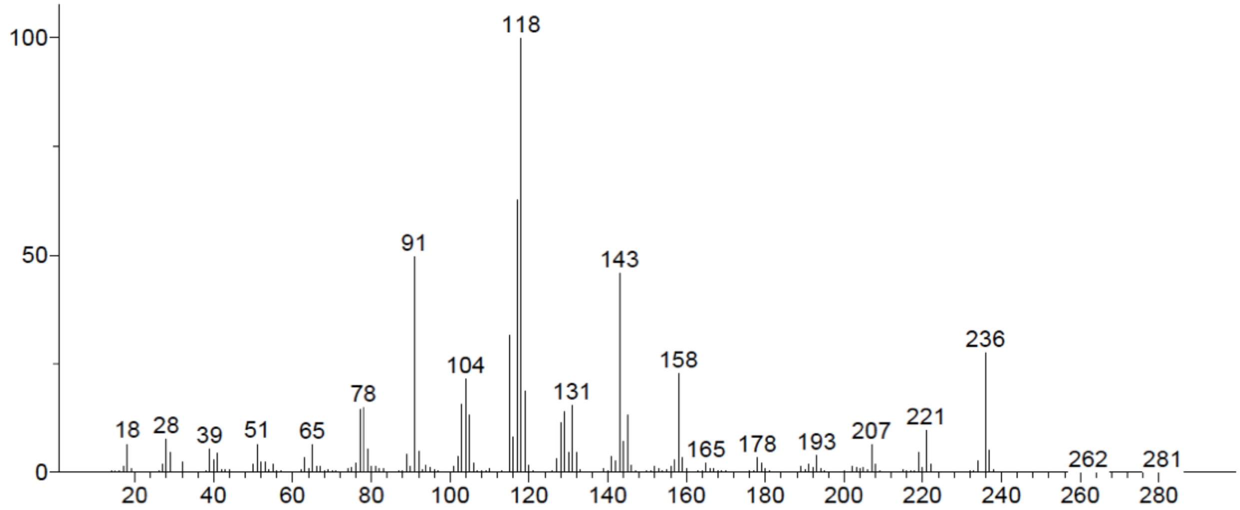

Figure B.24: Mass spectrum of compound G7.

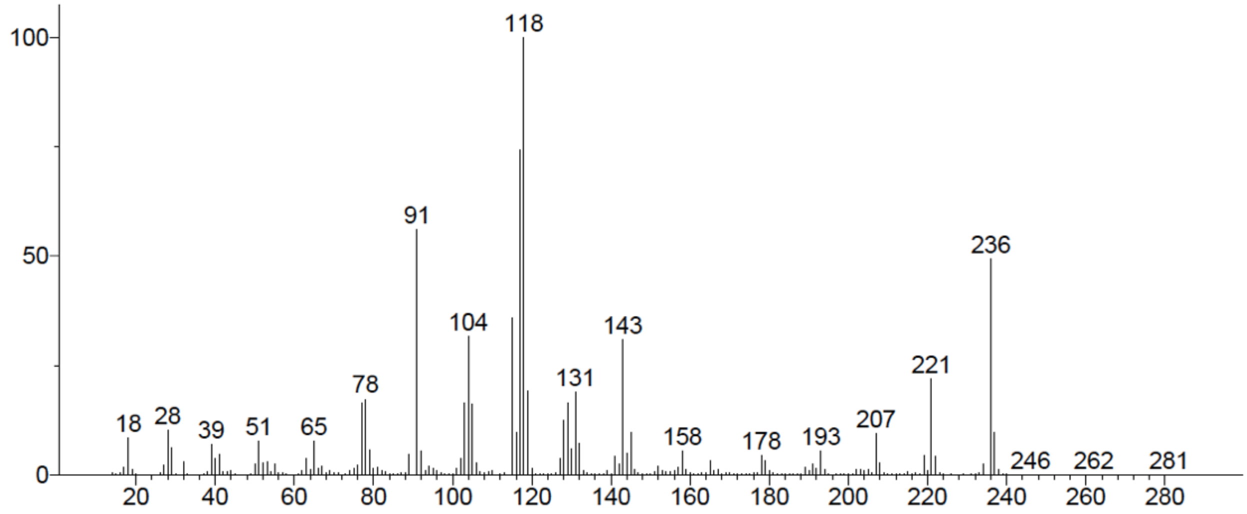

Figure B.25: Mass spectrum of compound G8.

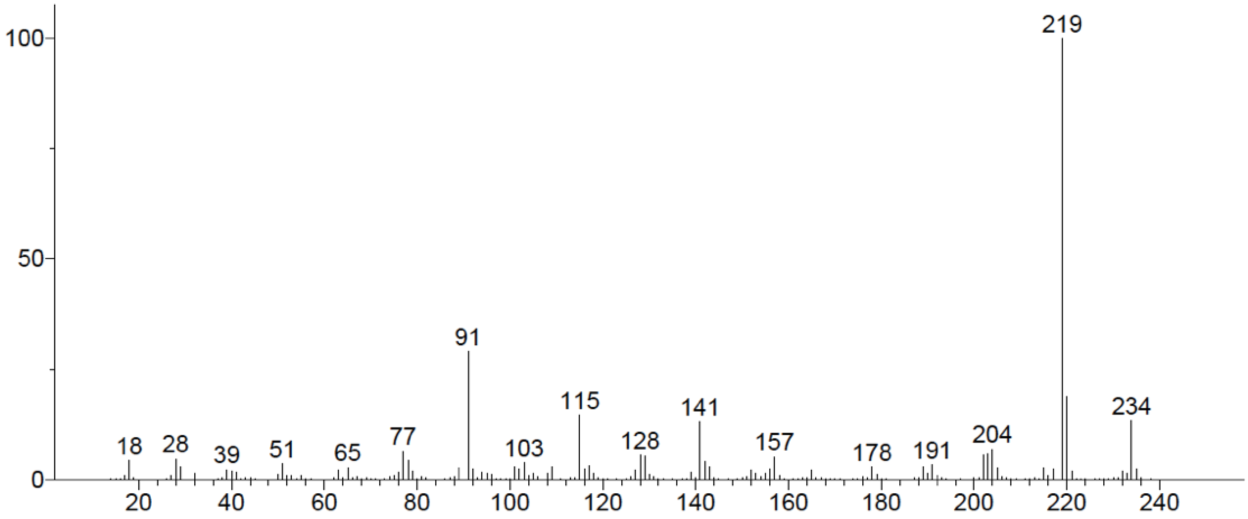

Figure B.26: Mass spectrum of compound G9.

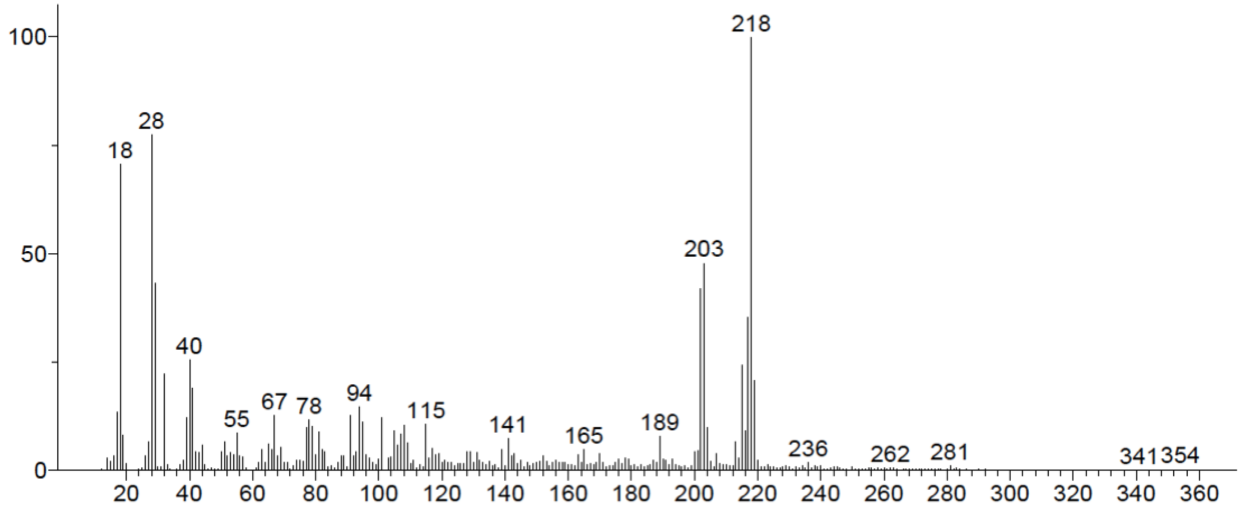

Figure B.27: Mass spectrum of compound G10.

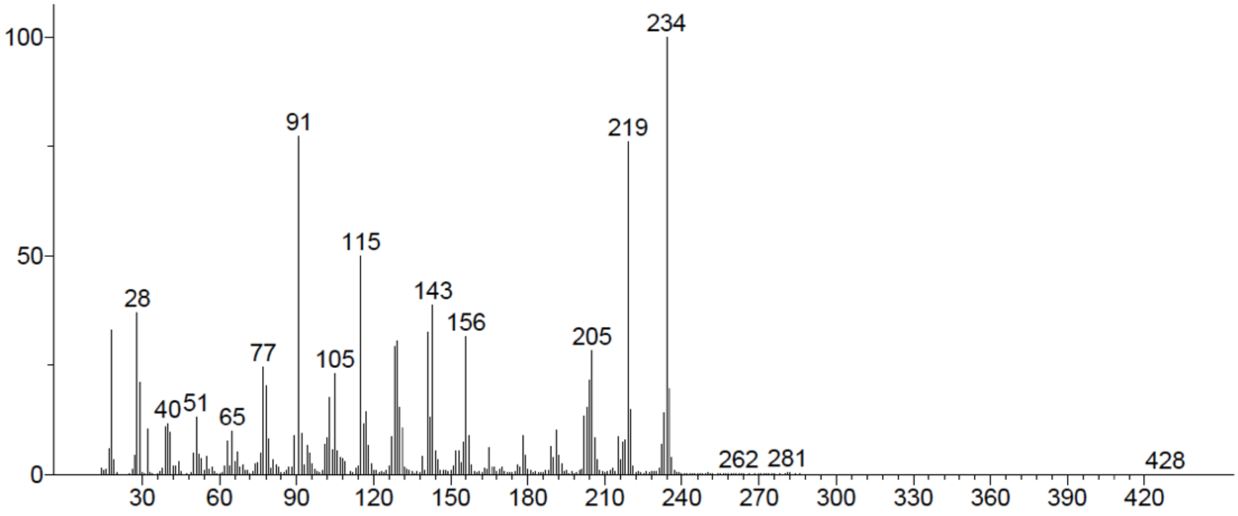

Figure B.28: Mass spectrum of compound G11.

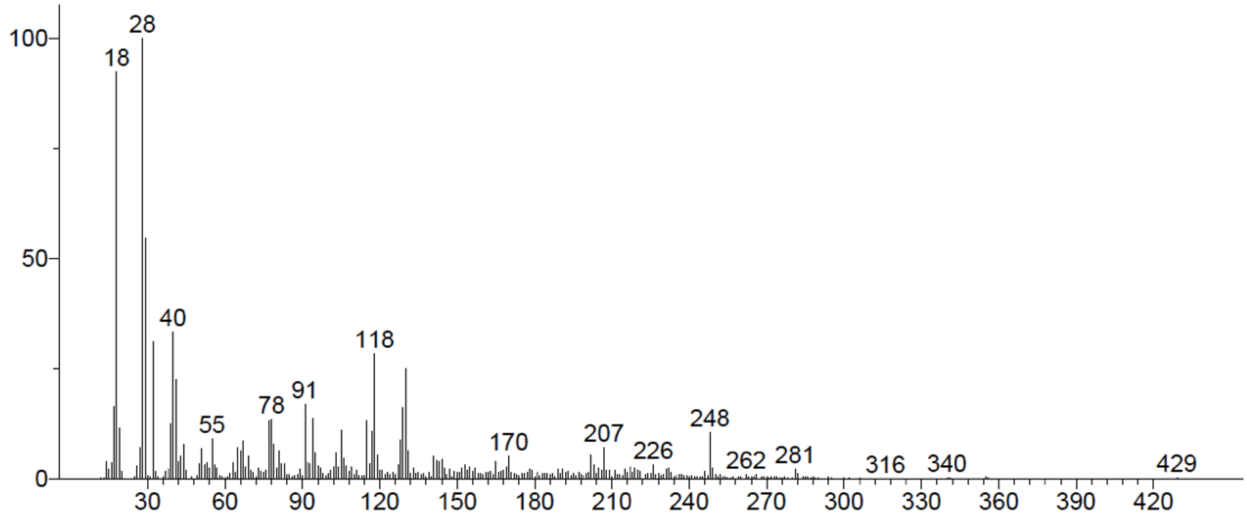

Figure B.29: Mass spectrum of compound H1.

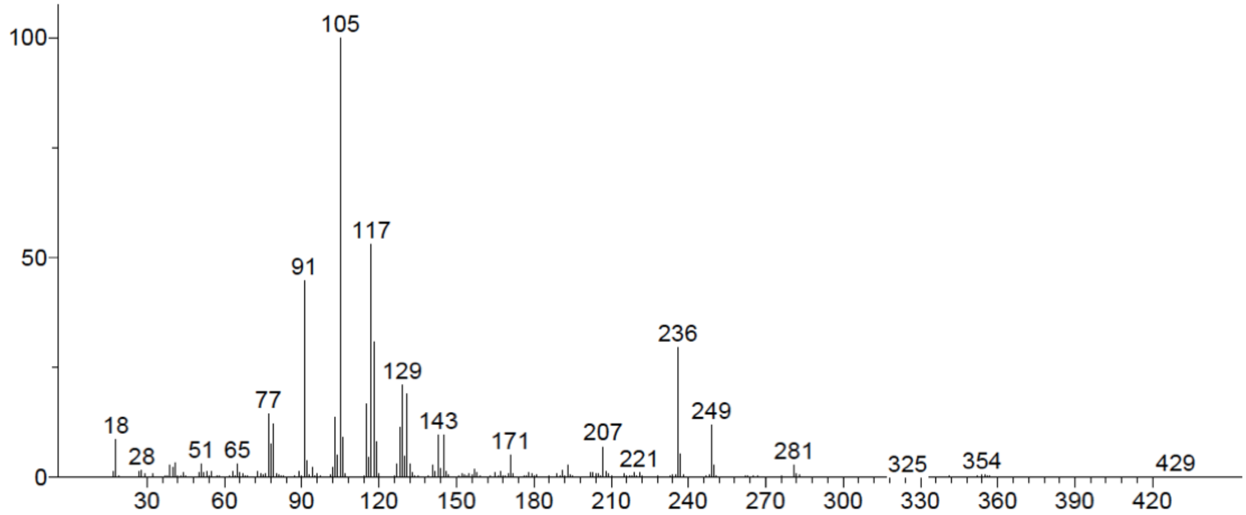

Figure B.30: Mass spectrum of compound H2.

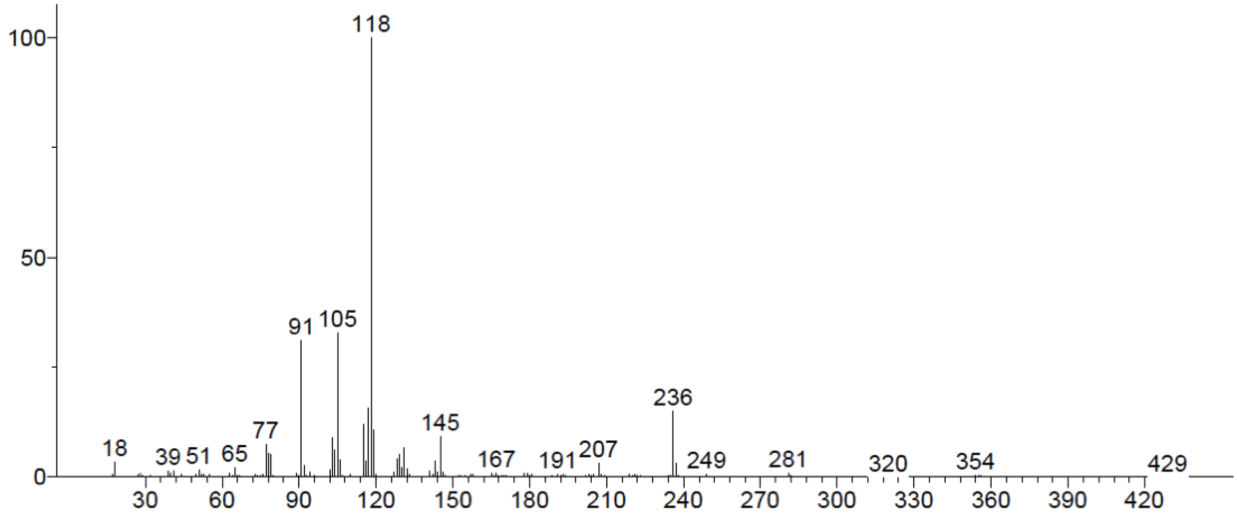

Figure B.31: Mass spectrum of compound H3.

B.8 Mass spectral assignment of selected species from regions G and H of the chromatograms

This section comprises the analysis of the mass spectra of selected compounds in the regions G and H of the chromatograms, which led to the assignment of the tentative structures shown in **Figure 4.2** of the manuscript. In addition to the MS library suggestions, a comprehensive analysis of the most abundant fragments in the mass spectra was performed, also taking into account energetic considerations.

B.8.1 $C_{18}H_{20}$ isomers

Compounds G1, G6, G7, and G8 presented a molecular ion peak at an m/z of 236, indicating that these species are products of AMS dimerization ($C_{18}H_{20}$ isomers). The possible structures for AMS dimers are shown in **Figure B.32**. The isomer with structure II in **Figure B.32** corresponds to 2,4-diphenyl-4-methyl-1-pentene, for which a commercial standard was available, but that isomer was not detected in the chromatograms.

The AMS dimer I in **Figure B.32** was previously identified in the study by Turuga and de Klerk,[1] on the thermal treatment of AMS at 250 °C in the presence of clays. The authors performed a comprehensive analysis of the MS spectrum to attribute structure I to one of the AMS dimers identified in their study. In the present study, the mass spectra of compound G1 (**Figure B.19**) precisely matched the spectra associated with structure I, as identified by Turuga and de Klerk [1]. This compound presented an intense peak at an m/z of 221, corresponding to its tricycle nature.

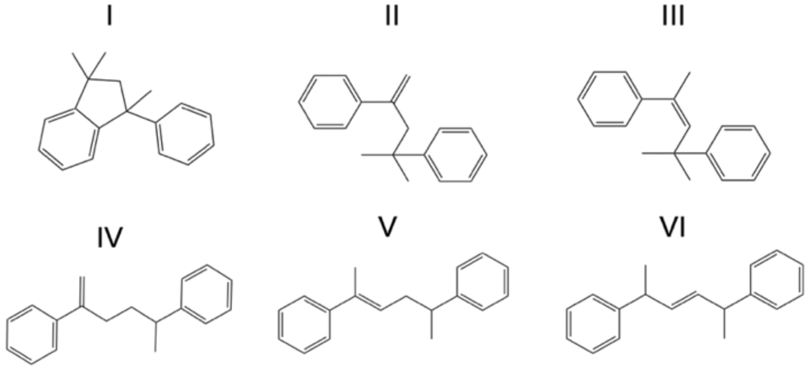

Figure B.32: Possible $C_{18}H_{20}$ isomers.

When comparing the RAP of compounds G6, G7, and G8 in the control reaction K+AMS (**Table B.14**), G6 was the most abundant product among them. Because the system K+AMS lacks hydrogen donors, it is likely that AMS dimerization in that system is initiated by hydrogen disproportionation between two AMS molecules. If this dimerization occurs within the cage (see **Figure B.33**), it is suspected that the primary product would be 2,5-diphenyl-1-hexene (structure IV in **Figure B.32**). The dimer G6 has a dominant peak at an m/z of 118 (**Figure B.23**), but it lacks heavier fragments, which suggests that the decomposition product of that species most easily forms cumyl-type fragments but does not readily lead to unsymmetrical fragmentation. Considering this feature of the G6 spectrum and the likelihood that structure IV is a product of a concerted bimolecular reaction (as depicted in **Figure B.33**), it is probable that G6 corresponds to the dimer with structure IV in **Figure B.32**.

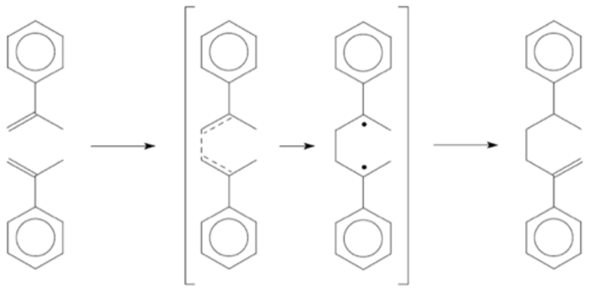

Figure B.33: Potential route for the AMS dimerization in the control system K+AMS.

Both isomers G7 and G8 have other noticeable features beyond the prominent 118 m/z fragment. For isomer G7 (**Figure B.24**), the most abundant peaks were the grouping around 118 > 91∼143 > 158∼104∼236 m/z. For isomer G8 (**Figure B.25**), the most abundant peaks were around 118 > 91∼236 > 104∼143 > 221 m/z. The noticeably higher peak at an m/z of 158 implies that fragmentation to lose the phenyl group directly is a meaningful decomposition pathway. For this to be stable, the fragmentation should typically have the C–phenyl bond fragment to create a stabilized C. This would make sense if that C could form an allylic radical conjugated to the remaining phenyl fragment, which suggests structure III in **Figure B.32** is a likely assignment for dimer G7.

The prominence of the peak at 236 m/z in compound G8 (**Figure B.25**) suggests that this is an isomer where the decomposition of the molecular ion is more challenging than in any other $C_{18}H_{20}$ isomers. The isomers II and V in **Figure B.32** are readily fragmented to produce allylic and benzylic radicals, making them less probable structures for G8. Since the C=C in structure VI is not conjugated with any of the phenyl groups, it could hinder fragmentation due to its position. This feature could explain the prominence of 236 m/z and the near absence of 158 m/z in the spectrum of compound G8, suggesting that structure VI is likely the G8 dimer.

In summary, the AMS dimers G1, G7, G8, and G9 were assigned to structures I, IV, III, and VI in **Figure B.32**, respectively.

B.8.2 $C_{18}H_{22}$ isomers

Compounds G3 and G4 presented a molecular ion peak at an m/z of 238, indicating that they correspond to hydrogenated AMS dimers ($C_{18}H_{22}$ isomers). It is reasonable that the saturated dimers must have skeletal structures derived from those of the $C_{18}H_{20}$ isomers, excluding isomer G1. The isomers G3, G4, and G5 represent primary-primary, primary-tertiary, and tertiary-tertiary addition products, as shown in **Figure B.34**. Compound G5 (structure III in **Figure B.34**) is dicumene, and a commercial standard was available for its identification; however, it was not detected in any of the reaction systems.

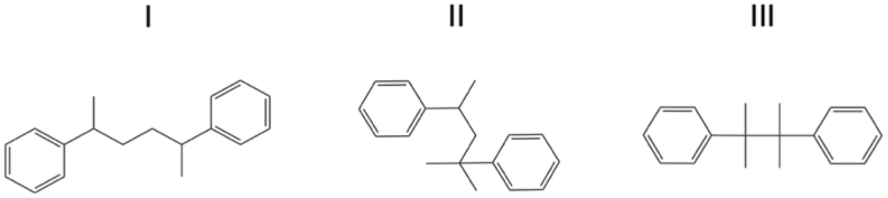

Figure B.34: Possible $C_{18}H_{22}$ isomers.

The mass spectra of G3 and G4 (**Figures B.21** and **B.22**) are almost identical. Also, their relative abundance in the products (**Tables B.13** and **B.14**) were comparable, not allowing for any consideration on the likelihood of specific compound formation. Therefore G3 and G4 could be any of the species depicted in structures I and II in **Figure B.34**.

B.8.3 $C_{18}H_{18}$ isomers

Compounds G9 and G11 presented a molecular ion peak at an m/z of 234 (**Figures B.26** and **B.28**), indicating that they correspond to C18H18 isomers. The possible products from AMS addition that could correspond to $C_{18}H_{18}$ isomers are the diene species shown in **Figure B.35**.

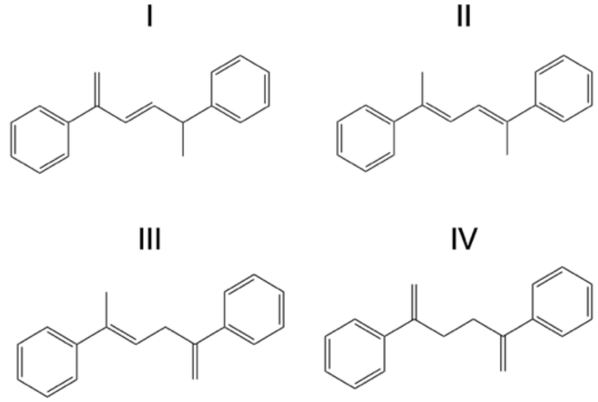

Figure B.35: Possible $C_{18}H_{18}$ isomers.

Compound G9 has a dominant peak with 219 m/z (**Figure B.26**), while all the other peaks are notably smaller. This suggests a compound that would readily lose a methyl group, which matches structure I in **Figure B.35**. Thus, it is likely that structure I corresponds to isomer G9.

The defining feature in the spectrum of isomer G11 (**Figure B.28**) is that its structure is resistant to fragmentation, with the peak at 234 m/z being the most abundant peak. This would rule out structure IV in **Figure B.35**, which would readily fragment. Based on energetic reasoning, conjugated dienes are expected to be more abundant than isolated ones, increasing the likelihood that compound G11 corresponds to structure II in **Figure B.35**.

B.9 References

(1) Turuga, A. S. S.; de Klerk, A. Free Radical and Cationic Addition due to Clay Minerals Found in Bitumen Froth at 250 °C Probed with Use of α-Methylstyrene and 1-Octene. *Energy Fuels* **2022**, *36* (23), 14148–14162.

Appendix C: Supporting information for Chapter 5

C.1 Characterization of minerals

The characterization properties of the minerals used in this study (i.e., kaolinite, rutile, and quartz) are given in **Table C.1**.

The particle size distribution was analyzed in the Institute of Oil Sands Innovation laboratory in the chemical engineering department at the University of Alberta. The equipment used was a Malvern Mastersizer 3000. Reverse osmosis water was used as a dispersant fluid. The particle size was measured in the range of 0.01 to 3500 μm at an acquisition rate of 10 kHz.

Table C.1: Characterization properties of kaolinite, rutile, and quartz used in this study.

Property	**Mineral**		
	kaolinite	**rutile**	**quartz**
Particle diameter range (μm)	0.7–67	0.2–4	163–670
Particle diameter (μm)			
10 vol%	<2	<0.4	<242
50 vol%	<7	<1	<314
90 vol%	<22	<2	<417
BET surface area (m^2/g)	9.37	5.18	1.53
Cumulative pore volume ($\times 10^{-5}$ m^3/kg)	6.4	2.9	0.2

The specific surface area and pore volume were assessed through nitrogen gas adsorption using a Quantacrome Autosorb iQ. This analysis relied on the Brunauer-Emmet-Teller (BET) theory for specific surface area determination. Around 0.5 g of sample was inserted in a 9-mm quartz cell and outgassed at 150 °C for 2 hours. Following this, the surface area and pore volume were determined using 7 BET, 21 adsorption, and 20 desorption data points.

The stereo-microscope pictures of the minerals used in this study are shown in **Figure C.1**.

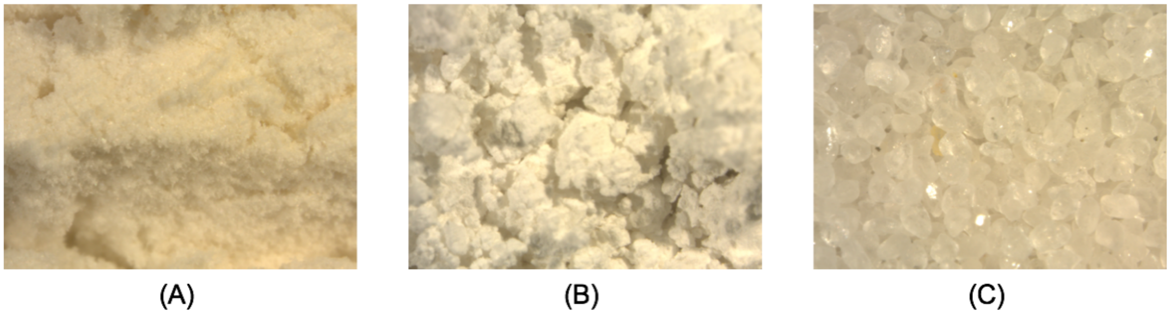

Figure C.1: Stereo-microscope pictures of (A) kaolinite, (B) rutile, and (C) quartz at 30x magnification.

C.2 Commercial standards used for identity confirmation of compounds detected in the GC-MS spectra

The list of commercial standards used for identity confirmation of products in this study is shown in **Table C.2**.

Table C.2: Commercial standards used for compound identification through GC-MS.

Compound	Formula	CASRN[a]	Purity (%)[b]	Supplier	Molecular weight (g/mol)	RT (min)[c]
hexane	C_6H_{14}	110-54-3	95	Sigma Aldrich	86.18	4.7
benzene	C_6H_6	71-43-2	99.8	Sigma Aldrich	78.11	6.3
heptane	C_7H_{16}	142-82-5	98	Fisher Scientific	100.21	8.3
toluene	C_7H_8	108-88-3	99.9	Fisher Scientific	92.14	11.0
octane	C_8H_{18}	111-65-9	95	Fisher Scientific	114.23	13.5

Continues on the next page

Compound	Formula	CASRN[a]	Purity (%)[b]	Supplier	Molecular weight (g/mol)	RT (min)[c]
ethylbenzene	C_8H_{10}	100-41-4	99	Sigma Aldrich	106.16	16.2
styrene	C_8H_8	100-42-5	99	Sigma Aldrich	104.15	17.7
nonane	C_9H_{20}	111-84-2	99	Thermo Scientific	128.26	19.4
cumene	C_9H_{12}	98-82-8	98	Sigma Aldrich	120.19	20.0
n-propylbenzene	C_9H_{12}	103-65-1	98	Sigma Aldrich	120.2	21.7
AMS (alphamethylstyrene)	C_9H_{10}	98-83-9	99	Sigma Aldrich	118.18	23.1
tert-butylbenzene	$C_{10}H_{14}$	1998-06-06	99	Sigma Aldrich	134.22	23.9
isobutylbenzene	$C_{10}H_{14}$	538-93-2	99	Sigma Aldrich	134.22	24.8
sec-butylbenzene	$C_{10}H_{14}$	135-98-8	99	Sigma Aldrich	134.22	24.9
decane	$C_{10}H_{22}$	124-18-5	94	Sigma Aldrich	142.28	25.1
indane	C_9H_{10}	496-11-7	95	Acros Organics	118.18	26.0
indene	C_9H_8	95-13-6	90	Sigma Aldrich	116.16	26.4
n-butylbenzene	$C_{10}H_{14}$	104-51-8	99	Sigma Aldrich	134.22	27.3
decalin (decahydronaphthalene (cis/trans))	$C_{10}H_{18}$	91-17-8	99	Sigma Aldrich	138.25	27.9 & 30.1

Continues on the next page

Compound	Formula	CASRN[a]	Purity (%)[b]	Supplier	Molecular weight (g/mol)	RT (min)[c]
2-phenyl-2-propanol	$C_9H_{12}O$	617-94-7	98	TCI	136.19	28.4
undecane	$C_{11}H_{24}$	1120-21-4	99	Sigma Aldrich	156.31	30.6
tetralin (1,2,3,4-tetrahydronaphthalene)	C10H12	119-64-2	99	Sigma Aldrich	132.2	32.8
naphthalene	$C_{10}H_8$	91-20-3	99	Sigma Aldrich	128.17	33.7
dodecane	$C_{12}H_{26}$	112-40-30	99	Honeywell	170.33	35.7
2-methylnaphthalene	$C_{11}H_{10}$	91-57-6	97	Alfa Aesar	142.2	38.8
1-methylnaphthalene	$C_{11}H_{10}$	90-12-0	96	Alfa Aesar	142.2	39.5
tridecane	$C_{13}H_{28}$	629-50-5	99	Acros Organics	184.37	39.9
biphenyl	$C_{12}H_{10}$	92-52-4	99.5	Sigma Aldrich	154.21	42.1
tetradecane	$C_{14}H_{30}$	629-59-4	99	Alfa Aesar	198.39	43.9
1,4-dimethylnaphthalene	$C_{12}H_{12}$	571-58-4	95	Sigma Aldrich	156.23	44.4
pentadecane	$C_{15}H_{32}$	629-62-9	99	Acros Organics	212.42	47.2

[a] Chemical Abstracts Services Registry Number (CASRN).[b] Purity of material provided by the supplier. Material was not further purified. [c] Retention time (RT).

C.3 Calibration data for compounds quantification through GC-FID

Table C.3 contains the linear regression data obtained from the calibration curves built for selected species in this study. Each calibration curve was obtained from four data points of concentration ratios (concentration of the compound to be quantified divided by the concentration of the internal standard) versus area ratios (area of the compound to be quantified divided by the area of the internal standard) using biphenyl as an internal standard and methanol as a solvent.

Table C.3: Linear regression data from calibration curves for selected species that were quantified through GC-FID.

Compound	Slope (*b*)[a]	R^2
AMS	1.0212	0.9999
benzene	1.0969	0.9998
cumene	1.0541	0.9998
ethylbenzene	1.0443	0.9998
n-pentadecane	1.0913	0.9999
naphthalene	0.9851	0.9995
n-propylbenzene	1.0264	0.9998
sec-butylbenzene	1.0358	0.9997
tetralin	1.0270	0.9999
toluene	1.1211	0.9995

[a] Slope (b) in the linear regression $y = bx$, where y is the concentration ratio between the species to be quantified and biphenyl, and x is the area ratio between the species to be quantified and biphenyl.

C.4 Temperature profiles inside the reactor

The temperature profiles of the ATP experiments conducted at a reaction time of 10 min are illustrated in **Figure C.2**. The systems ATP and ATP+K achieved the reaction temperature of 400 °C in approximately 10–12 min, whereas the water-containing systems required a longer time, approximately 14–16 min, to reach the same reaction temperature. The air-assisted cooling-down process took approximately 5–7 min to reach 50 °C in all the reaction systems. Although only the temperature profiles inside the reactor of the ATP experiments with a 10-min reaction time are shown in **Figure C.2**, it is noteworthy that all the other experiments exhibited comparable heating and cooling profiles.

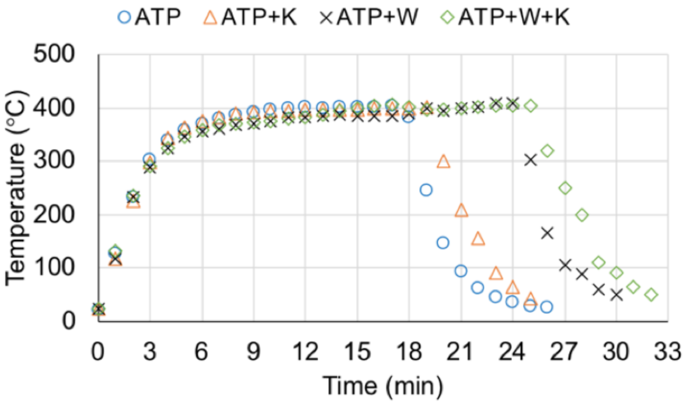

Figure C.2: Temperature profiles inside the reactors during the ATP experiments with planned reaction times of 10 min.

C.5 Data used for concentration calculations in the ATP experiments

The exact amount of product sample used for GC-FID quantification, the mass of formed gas, the density data at 25 °C, and the corrected sample volume used to calculate the concentration of species in the ATP experiment are listed in **Table C.4**. The mass of the formed gas during the reactions, which was lost after the reactor was opened, was added to the mass of the liquid sample used for GC-FID quantification, and the product density at 25 °C was used to calculate the volume of the corrected product sample volume. The density of the liquid product was assumed to not significantly change because of the small amount of gas formed during the experiments.

The mass fractions of AMS, tetralin, and *n*-pentadecane obtained through calibrated GC-FID data and the concentrations of each of these compounds are listed in **Tables C.5**, **C.6**, and **C.7**, respectively.

Table C.4: Data used for calculating and correcting the product sample volume used for concentration calculations.

System	Mass of product sample used for GC-FID quantification (g)	Relative mass of formed gas (mg of gas / g of ATP)	Total mass of formed gas (g)	Mass of product sample + Mass of formed gas (g)	Product density at 25 °C (g/cm^3)	Corrected product sample volume (cm^3)
ATP						
1 min	0.4960	7	0.0035	0.4995	0.8417	0.5935
5 min	0.4966	6	0.0031	0.4997	0.8474	0.5897
10 min	0.5047	12	0.0058	0.5105	0.8502	0.6005
30 min	0.4935	33	0.0162	0.5097	0.8503	0.5994
ATP+K						
1 min	0.4978	2	0.0011	0.4989	0.8429	0.5919
5 min	0.4993	2	0.0010	0.5003	0.8478	0.5901
10 min	0.5067	9	0.0045	0.5112	0.8495	0.6018
30 min	0.5045	14	0.0069	0.5114	0.8493	0.6021
ATP+W						
1 min	0.4988	4	0.0022	0.5010	0.8412	0.5955
5 min	0.4983	4	0.0020	0.5003	0.8463	0.5911
10 min	0.4980	32	0.0158	0.5138	0.8490	0.6052
30 min	0.4904	9	0.0046	0.4950	0.8499	0.5824
30 min (rep)[a]	0.5024	40	0.0201	0.5225	0.8503	0.6145
ATP+W+K						
1 min	0.5013	12	0.0060	0.5073	0.8418	0.6027
5 min	0.4939	18	0.0088	0.5027	0.8469	0.5936
10 min	0.4925	18	0.0090	0.5015	0.8489	0.5908
30 min	0.4970	22	0.0111	0.5081	0.8476	0.5995
30 min (rep)[a]	0.5115	69	0.0353	0.5468	0.8480	0.6448

[a] “rep” stands for replicate.

Table C.5: Mass fraction of AMS and AMS concentration (in kg/m^3) in the products of the ATP experiments.

System	Mass fraction of AMS in the product (wt/wt)	Mass of AMS in the product sample (g)	AMS concentration (kg/m^3)^a
ATP			
1 min	0.2241	0.1111	187.28
5 min	0.1415	0.0703	119.16
10 min	0.0838	0.0423	70.44
30 min	0.0233	0.0115	19.22
ATP+K			
1 min	0.1905	0.0948	160.19
5 min	0.1150	0.0574	97.33
10 min	0.0663	0.0336	55.79
30 min	0.0157	0.0079	13.14
ATP+W			
1 min	0.2311	0.1153	193.57
5 min	0.1600	0.0797	134.88
10 min	0.1046	0.0521	86.10
30 min	0.0441	0.0216	37.11
30 min (rep)^b	0.0373	0.0187	30.49
ATP+W+K			
1 min	0.2081	0.1043	173.06
5 min	0.1197	0.0591	99.62
10 min	0.0683	0.0337	56.98
30 min	0.0345	0.0171	28.60
30 min (rep)^b	0.0230	0.0118	18.28

[a] AMS concentration in the feed was calculated based on measured mass of AMS when preparing the feed and the density of feed at 25 °C (836.4 kg/m^3) and was found to be equal to 250.9 kg/m^3 for all reaction systems. [b] "rep" stands for replicate.

Table C.6: Mass fraction of tetralin and tetralin concentration (in kg/m^3) in the products of the ATP experiments.

System	Mass fraction of tetralin in the product (wt/wt)	Mass of tetralin in the product sample (g)	tetralin concentration (kg/m^3)[a]
ATP			
1 min	0.1678	0.0832	140.27
5 min	0.1537	0.0763	129.47
10 min	0.1358	0.0685	114.12
30 min	0.1193	0.0589	98.21
ATP+K			
1 min	0.1625	0.0809	136.70
5 min	0.1495	0.0746	126.45
10 min	0.1347	0.0683	113.45
30 min	0.1161	0.0586	97.29
ATP+W			
1 min	0.1697	0.0847	142.16
5 min	0.1549	0.0772	130.55
10 min	0.1436	0.0715	118.19
30 min	0.1245	0.0610	104.80
30 min (rep)[b]	0.1262	0.0634	103.16
ATP+W+K			
1 min	0.1661	0.0833	138.15
5 min	0.1477	0.0730	122.93
10 min	0.1328	0.0654	110.70
30 min	0.1215	0.0604	100.76
30 min (rep)[b]	0.1193	0.0610	94.67

[a] Tetralin concentration in the feed was calculated based on measured mass of tetralin when preparing the feed and the density of feed at 25 °C (836.4 kg/m^3), and was found to be equal to 167.3 kg/m^3 for all reaction systems. [b] "rep" stands for replicate.

Table C.7: Mass fraction of *n*-pentadecane and *n*-pentadecane concentration (in kg/m^3) in the products of the ATP experiments.

System	Mass fraction of *n*-pentadecane in the product (wt/wt)	Mass of *n*-pentadecane in the product sample (g)	n-pentadecane concentration (kg/m^3)^a
ATP			
1 min	0.3913	0.1941	327.08
5 min	0.3692	0.1833	310.88
10 min	0.3600	0.1817	302.61
30 min	0.3174	0.1566	261.28
ATP+K			
1 min	0.4080	0.2031	343.11
5 min	0.3692	0.1843	312.34
10 min	0.3640	0.1844	306.45
30 min	0.3397	0.1714	284.65
ATP+W			
1 min	0.4057	0.2024	339.82
5 min	0.3765	0.1876	317.42
10 min	0.3607	0.1796	296.80
30 min	0.3162	0.1551	266.25
30 min (rep)^b	0.3084	0.1549	252.15
ATP+W+K			
1 min	0.4012	0.2011	333.72
5 min	0.3635	0.1795	302.42
10 min	0.3532	0.1739	294.44
30 min	0.3283	0.1632	272.21
30 min (rep)^b	0.3315	0.1695	262.94

^{a} *n*-Pentadecane concentration in the feed was calculated based on measured mass of *n*-pentadecane when preparing the feed and the density of feed at 25 °C (836.4 kg/m^3), and was found to be equal to 418.2 kg/m^3 for all reaction systems. ^{b} "rep" stands for replicate.

C.6 Polynomial coefficients and plots of selected species

The coefficients of the interpolating polynomials that describe the concentration of selected species in feed and products as functions of the ERT at 400 °C for the time intervals of 1–10 min and 5–30 min are given in **Tables C.8–C.10**. These polynomial functions were used to evaluate the rates of reaction at 5 and 10 min. Since the interpolating polynomials were built to contain the exact data points used for obtaining their coefficients, it was not feasible to calculate the error associated with their data prediction. For this reason, the polynomials were graphed on concentration vs. ERT plots to facilitate a visual inspection of the trends they represented. The results are shown in **Figures C.3-C.17**. The trends described by the polynomial functions were consistent with the trends suggested by the measured concentration vs. ERT data points.

C.6.1 AMS, tetralin, and *n*-pentadecane

Table C.8: Coefficients of the polynomial functions of AMS, tetralin, and *n*-pentadecane, describing concentration over ERT at 400 °C within the time intervals of 1–10 min and 5–30 min.

Compound / System	Polynomial coefficients // $C_w = at^2+bt+c$ [a,b]					
	Δt = 1–10 min			Δt = 5–30 min		
AMS	a	b	c	a	b	c
ATP	0.809	-21.887	208.36	0.287	-14.054	182.25
ATP+K	0.823	-20.653	180.02	0.247	-12.013	151.22
ATP+W	0.546	-17.950	210.97	0.286	-14.041	197.94
ATP+W+K	1.092	-24.915	196.88	0.274	-12.638	155.96
tetralin						
ATP	-0.041	-2.453	142.76	0.091	-4.435	149.37
ATP+K	-0.004	-2.537	139.24	0.072	-3.675	143.03
ATP+W	0.048	-3.189	145.3	0.070	-3.529	146.43
ATP+W+K	0.151	-4.711	142.71	0.072	-3.524	138.75
***n*-pentadecane**						
ATP	0.266	-5.647	332.46	-0.016	-1.407	318.32
ATP+K	0.724	-12.035	354.42	0.003	-1.231	318.41
ATP+W	0.164	-6.584	346.24	0.090	-5.470	342.53
ATP+W+K	0.692	-11.978	345.00	0.010	-1.747	310.90

[a] Cw in units of kg/m^3 and t in units of min. [b] The independent variable t in the interpolating polynomial corresponds to the ERT at 400 °C.

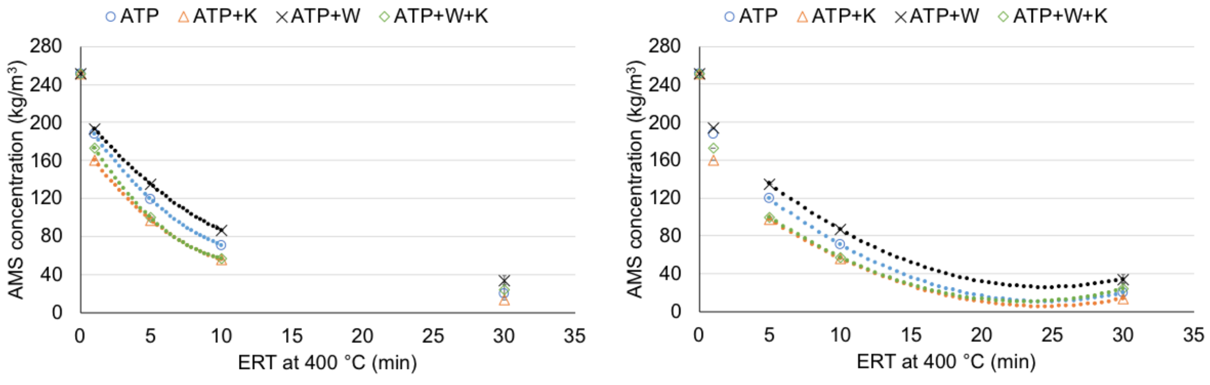

(A)

(B)

Figure C.3: Plot of the polynomial functions describing the AMS concentration over time for the time intervals of (A) 1–10 min and (B) 5–30 min.

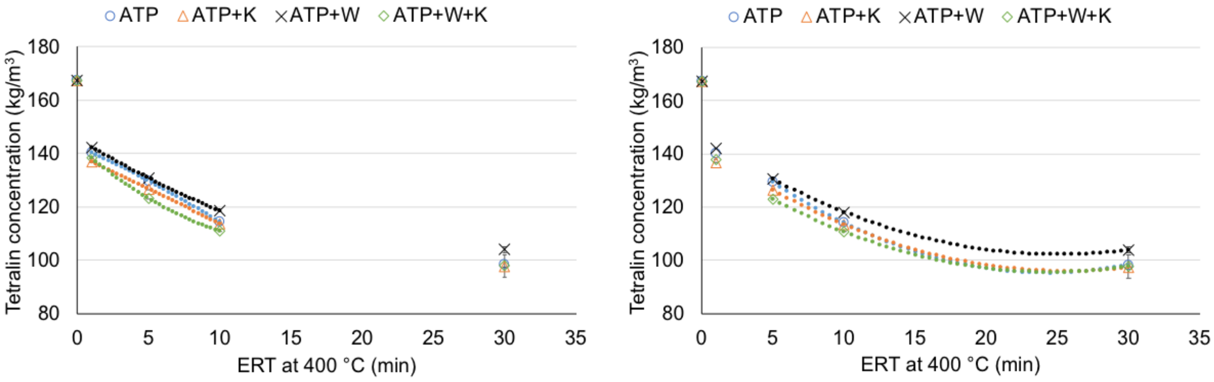

(A)

(B)

Figure C.4: Plot of the polynomial functions describing the tetralin concentration over time for the time intervals of (A) 1–10 min and (B) 5–30 min.

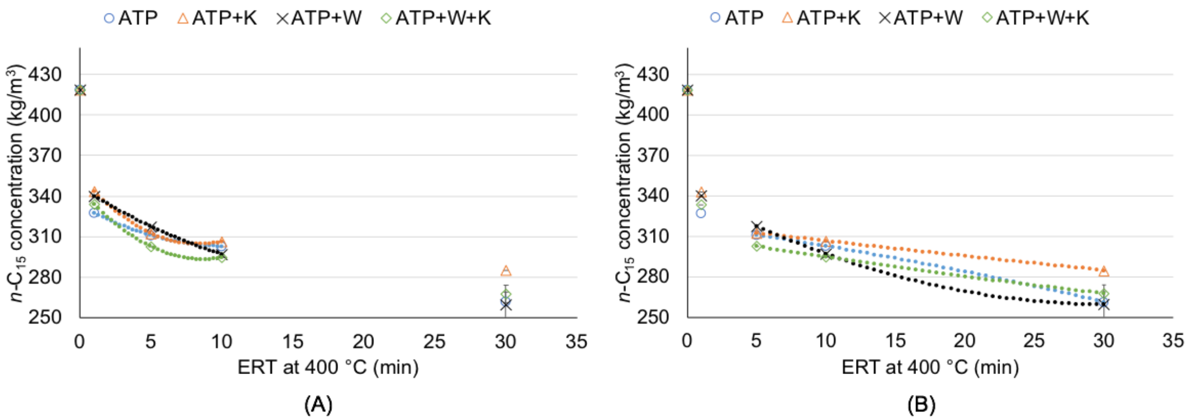

Figure C.5: Plot of the polynomial functions describing the n-pentadecane concentration over time for the time intervals of (A) 1–10 min and (B) 5–30 min.

C.6.2 Benzene, toluene, ethylbenzene, *n*-propylbenzene, cumene, and naphthalene

Table C.9: Coefficients of the polynomial functions of benzene, toluene, ethylbenzene, n-propylbenzene, cumene, and naphthalene, describing concentration over ERT at 400 °C within the time intervals of 1–10 min and 5–30 min.

Compound / System	Polynomial coefficients // $C_W = at^2 + bt + c^{a,b}$					
	Δt = 1-10 min			Δt = 5-30 min		
	a	b	c	a	b	c
benzene						
ATP	0.0005	-0.0024	0.0018	-0.0001	0.0069	-0.0290
ATP+K	0.0019	-0.0092	0.6672	-0.0006	0.0301	0.5322
ATP+W	-	-	-	0.0002	-0.0030	0.0100
ATP+W+K	-0.0002	0.0070	0.0249	0.0000	0.0048	0.0324
toluene						
ATP	0.0087	-0.0131	0.2078	-0.0023	0.1507	-0.3382
ATP+K	0.0011	0.0575	0.0053	-0.0005	0.0819	-0.0762
ATP+W	-0.0013	0.0716	0.0854	0.0008	0.0398	0.1914
ATP+W+K	-0.0008	0.0894	-0.0304	-0.0006	0.0871	-0.0225
ethylbenzene						
ATP	-0.0481	2.2528	1.9074	-0.0347	2.0508	2.5807
ATP+K	-0.0686	2.4462	0.9009	-0.0362	1.9605	2.5201

Continues on the next page

Compound / System	Polynomial coefficients // C_W = at^2 + bt + $c^{a,b}$					
	Δt = 1-10 min			Δt = 5-30 min		
	a	b	c	a	b	c
ATP+W	-0.0235	1.8976	1.9527	-0.0389	2.1287	1.1824
ATP+W+K	-0.1412	3.5102	0.3045	-0.0369	1.9452	5.5212
***n*-propylbenzene**						
ATP	0.0005	0.2282	-0.0228	-0.0043	0.3002	-0.2628
ATP+K	-0.0033	0.2568	-0.0586	-0.0039	0.2660	-0.0892
ATP+W	0.0033	0.1842	0.0038	-0.0043	0.2990	-0.3791
ATP+W+K	-0.0097	0.3316	-0.0867	-0.0031	0.2329	0.2422
cumene						
ATP	-0.0195	1.9373	1.4627	-0.0286	2.0735	1.0087
ATP+K	-0.0881	3.6252	10.7746	-0.0445	2.9706	12.9567
ATP+W	-0.0037	1.5614	1.3423	-0.0189	1.7894	0.5822
ATP+W+K	-0.1938	5.1724	6.3486	-0.0585	3.1425	13.1150
naphthalene						
ATP	0.0144	0.4774	0.3621	-0.0096	0.8373	-0.8375
ATP+K	-0.0084	1.1154	2.3135	-0.0160	1.2303	1.9306
ATP+W	0.0215	0.3557	0.4468	-0.0070	0.7836	-0.9795
ATP+W+K	-0.0677	2.0613	0.8352	-0.0251	1.4231	2.9625

[a] C_W in units of kg/m^3 and t in units of min. [b] The independent variable t in the interpolating polynomial corresponds to the ERT at 400 °C.

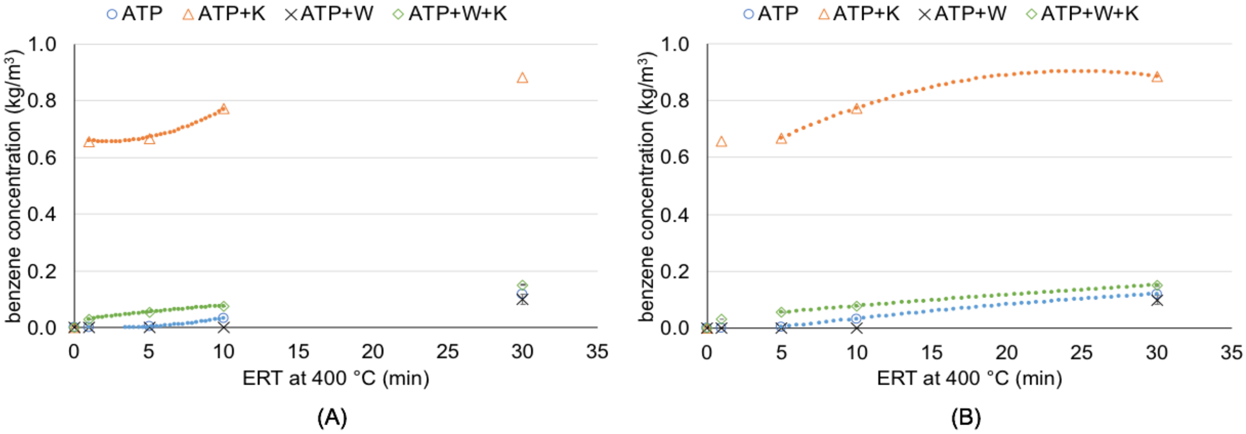

Figure C.6: Plot of the polynomial functions describing the benzene concentration over time for the time intervals of (A) 1–10 min and (B) 5–30 min.

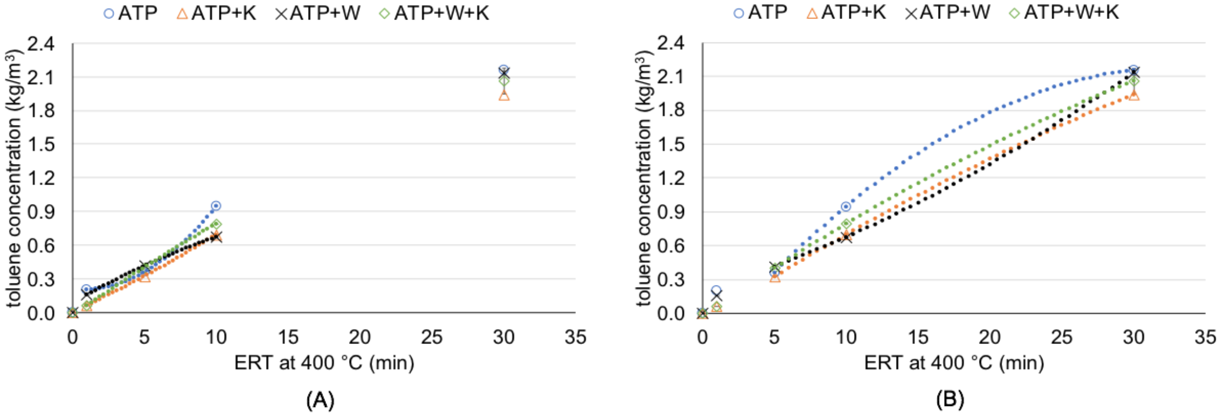

Figure C.7: Plot of the polynomial functions describing the toluene concentration over time for the time intervals of (A) 1–10 min and (B) 5–30 min.

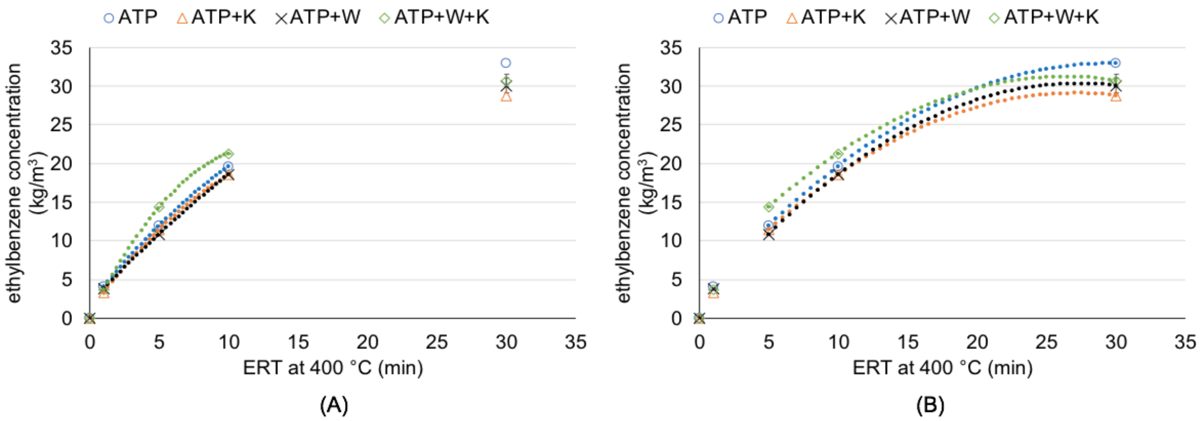

Figure C.8: Plot of the polynomial functions describing the ethylbenzene concentration over time for the time intervals of (A) 1–10 min and (B) 5–30 min.

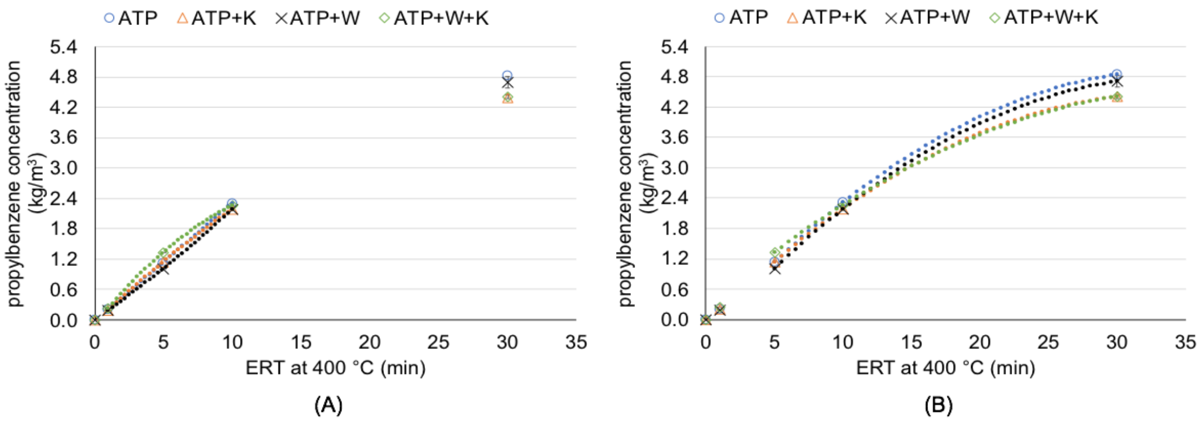

Figure C.9: Plot of the polynomial functions describing the *n*-propylbenzene concentration over time for the time intervals of (A) 1–10 min and (B) 5–30min.

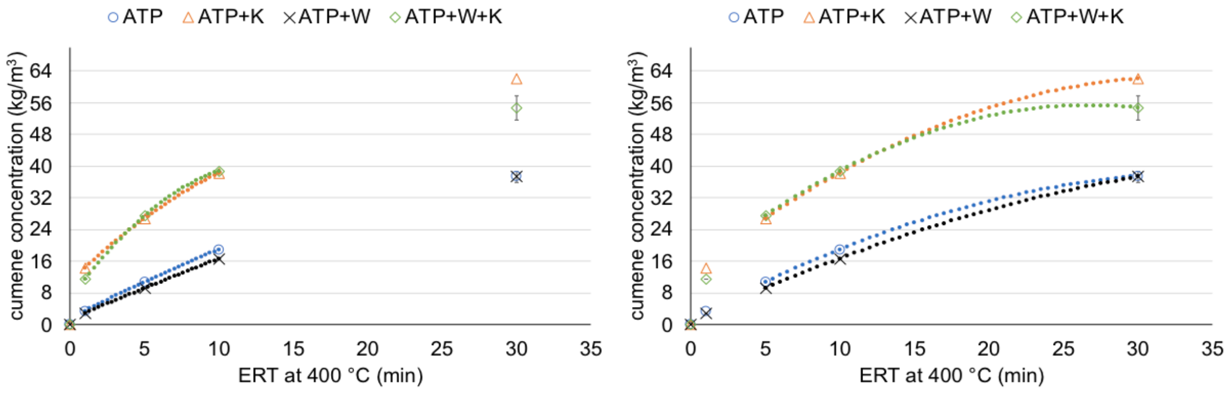

(A) (B)

Figure C.10: Plot of the polynomial functions describing the cumene concentration over time for the time intervals of (A) 1–10 min and (B) 5–30 min.

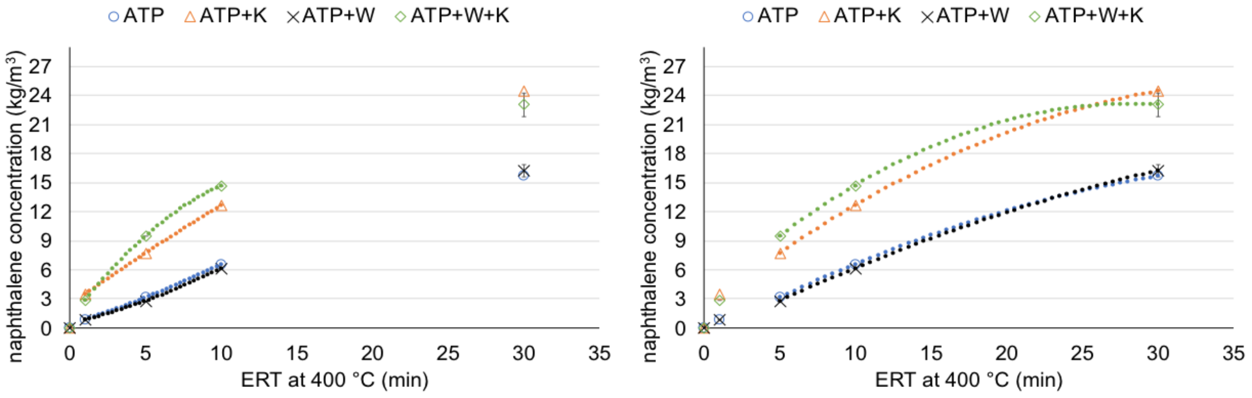

(A) (B)

Figure C.11: Plot of the polynomial functions describing the naphthalene concentration over time for the time intervals of (A) 1–10 min and (B) 5–30 min.

C.6.3 Species with retention time higher than 50 min (E1–E6)

Table C.10: Coefficients of the polynomial functions of species E1–E6, describing concentration over ERT at 400 °C within the time intervals of 1–10 min and 5–30 min.

Compound / System	Polynomial coefficients // $C_W = at^2 + bt + c^{a,b}$					
	Δt = 1-10 min			Δt = 5-30 min		
	a	*b*	*c*	*a*	*b*	*c*
E1						
ATP	-	-	-	-	-	-
ATP+K	-0.0001	-0.0316	2.7455	0.0022	-0.0671	2.8639
ATP+W	-	-	-	-	-	-
ATP+W+K	-0.0119	0.2648	1.0915	-0.0065	0.1835	1.3626
E2						
ATP	0.0002	0.0248	0.0209	-0.0009	0.0417	-0.0355
ATP+K	0.0030	-0.0397	0.3313	0.0000	0.0055	0.1804
ATP+W	0.0001	0.0200	0.0176	-0.0007	0.0332	-0.0266
ATP+W+K	0.0004	0.0081	0.0992	-0.0005	0.0213	0.0552
E3						
ATP	-0.0003	0.0441	0.0138	-0.0013	0.0600	-0.0393
ATP+K	-0.0025	0.0573	0.0061	-0.0005	0.0277	0.1048
ATP+W	-0.0004	0.0372	0.0122	-0.0010	0.0458	-0.0162
ATP+W+K	-0.0028	0.0617	0.0203	-0.0008	0.0310	0.1227
E4						
ATP	-0.0203	0.0323	3.6845	0.0073	-0.3816	5.0639
ATP+K	-0.0198	0.0598	2.3156	0.0078	-0.3544	3.6963
ATP+W	-0.0185	0.0240	3.2726	0.0075	-0.3668	4.5753
ATP+W+K	0.0153	-0.2863	1.7392	0.0016	-0.0805	1.0535
E5						
ATP	-0.0187	0.4453	0.3592	-0.0062	0.2579	0.9841
ATP+K	-0.0254	0.4284	0.2887	-0.0011	0.0640	1.5033
ATP+W	-0.0162	0.3932	0.3142	-0.0051	0.2274	0.8670
ATP+W+K	-0.0182	0.3683	0.3326	-0.0035	0.1467	1.0714
E6						

Continues on the next page

Compound / System	Polynomial coefficients // $C_W = at^2 + bt + c^{a,b}$					
	Δt = 1-10 min			Δt = 5-30 min		
	a	b	c	a	b	c
ATP	-0.0120	0.3219	0.2232	-0.0047	0.2130	0.5860
ATP+K	-0.0174	0.3103	0.1801	-0.0010	0.0644	0.9998
ATP+W	-0.0101	0.2805	0.1957	-0.0039	0.1884	0.5026
ATP+W+K	-0.0131	0.2811	0.1995	-0.0027	0.1255	0.7183

[a] C_W was calculated using the relative area percentage (RAP) of each species. [b] The independent variable t in the interpolating polynomial corresponds to the ERT at 400 °C.

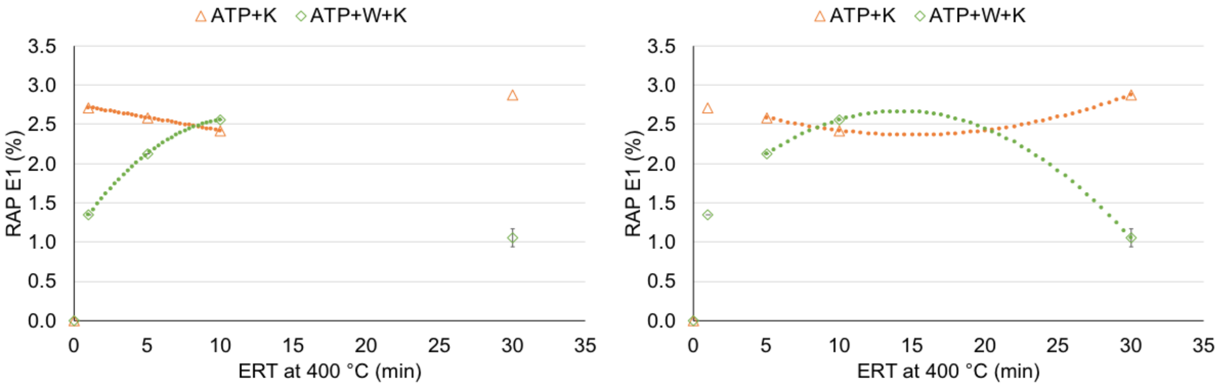

(A) (B)

Figure C.12: Plot of the polynomial functions describing the RAP of E1 over time for the time intervals of (A) 1–10 min and (B) 5–30 min.

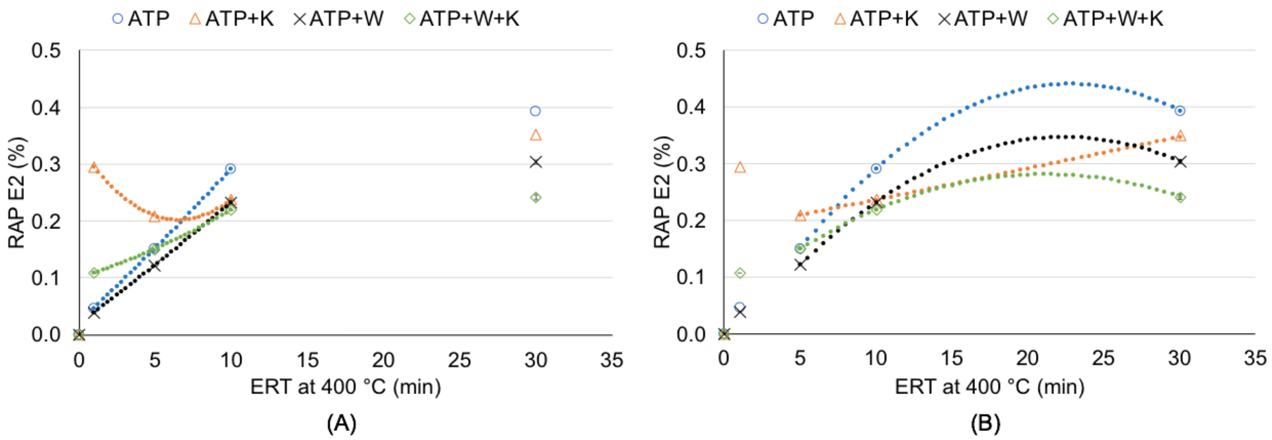

Figure C.13: Plot of the polynomial functions describing the RAP of E2 over time for the time intervals of (A) 1–10 min and (B) 5–30 min.

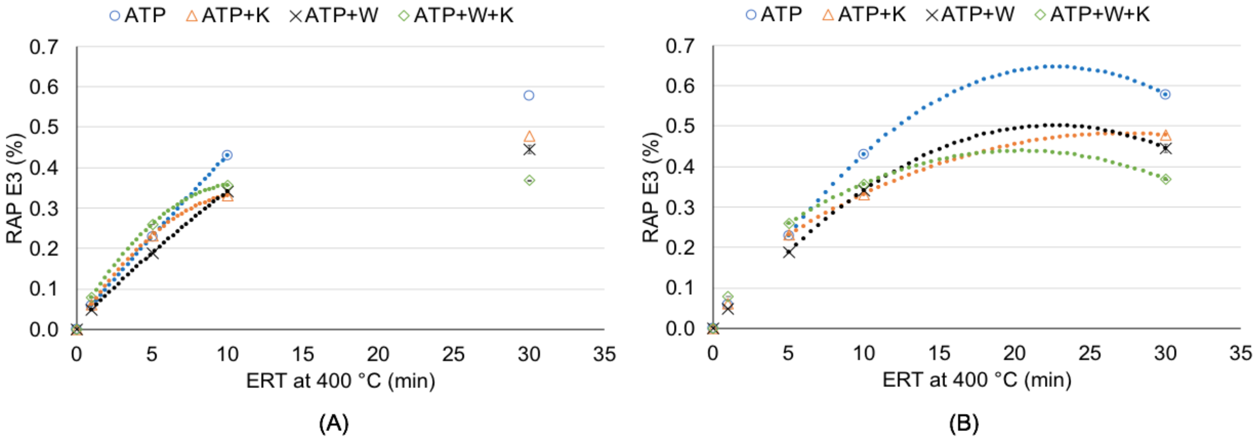

Figure C.14: Plot of the polynomial functions describing the RAP of E3 over time for the time intervals of (A) 1–10 min and (B) 5–30 min.

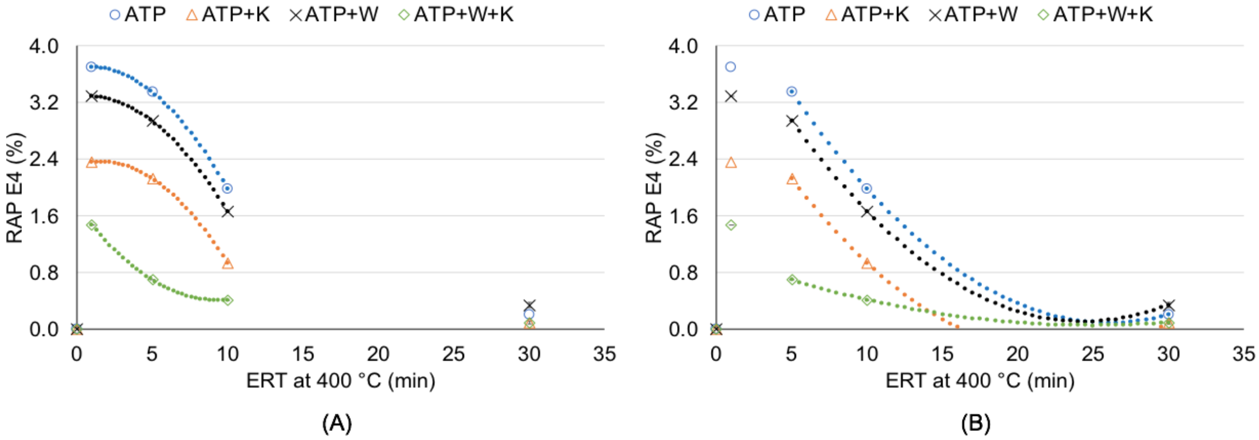

Figure C.15: Plot of the polynomial functions describing the RAP of E4 over time for the time intervals of (A) 1–10 min and (B) 5–30 min.

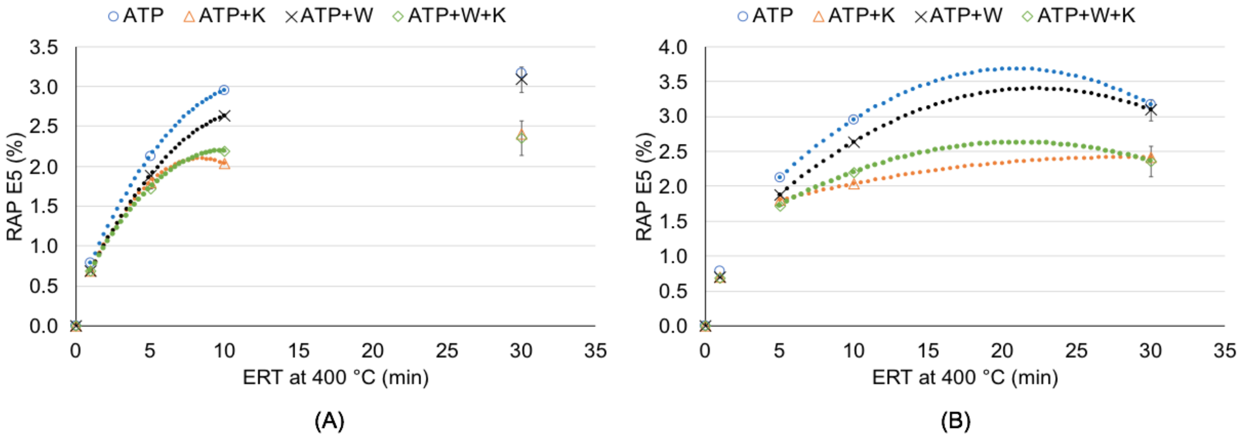

Figure C.16: Plot of the polynomial functions describing the RAP of E5 over time for the time intervals of (A) 1–10 min and (B) 5–30 min.

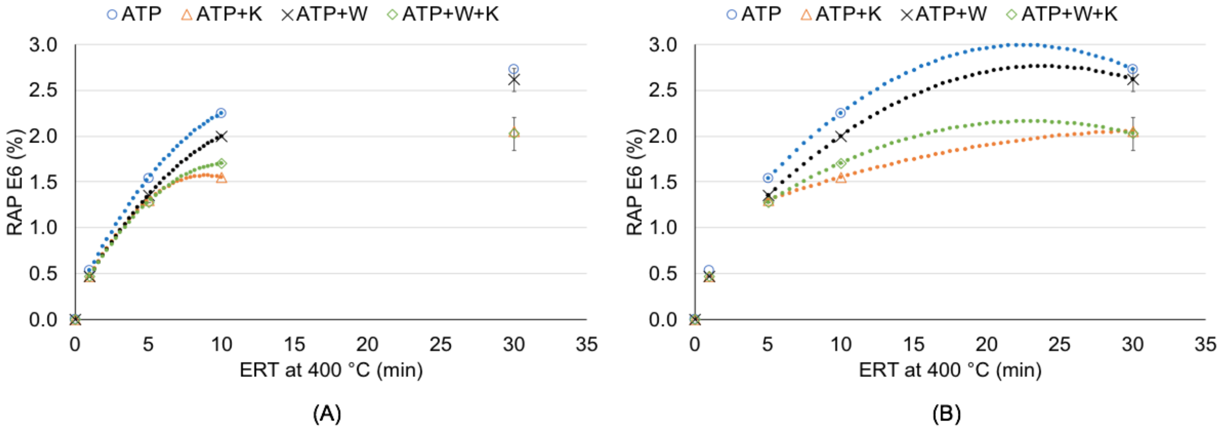

Figure C.17: Plot of the polynomial functions describing the RAP of E6 over time for the time intervals of (A) 1–10 min and (B) 5–30 min.

C.7 Concentration versus time plots of AMS, tetralin, and *n*-pentadecane conversion in the ATP experiments

C.7.1 Concentration versus reaction time plots of AMS

The plot of the natural logarithm of the AMS concentration versus time and the plot of the inverse of the AMS concentration versus time are shown in **Figures C.18** and **C.19**, respectively. The linear regressions were calculated for each reaction system and the R^2 of the regressions are given in the figures.

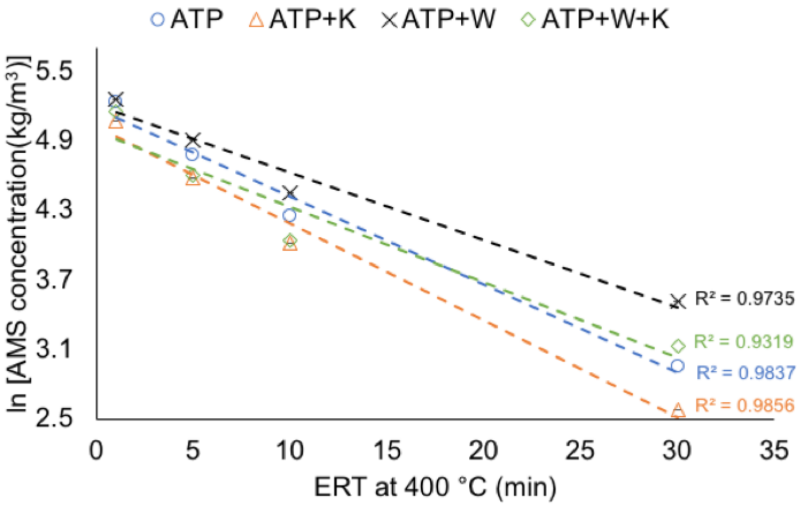

Figure C.18: Plot of the natural logarithm of AMS concentration vs. reaction time.

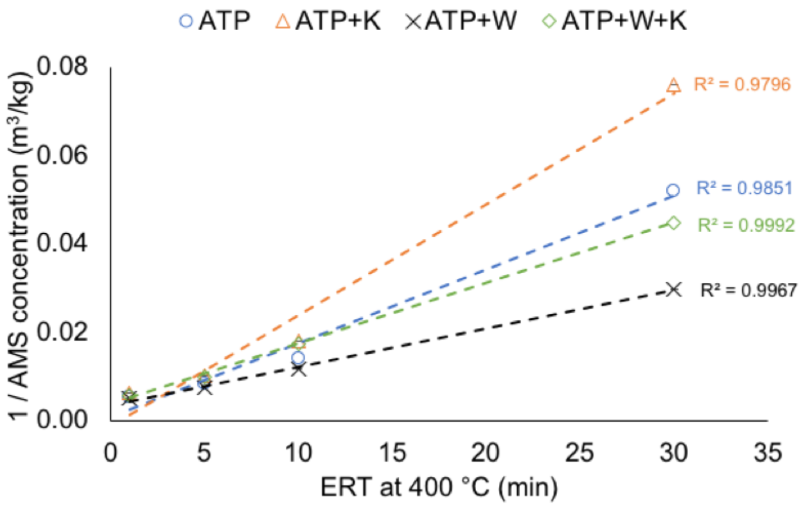

Figure C.19: Plot of the inverse of AMS concentration vs. reaction time.

C.7.2 Concentration versus time plots of tetralin

The plot of the natural logarithm of the tetralin concentration versus time and the plot of the inverse of the tetralin concentration versus time are shown in **Figures C.20** and **C.21**, respectively. The linear regressions were calculated for each reaction system and the R^2 of the regressions are given in the figures.

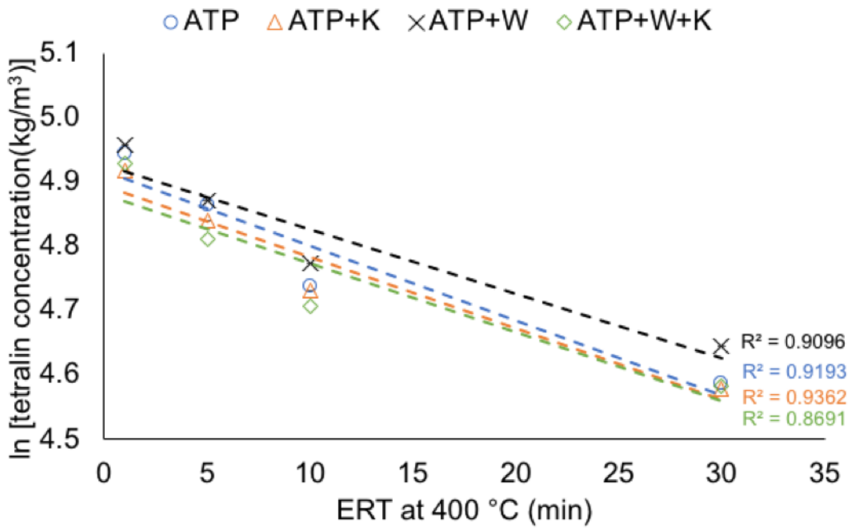

Figure C.20: Plot of the natural logarithm of tetralin concentration vs. reaction time.

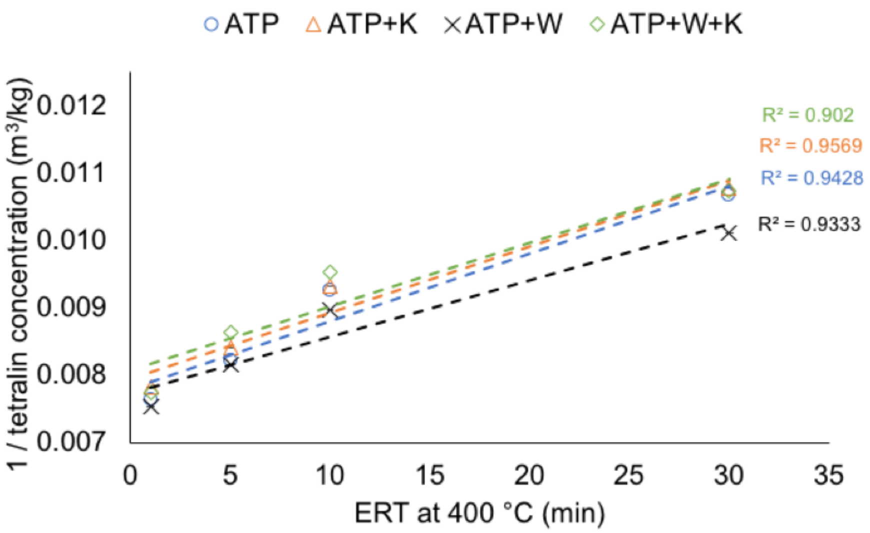

Figure C.21: Plot of the inverse of tetralin concentration vs. reaction time.

C.7.3 Concentration versus time plots of *n*-pentadecane

The plot of the natural logarithm of the *n*-pentadecane concentration versus time and the plot of the inverse of the *n*-pentadecane concentration versus time are shown in **Figures C.22** and **C.23**, respectively. The linear regressions were calculated for each reaction system and the R^2 of the regressions are given in the figures.

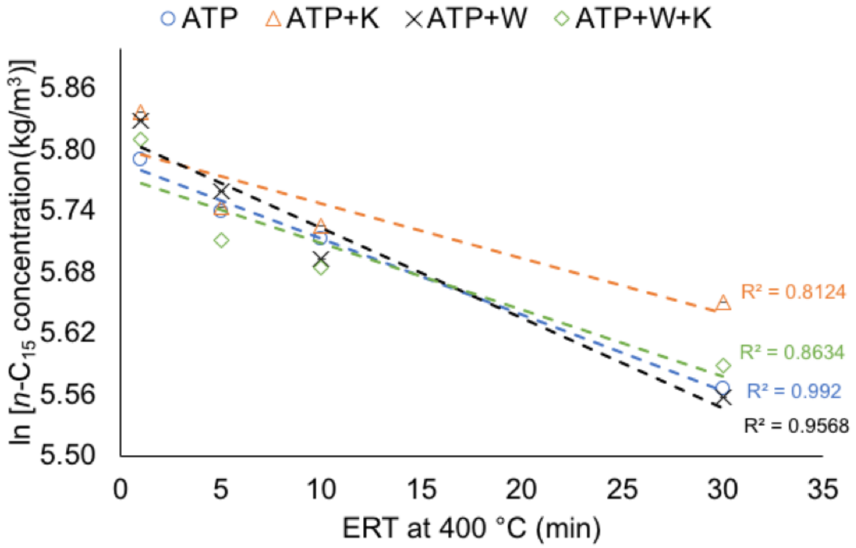

Figure C.22: Plot of the natural logarithm of *n*-pentadecane concentration vs. reaction time.

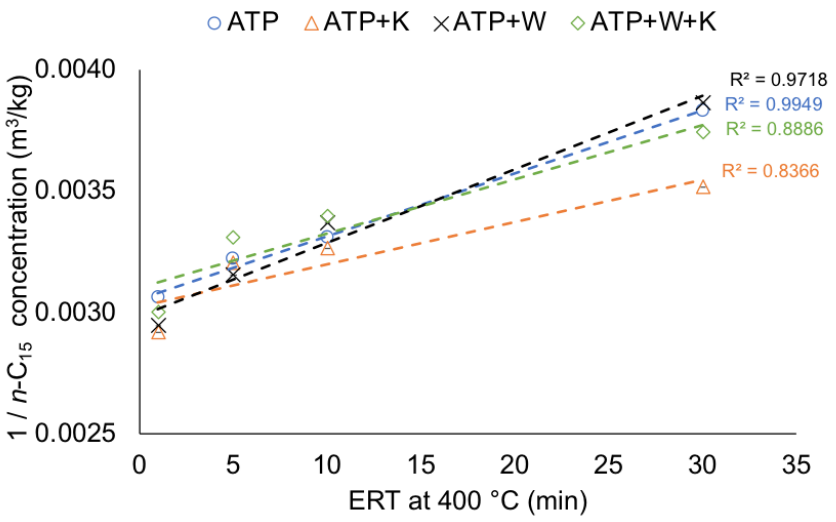

Figure C.23: Plot of the inverse of *n*-pentadecane concentration vs. reaction time.

C.8 GC-MS chromatograms with RT lower than 50 min from the ATP experiments

To improve clarity for peak identification, the chromatograms from the ATP experiments obtained by GC-MS in the region with a retention time (RT) between 4.2 and 50 minutes were split into four regions (A to D). The chromatograms for each region are shown in the next subsections. The peaks were assigned peak identifiers, which are listed in the tables contained in each one of the following subsections. The compounds with an RT lower than 50 min were identified by the use of the commercial standards that were listed in **Table C.2**. Only the chromatograms containing the experiments with reaction time of 10 min were reported in this section because they contained all species identified in the other reaction times as well.

C.8.1 Region A – RT between 4.2 and 14.5 min

Table C.11: Peak identifier and RT of compounds identified in the region A of the GC-MS chromatograms of the ATP experiments.

Compound	Peak identifier	RT (min)
hexane	A1	4.7
benzene	A2	6.3
heptane	A3	8.3
toluene	A4	11.0
octane	A5	13.5

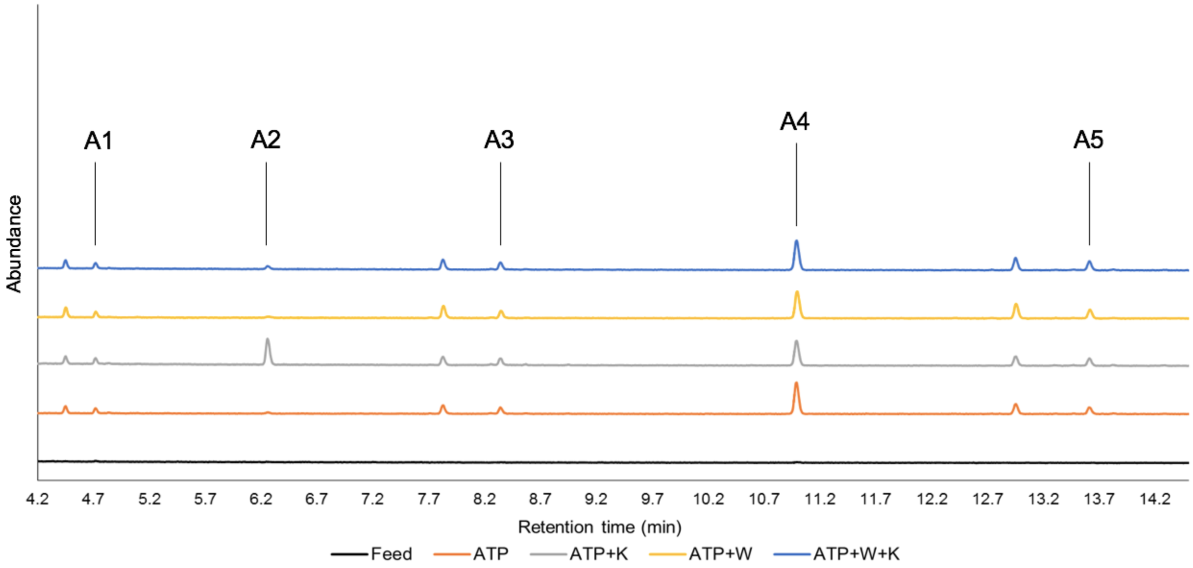

Figure C.24: GC-MS chromatograms from the ATP experiments (reaction time of 10 min) - Region A (RT between 4.2 and 14.5 min).

C.8.2 Region B – RT between 14.5 and 20.5 min

Table C.12: Peak identifier and RT of compounds identified in the region B of the GC-MS chromatograms of the ATP experiments.

Compound	Peak identifier	RT (min)
ethylbenzene	B1	16.2
styrene	B2	17.7
nonane	B3	19.4
cumene	B4	20.0

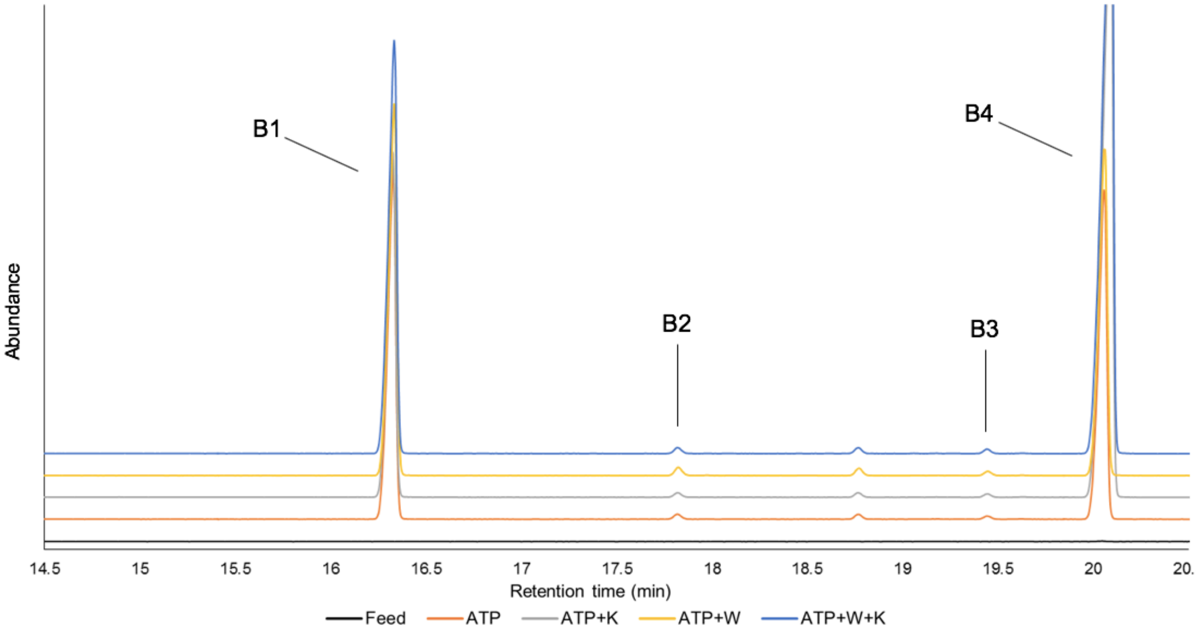

Figure C.25: GC-MS chromatograms from the ATP experiments (reaction time of 10 min) - Region B (RT between 14.5 and 20.5 min).

C.8.3 Region C – RT between 20.5 and 34.5 min

Table C.13: Peak identifier and RT of compounds identified in the region C of the GC-MS chromatograms of the ATP experiments.

Compound	Peak identifier	RT (min)
n-propylbenzene	C1	21.7
AMS	C2	23.1
sec-butylbenzene	C3	24.9
decane	C4	25.1
n-butylbenzene	C5	27.3
2-phenyl-2-propanol	C6	28.4
undecane	C7	30.6
tetralin	C8	32.8
naphthalene	C9	33.7

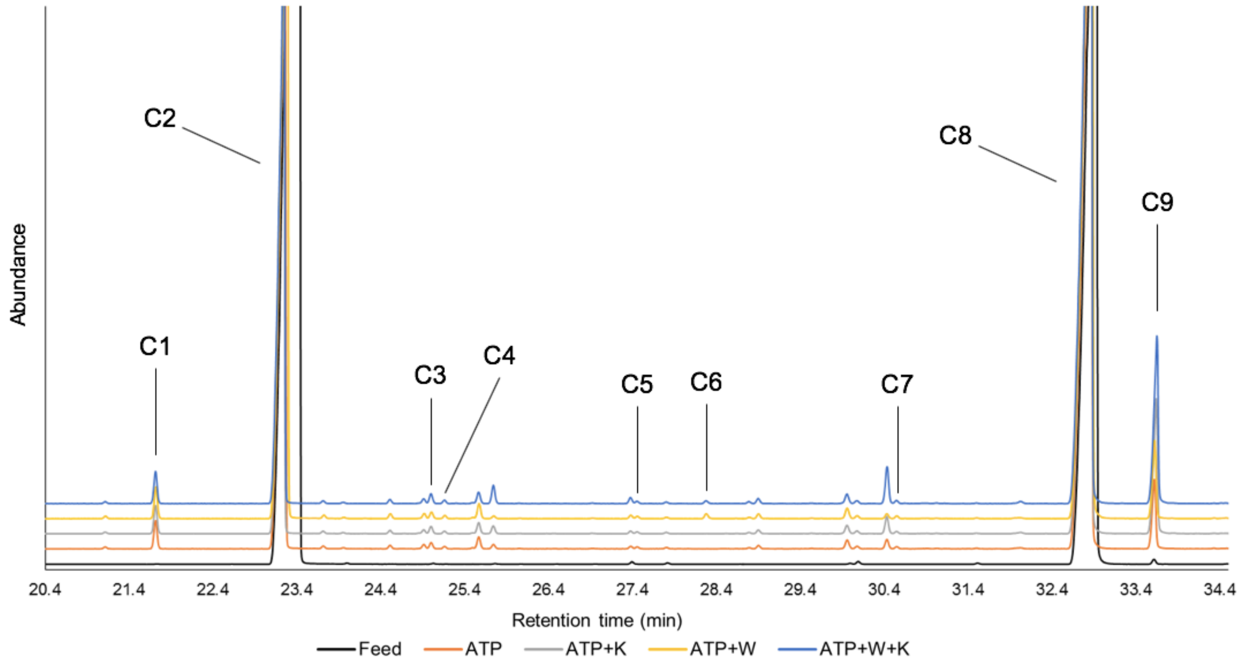

Figure C.26: GC-MS chromatograms from ATP experiments (reaction time of 10 min) - Region C (RT between 20.5 and 34.5 min).

C.8.4 Region D – RT between 34.5 and 50.0 min

Table C.14: Peak identifier and RT of compounds identified in the region D of the GC-MS chromatograms of the ATP experiments.

Compound	Peak identifier	RT (min)
dodecane	D1	35.7
2-methylnaphthalene	D2	38.8
1-methylnaphthalene	D3	39.5
tridecane	D4	39.9
biphenyl	D5	42.1
tetradecane	D6	43.9
1,4-dimethylnaphthalene	D7	44.4
pentadecane	D8	47.2

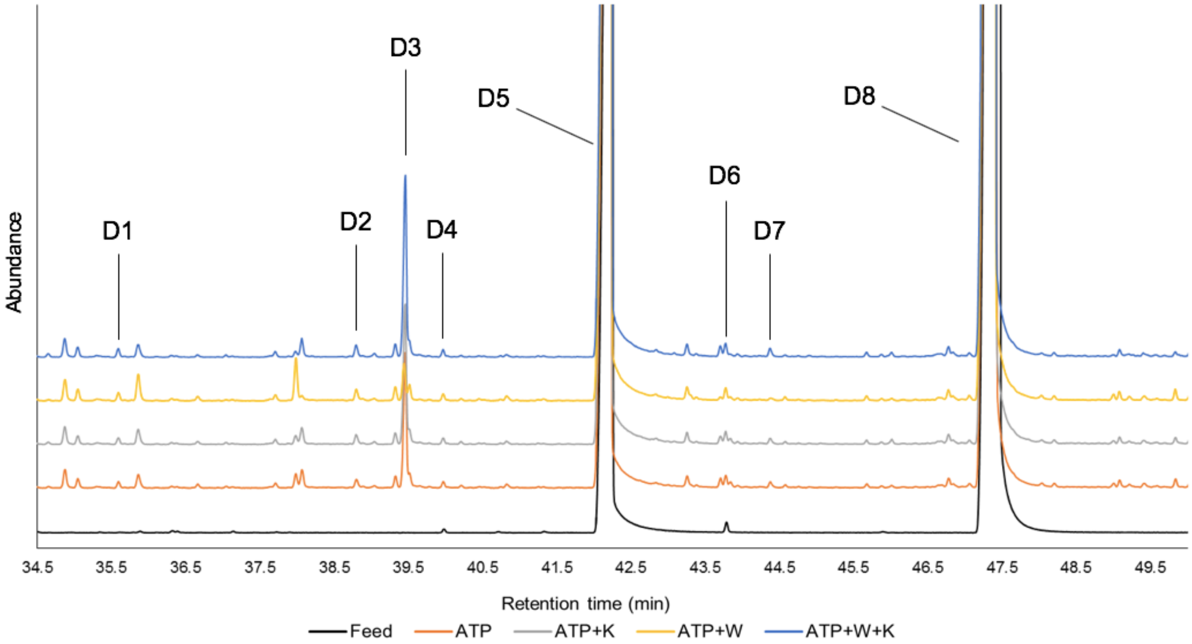

Figure C.27: GC-MS chromatograms from ATP experiments (reaction time of 10 min) - Region D (RT between 34.5 and 50 min).

C.9 GC-MS chromatograms with RT lower than 50 min from the AWM experiments

Although several common products were formed in both the ATP and AWM experiments, there were some species that were exclusively formed in only one of the experiments because their feed differed. To improve clarity, different labels for the regions with RT lower than 50 min were used for both experiments, even for common products. The chromatograms from the AWM experiments were split into three regions (I, J, and K).

C.9.1 Region I – RT between 4.2 and 20.5 min

Table C.15: Peak identifier and RT of compounds identified in the region I of the GC-MS chromatograms of the AWM experiments.

Compound	Peak identifier	RT (min)
benzene	I1	6.3
toluene	I2	11.0
ethylbenzene	I3	16.2
styrene	I4	17.7
cumene	I5	20.0

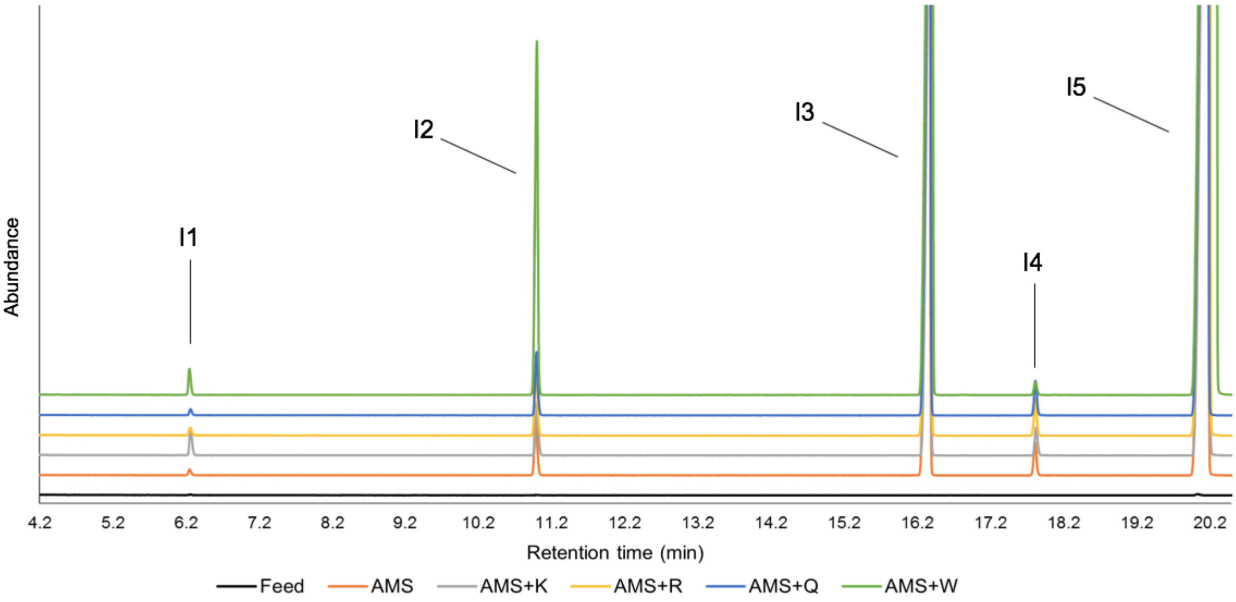

Figure C.28: GC-MS chromatograms from AWM experiments - Region I (RT between 4.2 and 20.5 min).

C.9.2 Region J – RT between 20.5 and 34.5 min

Table C.16: Peak identifier and RT of compounds identified in the region J of the GC-MS chromatograms of the AWM experiments.

Compound	Peak identifier	RT (min)
n-propylbenzene	J1	21.7
AMS	J2	23.1
sec-butylbenzene	J3	24.9
n-butylbenzene	J4	27.3
2-phenyl-2-propanol	J5	28.4

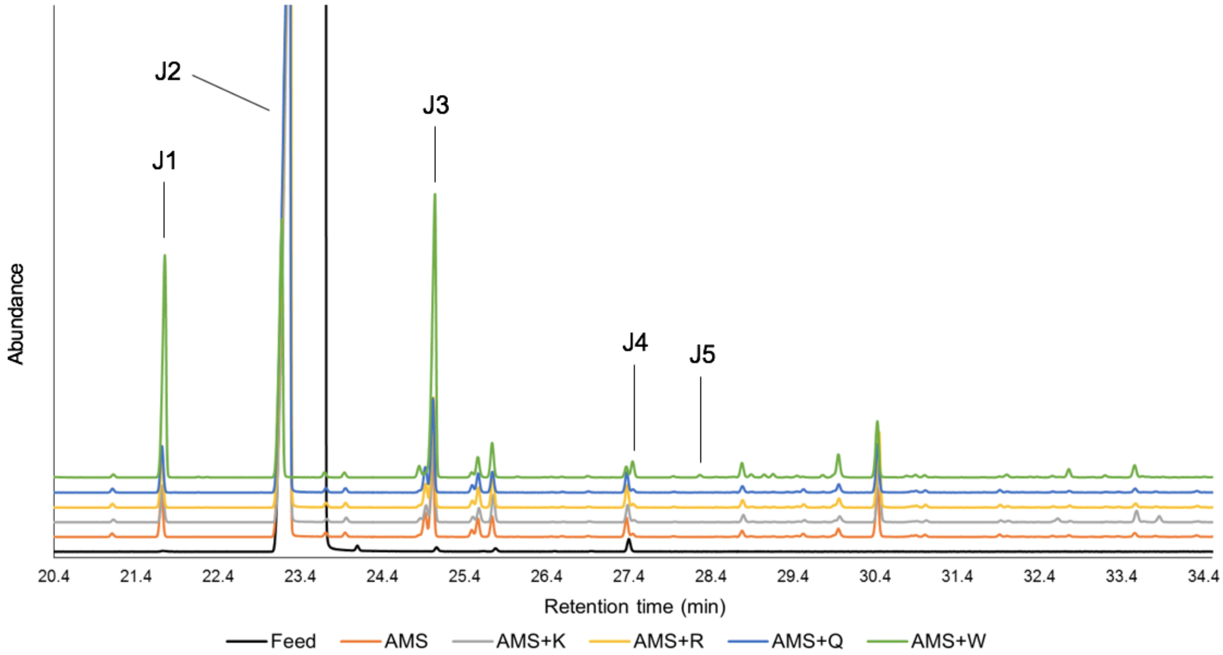

Figure C.29: GC-MS chromatograms from AWM experiments - Region J (RT between 20.5 and 34.5 min).

C.9.3 Region K – RT between 34.5 and 50.0 min

Table C.17: Peak identifier and RT of compounds identified in the region K of the GC-MS chromatograms of the AWM experiments.

Compound	Peak identifier	RT (min)
biphenyl	K1	42.1

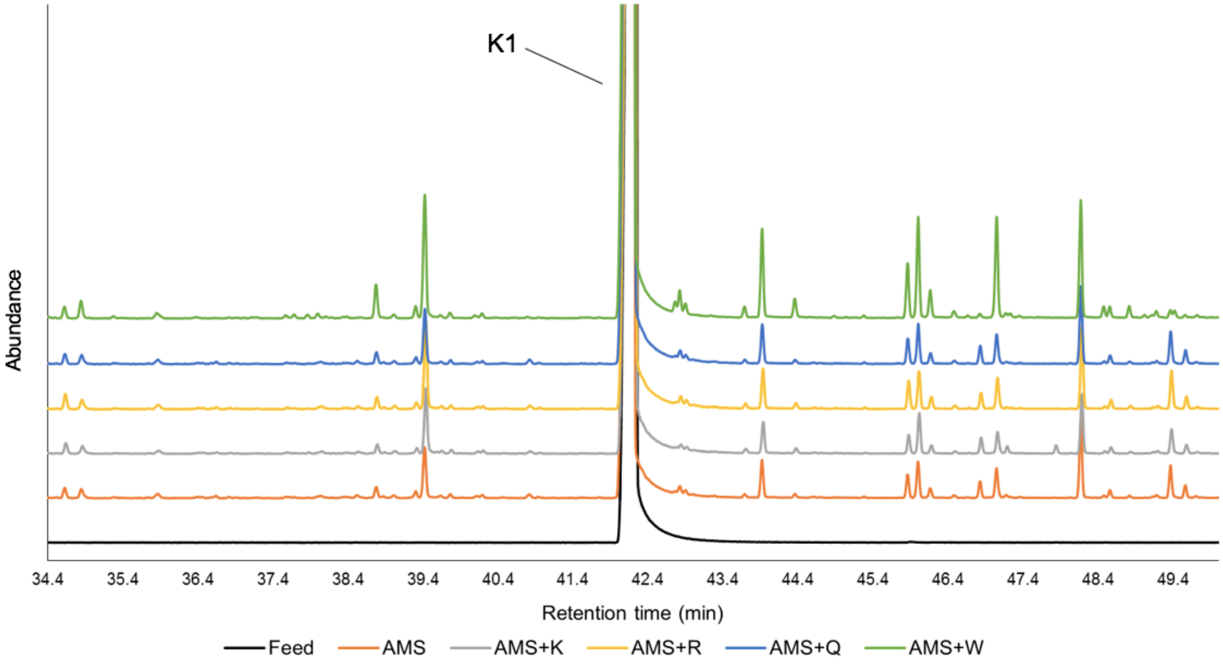

Figure C.30: GC-MS chromatograms from AWM experiments - Region K (RT between 34.5 and 50 min).

C.10 GC-MS chromatograms with RT higher than 50 min from ATP and AWM experiments

The selected compounds in the chromatogram region with an RT higher than 50 min were identified through mass spectral assignment only. These selected compounds, detected in both ATP and AWM experiments, were assigned the same peak identifier. This standardization was applied to improve clarity in data presentation and to facilitate the comparison of identical species across different experiments.

The selected compounds in the Region E of the chromatograms are shown in **Table C.18**.

Table C.18: Peak identifier and RT of compounds identified in the region E of the GC-MS chromatograms from the ATP and AWM experiments.

Compound[a]	**Formula**	**Peak identifier**	**RT (min)**	**Tentative structure**[b]
$C_{18}H_{20}$ – isomer (1,1,3-trimethyl-3-phenyl indane)	$C_{18}H_{20}$	E1	53.2	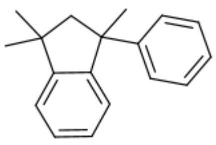
$C_{18}H_{22}$ – isomer	$C_{18}H_{22}$	E2[e]	55.2	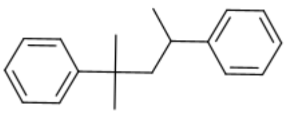 or 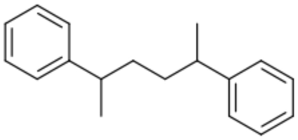
$C_{18}H_{22}$ – isomer	$C_{18}H_{22}$	E3[e]	55.5	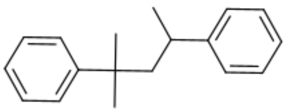 or 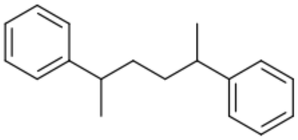
$C_{18}H_{20}$ – isomer	$C_{18}H_{20}$	E4	56.6	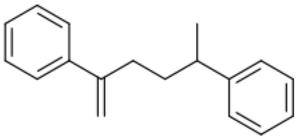

Continues on the next page

Compound[a]	**Formula**	**Peak identifier**	**RT (min)**	**Tentative structure**[b]
$C_{18}H_{20}$ – isomer	$C_{18}H_{20}$	E5	59.2	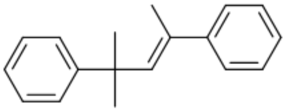
$C_{18}H_{20}$ – isomer	$C_{18}H_{20}$	E6	59.4	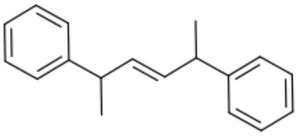

[a] Compound identification based on mass spectral assignment only. [b] Tentative structures for unconfirmed compounds based on mass spectral assignment. [e] The mass spectra of E2 and E3 were almost identical, and their structure assignment corresponded to both isomers depicted in their tentative structures.

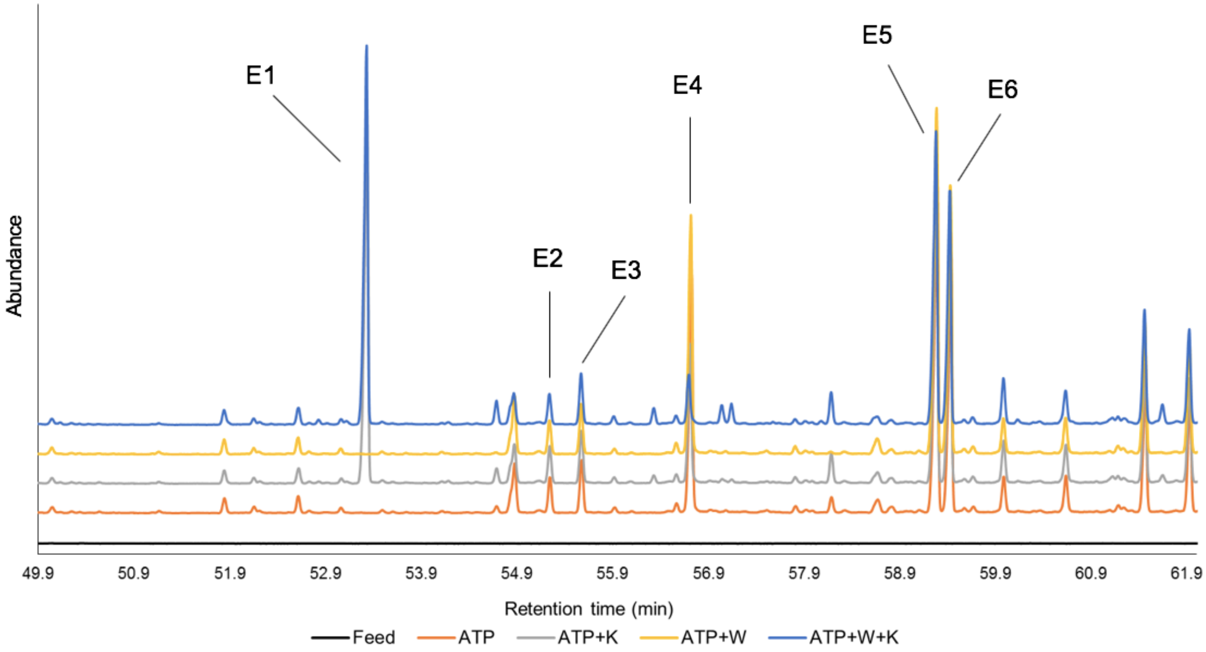

Figure C.31: GC-MS chromatograms from the ATP experiments (reaction time of 10 min) - Region E (RT between 50.0 and 62.0 min).

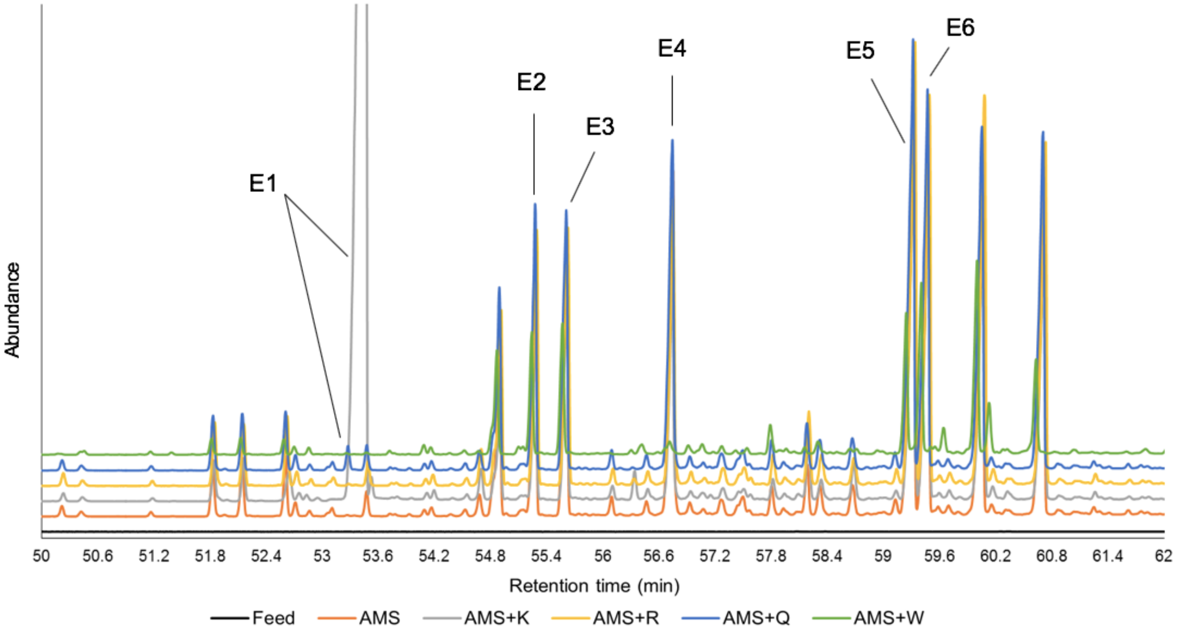

Figure C.32: GC-MS chromatograms from the AWM experiments - Region E (RT between 50.0 and 62.0 min).

C.11 Total RAP of *n*-alkanes from hexane to nonane

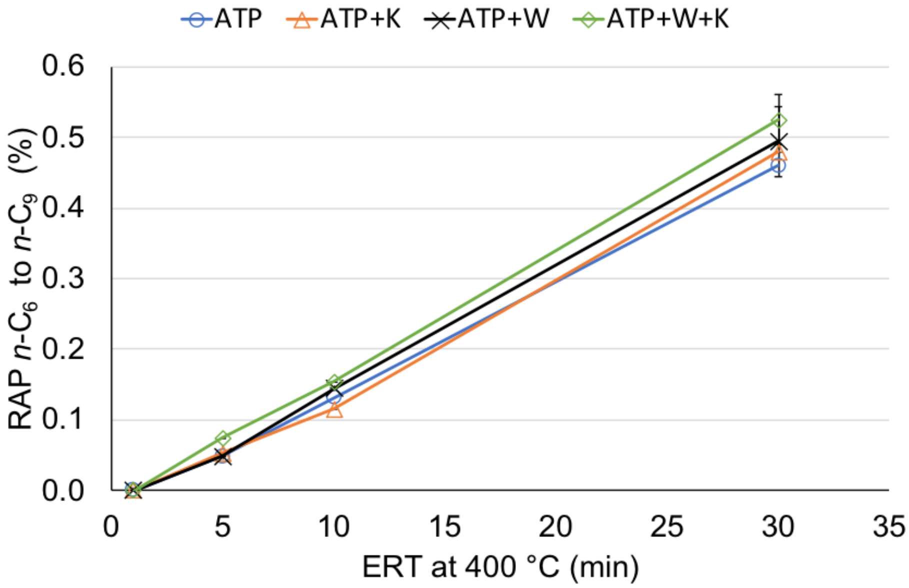

Figure C.33: Total RAP of *n*-alkanes in the range of C6 to C9 in the ATP experiments.

C.12 Thermogravimetric analyses (TGA) of minerals after the reactions in the ATP and AWM experiments

Thermogravimetric analysis of solids was carried out using a Mettler Toledo TGA/DSC1. Each analysis used approximately 10 mg of sample placed in a 70 μL alumina crucible. The temperature program encompassed three phases: first, the sample was heated from 25 to 600 °C at a rate of 10 °C/min under a nitrogen atmosphere; second, the temperature was held constant at 600 °C for 30 minutes under a nitrogen atmosphere; and third, the temperature was maintained at 600 °C for 1 hour under an air atmosphere.

The TGA results for the minerals collected after reactions in the ATP and AWM experiments are given in **Table C.19**.

Table C.19: Weight Loss Obtained from TGA Analysis of solids separated from products.

Experiment	Weight loss (wt%)[a]						Mineral content (wt%)	Fixed organic matter / Mineral content
	250–600 °C / N_2		600 °C / N_2 / 30 min		Fixed organic matter 600 °C / Air / 60 min			
	x	*s*	*x*	*s*	*x*	*s*		
ATP+K								
1 min	40.7	0.2	1.0	0.0	0.5	0.1	57.7	0.009
5 min	44.8	0.2	0.9	0.0	0.3	0.0	53.9	0.006
10 min	47.5	1.0	0.9	0.1	0.5	0.1	51.2	0.009
30 min	44.0	0.3	0.9	0.0	0.5	0.1	54.6	0.010
ATP+W+K								
1 min	13.1	0.5	1.5	0.0	0.4	0.0	85.0	0.005
5 min	15.2	0.5	1.5	0.1	0.4	0.1	82.8	0.005
10 min[b]	61.2	1.7	0.7	0.0	0.3	0.1	37.9	0.008
30 min	35.5	0.3	1.0	0.1	0.6	0.0	62.9	0.009
AMS+K	49.8	3.2	0.8	0.1	0.7	0.0	48.7	0.014
AMS+R	31.8	3.1	0.1	0.0	0.0	0.7	68.1	0.000
AMS+Q	14.7	0.2	0.0	0.0	0.1	0.0	85.2	0.001

[a] Average (*x*) and standard deviation (*s*) of experiments in duplicate for the AWM experiments and analyses in duplicate for the ATP experiments. [b] Most of the solids from the ATP+W+K experiment at 10-min reaction were left inside the reactor and only a small amount was collected in the centrifuge tube. As a consequence, the relative high amount of volatized organic matter in that system is probably due to sampling of more organic matter than solids for the TGA analysis.